Neurite Response to Topographical and Molecular Cues

by

Julie Ann Richardson

Sc.B. Brown University, Providence, RI, 2007

Submitted in partial fulfillment of the requirements

for the degree of Doctor of Philosophy in the

Division of Biology and Medicine at Brown University

Department of Molecular Pharmacology, Physiology, and Biotechnology

and

Center for Biomedical Engineering

Providence, Rhode Island

May 2012

This dissertation by Julie A. Richardson is accepted in its present form by the Division of Biology and Medicine as satisfying the dissertation requirement for the degree of Doctor of Philosophy.

Date_____ _____

Diane Hoffman-Kim, Ph.D., Advisor

Date_____ _____

Eric Darling, Ph.D., Reader

Date_____ _____

Jeffrey Morgan, Ph.D. Reader

Date_____ _____

Anubhav Tripathi, Ph.D., Reader

Date_____ _____

Shawn Mulvaney, Ph.D., External Reader

Approved by the Graduate Council

Date_____ _____

Peter Weber, Dean of the Graduate School

CURRICULUM VITAE

Name: Julie Ann Richardson

Date of Birth: November 19, 1984

Place of Birth: Long Branch, NJ, USA

I. EDUCATION

- Ph.D. candidate, Biomedical Engineering. Thesis title: Neurite Response to Topographical and Molecular Cues. Brown University, Providence, RI. Expected graduation date, May 2012.
- Sc.B. Biomedical Engineering with Honors. Brown University, Providence, RI, May 2007.

II. ABSTRACTS

- D Chau, JA Richardson, D Hoffman-Kim. TREK-1 channels and navigation: A study in neurite contact guidance. Brown Undergraduate Summer Research Symposium. August 2011.

- JA Richardson, CW Rementer, DB Chau, D Hoffman-Kim. Directed nerve growth in complex environments exhibiting biomimetic topographic features. Gordon Research Conferences: Biomaterials and Tissue Engineering, July 2011.
- JA Richardson, CW Rementer, D Hoffman-Kim. Guidance of dorsal root ganglion neurites and Schwann cells by isolated Schwann cell topography. New England Science Symposium, April 2011.
- JA Richardson, CW Rementer, D Hoffman-Kim. Guidance of dorsal root ganglion neurites and Schwann cells by biomimetic topography. Biomedical Engineering Society Annual Meeting, October 2010.
- D Chau, E Hsieh, T Ramchal, C Lopez-Fagundo, J Richardson, D Hoffman-Kim. Analyzing nerve growth in complex in vitro environments. Brown Undergraduate Summer Research Symposium. August 2010.
- JA Richardson, D Hoffman-Kim. Biomimetic Schwann cell features within polymeric conduits direct neurite extension. Biomedical Engineering Society Annual Meeting, October 2009.
- CW Rementer, JA Richardson, D Hoffman-Kim. Schwann cell migration and alignment from dorsal root ganglia are directed by biomimetic topography. Biomedical Engineering Society Annual Meeting, October 2009.
- KM Kim, SY KIM, JA Richardson, C Kofron, D Hoffman-Kim, GTR Palmore. Electrical stimulation of nerve cells: image analysis of cell behavior. Materials Research Society Annual Meeting, December, 2008.
- JA Richardson, K-M Kim, C Kofron, SY Kim, GT Palmore, D Hoffman-Kim. Neurite outgrowth in response to electrical and molecular cues. Biomedical Engineering Society Annual Meeting, October 2008.

- JA Richardson, KM Kim, CM Kofron, SY Kim, GTR Palmore, D Hoffman-Kim. Novel Platform to Assess Neurite Outgrowth in Response to Multiple Cues. Northeast Bioengineering Conference, April 2008.
- JA Richardson, GN Li, D Hoffman-Kim. Characterization of Cellular Behavior in the Presence of Complex Topographical and Molecular Cues for Application to Central Nervous System Repair. Biomedical Engineering Undergraduate Research Symposium, April 2007.
- JA Richardson, GN Li, D Hoffman-Kim. Schwann Cell Bridging is Influenced by the Combination of Topography and Molecular Guidance Cues. Biological Sciences Undergraduate Research Poster Session, April 2007.
- JA Richardson, GN Li, D Hoffman-Kim. Selective Coating of Permissive Molecular Cue on Topographical Poly(dimethyl siloxane) Influences Bridging of Schwann Cells. Biomedical Engineering Society Annual Meeting, October 2006.
- JA Richardson, GN Li, D Hoffman-Kim. Axon Guidance by Overlapping Permissive and Inhibitory Protein Gradients. Brown Undergraduate Teaching and Research Assistantship Symposium, August 2006.
- JA Richardson, D Haders. Adsorption and Release of PolyAspirin to and from Hydroxyapatite Crystals. Rutgers Summer Undergraduate Research Frontiers and Nanomaterials Science and Engineering Internship, August 2004.

III. PUBLICATIONS

- JA Richardson, C Kofron, C Johnson, J Mitchel, D Chau, J Bruder, D Hoffman-Kim. “Cooperating and competing combinations of Schwann cell topography and micropatterned laminin influence neurite growth”. Manuscript in preparation.

- JA Richardson, CW Rementer, J Bruder, D Hoffman-Kim. “Guidance of dorsal root ganglion neurites and Schwann cells by isolated Schwann cell topography on poly(dimethyl siloxane) films and conduits” 2011. *Journal of Neural Engineering*, 8(4):046015. Epub 2011 Jun 15.
- JA Richardson, D Hoffman-Kim. “The importance of defining ‘data’ in data management policies” 2010. *Science and Engineering Ethics*, 16(4):749-751.
- TK Kayagil, JA Richardson, MJ Archer, JS Erickson, FS Ligler. “The Beadwhacker for maintaining even dispersion of micron-sized beads” 2007. *Measurement Science and Technology*, 18 N1-N4.

IV. INVITED SEMINARS AND LECTURES

- “Following the leader: Directing nerves and Schwann cells with biomimetic guidance channels” Graduate Student Research Seminar Series, Brown University, Providence, RI, December 2011.
- "Directed nerve growth in complex environments exhibiting biomimetic topographic features" Naval Research Laboratory, Washington, DC, September 2011.
- “Directed nerve growth in complex environments exhibiting biomimetic topographic features” VA Center for Restorative and Regenerative Medicine Seminar Series, Providence, RI, March 2011.
- “Introduction to Biomedical Engineering” National Student Leadership Conference Seminar Series, Berkeley, CA, July 2007.

V. AWARDS AND LEADERSHIP

- Predoctoral Associated Health Rehabilitation Research Fellowship Program. Veterans Administration (VA). "Engineering Nanoscale Biomimetic Materials for Nerve Regeneration and Rehabilitation" October 2010 – October 2011.
- Susan and Robert Kaplan Fellowship Travel Award, June 2010.
- Graduate Biomedical Engineering Society (gBMES). Organized seminars, banquet functions, and collaborated with department leaders to develop gBMES. Communicated with biomedical engineering students and faculty to enrich the program across campus. Providence, RI. Vice President August 2010 – August 2011; Secretary October 2009 – August 2010.
- NSF GK-12 Fellowship. Developed lesson plans and delivered lessons to high school science students. Brought hands-on science into the classroom and led students in instruction of course materials. Providence, RI. June 2007 – June 2008.
- National Student Leadership Council. Team Advisor. Mentored and managed high school students at an intensive engineering leadership conference. Led students in the design and construction of underwater, motorized robots. Responsibilities included instructing group activities, facilitating group discussions, supervising a group of 13 students, and designing and delivering lectures and lessons. Berkeley, CA. July 2007 – August 2007.
- Biomedical Engineering Society Membership Chair. Providence, RI. September 2006 – April 2007.
- The Adolescent Leadership Council. Mentored teens with chronic illness at Hasbro Children's Hospital. Providence, RI. August 2006 – August 2009.
- Chattertocks, all-female a cappella group. Planned and ran rehearsals, initiated and arranged performance pieces. Recognized by a cappella review board as 'Best all-female Album' and 'Best all-female Song' 2004. Co-Musical Director (F'06), Musical Director (S'05,'06); Tour

Manager (W'03,'05), CD Mixing Committee (S'05,'07), CD Coordinator (F'04). Providence, RI. September 2003 – May 2007.

- Avaya Academic Awards Program. September 2003 – May 2007.
- Teaching Assistantships. Organ Replacement (S'07); Introduction to Engineering (F'06). Providence, RI. September 2006 – December 2006; January 2007 – May 2007.

VI. TRAINING

- Laboratory: Experimental animal surgical technique, sterile cell culture, soft lithography, photolithography, replica molding, microcontact protein printing, immunocytochemistry, phase, epifluorescence, and scanning electron microscopy, clean room training, PCR (real time- and RT-PCR), nucleic acid extraction, magnetic and glass bead separation techniques.
- Software: SigmaPlot, OpenLab, SPSS, Oriana, ImageJ, Photoshop, Excel, PowerPoint, LabView, MS Word.

VII. PROFESSIONAL DEVELOPMENT

- Brown Ethical and Responsible Conduct of Research Education (BEARCORE) program. Providence, RI. January 2012.
- Navigating the Publication Process Workshop. Providence, RI. January 2011.
- Responsible conduct in research training. Providence, RI. September 2008 – December 2008.

VIII. UNDERGRADUATE RESEARCH EXPERIENCE

- Undergraduate Thesis Research. Characterization of CNS-supporting bridging of Schwann cells in response to topographical and molecular cues in the laboratory of Diane Hoffman-Kim, Ph.D. Providence, RI. August 2006 – May 2007.
- Undergraduate Teaching and Research Assistantship. Investigated effects of permissive and inhibitory protein gradients on dorsal root ganglion adhesion and neurite outgrowth for application to CNS nerve regeneration. Providence, RI. June 2006 – August 2006.
- Naval Research Laboratory (NRL) Internship. Developed and optimized parameters of nucleic acid subtraction and concentrated elution. Improved efficiency and tested full pathogen recovery protocol from human nasal washings spiked with Ad4/7 and FluA pathogens, recovering both from initial spiking on the nano- and pico-scale, respectively. Co-invented Beadwhacker device (patent pending) to maintain even and continuous dispersion of micron-sized beads. Washington, DC. June 2005 – August 2005.
- Rutgers University Internships. IGERT Graduate Fellowship Program on Integratively Engineered Biointerfaces Summer Undergraduate Research Frontiers Program and Nanomaterials Science and Engineering Internship. Designed and implemented an experimental protocol to monitor the adsorption and release of PolyAspirin to and from hydroxyapatite crystals. Piscataway, NJ. June 2004 – August 2004.
- Research Assistantship. Artificial Organs Lab. Conducted a degradation study of polyadipic anhydride. Optimized parameters of microsphere formation by Phase Inversion Nanoencapsulation (PIN). Providence, RI . January 2004 – May 2004.

IX. PATENT

- TA Kayagil, JA Richardson. Beadwhacker. Pub. No. US2008/1008406 A1. May 22, 2008.

ACKNOWLEDGEMENTS

First of all, I must thank Diane Hoffman-Kim for her guidance and for her mentorship throughout this journey. Over the past six years Diane has taught me the importance of conducting good science, how to ask complex questions and follow through by designing experiments to answer them. Thank you, Diane, for instilling and confirming my scientific passions and for demonstrating how a career in science can be fulfilling and rewarding.

Thank you also to my thesis committee, Jeffrey Morgan, Anubhav Tripathi, Eric Darling, and Shawn Mulvaney for providing me with thought-provoking discussion, scientific insight, and encouragement, and for pushing me to become a better scientist through this process. I cherish your mentorship and sincerely feel honored to have you as my thesis committee.

Thank you to Carol Folan, Cheryl Pariseau, and all of the faculty and staff who made any and all logistical maneuvers seem like a walk in the park. You are the nuts and bolts of the program and I am thankful for your assistance and support through it all.

Thank you to my labmates, past and present, for your insights, discussions, and camaraderie. I consider myself very lucky that I entered grad school having co-workers but I am leaving with some of the best friends I've ever had. Thank you Liane Livi and UT Liu for answering tough questions and attacking troubleshooting issues head-on to help me through challenging lab dilemmas. Thank you Talisha Ramchal and Molly Boutin not only for your thoughtfulness and thorough help with interpretation and reflections of my data, but for somehow making me laugh through it all. Thank you Jen Mitchel for literally having my back over the last five years. I'm going to miss being able to turn around and talk, even if you usually have your headphones on and I have to wave like a lunatic to get your attention. I'm thankful that I've had such a wonderful buddy to step through grad school with, to laugh, cry, complain, and understand with, and I look forward to having you as my colleague for decades to come. Thank you Cristina López-Fagundo for being a brilliant collaborator, a truly great friend, and for being one of the most wholesome people I have ever met. I am so glad we were able to become such great friends over the past few years, and your companionship helped me in so many ways.

This work would not have been possible without the help and scientific drive of my undergraduate students Cameron Rementer and Danielle Chau. I feel so lucky that I was able to teach and learn from such passionate scientists. I know both of you will go on to change the world, and I'll be proud to say that you were once my little scientists in training.

Thank you to my family, Mom, Dad, and Gina, for supporting me in every way imaginable as I took a head-first dive into this whole PhD thing. Thank you for listening to me talk about my projects, even if you had to nod and smile through it all. You never questioned my ability and believed in me every step of the way, often more than I did myself. You've taught me how to go

for my dreams and not to settle for mediocrity. None of this would have come true without your support and moral guidance. I love you guys.

Finally, thank you Kenny. Over the last five years, you have become my companion, my sounding board, and the love of my life. You have been my number one fan from day one, and not once have you doubted me. You have been my rock through all of the good and all of the challenges. I don't believe that this kind of love and support comes around very often, and I am the luckiest to have found all of it in you. Thank you.

CONTENTS

FIGURES AND TABLES

ABSTRACT

Nerves must navigate through complex sets of environmental cues during development and after injury to connect and reconnect with their proper targets to generate and regenerate function of the nervous system. In order to develop strategies for nerve repair and to understand the basic biology of how nerves are guided and respond to the complex cues of their environment, neurite outgrowth and alignment must be quantified in response to systematic presentations of such cues via in vitro culture platforms. In this thesis, neurite outgrowth and alignment strength was determined on in vitro culture platforms presenting molecular and topographical guidance cues as permissive extracellular matrix molecule laminin (LN) and biomimetic or cell-based microfabricated topographical features. These studies revealed several characteristics of nerve growth and decision making in response to such cues.

Neurites responded directly to underlying biomimetic topographical features on two-dimensional polymeric films and within nerve guidance conduits. Neurite outgrowth on micropatterned repeating LN stripes depended on the micropattern characteristics, and neurite outgrowth and

alignment was complex on multi-cue platforms exhibiting strategic and simultaneous presentation of combinations of molecular and topographical cues. Neurite outgrowth was enhanced on platforms where cues were combined in parallel, while neurites preferentially aligned to one cue when cues were orthogonally opposed. This alignment depended on the characteristics of the opposed cues, and did not always occur as expected. These data provide justification for the study of multi-cue systems to improve our understanding of how nerves make decisions in complex environments.

Asymmetric cell-shape based topographical features were fabricated and Schwann cell alignment and neurite outgrowth response was assessed. Schwann cells and neurons interacted with the asymmetric features directly, exhibiting alignment and outgrowth response that depended on the feature shape and dimensions.

We assessed neuronal adhesion and neurite outgrowth in the presence of TREK-1, a pharmacological inhibitor of ion channels implicated in mechanosensation of environmental topographical cues to determine whether and how such mechanistic pathways are involved in neurite guidance on biomimetic topographical features. Through initial studies, we found that there was a dose-dependent response to the inhibitor, wherein neuronal adhesion and neurite alignment were impacted as inhibitor concentration increased. This type of study has not yet been performed on whole cell cultures, and as such, provides significant insights and preliminary steps toward a mechanistic approach to understanding how nerves make decisions on cell-based biomaterials.

The work presented in this thesis illuminates several key aspects of neurite guidance in response to complex molecular and topographical features. This research improves our understanding of

basic biological questions surrounding how nerves make navigational decisions, and will contribute to informing strategies of biomaterial design for therapeutic approaches toward nerve repair.

OVERVIEW OF THESIS CHAPTERS

The work presented in this thesis covers the investigation of neurite outgrowth in response to related, albeit diverse environmental cues, and as such is divided into distinct chapters. Chapter 1 details the background information and motivation relevant to nerve tissue engineering in response to environmental cues, highlighting the current status of the field and orienting the reader to obstacles that are yet to be overcome.

Chapter 2 reports a study published in the Journal of Neural Engineering wherein neurite outgrowth and alignment response were assessed within nerve guidance conduits and on polymeric films presenting cell-based topographical features. In addition, this work explored the relative extension and migration of neurites and their supporting glial cells on these novel biomaterial platforms, implicating biomimetic topographical features as promising components of therapeutic strategies for nerve repair.

Chapter 3 reports a complex study that investigated neuronal decision making and growth response to micropatterned permissive protein stripes and cell-based topographical features presented individually and in cooperative and competitive combinations. This work revealed several characteristics of nerve growth in complex multi-cue environments and illuminated key aspects of nerve growth decisions. The results of this work have led to the suggestion of the physical mechanisms underlying neurite outgrowth in response to protein micropatterns and competitively arranged molecular and topographical cues, which were further investigated through the work presented in Chapter 4.

The work of Chapter 4 investigated nerve growth characteristics in a dynamic setup, combining endpoint experiments with timelapse microscopy to elucidate nerve growth dynamics as alignment takes place on protein micropatterns and in the presence of competing micropatterns and cell-based topographical features.

Chapter 5 explores the intracellular mechanism surrounding neurite alignment response to cell-based topographical features. In particular, the mechanosensitive TREK-1 potassium channel was targeted as having a role in the mechanotransduction of cell-based topography for subsequent nerve growth decision making and alignment. Fluoxetine, a direct pharmacological inhibitor of TREK-1 was used to determine interruption of neurite alignment with decreased TREK-1 activity. This Chapter implicates TREK-1 activity as having a significant role in directing neuronal response to directive topographical features, and provides insight to the intracellular mechanisms surrounding such guidance.

Chapter 6 summarizes the key findings of this research, and explores possibilities for future work to enhance that presented here.

CHAPTER 1

INTRODUCTION

1.1. Relevance

Nerves must interpret and integrate a wide range of environmental cues during development in order to reach and connect with their intended target cells and tissues. These precise connections develop into a complex neuronal network that allows for the transmission of signals from the brain to and from the organs, muscles, and tissues of the body. The pathfinding process is highly regulated, as the navigating neuronal processes, known as neurites, interact with directive cues of their microenvironment to steer along the intended course. The microenvironmental cues are complex, as several types of cues, including soluble, topographical, galvanotropic, and substrate-bound cues are present at diverse strengths and spatial and temporal arrangements throughout development. Thus, navigating neurites are posed with the rigorous necessity to connect with

precisely intended targets while undergoing a complex navigational course through which growth and steering decisions must be accurately made in response to a complex milieu of environmental guidance cues.

After injury to the nervous system, damaged nerves must reconnect with their proper targets in order for regeneration and recovery to take place. Once again, nerves must navigate among complex sets of environmental cues to reconnect with their targets, but the post-injury environment poses additional complexities and obstacles to precise pathfinding, and regeneration is often not achievable following injury. Toward interventions to aid nerve repair, it is imperative to understand how nerve growth decisions take place in response to microenvironmental cues. With such information, strategies to promote nerve guidance and subsequent nerve regeneration among complex sets of environmental cues may be developed. The research presented in this dissertation addresses the assessment of nerve outgrowth and guidance in response to engineered platforms presenting chemical and topographical environmental cues, and sheds light on several attributes of nerve decision making among such cues.

1.2. Background and significance

It is estimated that there are forty spinal cord injuries (SCI) per million people in the United States, with approximately 12,000 new cases of SCI occurring each year[1]. SCI results from compression or severing of the nerves within the spinal cord by direct injury to the cord or indirect injury by surrounding tissues[2]. As of 2009, 262,000 people in the United States suffered from SCI, and these injuries predominantly affect young adults, as they are commonly results of vehicular or sports-related accidents. The average age of injury is 28.7 years, and the most common status upon hospital discharge is incomplete tetraplegia of the patient at 38.3% of all SCI. Less than one percent of people experiencing SCI experience full recovery. Aside from pain

and loss of motor and sensory function, nerve injury accounts for loss of occupational status for sufferers, and large economic expenses surrounding post injury medical services. The estimated lifetime cost of a person injured at age 25 with high tetraplegia totals $3,273,270, which poses significant financial incentive for investigating cures for SCI[1]. In addition to SCI, traumatic brain injury affects over two million people, and more than 500,000 people suffer from stroke in the United States[3-4], overall making CNS injury highly prevalent and in need of intervention efforts.

Peripheral nerve injury (PNI) affects the nerves responsible for signaling to and from the brain and the peripheral nerves of the body and occurs where there has been transection, crush, or compression injury to peripheral nerves[5-6]. PNI vary widely in etiology and severity, depending on whether and how severely motor, sensory, or autonomic nerves are involved. Such injuries can result in partial or full loss of motor function to limb or digital muscles, loss of sensory capacity in regions of the skin, and loss of innervations to organ systems by autonomic nerves [5]. PNI are often devastating injuries, as quality of life may be critically impaired, several surgical interventions are often required, and full functional recovery is limited by the size, severity, and type of injury obtained.

Research must move toward understanding nerve injury so that therapeutic means to achieve nerve regeneration and subsequent functional recovery may be developed. Toward this end, tissue engineered strategies incorporating growth-promoting environmental cues are being investigated to enhance nerve regeneration. To generate such strategies for repair, an understanding of nerve injury is necessary. The research presented in this thesis addresses several components of nerve outgrowth and guidance in response to environmental cues, toward improving the understanding of how nerves make growth decisions in complex environments.

1.3. Overview of nerve injury

1.3.1. Injury to the CNS

The CNS includes nerves of the brain and spinal cord, while the PNS constitutes the motor, sensory, and autonomic nerves that innervate muscles, skin, organs, and other tissues of the body outside the CNS. The post-injury environment of the CNS is inhibitory toward regeneration, and CNS injury to the spinal cord generally progresses in three phases. The first phase occurs minutes after injury and is sustained for a few days thereafter. During this initial phase, mechanical damage to central nerves takes place, resulting in local necrosis of affected neurons, glia, and supportive cells, and electrolyte imbalances that lead to massive misfiring of action potentials and failure of normal impulse conduction among the spinal circuitry[7]. Following the first phase, the secondary injury phase lasts from minutes after the time of injury to weeks following the injury. During the second phase of SCI, chemical changes at the post-injury environment are cytotoxic and lead to further cell death, while apoptosis of the surrounding cells occurs as a result of reactive gliosis, whereby the local glial cells proliferate and overexpress glial fibrillary acidic protein (GFAP), signaling increased reactivity of glia and glial scar formation, inhibiting neuronal growth at the injury site[8]. Concurrently, inflammatory cells invade the injury site and the surrounding area to generate an overall chemically inhibitory environment to neuron growth at the injury site and throughout the surrounding tissue. Additionally, damage to myelinating oligodendrocytes of the CNS results in injury-site myelin-associated debris, including Nogo, myelin-associated glycoprotein (MAG), and oligodendrocyte myelin glycoprotein (OMgp), all of which are inhibitors of axon outgrowth[9-11].

In the third, or chronic, stage of SCI, the formation of an astrocytic glial scar inhibits neurite growth beyond the injury site by a combination of physical obstruction to directed growth and molecular inhibition of neurite growth[9, 12-13]. The chronic phase of SCI may begin days after

injury and can persist for years, as apoptosis and further scarring occur, interrupting the neural circuitry and, ultimately, the potential for regeneration. The glial scar is primarily composed of reactive astrocytes which upregulate secretion of inhibitory chondroitin sulfate proteoglycans, causing neurite retraction and growth cone collapse at the post-injury location[14]. Growth cones are sensory structures at the distal ends of neurites that sample environmental cues leading to directed neurite extension, and growth cone collapse leads to neurite retraction and inhibition of outgrowth[15].

Injury to the CNS poses significant, overall insurmountable obstacles for nerve regeneration, as such injuries are followed by complex cellular and intracellular events that inhibit neurite outgrowth both physically and chemically, as discussed above. Interestingly, it has been shown that neurons of the CNS do have the inherent capacity for regeneration, but that the local inhibitory environment precludes regrowth and recovery[16-19]. In order to promote regeneration after CNS injury, strategies to alter or overcome the post-injury microenvironment must be explored, such that damaged CNS neurites are promoted and directed to navigate and reconnect with their original targets. An overview of these strategies is discussed in sections to follow.

1.3.2. Injury to the PNS: Schwann cells maintain health and support regeneration

The PNS consists of the motor, sensory, and autonomic neurons outside the brain and spinal cord and their supportive glia, Schwann cells (SC). In the healthy PNS, SC exhibit biomolecular and topographical features that promote and maintain neuronal health. SC are responsible for the myelination of axonal processes, which permits saltatory conduction of action potentials along neuronal processes [20-21]. SC are also responsible for the formation of a basal lamina, rich in extracellular nutrients that maintain neuronal health [22-23]. Additionally, SC are present in longitudinally aligned spatial arrangements along neuronal processes as Bands of Büngner, which

aid axonal directedness toward their targets [24]. SC also secrete neurotrophic factors including nerve growth factor (NGF), brain derived growth factor (BDNF), and ciliary neurotrophic factor (CNTF), and express surface proteins such as N-cadherin and neuronal cell adhesion molecule (N-CAM) that maintain neuronal health [25-26].

In contrast to CNS injury sites, the post-injury environment of the PNS holds potential for regeneration depending on the extent and severity of the injury [27]. It is well understood that SC present several coordinated cues to neurons following injury, and PNS regeneration is largely attributed to the growth-promoting roles of SC in the post-injury state[28]. The role of SC shifts upon PNS injury, wherein SC present both molecular and topographical guidance stimuli to damaged peripheral nerves [22-23]. Their surfaces provide a topographical guidance component via their longitudinally aligned spatial orientation, as well as permissive molecular cues in the form of surface-expressed proteins including cell adhesion molecules such as neural cell adhesion molecule (NCAM) and L1, and extracellular matrix molecules laminin (LN), fibronectin (FN), and collagen IV [29].

Injury site debris is removed during Wallerian degeneration, a process by which SC, macrophages, and microglia migrate to the site of peripheral nerve injury and clear away cytotoxic myelin debris. Once the injury site is clear of debris, SC upregulate secretion of neurotrophic factors and proliferate as they align to and encompass sprouting axonal processes and guide them toward their distal targets [29]. After sprouted axon stumps are guided to their proper targets, SC resume the role of maintaining axonal health and remyelinate axonal processes to enhance signal propagation once again[30]. Although SC are a vital component of peripheral nerve regeneration, injuries are not always fully recovered by the help of native SC alone [31]. The type and severity of peripheral nerve injury is often too severe for the native regeneration process

to achieve full recovery. Axonal sprouts which do not reconnect to the proper targets result in incomplete recovery, and sprouts which fail to reach targets degenerate. Upon incomplete recovery, painful neuromas may develop, in which aberrant axonal sprouts tangle and create bundles of misguided sensory nerve fibers[32-34].

When PNS injury is greater than 2 to 5 mm in length in humans, surgical intervention is often necessary. There are, however, significant challenges associated with surgical repair of damaged peripheral nerve. Interventions to repair peripheral nerve injury involving tissue engineered approaches to promote nerve growth and guidance are currently under pursuit, as the native biological and current surgical techniques for repair are often not adequate to promote complete recovery. An overview of current treatments aimed at CNS and PNS regeneration is presented in the following section. Ultimately, damaged nerves must be promoted to navigate through and around a complex environment to ultimately connect with their proper targets for regeneration after injury to take place.

1.4. Methods of intervention following nervous system injury

1.4.1. Intervention after CNS injury

CNS injury comprises a vast range of modalities, including traumatic brain injury (TBI) and SCI. A significant amount of research has been done regarding tissue engineered approaches to repair SCI and as such, SCI will be the focus of this section. Currently standard clinical treatments for SCI include multiple stages. The first stage of SCI treatment is to curtail the amount of damage done from the injury and from the secondary effects, including ischemia and edema[35]. Such damage is typically minimized with pharmaceutical methods, including corticosteroids to reduce swelling surrounding the injury site. More recently neuroprotection by therapeutic hypothermia, or patient cooling, has shown to reduce the spread of the injury site when applied immediately

following trauma[36-37]. Once the injury is stabilized, surgical intervention may be necessary to remove injury site debris, inflammatory fluid, or tissue that may be causing compression on the injured spinal cord[38-40].The spine may also be immobilized with spinal traction to reduce chances of further injury, and finally, physical therapy and rehabilitation aim to help patients adjust to secondary results of SCI, such as paralysis[41-42]. Ultimately there are no therapeutic interventions that are capable of encouraging full recovery after SCI, so investigation of tissue engineered approaches to such therapies is an area of much research.

Regenerative approaches using cellular and molecular therapy are currently being investigated for their effectiveness and safety concerning SCI repair. Transplantation of healthy glial cells or neurons to the site of spinal cord injury aims to bridge the inhibitory environment local to the injury site[43]. Peripheral nerve, SC, olfactory nerves, embryonic CNS tissue, embryonic and adult stem cells, and activated macrophages are currently being transplanted in animal models of SCI injury and various stages of clinical trials to better understand their role in enabling regeneration following SCI injury. Additionally, neuroprotective molecular therapies, employing antibodies, steroids, growth factors, and extracellular matrix modifiers are molecular approaches to enhancing SCI regeneration, also in animal models and various stages of clinical trials. Overall, each of these interventions has resulted in marginal improvement when examined, but this improvement was only marginal, indicating that alternate or combinatorial methods of intervention must be developed to improve SCI regeneration.

1.4.2. Intervention after PNS injury

For full functional recovery after PNS injury, proper axon-to-target reconnections must be made, and the size and severity of the injury often results in improper or incomplete regeneration. For small injuries less than approximately 5 mm in length, spontaneous regeneration is possible and

has potential to occur over time without treatment. Primary suturing of distal and proximal nerve stumps can achieve regeneration for injuries without a large nerve gap, as nerves under tension will not survive. Primary anastomoses are suitable for injuries less than 5 mm in length, since nerves do not survive under tension. Although this is the preferred method of repair, such minor injuries are often not the case, and therefore more involved methods of repair are necessitated[44-46]. Nerve autografts are the current gold standard for PNS repair for injuries up to 4 cm in length [47-48]. Autografts involve the use of donor nerve, commonly the sural nerve, sutured between the distal and proximal injured nerve stumps to bridge the region of trauma [49-50]. Nerve autografts are best suited for relatively short sensory nerve repair, but even so, they have only a 50% success rate[45], and thereby present limitations regarding applicability. Additionally, nerve autografts involve donor site morbidity, are subject to lack of suitable nerve for harvest, and create secondary injury that is prone to infection, scarring, and neuroma formation, so there remains a need for improvement in strategies for PNS regeneration [51-52]. When nerve autografts are not an option for repair, nerve guidance conduits (NGC) may be used to contain axonal sprouts and serve as a macroscale channel to bridge nerve gaps and promote directed nerve growth[53].

Hollow NGC are a clinically available alternative to autologous nerve grafts for peripheral nerve injuries less than 4 cm in length. The idea behind NGC is to promote sprouting axons to properly reconnect with their targets following injury with a macroscale tubular biomaterial construct[54-55]. Guidance conduits represent a means by which microsurgical techniques may abut proximal and distal stumps of damaged axons with a biocompatible tubular structure so that proper process-target reconnections may be accomplished as axons travel through the conduit. Guidance conduits have been used to confine neurites and encourage their growth toward their distal targets [56-57]. NGC, however, have not performed as well as nerve autografts as of yet, and often result in poor functional recovery from peripheral nerve injury[58-59].

The lack of significant success in NGC for larger injury gaps is thought to be due to poor or no formation of a fibrin cable within the conduit[58]. When NGC are utilized as an intervention for short injury gaps, regeneration between the proximal and distal nerve stumps proceeds via the formation of a fibrin cable between the stumps, which facilitates cell migration into the conduit and progressive regeneration. It is suggested, therefore, that hollow nerve tubes are not adequate promoters of regeneration for larger nerve gaps, and that as NGC offer a highly tailorable platform for the incorporation of cues known to guide axon growth, several strategies toward implementing a combinatorial approach are under investigation. An overview of these strategies is discussed in the section to follow. It is of importance that such additional guidance features to be employed within NGC to guide neurite outgrowth toward distal targets are well understood, such that efficient and optimal design of NGC components can be achieved and lead to enhanced nerve regeneration. More detail on guidance cues that may be incorporated into nerve guidance conduits is presented in the sections to follow.

Much of the research in this thesis investigates *in vitro* strategies of nerve regeneration by exploiting SC-derived guidance cues. Tissue engineering strategies to promote nerve growth, guidance, and reconnection with targets is a highly pursued area of research, as it offers potential to direct regeneration by employing basic concepts of nerve guidance biology to biomaterials approaches for repair. Engineered patterns of chemical cues and fabricated topographical features that direct nerve growth are among the primary features being investigated for tissue engineered approaches to nerve regeneration, and as such will be the focus of the following sections.

1.5. Molecular control of neurite guidance

During embryogenesis and development of the nervous system, neurites extend and navigate through complex arrays of environmental cues to reach their appropriate target cells and ultimately mature into complex neuronal networks. Molecular cues are a significant environmental component to which neurite outgrowth responds, present in highly controlled spatiotemporal arrangements in the developing organism. Molecular guidance cues may be soluble or substrate-bound, and may effectively attract or repel neurite attachment and extension[60-61].

Neurotrophic factors are typically secreted by glial cells and by target cells and tissues, and promote nerve guidance during development and survival and maintenance of neuronal health[62]. A family of transmembrane receptors known as tropomycin receptor kinase (Trk) receptors specifically bind neurotrophins, leading to signal transduction and ultimately neuronal response[63]. The signal transduction depends on several factors, including timing, type, and location of neurotrophin binding to Trk receptors, but general Trk binding relays growth-promoting and survival signals to neurons.

During development, soluble neurotrophic factors, cell adhesion molecules (CAMs), and extracellular matrix (ECM) proteins are molecular directors of nerve growth, leading to development of the nervous system. Neurotrophic factors, including nerve growth factor (NGF), brain derived neurotrophic factor (BDNF), and neurotrophin-3 (NT-3) have been implicated in directing axonal growth and survival in distinct subpopulations of neurons during development of the CNS and PNS[60].

Nerves are also directed by CAMs, another class of molecular guidance molecules, during development[64-65]. CAMs are typically transmembrane receptors that are part of or linked to the

plasma membrane of cells. The extracellular portion of CAMs interact homotypically or heterotypically with other CAMs or the surrounding ECM and promote cell adhesion. Neuronal CAM, or NCAM, is expressed in several forms on the surfaces of neurons and glia, including SC[66-67]. NCAM promotes neurite elongation and guidance along other neurites as well as along adhesive pathways created by elongated SC and central glia during development and in the healthy nervous system[68].

Extracellular matrix (ECM) molecules are insoluble, typically multifunctional glycoproteins that have been shown to promote neuronal adhesion, differentiation, and guidance during development. Collagen IV, fibronectin, LN, and hyaluronic acid are ECM molecules that have all been implicated as having permissive roles in guiding neurites during development[69]. As early as 1975, Letourneau hypothesized that navigating neurites exposed to several types of surfaces will turn toward and follow the direction of the surface with higher adhesivity[70-71]. The balance of neuronal adhesion and neurite outgrowth must be considered when using molecular cues to guide neurite growth, as neurite elongation and extension typically occur more quickly on less adhesive substrates, such as LN, when compared with polylysine, which is highly adhesive. Thus, an optimal protein patterning should present optimal levels of adhesivity to promote and direct neurite outgrowth. LN is strongly implicated in nerve guidance during development[72-76]. LN is a basement-membrane associated ECM molecule associated with several tissue types, including those of the CNS and PNS[77-80]. It has been shown that navigating neurites associate with linear tracks of LN present in the basement membrane as they pathfind in the developing nervous system[81]. SC of the PNS produce LN, depositing it into the local basement membrane to maintain neuronal health and promote guidance[82-83].

Following nerve injury, injured or damaged nerves encounter complex sets of molecular cues in response to trauma and toward regeneration. Damage to neurons, glia, and surrounding cells results in a variety of permissive and inhibitory molecular signals which must be integrated and interpreted by damaged neurons in order for them to regenerate, but such post-injury environments often limit the extent of repair, especially in the CNS and severe injuries of the PNS.

Certain elements of the regenerative process that occurs to an extent after PNS injury provide motivation for adaptation of such injury response in tissue engineered strategies for nerve repair. Following the removal of cellular and matrix debris by Wallerian degeneration after severe PNS injury, columns of SC processes that formerly encompassed and maintained neuronal health serve as directive guides for axons sprouting from the distal stump at the injury site[84]. In ideal scenarios where regeneration is possible, these SC tubes, known as Bands of Büngner, promote guidance and reinnervation of axon sprouts with their target cells, continually producing LN on their surfaces to effectively present longitudinally aligned LN pathways along which axonal sprouts may be guided[82, 85-86]. The compelling substantiation of neurite guidance by molecular signals during development has prompted significant research in the area of directing nerve outgrowth and guidance by engineered patterns of molecular cues towards the development of strategies to guide nerves after injury.

Microfabricated protein patterns have been widely used to direct the adhesion and growth of several cell types[87-88]. Through these approaches, researchers strategically present patterns of proteins of interest to cells in vitro or in conjunction with biomaterials in vivo in order to direct cell attachment or growth by preferential or repulsive interactions between cells and the patterned proteins[89-92].

As discussed above, LN has been of particular interest in the study of nerve guidance, and as such will be the nerve guidance protein of focus within this research. LN is a strong promoter of neuronal adhesion and neurites preferentially grew toward the direction of higher LN concentration when presented with concentration gradients decreasing from 50 μg/ml to 10 μg/ml[93].

In a study by Song and Uhrich, embryonic chick DRG neurons were grown on poly(methyl methacrylate) (PMMA) with repeating parallel stripes of 100 μg/ml LN to determine the optimal micropattern dimensions for directing neurite outgrowth[88]. In this study, when LN stripe width was varied, optimal neurite alignment was observed on 40 μm wide LN stripes separated by 40 μm spaces. This study did not investigate neurite outgrowth response to different space widths or LN concentrations, leaving room for further investigation. In the research presented in Chapter 3, an investigation of neurite response to several stripe widths, space widths, and LN concentrations was quantified.

Microcontact printing is a technique by which predetermined engineered protein or biomolecule patterns are transferred to cell culture substrates to determine how such patterns may affect cell behavior. Several groups, including ours, have developed specific microcontact printing methods to transfer protein patterns with specific dimensions to glass or polymer substrates, and it has been found that nerve guidance response may be highly dependent on micropattern dimensions[94].

In order to understand how nerves grow in response to the molecular guidance cues of their environment, systematic *in vitro* studies must be done wherein neurite alignment and outgrowth response are quantified and compared among sets of strategically engineered micropatterns. In

the work presented in Chapter 3, neurite alignment response is assessed in the presence of distinct micropatterned LN stripes, cell-based topographical cues, and systematic combinations therein. An overview of topographical control of neurite outgrowth is addressed in the following section.

1.6. Topographical control of neurite guidance

During development of the nervous system, navigating neurites respond to the topographical features of their surroundings. For example, developing neurons of the cortex migrate along projections of radial glial cells to reach their appropriate location[95], and it has been found that several other types of neurons follow tracts produced by glial cells and ECM fibers during development[96-97]. This form of interaction with topographical features is known as contact guidance and has been reported in the developing nervous system and implicated in strategies for intervention following nerve injury.

After injury, nerves respond to the topographical features of the post-injury environment. In the PNS, SC align to form Bands of Büngner, which provide a favorable substrate for longitudinal guidance of axonal sprouts toward target cells[98]. Contrastingly, the CNS is not conducive to repair after injury, due to inhibitory molecular secretions of hypertrophic astrocytes and the formation of an obstructive cyst surrounded by scarring, which presents a physical barrier to regrowth beyond the injury site[99-100]. The potential for nerve repair in the PNS combined with inhibition of repair in the CNS has prompted researchers to investigate neurite response to engineered presentation of in vitro and in vivo topographical guidance cues.

Guidance of neurite outgrowth has been documented in response to several types of in vitro topographical features. These experimental setups have used pillar microarrays[101], repeating grooves and plateaus[102-105], oriented micro- and nanofibers[106-107], surface roughness[108-109], cellular

based topographical features[110], and nerve guidance conduits to promote nerve guidance and outgrowth and observe and quantify nerve behavior in response to such cues. These studies have found that guidance depends on feature dimensions, level of orientation, and spacing, and that different cell types may have different responses to the same features. These observations indicate that the design of therapeutic biomaterials should incorporate topographical features to promote nerve guidance, but that these features should be thoroughly investigated such that optimal feature design is implemented to produce maximal neurite response.

1.6.1. Isolated SC topography promotes nerve guidance

Isolated SC topography influences neurite outgrowth and orientation. Our lab has developed a replica molding technique to reproduce and isolate SC topographical features in random and aligned orientations. Aligned micro- and nanoscale SC topographical features enhanced DRG neurite outgrowth and directedness over random SC topography [111]. The biomimetic technique of isolating cellular topography presents the ability for researchers to use biocompatible materials with cellular mimicry to avoid immunogenic responses that may come with using live cellular components in an implantable construct, incorporating the tissue engineering scaffold with a topographical cue to achieve desired cellular behavior.

1.7. SC promote nerve regeneration

Because they are capable of encouraging regeneration following injury, live SC have been employed as a strategy to improve neurite outgrowth and directedness [112-114]. In a study by Miller et al., SC were aligned to underlying biodegradable polymeric microgrooves [114]. Aligned SC promoted neurite elongation and alignment along the direction of the underlying SC and neurite alignment persisted after the underlying polymer was degraded [114]. Longitudinally aligned SC monolayers resulted in alignment of rat spinal neurites along the SC orientation in a study by

Thompson and Buettner [112]. The correlation of neurite outgrowth along the SC monolayer suggested that both SC topography and molecular cues are responsible for encouraging neurite outgrowth and alignment.

1.8. Molecular and topographical cues within nerve guidance conduits

Several molecular and topographical cues have been incorporated to tailorable guidance conduits to encourage regeneration. A variety of growth-permissive cues have been employed within conduits to encourage growth specifically along the longitudinal axis of the conduit [56, 115]. Additionally, nerve guidance conduits presenting topographical cues including multiple lumens, electrospun microfibers, and microgrooves have been fabricated and investigated for their potential to promote nerve regeneration [104, 116-117]. Currently, nerve guidance conduits lead the efforts in enhancing nerve regeneration, and incorporation of appropriate permissive molecular and topographical cues or combinations thereof is the focus of such research [118-122].

1.8.1. SC within NGC

SC are an appealing strategy of encouraging neurite outgrowth and directionality, and have therefore been investigated as guidance features within nerve guidance conduits to promote neurite regeneration to targets along the longitudinal axis of the conduit [123-126]. In an in vivo study by Guenard et al., SC at high, moderate, and low densities were suspended in Matrigel and seeded into semipermeable acrylonitrile vinylchloride conduits and inserted to 8 mm rat sciatic nerve gaps [127]. There was a graded regeneration response which increased proportionately to the initial SC seeding density, which suggests that SC promote peripheral nerve regeneration through the conduits. In all cases, however, regeneration did not match or exceed that of nerve autografts. These results indicate that SC provide potential to encourage nerve regeneration through conduits, but that SC properties must be properly exploited and executed in order to achieve

regeneration superior to nerve autografts. As an alternative to employing suspended SC to encourage nerve regeneration, Hadlock et al., used conduits containing multiple longitudinally aligned channels within one larger conduit seeded with SC [128]. SC adhered to the luminal surfaces of the inner channels and promoted nerve regeneration similar to nerve autografts, suggesting that the approach of lining SC on the luminal conduit surface may encourage regeneration.

To encourage longitudinal SC orientation along the conduit long axis, Rutkowski et al. explored nerve regeneration through conduits lined with longitudinally oriented pre-seeded SC [129]. A microgrooved conduit lumen was used to align SC longitudinally along the length of poly(D,L-lactic acid) conduits. In a sciatic nerve regeneration experiment, conduits seeded with longitudinally aligned SC promoted regeneration over control conduits without microgrooves or SC, or both. Although the effect of aligned-SC conduits was not compared to autologous grafts, these results suggest that aligned SC along the lumen of polymeric conduits encourages nerve regeneration through the conduits.

Although neurite outgrowth has been studied in the presence of live SC, the individual effects that SC topography and chemical cues have on neurite outgrowth have not been fully elucidated. Our approach is to isolate the topographical component of SC in order to observe guidance of DRG neurites along SC topographical cues alone. Our lab has developed a polymer replica molding technique to isolate SC topography alone [130]. Through this technique, questions regarding the relative effects of supportive SC components may be addressed. This approach eliminates the concern of immunologic response, described in several studies using non-autologous live SC [124-125, 127]. Additionally, our approach will enable us to reveal how isolated SC components serve to guide neurite outgrowth. The focus of the work presented in Chapter 1 will be based on neurite interaction with isolated SC topographical features, and a subset of the experiments described in

the research in Chapter 1 highlights nerve alignment response to isolated SC topography featured on the luminal surface of polymeric conduits.

1.9. Neurite guidance by multiple simultaneous extracellular cues

Throughout development of the nervous system and during repair after nerve injury, navigating neurites must interact with and assimilate the directive information of their surroundings in order to successfully reach their proper target cells and tissues. In vitro approaches to investigate neuronal response to guidance cues individually is a powerful means to determine how such cues elicit neuronal response, such that they may be utilized in therapeutic approaches toward nerve repair and to understand and quantify these interactions to understand the basic biology of nerve guidance. Although approaches using single extracellular cues to investigate neurite outgrowth are valuable, studies of neurite guidance response to combinations of multiple cues should complement single cue research in order to determine neuronal response to the complex sets of cues encountered in vivo. With an improved understanding of how nerves are guided by sets of extracellular cues, we can better understand how to augment nerve guidance in response to cooperative cues, and we can improve our understanding of how nerves make growth decisions when faced with competitive sets of cues.

Although there is a limited volume of work that has investigated neuronal response to simultaneous presentation of cooperative extracellular cues, this body of work is growing and shows some promise in determining where combinations of cues have additive or synergistic effects on neurite outgrowth and guidance[131-133]. Combinations of cooperative guidance cues allow researchers to determine whether such combinations have additive or synergistic effects on nerve guidance[103, 134]. For example, neurite outgrowth response was enhanced with the parallel combination of adhesive tracks of vitronectin and topographical gratings when compared to

topographical gratings only for shallow groove depths[135]. Ultimately, optimal parallel combinations of extracellular cues may enhance neurite alignment strength to develop therapeutic means for nerve repair which succeed the current autograft and hollow lumen NGC techniques available.

Identification of neurite growth and behavior in response to simultaneous presentation of orthogonal guidance cues has not been well established in the field of neuronal tissue engineering. Such experimental setups typically oppose two directive cues in perpendicular arrangements, such that navigating neurites are simultaneously presented with two favorable cues, but at competing orientations[136-137]. Charest et al., observed decreased osteoblast alignment to fibronectin lanes when they were orthogonally opposed to topographical grooves and mesas when compared to fibronectin lanes or topographical cues presented individually[136]. Of the features examined, cell alignment response appeared to be dominated by topographical cues versus protein micropatterns. Contrastingly, a study by Britland et al. demonstrated preferential neurite alignment to adsorbed vitronectin tracts when presented orthogonally to shallow (< 1μm) but not deep (> 1μm) grooves. In these experimental setups, neurite alignment response may be quantified, such that researchers may determine which cue elicited higher alignment response, or preference, for neurite outgrowth. With such experimental setups it is possible to determine whether cue hierarchy exists among sets of environmental cues. Additionally, in the case where neurite response to simultaneous presentation of two competing cues is not preferential toward one cue over the other, then the assessment of how nerves make decisions in complex environments may be explored. This is particularly relevant to neurite navigation after injury in vivo, where neurites encounter complex combinations of cues at different orientations, strengths, and directions[138-139]. It is in these complex multi-cue environments where nerve growth decisions

are interesting, and improvement upon the understanding of how nerves make complex growth and directional decisions is necessary in order to target and direct nerve growth therapeutically.

Chapter 3 consists of a set of experiments which assess neurite alignment response to micropatterned LN stripes and SC replica topography presented individually and as cooperative and competitive simultaneous cues.

1.10. Dynamic and sequential observations of neurite interaction with molecular and topographical features

Sequential endpoint and dynamic imaging studies are employed to determine cell behavior in response to environmental cues over time[140-142]. Advantages of sequential endpoint studies, wherein cell cultures are fixed and immunolabeled at incremental timepoints, include the ability to sample and quantify cell behavior and response to culture platforms. To support the quantification of sequential endpoint studies, timelapse microscopy, in which images of live cells are captured at frequent intervals and merged to generate a video file, allows researchers to visualize real-time cell response and movements that are not observable by standard endpoint studies. The strength of a combinatorial approach that joins sequential endpoint and dynamic imaging studies is that each type of study informs the other to develop clear explanations and quantification of how cells respond to their environmental cues over time. This information is critical to the optimal design of biomaterials for nerve guidance and may be used to explain cell behavior in complex environments. Chapter 4 utilized sequential endpoint and timelapse microscopy to test hypotheses regarding how nerves make growth decisions in response to molecular and topographical cues presented individually and in combinations, as initially described in Chapter 3.

1.11. Mechanistic response to molecular and topographical features

The growth cone is the structure located at neurite tips that is predominantly responsible for sensing environmental cues during neurite navigation. Growth cones consist of finger-like lamellar and filopodial projections that undergo rapid extension, retraction, and morphological change in response to permissive and inhibitory environmental cues[15, 61, 89, 139, 143-144]. The extracellular information sensed by the growth cone results in subsequential further growth toward or away from permissive or inhibitory cues, or persistence of neurite growth along a path. This was demonstrated in a study where dissociated DRG were cultured on gradients of permissive LN, neurite growth cones turned in response to increasing LN concentration[93].

Mechanotransduction is the process by which mechanical stimulus is sensed and subsequently relayed to the cell nucleus, ultimately informing intracellular changes which result in cytoskeletal rearrangement and morphological responses by the cell. Contact guidance is a form of mechanotransduction, wherein navigating neurons respond to topographical features by aligning to and growing along oriented features, ultimately aligning along the direction of the topographical cue[145-152].

The plasma membrane of the growth cone exhibits a rich collection of proteins, including integrins, cell adhesion molecules, and ion channels all of which relay environmental information to the neuron[60, 68, 75, 153]. A potassium ion channel present on neuronal membranes known as TREK-1 is a polymodal channel, activated by a range of environmental stimuli, including pH of the surrounding fluid, voltage, and membrane stretch, or mechanical stimulation[145, 154-157]. TREK-1 is a two-pore transmembrane potassium channel with two subunits each composed of four transmembrane segments, with both the C- and –N termini residing in the intracellular space. It is suggested that the TREK-1 channel C-terminus is involved in TREK-1 channel activation[155, 158].

The features of TREK-1 channels make them an attractive target to investigate for their role in mechanosensing of SC topographical features and subsequent neurite guidance by these features.

The role of TREK-1 channels in mechanotransduction of extracellular topographical features by neurons has yet to be determined. Our lab has developed a replica molding technique to isolate Schwann cell (SC) topographical features as inverted and protruding replicas. Electrophysiological studies, through which patch-clamping of neuronal membranes in inside-out and outside-in configurations have revealed that TREK-1 channels may exhibit higher sensitivity to convex membrane deformation[159]. This data has led to the hypothesis that concave and convex extracellular topographical features may produce different degrees of TREK-1 activation, such that inhibition of TREK-1 channel activity in the presence of either convex or concave topographical features will lead to differential reduction in neurite alignment to those features.

Fluoxetine hydrochloride (FLX) is a pharmacological inhibitor of TREK-1 channels. Although the mechanism of action is not well understood, TREK-1 channels were selectively inactivated in the presence of FLX in both inside-out and membrane-out configurations[156, 158]. When FLX was applied in a bath solution during electrophysiological experiments, 84% TREK-1 channel inactivation occurred[156]. In the work described in Chapter 5, we have optimized FLX dosing for dissociated DRG cultures, and used FLX to better elucidate the mechanistic role behind neurite guidance by SC-based topographical features.

1.12. Dorsal root ganglia as a model for neurite outgrowth

For a predominant portion of the studies presented in this thesis, postnatal (P1-P5) rat dorsal root ganglion (DRG) were used as a source of primary neurons. Different neuronal subpopulations are differentially preferred as models of specific neuronal events. DRG are commonly used as a

model to assess neurite outgrowth and directionality[160-161], and as such, apply well to the sets of experiments presented in this research. DRG are a heterotypic cell source, composed of neurons, SC, and a small percentage of fibroblasts, thereby providing a complex cell culture model which correlates more closely with events that occur in the body, as cell-cell interactions are permitted to occur. DRG are clusters of sensory neurons located along the spinal nerves. DRG contain neuronal bodies that transmit sensory information acquired by their sensory dendrites to the central nervous system as they terminate in the dorsal horn of the spinal cord[162].

1.13. Poly(dimethyl siloxane) for in vitro studies of neurite outgrowth

Poly(dimethyl siloxane) (PDMS) is a biocompatible, transparent polymer commonly used for in vitro cell culture experimentation[163-164]. For the applications described in this thesis, PDMS has been used, as it is flexible, mimicking mechanical properties of bodily tissues, and can be manipulated to form thin films which can subsequently be used in the fabrication of NGC.

1.14 Lithography for microcontact printing and replica molding

Photolithography was used to crosslink repeating parallel lanes of photoresist to silicon wafers. Soft lithography of PDMS on the wafers was used to microcontact print repeating parallel stripes of LN onto substrates used for cell culture. Detailed methods are described where applicable throughout the text.

1.15. Literature cited

1. Paralysis, T.M.P.t.C. *The Miami Project to Cure Paralysis*. 2012 [cited 2012 January 15, 2012]; Available from: http://www.themiamiproject.org/.

2. Medicine, U.S.N.L.o. *Spinal Cord Trauma. Spinal cord injury; Compression of spinal cord; SCI; Cord compression*. 2012 June 16, 2010 [cited 2012 January 15]; Available from: http://www.ncbi.nlm.nih.gov/pubmedhealth/PMH0002061/.

3. Institute, M.B. *CNS Injury*. Cores to Translate Therapies August 18, 2009 [cited 2012 January 15]; Available from: http://www.mbi.ufl.edu/research/cores-to-translate-therapies/cns-injury/.

4. Wood, M.D., et al., *Outcome measures of peripheral nerve regeneration.* Ann Anat, 2011. **193**(4): p. 321-33.

5. *Peripheral Neuropathy Types*. Neuropathy [cited 2012 January 15]; Available from: http://www.healthcommunities.com/neuropathy/types.shtml.

6. Clarke, D. and P. Richardson, *Peripheral nerve injury.* Curr Opin Neurol, 1994. **7**(5): p. 415-21.

7. Hulsebosch, C.E., *Recent advances in pathophysiology and treatment of spinal cord injury.* Adv Physiol Educ, 2002. **26**(1-4): p. 238-55.

8. Smith, M.E. and L.F. Eng, *Glial fibrillary acidic protein in chronic relapsing experimental allergic encephalomyelitis in SJL/J mice.* J Neurosci Res, 1987. **18**(1): p. 203-8.

9. Mukhopadhyay, G., et al., *A novel role for myelin-associated glycoprotein as an inhibitor of axonal regeneration.* Neuron, 1994. **13**(3): p. 757-67.

10. Grados-Munro, E.M. and A.E. Fournier, *Myelin-associated inhibitors of axon regeneration.* Journal of Neuroscience Research, 2003. **74**(4): p. 479-485.

11. McKerracher, L., et al., *Identification of myelin-associated glycoprotein as a major myelin-derived inhibitor of neurite growth.* Neuron, 1994. **13**(4): p. 805-11.

12. Schmidt, C.E. and J.B. Leach, *Neural tissue engineering: Strategies for repair and regeneration.* Annual Review of Biomedical Engineering, 2003. **5**: p. 293-347.

13. Rolls, A., R. Shechter, and M. Schwartz, *NEURON - GLIA INTERACTIONS - OPINION The bright side of the glial scar in CNS repair.* Nature Reviews Neuroscience, 2009. **10**(3): p. 235-U91.

14. Mckeon, R.J., et al., *Reduction of Neurite Outgrowth in a Model of Glial Scarring Following Cns Injury Is Correlated with the Expression of Inhibitory Molecules on Reactive Astrocytes.* Journal of Neuroscience, 1991. **11**(11): p. 3398-3411.

15. Huber, A.B., et al., *Signaling at the growth cone: ligand-receptor complexes and the control of axon growth and guidance.* Annu Rev Neurosci, 2003. **26**: p. 509-63.

16. David, S. and A.J. Aguayo, *Axonal elongation into peripheral nervous system "bridges" after central nervous system injury in adult rats.* Science, 1981. **214**(4523): p. 931-3.

17. Richardson, P.M., U.M. McGuinness, and A.J. Aguayo, *Axons from CNS neurons regenerate into PNS grafts.* Nature, 1980. **284**(5753): p. 264-5.

18. Crutcher, K.A., *Tissue sections from the mature rat brain and spinal cord as substrates for neurite outgrowth in vitro: extensive growth on gray matter but little growth on white matter.* Exp Neurol, 1989. **104**(1): p. 39-54.

19. Crutcher, K.A. and M. Privitera, *Axonal regeneration on mature human brain tissue sections in culture.* Ann Neurol, 1989. **26**(4): p. 580-3.

20. Edgar, J.M. and J. Garbern, *The myelinated axon is dependent on the myelinating cell for support and maintenance: Molecules involved.* Journal of Neuroscience Research, 2004. **76**(5): p. 593-598.

21. Nave, K.A. and B.D. Trapp, *Axon-glial signaling and the glial support of axon function.* Annual Review of Neuroscience, 2008. **31**: p. 535-561.

22. Bunge, R.P., *The Role of the Schwann-Cell in Trophic Support and Regeneration.* Journal of Neurology, 1994. **242**(1): p. S19-S21.

23. Buss, A., et al., *Growth-modulating molecules are associated with invading Schwann cells and not astrocytes in human traumatic spinal cord injury.* Brain, 2007. **130**: p. 940-953.

24. Brook, G.A., et al., *Spontaneous longitudinally orientated axonal regeneration is associated with the Schwann cell framework within the lesion site following spinal cord compression injury of the rat.* Journal of Neuroscience Research, 1998. **53**(1): p. 51-65.

25. Bixby, J.L., J. Lilien, and L.F. Reichardt, *Identification of the major proteins that promote neuronal process outgrowth on Schwann cells in vitro.* J Cell Biol, 1988. **107**(1): p. 353-61.

26. Frostick, S.P., Q. Yin, and G.J. Kemp, *Schwann cells, neurotrophic factors, and peripheral nerve regeneration.* Microsurgery, 1998. **18**(7): p. 397-405.

27. Fawcett, J.W. and R.J. Keynes, *Peripheral-Nerve Regeneration.* Annual Review of Neuroscience, 1990. **13**: p. 43-60.

28. Mehta, A., M.L. Reynolds, and C.J. Woolf, *Partial Denervation of the Medial Gastrocnemius-Muscle Results in Growth-Associated Protein-43 Immunoreactivity in Sprouting Axons and Schwann-Cells.* Neuroscience, 1993. **57**(2): p. 433-442.

29. Bunge, R.P., *Tissue-Culture Observations Relevant to the Study of Axon Schwann-Cell Interactions during Peripheral-Nerve Development and Repair.* Journal of Experimental Biology, 1987. **132**: p. 21-34.

30. Fu, S.Y. and T. Gordon, *The cellular and molecular basis of peripheral nerve regeneration.* Mol Neurobiol, 1997. **14**(1-2): p. 67-116.

31. Brushart, T.M. and M.M. Mesulam, *Alteration in Connections between Muscle and Anterior Horn Moto-Neurons after Peripheral-Nerve Repair.* Science, 1980. **208**(4444): p. 603-605.

32. Devor, M. and P.D. Wall, *Type of sensory nerve fibre sprouting to form a neuroma.* Nature, 1976. **262**(5570): p. 705-8.

33. Dagum, A.B., *Peripheral nerve regeneration, repair, and grafting.* J Hand Ther, 1998. **11**(2): p. 111-7.

34. Carlton, S.M., et al., *Neuroma formation and numbers of axons in a rat model of experimental peripheral neuropathy.* Neurosci Lett, 1991. **131**(1): p. 88-92.

35. Hurlbert, R.J., *Strategies of medical intervention in the management of acute spinal cord injury.* Spine (Phila Pa 1976), 2006. **31**(11 Suppl): p. S16-21; discussion S36.

36. Dietrich, W.D., 3rd, *Therapeutic hypothermia for spinal cord injury.* Crit Care Med, 2009. **37**(7 Suppl): p. S238-42.

37. Bernard, S., *New indications for the use of therapeutic hypothermia.* Crit Care, 2004. **8**(6): p. E1.

38. Vaccaro, A.R., et al., *Neurologic outcome of early versus late surgery for cervical spinal cord injury.* Spine (Phila Pa 1976), 1997. **22**(22): p. 2609-13.

39. Mirza, S.K., et al., *Early versus delayed surgery for acute cervical spinal cord injury.* Clin Orthop Relat Res, 1999(359): p. 104-14.

40. Fehlings, M.G. and R.G. Perrin, *The timing of surgical intervention in the treatment of spinal cord injury: a systematic review of recent clinical evidence.* Spine (Phila Pa 1976), 2006. **31**(11 Suppl): p. S28-35; discussion S36.

41. Vissers, M., et al., *Barriers to and facilitators of everyday physical activity in persons with a spinal cord injury after discharge from the rehabilitation centre.* J Rehabil Med, 2008. **40**(6): p. 461-7.

42. Jones, C.F., B.K. Kwon, and P.A. Cripton, *Mechanical indicators of injury severity are decreased with increased thecal sac dimension in a bench-top model of contusion type spinal cord injury.* J Biomech, 2012.

43. Thuret, S., L.D. Moon, and F.H. Gage, *Therapeutic interventions after spinal cord injury.* Nat Rev Neurosci, 2006. **7**(8): p. 628-43.

44. Flores, A.J., C.J. Lavernia, and P.W. Owens, *Anatomy and physiology of peripheral nerve injury and repair.* Am J Orthop (Belle Mead NJ), 2000. **29**(3): p. 167-73.

45. Lee, S.K. and S.W. Wolfe, *Peripheral nerve injury and repair.* J Am Acad Orthop Surg, 2000. **8**(4): p. 243-52.

46. Ogun, T.C., et al., *End-to-side neurorrhaphy as a salvage procedure for irreparable nerve injuries. Technical note.* J Neurosurg, 2003. **99**(1): p. 180-5.

47. Millesi, H., G. Meissl, and A. Berger, *The interfascicular nerve-grafting of the median and ulnar nerves.* J Bone Joint Surg Am, 1972. **54**(4): p. 727-50.

48. Millesi, H., G. Meissl, and A. Berger, *Further experience with interfascicular grafting of the median, ulnar, and radial nerves.* J Bone Joint Surg Am, 1976. **58**(2): p. 209-18.

49. Maeda, T., et al., *Effects of tension at the site of coaptation on recovery of sciatic nerve function after neurorrhaphy: evaluation by walking-track measurement, electrophysiology, histomorphometry, and electron probe X-ray microanalysis.* Microsurgery, 1999. **19**(4): p. 200-7.

50. Miyamoto, Y., *Experimental study of results of nerve suture under tension vs. nerve grafting.* Plast Reconstr Surg, 1979. **64**(4): p. 540-9.

51. Nichols, C.M., et al., *Effects of motor versus sensory nerve grafts on peripheral nerve regeneration.* Exp Neurol, 2004. **190**(2): p. 347-55.

52. Mackinnon, S.E. and A.L. Dellon, *Clinical nerve reconstruction with a bioabsorbable polyglycolic acid tube.* Plast Reconstr Surg, 1990. **85**(3): p. 419-24.

53. Hudson, T.W., G.R. Evans, and C.E. Schmidt, *Engineering strategies for peripheral nerve repair.* Orthop Clin North Am, 2000. **31**(3): p. 485-98.

54. Kehoe, S., X.F. Zhang, and D. Boyd, *FDA approved guidance conduits and wraps for peripheral nerve injury: A review of materials and efficacy.* Injury, 2011.

55. Nectow, A.R., K.G. Marra, and D.L. Kaplan, *Biomaterials for the development of peripheral nerve guidance conduits.* Tissue Eng Part B Rev, 2012. **18**(1): p. 40-50.

56. Pfister, L.A., et al., *Nerve conduits and growth factor delivery in peripheral nerve repair.* Journal of the Peripheral Nervous System, 2007. **12**(2): p. 65-82.

57. Evans, G.R.D., et al., *In vivo evaluation of poly(L-lactic acid) porous conduits for peripheral nerve regeneration.* Biomaterials, 1999. **20**(12): p. 1109-1115.

58. Daly, W., et al., *A biomaterials approach to peripheral nerve regeneration: bridging the peripheral nerve gap and enhancing functional recovery.* J R Soc Interface, 2012. **9**(67): p. 202-21.

59. Bell, J.H. and J.W. Haycock, *Next Generation Nerve Guides: Materials, Fabrication, Growth Factors, and Cell Delivery.* Tissue Eng Part B Rev, 2011.

60. Tessier-Lavigne, M. and C.S. Goodman, *The molecular biology of axon guidance.* Science, 1996. **274**(5290): p. 1123-33.

61. Dickson, B.J., *Molecular mechanisms of axon guidance.* Science, 2002. **298**(5600): p. 1959-64.

62. Deister, C. and C.E. Schmidt, *Optimizing neurotrophic factor combinations for neurite outgrowth.* J Neural Eng, 2006. **3**(2): p. 172-9.

63. Segal, R.A., *Selectivity in neurotrophin signaling: theme and variations.* Annu Rev Neurosci, 2003. **26**: p. 299-330.

64. Rutishauser, U., *Adhesion molecules of the nervous system.* Curr Opin Neurobiol, 1993. **3**(5): p. 709-15.

65. Cunningham, B.A., et al., *Neural cell adhesion molecule: structure, immunoglobulin-like domains, cell surface modulation, and alternative RNA splicing.* Science, 1987. **236**(4803): p. 799-806.

66. Triolo, D., et al., *Loss of glial fibrillary acidic protein (GFAP) impairs Schwann cell proliferation and delays nerve regeneration after damage.* J Cell Sci, 2006. **119**(Pt 19): p. 3981-93.

67. Martini, R., Y. Xin, and M. Schachner, *Restricted localization of L1 and N-CAM at sites of contact between Schwann cells and neurites in culture.* Glia, 1994. **10**(1): p. 70-4.

68. Rutishauser, U., *Influences of the neural cell adhesion molecule on axon growth and guidance.* J Neurosci Res, 1985. **13**(1-2): p. 123-31.

69. Deister, C., S. Aljabari, and C.E. Schmidt, *Effects of collagen 1, fibronectin, laminin and hyaluronic acid concentration in multi-component gels on neurite extension.* J Biomater Sci Polym Ed, 2007. **18**(8): p. 983-97.

70. Letourneau, P.C., *Possible roles for cell-to-substratum adhesion in neuronal morphogenesis.* Dev Biol, 1975. **44**(1): p. 77-91.

71. Letourneau, P.C., *Cell-to-substratum adhesion and guidance of axonal elongation.* Dev Biol, 1975. **44**(1): p. 92-101.

72. Lentz, S.I., et al., *Distribution of the ten known laminin chains in the pathways and targets of developing sensory axons.* J Comp Neurol, 1997. **378**(4): p. 547-61.

73. Miner, J.H., *Laminins and their roles in mammals.* Microsc Res Tech, 2008. **71**(5): p. 349-56.

74. Bixby, J.L. and W.A. Harris, *Molecular mechanisms of axon growth and guidance.* Annu Rev Cell Biol, 1991. **7**: p. 117-59.

75. Keynes, R. and G.M. Cook, *Axon guidance molecules.* Cell, 1995. **83**(2): p. 161-9.

76. Hunter, D.D., et al., *Expression of s-laminin and laminin in the developing rat central nervous system.* J Comp Neurol, 1992. **323**(2): p. 238-51.

77. Grumet, M., D.R. Friedlander, and G.M. Edelman, *Evidence for the binding of Ng-CAM to laminin.* Cell Adhes Commun, 1993. **1**(2): p. 177-90.

78. Garcia-Alonso, L., R.D. Fetter, and C.S. Goodman, *Genetic analysis of Laminin A in Drosophila: extracellular matrix containing laminin A is required for ocellar axon pathfinding.* Development, 1996. **122**(9): p. 2611-21.

79. Riggott, M.J. and S.A. Moody, *Distribution of laminin and fibronectin along peripheral trigeminal axon pathways in the developing chick.* J Comp Neurol, 1987. **258**(4): p. 580-96.

80. Dertinger, S.K., et al., *Gradients of substrate-bound laminin orient axonal specification of neurons.* Proc Natl Acad Sci U S A, 2002. **99**(20): p. 12542-7.

81. Krayanek, S. and S. Goldberg, *Oriented extracellular channels and axonal guidance in the embryonic chick retina.* Dev Biol, 1981. **84**(1): p. 41-50.

82. Cornbrooks, C.J., et al., *In vivo and in vitro observations on laminin production by Schwann cells.* Proc Natl Acad Sci U S A, 1983. **80**(12): p. 3850-4.

83. Palm, S.L. and L.T. Furcht, *Production of laminin and fibronectin by Schwannoma cells: cell-protein interactions in vitro and protein localization in peripheral nerve in vivo.* J Cell Biol, 1983. **96**(5): p. 1218-26.

84. Burnett, M.G. and E.L. Zager, *Pathophysiology of peripheral nerve injury: a brief review.* Neurosurg Focus, 2004. **16**(5): p. E1.

85. Tomaselli, K.J. and L.F. Reichardt, *Peripheral motoneuron interactions with laminin and Schwann cell-derived neurite-promoting molecules: developmental regulation of laminin receptor function.* J Neurosci Res, 1988. **21**(2-4): p. 275-85.

86. Martini, R., *Expression and functional roles of neural cell surface molecules and extracellular matrix components during development and regeneration of peripheral nerves.* J Neurocytol, 1994. **23**(1): p. 1-28.

87. Kofron, C.M. and D. Hoffman-Kim, *Optimization by Response Surface Methodology of Confluent and Aligned Cellular Monolayers for Nerve Guidance.* Cell Mol Bioeng, 2009. **2**(4): p. 554-572.

88. Song, M. and K.E. Uhrich, *Optimal micropattern dimensions enhance neurite outgrowth rates, lengths, and orientations.* Ann Biomed Eng, 2007. **35**(10): p. 1812-20.

89. Clark, P., S. Britland, and P. Connolly, *Growth cone guidance and neuron morphology on micropatterned laminin surfaces.* J Cell Sci, 1993. **105 (Pt 1)**: p. 203-12.

90. von Philipsborn, A.C., et al., *Microcontact printing of axon guidance molecules for generation of graded patterns.* Nat Protoc, 2006. **1**(3): p. 1322-8.

91. Oliva, A.A., Jr., et al., *Patterning axonal guidance molecules using a novel strategy for microcontact printing.* Neurochem Res, 2003. **28**(11): p. 1639-48.

92. Shi, P., K. Shen, and L.C. Kam, *Local presentation of L1 and N-cadherin in multicomponent, microscale patterns differentially direct neuron function in vitro.* Dev Neurobiol, 2007. **67**(13): p. 1765-76.

93. Li, G.N., J. Liu, and D. Hoffman-Kim, *Multi-molecular gradients of permissive and inhibitory cues direct neurite outgrowth.* Ann Biomed Eng, 2008. **36**(6): p. 889-904.

94. Wheeler, B.C., et al., *Microcontact printing for precise control of nerve cell growth in culture.* J Biomech Eng, 1999. **121**(1): p. 73-8.

95. Nadarajah, B., et al., *Two modes of radial migration in early development of the cerebral cortex.* Nat Neurosci, 2001. **4**(2): p. 143-50.

96. Hoffman-Kim, D., J.A. Mitchel, and R.V. Bellamkonda, *Topography, cell response, and nerve regeneration.* Annu Rev Biomed Eng, 2010. **12**: p. 203-31.

97. Webb, A., et al., *Guidance of oligodendrocytes and their progenitors by substratum topography*. J Cell Sci, 1995. **108 (Pt 8)**: p. 2747-60.

98. Weidner, N., et al., *Nerve growth factor-hypersecreting Schwann cell grafts augment and guide spinal cord axonal growth and remyelinate central nervous system axons in a phenotypically appropriate manner that correlates with expression of L1*. J Comp Neurol, 1999. **413**(4): p. 495-506.

99. Fawcett, J.W. and R.A. Asher, *The glial scar and central nervous system repair.* Brain Res Bull, 1999. **49**(6): p. 377-91.

100. Silver, J. and J.H. Miller, *Regeneration beyond the glial scar.* Nat Rev Neurosci, 2004. **5**(2): p. 146-56.

101. Dowell-Mesfin, N.M., et al., *Topographically modified surfaces affect orientation and growth of hippocampal neurons.* J Neural Eng, 2004. **1**(2): p. 78-90.

102. Li, G.N. and D. Hoffman-Kim, *Tissue-engineered platforms of axon guidance.* Tissue Eng Part B Rev, 2008. **14**(1): p. 33-51.

103. Miller, C., S. Jeftinija, and S. Mallapragada, *Synergistic effects of physical and chemical guidance cues on neurite alignment and outgrowth on biodegradable polymer substrates.* Tissue Eng, 2002. **8**(3): p. 367-78.

104. Hsu, S.H. and H.C. Ni, *Fabrication of the Microgrooved/Microporous Polylactide Substrates as Peripheral Nerve Conduits and In Vivo Evaluation.* Tissue Engineering Part A, 2009. **15**(6): p. 1381-1390

105. Li, N. and A. Folch, *Integration of topographical and biochemical cues by axons during growth on microfabricated 3-D substrates.* Exp Cell Res, 2005. **311**(2): p. 307-16.

106. Corey, J.M., et al., *Aligned electrospun nanofibers specify the direction of dorsal root ganglia neurite growth.* J Biomed Mater Res A, 2007. **83**(3): p. 636-45.

107. Xie, J., et al., *Neurite outgrowth on nanofiber scaffolds with different orders, structures, and surface properties.* ACS Nano, 2009. **3**(5): p. 1151-9.

108. Johansson, F., et al., *Axonal outgrowth on nano-imprinted patterns.* Biomaterials, 2006. **27**(8): p. 1251-8.

109. Simon, K.A., et al., *Enhancing cell adhesion and confinement by gradient nanotopography.* J Am Chem Soc, 2007. **129**(16): p. 4892-3.

110. Bruder, J.M., A.P. Lee, and D. Hoffman-Kim, *Biomimetic materials replicating Schwann cell topography enhance neuronal adhesion and neurite alignment in vitro.* J Biomater Sci Polym Ed, 2007. **18**(8): p. 967-82.

111. Bruder, J.M., A.P. Lee, and D. Hoffman-Kim, *Biomimetic materials replicating Schwann cell topography enhance neuronal adhesion and neurite alignment in vitro.* Journal of Biomaterials Science-Polymer Edition, 2007. **18**(8): p. 967-982.

112. Thompson, D.M. and H.M. Buettner, *Neurite outgrowth is directed by Schwann cell alignment in the absence of other guidance cues.* Annals of Biomedical Engineering, 2006. **34**(4): p. 669-676.

113. Thompson, D.M. and H.M. Buettner, *Oriented Schwann cell monolayers for directed neurite outgrowth.* Annals of Biomedical Engineering, 2004. **32**(8): p. 1120-1130.

114. Miller, C., S. Jeftinija, and S. Mallapragada, *Micropatterned Schwann cell-seeded biodegradable polymer substrates significantly enhance neurite alignment and outgrowth.* Tissue Engineering, 2001. **7**(6): p. 705-715.

115. Yang, Y., et al., *Neurotrophin releasing single and multiple lumen nerve conduits.* Journal of Controlled Release, 2005. **104**(3): p. 433-446.

116. Wang, A.J., et al., *Physical properties and biocompatibility of a porous chitosan-based fiber-reinforced conduit for nerve regeneration.* Biotechnology Letters, 2007. **29**(11): p. 1697-1702.

117. Panseri, S., et al., *Electrospun micro- and nanofiber tubes for functional nervous regeneration in sciatic nerve transections.* Bmc Biotechnology, 2008. **8**: p. -.

118. Moore, A.M., et al., *Limitations of conduits in peripheral nerve repairs.* Hand (N Y), 2009. **4**(2): p. 180-6.

119. Johnson, E.O. and P.N. Soucacos, *Nerve repair: Experimental and clinical evaluation of biodegradable artificial nerve guides.* Injury-International Journal of the Care of the Injured, 2008. **39**: p. S30-S36.

120. Hazari, A., et al., *A resorbable nerve conduit as an alternative to nerve autograft in nerve gap repair.* British Journal of Plastic Surgery, 1999. **52**(8): p. 653-657.

121. Pierucci, A., E.A.R. De Duek, and A.L.R. De Oliveira, *Peripheral nerve regeneration through biodegradable conduits prepared using solvent evaporation.* Tissue Engineering Part A, 2008. **14**(5): p. 595-606.

122. Nomura, H., et al., *Extramedullary chitosan channels promote survival of transplanted neural stem/progenitor cells and create a tissue bridge after complete spinal cord transection.* Journal of Neurotrauma, 2008. **25**(7): p. 899-899.

123. Evans, G.R.D., et al., *Bioactive poly(L-lactic acid) conduits seeded with Schwann cells for peripheral nerve regeneration.* Biomaterials, 2002. **23**(3): p. 841-848.

124. Rodriguez, F.J., et al., *Nerve guides seeded with autologous Schwann cells improve nerve regeneration.* Experimental Neurology, 2000. **161**(2): p. 571-584.

125. Ansselin, A.D., T. Fink, and D.F. Davey, *Peripheral nerve regeneration through nerve guides seeded with adult Schwann cells.* Neuropathology and Applied Neurobiology, 1997. **23**(5): p. 387-398.

126. Bozkurt, A., et al., *In vitro cell alignment obtained with a Schwann cell enriched microstructured nerve guide with longitudinal guidance channels.* Biomaterials, 2009. **30**(2): p. 169-79.

127. Guenard, V., et al., *Syngeneic Schwann-Cells Derived from Adult Nerves Seeded in Semipermeable Guidance Channels Enhance Peripheral-Nerve Regeneration.* Journal of Neuroscience, 1992. **12**(9): p. 3310-3320.

128. Hadlock, T., et al., *A polymer foam conduit seeded with Schwann cells promotes guided peripheral nerve regeneration.* Tissue Engineering, 2000. **6**(2): p. 119-127.

129. Rutkowski, G.E., et al., *Synergistic effects of micropatterned biodegradable conduits and Schwann cells on sciatic nerve regeneration.* Journal of Neural Engineering, 2004(3): p. 151.

130. Bruder, J.M., et al., *Fabrication of polymeric replicas of cell surfaces with nanoscale resolution.* Langmuir, 2006. **22**(20): p. 8266-70.

131. Cao, X. and M.S. Shoichet, *Investigating the synergistic effect of combined neurotrophic factor concentration gradients to guide axonal growth.* Neuroscience, 2003. **122**(2): p. 381-9.

132. Moore, K., M. MacSween, and M. Shoichet, *Immobilized concentration gradients of neurotrophic factors guide neurite outgrowth of primary neurons in macroporous scaffolds.* Tissue Eng, 2006. **12**(2): p. 267-78.

133. Madduri, S., M. Papaloizos, and B. Gander, *Synergistic effect of GDNF and NGF on axonal branching and elongation in vitro.* Neurosci Res, 2009. **65**(1): p. 88-97.

134. Koh, H.S., et al., *Enhancement of neurite outgrowth using nano-structured scaffolds coupled with laminin.* Biomaterials, 2008. **29**(26): p. 3574-82.

135. Britland, S., Perridge, C., Denyer, M., Morgan, H., Curtis, A., Wilkinson, C., *Morphogenetic guidance cues can interact synergistically and hierarchically in steering nerve cell growth.* Exp biol online, 1996. **1**(2): p. 1-15.

136. Charest, J.L., et al., *Combined microscale mechanical topography and chemical patterns on polymer cell culture substrates.* Biomaterials, 2006. **27**(11): p. 2487-94.

137. Britland, S., et al., *Synergistic and hierarchical adhesive and topographic guidance of BHK cells.* Exp Cell Res, 1996. **228**(2): p. 313-25.

138. Jagoda, A.S., et al., *Clinical policy: neuroimaging and decisionmaking in adult mild traumatic brain injury in the acute setting.* J Emerg Nurs, 2009. **35**(2): p. e5-40.

139. Dent, E.W., F. Tang, and K. Kalil, *Axon guidance by growth cones and branches: common cytoskeletal and signaling mechanisms.* Neuroscientist, 2003. **9**(5): p. 343-53.

140. Lal, R., et al., *Imaging real-time neurite outgrowth and cytoskeletal reorganization with an atomic force microscope.* Am J Physiol, 1995. **269**(1 Pt 1): p. C275-85.

141. Buettner, H.M. and R.N. Pittman, *Quantitative effects of laminin concentration on neurite outgrowth in vitro.* Dev Biol, 1991. **145**(2): p. 266-76.

142. Pittman, R.N., J.K. Ivins, and H.M. Buettner, *Neuronal plasminogen activators: cell surface binding sites and involvement in neurite outgrowth.* J Neurosci, 1989. **9**(12): p. 4269-86.

143. Britland, S. and C. McCaig, *Embryonic Xenopus neurites integrate and respond to simultaneous electrical and adhesive guidance cues.* Exp Cell Res, 1996. **226**(1): p. 31-8.

144. Kalil, K., G. Szebenyi, and E.W. Dent, *Common mechanisms underlying growth cone guidance and axon branching.* J Neurobiol, 2000. **44**(2): p. 145-58.

145. Chemin, J., et al., *A phospholipid sensor controls mechanogating of the K+ channel TREK-1.* Embo Journal, 2005. **24**(1): p. 44-53.

146. Hamill, O.P., *Twenty odd years of stretch-sensitive channels.* Pflugers Archiv-European Journal of Physiology, 2006. **453**(3): p. 333-351.

147. Kung, C., *A possible unifying principle for mechanosensation.* Nature, 2005. **436**(7051): p. 647-54.

148. Lauritzen, I., et al., *Cross-talk between the mechano-gated K-2P channel TREK-1 and the actin cytoskeleton.* Embo Reports, 2005. **6**(7): p. 642-648.

149. McCarter, G.C., D.B. Reichling, and J.D. Levine, *Mechanical transduction by rat dorsal root ganglion neurons in vitro.* Neuroscience Letters, 1999. **273**(3): p. 179-182.

150. Pellegrino, M. and M. Pellegrini, *Mechanosensitive channels in neurite outgrowth.* Mechanosensitive Ion Channels, Pt B, 2007. **59**: p. 111-125.

151. Raoux, M., et al., *Mechanosensor channels in mammalian somatosensory neurons.* Sensors, 2007. **7**(9): p. 1667-1682.

152. Vogel, V. and M. Sheetz, *Local force and geometry sensing regulate cell functions.* Nat Rev Mol Cell Biol, 2006. **7**(4): p. 265-75.

153. Schmidt, C.E., et al., *Integrin-cytoskeletal interactions in neuronal growth cones.* J Neurosci, 1995. **15**(5 Pt 1): p. 3400-7.

154. Dedman, A., et al., *The mechano-gated K(2P) channel TREK-1*. Eur Biophys J, 2009. **38**(3): p. 293-303.

155. Heurteaux, C., et al., *Deletion of the background potassium channel TREK-1 results in a depression-resistant phenotype.* Nature Neuroscience, 2006. **9**(9): p. 1134-1141.

156. Kennard, L.E., et al., *Inhibition of the human two-pore domain potassium channel, TREK-1, by fluoxetine and its metabolite norfluoxetine.* Br J Pharmacol, 2005. **144**(6): p. 821-9.

157. Maingret, F., et al., *Mechano- or acid stimulation, two interactive modes of activation of the TREK-1 potassium channel.* J Biol Chem, 1999. **274**(38): p. 26691-6.

158. Eckert, M., et al., *TREK-1 isoforms generated by alternative translation initiation display different susceptibility to the antidepressant fluoxetine.* Neuropharmacology, 2011. **61**(5-6): p. 918-23.

159. Patel, A.J., et al., *A mammalian two pore domain mechano-gated S-like K+ channel.* Embo Journal, 1998. **17**(15): p. 4283-90.

160. Jin, G.Z., et al., *Neurite outgrowth of dorsal root ganglia neurons is enhanced on aligned nanofibrous biopolymer scaffold with carbon nanotube coating.* Neurosci Lett, 2011. **501**(1): p. 10-4.

161. Wright, K.T., et al., *Extracellular Nm23H1 stimulates neurite outgrowth from dorsal root ganglia neurons in vitro independently of nerve growth factor supplementation or its nucleoside diphosphate kinase activity.* Biochem Biophys Res Commun, 2010. **398**(1): p. 79-85.

162. Shen, J., et al., *Morphologic analysis of normal human lumbar dorsal root ganglion by 3D MR imaging.* AJNR Am J Neuroradiol, 2006. **27**(10): p. 2098-103.

163. Peterson, S.L., et al., *Poly(dimethylsiloxane) thin films as biocompatible coatings for microfluidic devices: cell culture and flow studies with glial cells.* J Biomed Mater Res A, 2005. **72**(1): p. 10-8.

164. Folch, A. and M. Toner, *Cellular micropatterns on biocompatible materials.* Biotechnol Prog, 1998. **14**(3): p. 388-92.

CHAPTER 2

GUIDANCE OF DORSAL ROOT GANGLION NEURITES AND SCHWANN CELLS BY ISOLATED SCHWANN CELL TOPOGRAPHY ON POLY(DIMETHYL SILOXANE) CONDUITS AND FILMS

J A Richardson, C W Rementer, Jan M. Bruder, and D Hoffman-Kim, Ph.D.

Journal of Neural Engineering, 2011. 8(4):046015. Epub 2011 Jun 15.

2.1. Abstract

Biomimetic replicas of cellular topography have been utilized to direct neurite outgrowth. Here we cultured postnatal rat dorsal root ganglion (DRG) explants in the presence of Schwann cell (SC) topography to determine the influence of SC topography on neurite outgrowth. Four distinct poly(dimethyl siloxane) (PDMS) conduits were fabricated within which DRG explants were cultured. To determine the contribution of SC topographical features to neurite guidance, the extent of neurite outgrowth into unpatterned conduits, conduits with randomly oriented SC replicas, and conduits with SC replicas parallel or perpendicular to the conduit long axis was measured. Neurite directionality and outgrowth from DRG were also quantified on two-dimensional SC replicas with orientations corresponding to the four conduit conditions. Additionally, live SC migration and neurite extension from DRG on SC replicas were examined as a first step toward quantification of the interactions between live SC and navigating neurites on SC replicas. DRG neurite outgrowth and morphology within conduits and on two-dimensional SC replicas were directed by the underlying SC topographical features. Maximal neurite outgrowth and alignment to the underlying features were observed into parallel conduits and on parallel two-dimensional substrates, whereas least extent of outgrowth was observed into perpendicular conduits and on perpendicular two-dimensional replica conditions. Additionally, neurites on perpendicular conditions turned to extend along the direction of underlying SC topography. Neurite outgrowth exceeded SC migration in the direction of the underlying anisotropic SC replica after 2 days in culture. This finding confirms the critical role that SC have in guiding neurite outgrowth and suggests that the mechanism of neurite alignment to SC replicas depends on direct contact with cellular topography. These results suggest that SC topographical replicas may be used to direct and optimize neurite alignment, and emphasize the importance of SC features in neurite guidance.

2.2. Introduction

Following neuronal injury, accurate navigation of axons to their proper targets is necessary for functional regeneration. Schwann cells (SC), the glia of the peripheral nervous system (PNS), promote and maintain neuronal health in the PNS, and present both molecular and topographical guidance stimuli to damaged peripheral nerves [1-3]. Migration of SC to the injury site is necessary to promote regeneration in the PNS [2, 4]. Additionally, SC are present in longitudinally aligned spatial arrangements along neuronal processes as Bands of Büngner, which promote the maintenance of axonal directedness toward their targets [1, 5].

Although SC promote the regenerative process, complete recovery following PNS injury is difficult, as the size and severity of the injury often limit proper regeneration [6-7]. Nerve autografts are the current gold standard for PNS repair, but there remains a need for improved methods of PNS regeneration, as autografts can result in incomplete functional recovery due to incorrect reinnervation to distal targets and the lack of complete axonal regeneration [8-11]. Toward this end, many are investigating tissue-engineered approaches.

Polymeric nerve guidance conduits have been explored to promote sprouting axons to properly reconnect with their targets following injury [12-13]. Incorporation of permissive molecular and topographical cues or combinations thereof into guidance conduits is one focus of such research [14-18]. SC are an appealing strategy of enhancing neurite outgrowth and directionality, and have therefore been investigated as guidance features within nerve guidance conduits to promote neurite regeneration to targets along the longitudinal axis of the conduit [19-23]. To investigate how SC guide nerves, our lab has developed a replica molding technique to reproduce and isolate SC topographical features [24]. With this approach, the effects of SC topography in various orientations on neurite directionality can be quantified.

In this study we have utilized isolated SC topography as a guidance cue for DRG explants. Thin poly(dimethyl siloxane) (PDMS) films were fabricated to replicate SC topography in distinct orientations and without other cellular components. Toward an application-based approach, three types of guidance conduits were formed from SC replica films to investigate the abilities of the tubular conduit geometry and the SC topography to direct neurite outgrowth. Conduits of unpatterned PDMS films were used as controls. For further analysis of these phenomena, neurite and SC growth and orientation were quantified on two-dimensional replicas. Here we show that the orientation of SC replicas differentially directs neurites through conduits and on two-dimensional SC replicas. These studies also indicate that complex dynamics exist between navigating neurites, migrating SC, and SC topography.

2.3. Materials and Methods

2.3.1. Schwann cell culture

Cell culture reagents were obtained from Invitrogen Life Science (Carlsbad, CA, USA), unless otherwise indicated. SC from adult rat sciatic nerve (generous gift from Dr. Mary Bunge) were cultured on tissue culture plastic flasks pre-coated with 100 µg/ml poly(L-lysine) (PLL; Sigma, St. Louis, MO, USA) in Dulbecco's modified eagle's medium (DMEM) with 10% fetal bovine serum (FBS), 4 mM L-glutamine, 100 U/ml penicillin and 100 µg/ml streptomycin (base media) supplemented with 2 µM forskolin (Sigma), 10µg/ml bovine pituitary extract (Sigma) and 2 µM heregulin (gift from Genentech, Vacaville, CA, USA) (SC media). SC from passages 4-9 were used in these experiments.

2.3.2. Fabrication of SC replicas

Photolithographic and soft lithographic techniques were used to generate micropatterned photoresist on silicon wafers to be used as templates for PDMS soft lithography as described by

Bruder et al. [24]. To generate aligned SC templates, glass coverslips (Fisher Scientific, Pittsburgh, PA, USA) were microcontact printed with 50 µm stripes separated by 20 µm spaces of 50 µg/mL mouse laminin (LN) in Hank's Balanced Salt Solution (HBSS) as described by Kofron et al. [25]. To generate randomly oriented SC templates, glass cover slips were fully adsorbed with 50 µg/mL LN. SC were seeded at 88,000 cells/cm^2 and 25,000 cells/cm^2 to generate aligned and randomly oriented cell templates, respectively, and were cultured approximately 2 days until they reached confluence[26]. Cell cultures were fixed with 2% paraformaldehyde in 0.1M phosphate-buffered saline, pH 7.4 (PBS) for 20 minutes at room temperature and rinsed with PBS. To confirm cellular orientation, cells were stained with 50 µg/mL 4-,6-diamidino-2-phenylindole (DAPI, Sigma) in PBS and analyzed for alignment as described below. Samples were post-fixed as the final step of cell template generation. All post-fixing reagents were from Electron Microscopy Sciences. Samples were incubated at room temperature in Karnovsky's fixative overnight, rinsed with 0.1 M sodium cacodylate buffer, incubated in 1% OsO_4 in 0.1 M sodium cacodylate buffer for 1 h, rinsed with dH_2O, incubated in 1% thiocarbohydrazide in dH_2O for 30 min, rinsed with dH_2O, incubated with 1% OsO_4 in dH_2O for 20 min, dehydrated with graded ethanols to 100% ethanol, air dried, and sputter-coated with gold-palladium. A replica-molding technique was used to generate PDMS impression replicas. Sylgard 184 elastomer base was mixed with Sylgard 184 curing agent (10:1 wt/wt) and applied to the template. The template was rotated to evenly distribute PDMS as a film of uniform thickness. The solution was heated to 95°C for 1 h, and the resulting PDMS layer was peeled and inverted to generate the SC replica. To generate control substrates of unpatterned PDMS, a similar replica-molding technique was used with clean glass cover slips as templates.

2.3.3. Cell template alignment analysis

To assess cell template alignment, 10 fields of view (FOV) per sample of DAPI-stained SC nuclei were acquired at 10x magnification with a Nikon Eclipse TE2000-S phase-contrast and epifluorescence microscope, equipped with a software-controlled motorized stage. Patterned samples were oriented so that substrate pattern direction was uniform between samples. Images were captured using a Hamamatsu Orca-ER camera, an Orbit shutter controller, and a Ludl stage controller, outputting to OpenLab v4.0.4 (Improvision, Lexington, MA, USA). DAPI images of SC for alignment analysis were converted to 8-bit grayscale with Adobe Photoshop CS2, inverted, and the contrast was adjusted using the level and curve functions. Nuclei number and orientation were assessed with ImageJ v1.36, using the Otsu function of the multithresholder plugin and the particle analyzer plugin with size filter set to 50–850 pixels to exclude image artifacts and cell clusters. Data were analyzed with Oriana v2.02c (Kovach Computing Services, Pentraeth, UK).

2.3.4. Conduit preparation

SC replicas were trimmed to create films measuring 1x2 cm. The short axis of the replica was rolled around a glass mandrel (1 mm diameter) with the patterned side forming the conduit lumen, and approximately 100 µL of 10:1 (wt/wt) mixture of Sylgard 184 elastomer base and curing agent was used to secure the wrapped replica around the mandrel. Samples were heated to 175°C for 10 minutes to allow the sealing PDMS to cure. Aligned replicas were wrapped with the pattern parallel to the mandrel or rotated 90° to generate parallel or perpendicularly aligned replica conduits. Random replica and unpatterned PDMS films were also wrapped around mandrels, resulting in conduits with four lumen topography conditions. Conduits were removed from the mandrels and sliced orthogonally in half to result in 5 mm long conduits. Conduit surfaces were plasma activated for 60 s, filled with 50 µg/mL LN, and incubated at room

temperature for 1 h. Immediately before DRG explants were seeded, LN was removed, conduits were flushed with dH_2O, and conduits were dried using a pressurized air stream.

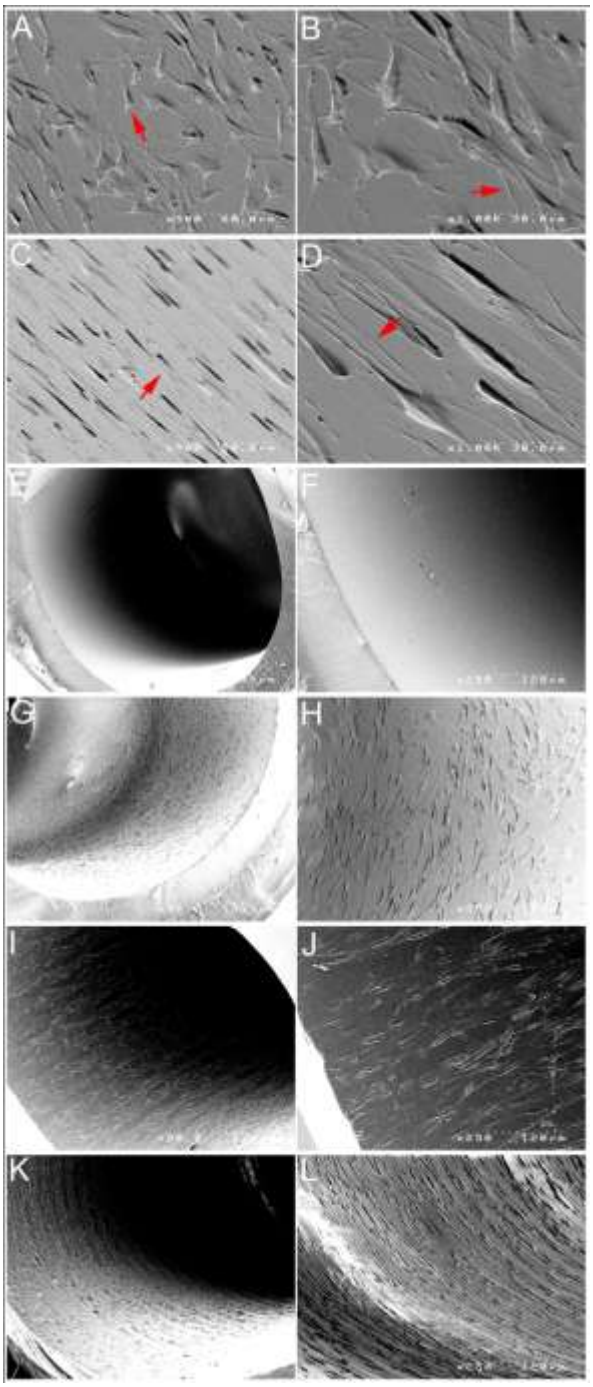

Figure 2.1. A-D. Scanning electron micrographs of random (A,B) and aligned (C,D) SC topographical replicas. Arrows indicate replicas of cell soma and processes. Replicas are shown at low (500x; A,C) and high (1000x; B,D) magnifications. E-L. Conduits presented four distinct topographical orientations**.** Unpatterned (E,F), random (G,H), parallel (I,J), and perpendicular (K,L) conduit lumens are shown at low (90x; C,E,G,I,K) and high (250x; D,F,H,J,L) magnifications.

2.3.5. Conduit analysis

Image analysis of rolled conduit cross sections was used to assess the uniformity of inner and outer conduit diameter, individual layer thickness, and number of PDMS film wraps. Images were taken at 4x and 10x magnification. The straight line segment measure tool in Openlab v4.0.4 software was used to determine conduit dimensions. Conduits were also examined for surface morphology with a Hitachi S-2700 scanning electron microscope using an acceleration voltage of 8 kV.

2.3.6. DRG explant harvest and culture

DRG explants were dissected from the spinal columns of postnatal (P0-P4) rat pups and cleaned of remaining axons, blood, and connective tissue. Each explant was plated to the inner conduit wall at one end of the conduit. Conduits with explants were cultured in 6-well tissue culture plates with base media supplemented with 50 ng/ml nerve growth factor (NGF) at 37°C with 100% humidity and 5% CO_2 for 1, 2, or 3 days. Conduits with explants were fixed with 2% paraformaldehyde in PBS and rinsed with PBS. NIH guidelines for the care and use of laboratory animals were observed throughout all studies.

2.3.7. Neurite analysis

Immunocytochemistry of the DRG explants was performed according to Goldner et al. [27] using the primary mouse monoclonal antibody RT97 directed against the phosphorylated epitopes of neurofilament (NF) (developed by Dr. John Wood and obtained from the Developmental Studies Hybridoma Bank) and a Cy2-conjugated goat anti-mouse secondary antibody (Jackson Laboratories). In conduits, NF-stained DRG neurites were analyzed at 10x magnification. NF-stained DRG neurites within conduits were assessed for the maximum growth achieved along the

conduit long axis. Measurements of this length were obtained using the measure tool in Openlab v4.0.4.

To assess neurite directionality on two-dimensional SC replicas, all in-focus NF-labeled neurites present in each FOV analyzed were manually traced using the straight line segment tool of Openlab v.4.0.4 software, and their angles of orientation and lengths were recorded and grouped into 5˚ angle bins from -90˚ to +90˚, as depicted by Fig. 2.5. Directional bias along and opposing the direction of the underlying SC topographical features was quantified. Percent neurite alignment within 10° regions depicted by the shaded regions i and ii in Fig. 2.4A, was calculated. Percent neurite alignment was compared between regions i and ii for all conditions.

Neurite outgrowth and arbor orientation on unpatterned, random, and aligned replicas were assessed by an adaptation of the technique described by Thompson and Buettner [28]. Briefly, an ellipse was fit to a tracing of the perimeter of the neurite arbor. The area of the ellipse was recorded as well as the lengths of the major and minor axes of the ellipse. The aspect ratio of the neurite arbor was used as an indication of neurite alignment, where aspect ratio = $length_{major}$ / $length_{minor}$.

2.3.8. SC analysis

Immunocytochemistry was performed to identify SC which had migrated from DRG explants on two-dimensional replicas. SC were labeled using the primary rabbit polyclonal anti-S-100 protein antibody (Chemicon International, Temecula, CA, USA) and a Cy-2 secondary conjugated goat anti-rabbit antibody. SC arbor was analyzed for area and aspect ratio as described above.

2.3.9. Statistical analysis

To confirm the orientation of SC on cell templates, circular analysis was used to analyze the angular distributions of the major axes of the SC nuclei, as described by Li et al., 2009 [29]. Circular mean vectors and standard errors of the mean were calculated, where the length of the mean vector corresponds to the degree of clustering of the data, and the direction of the mean vector corresponds to the mean direction of the data. Uniformity of the distribution of nuclei and of the angles of neurite segments were assessed using the Rayleigh's test and Rao's spacing test. Oriana 2.02c software was used for circular analysis. One-way ANOVAs with post-hoc Bonferroni tests were used to compare percentages of neurite outgrowth in distinct 10° regions among the four two-dimensional conditions presenting SC replicas or no topographical features. Student t-tests assuming equal variances were used to compare maximum neurite distance and rates of extension along the conduit longitudinal axis among the four lumen topographical conditions, rates of neurite extension and neurite and SC arbor areas and aspect ratios among the two-dimensional topographical conditions, and neurite angle distributions. A P-value less than 0.05 was considered significant for all statistical tests performed.

2.4. Results

2.4.1. SC templates exhibiting random or aligned orientations were used to fabricate PDMS SC replicas and conduits.

We fabricated SC replica substrates that exhibited indented SC topography with random or aligned orientations. SC were cultured to confluence on glass fully coated with LN or microcontact-printed with LN stripes to generate randomly oriented and aligned SC templates, respectively. Cellular orientation assessed by nuclear alignment with a circular analysis approach [29] confirmed that random SC templates had angular distributions that were not different from a uniform distribution. The aligned SC templates had angular distributions that were significantly different from a uniform distribution ($P<0.05$, Rao's spacing test, Rayleigh's test of uniformity),

and had a mean vector angle of 88.30˚ with a length of 0.681, which indicated alignment in the direction of the underlying LN stripes.

A replica molding approach was used to generate replicas and guidance conduits as described previously by our lab [24]. Briefly, a layer of PDMS of thickness 153.84 ± 50.35 μm was cured over the fixed cell templates and subsequently peeled and inverted to generate replicas with either aligned or random topographical features. Scanning electron microscopy showed replication of cellular features including soma and processes. The PDMS replicas were wrapped around glass mandrels to form guidance conduits with inner diameter of 1.28 ± .045 mm.

To investigate the effects of SC replica topography on neurite guidance through channels, guidance conduits were fabricated from SC replicas, such that four lumen topographical conditions were generated: unpatterned (Figure 2.1E, F), random replicas (Figure 2.1G, H), parallel replicas (Figure 2.1I, J), and perpendicular replicas (Figure 2.1K, L). Parallel replica conduits presented aligned replica topography with a longitudinal axis of alignment corresponding to the long axis of the conduit, while perpendicular replica conduits presented aligned replica topography in a direction orthogonal to the long axis of the conduit.

2.4.2. DRG neurite outgrowth and morphology were directed by lumen replica topography.

A single DRG was cultured at one end of each tubular conduit for 3 days. DRGs were positioned within 1 mm of the conduit opening. To assess the furthest extent of neurite outgrowth within the conduits, the distance from the DRG edge furthest along the length of the conduit to the furthest NF-stained neurite along the conduit long axis was measured (Figure 2.2). Extent of neurite outgrowth was greatest in parallel replica conduits at 2909.13$\pm$314.68 μm ($P<0.05$). Neurites in unpatterned and random replica conduits grew 1839.81$\pm$165.09 μm and 2102.14$\pm$150.95 μm,

respectively, into the conduits. The neurite outgrowth front within perpendicular replica conduits was shortest at 1121.40±194.88 μm ($P<0.05$). Neurites within unpatterned conduits grew in the direction of the longitudinal axis of the conduit, with limited directional changes and bifurcations and minimal morphological complexity (Figure 2.3A, B). Neurites within randomly oriented SC replica conduits displayed a high degree of complexity with many turning and branching morphological characteristics (Figure 2.3C, D). Neurites within parallel oriented SC replica conduits grew in the direction of the longitudinal axis of the conduit and of the lumen topography and were less morphologically complex. These neurites showed limited directional changes and bifurcations (Figure 2.3E, F). Neurites within perpendicular oriented SC replica conduits demonstrated sharp turning in the direction of the orthogonally oriented SC replica pattern as they grew away from the explant body (Figure 2.3G, H).

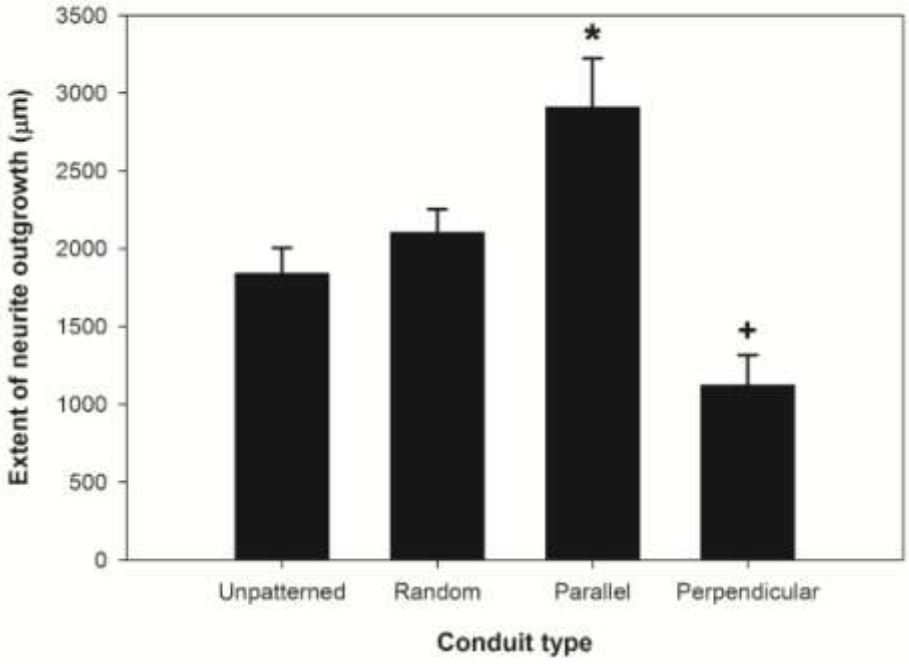

Figure 2.2. Distance of neurite outgrowth within conduits varied with underlying replica topography. *,$^{+}$$P<0.05$ significantly different from all other conditions by two-tailed Student's *t*-test assuming equal variances. Unpatterned, parallel: n=6, random, perpendicular: n=8; error bars are standard error of means.

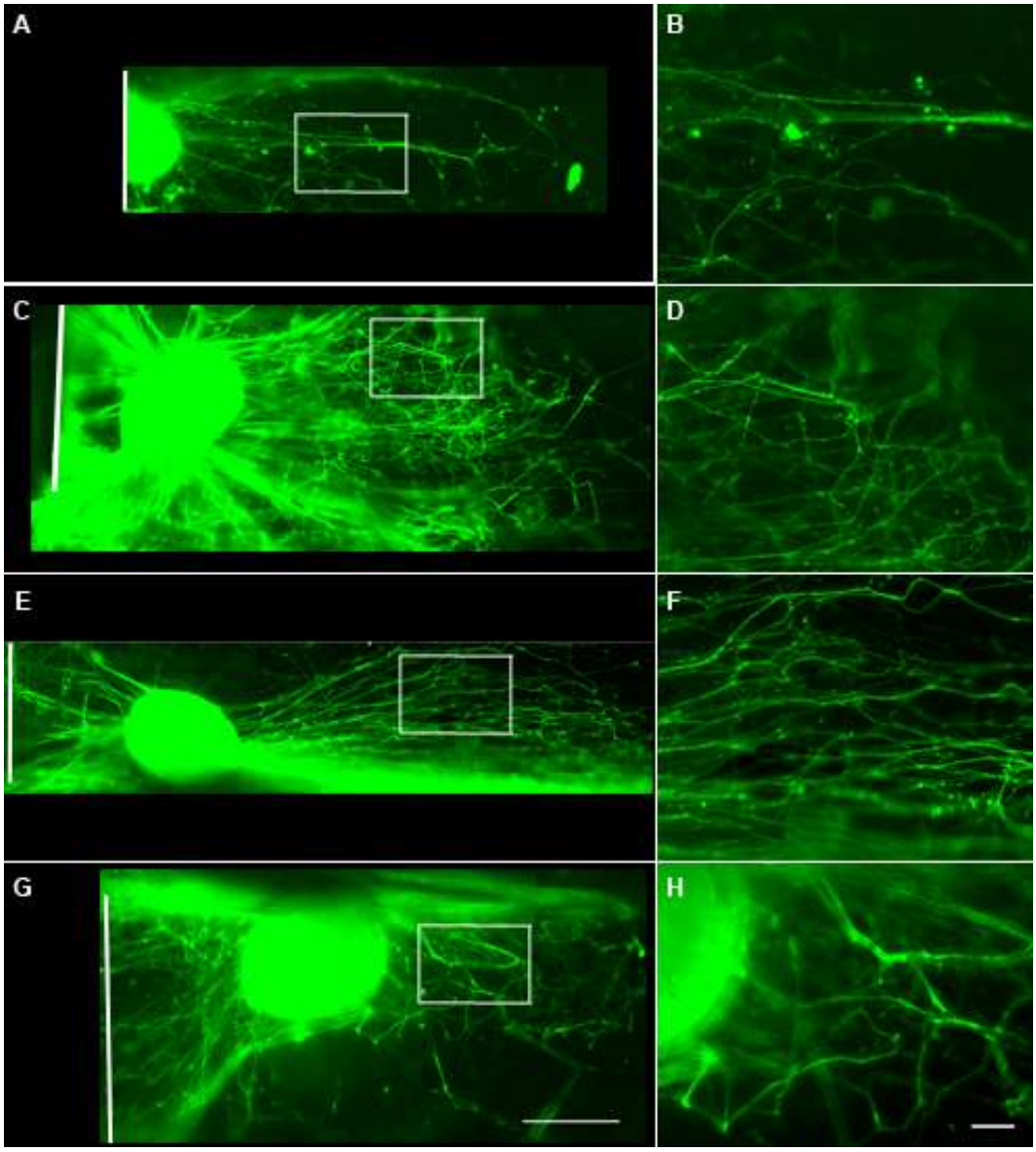

Figure 2.3. DRG neurite outgrowth and morphology in conduits were directed by underlying conduit lumen topography. Neurite extension patterns and overall neurite morphology differed among unpatterned (A,B), random (C,D), parallel (E,F), and perpendicular (G,H) conduits. B,D,F,H. FOVs corresponding to white boxed areas in adjacent left panels show higher magnification views of neurite outgrowth. White lines represent conduit openings. Scale bars represent 500 μm (A,C,E,G) and 100 μm (B,D,F,H).

2.4.3. Neurite directionality and morphology depended on underlying replica topography.

Based on the varied extents of neurite outgrowth and distinct neurite morphologies within the different types of conduits, we hypothesized that the underlying growth mechanism included

alignment of neurites from explants along the SC replica topographical features. We analyzed quantitatively the specific cell-biomaterial interactions by culturing DRG explants on two-dimensional SC replicas (Figure 2.4A-D). DRG explants in two-dimensional tissue culture typically extend neurites in all 360°; thus, we oriented our image acquisition so the aligned substrate could provide a representation of both parallel and perpendicular conduits. Specifically, images were obtained adjacent to the explant body at 90˚ offset such that the underlying aligned replica topography was either parallel or perpendicular relative to the perimeter of the explant body. Neurite orientations and morphologies with respect to the underlying SC replicas (Figure 2.4E-L) were similar to those that the neurites had displayed in the corresponding SC replica conduits (Figure 2.3). Neurite tracing analysis showed that neurite directionality was relatively evenly distributed on unpatterned and randomly oriented replicas (Figure 2.5A, B). Neurite growth was directed on parallel and perpendicular replica conditions (Figure 2.5C, D). Neurites analyzed on parallel replica conditions demonstrated peak outgrowth at 0°, corresponding to the orientation of the underlying replica. Neurites analyzed on perpendicular replica conditions were preferentially directed toward -90° and +90°, corresponding to the perpendicular orientation of the underlying replica.

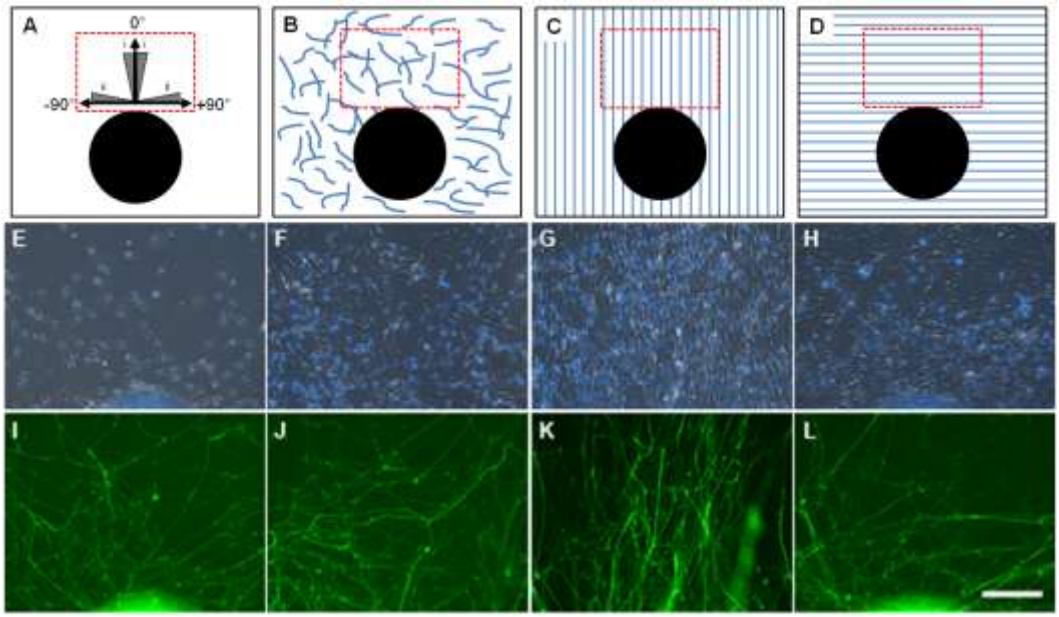

Figure 2.4. DRG neurite outgrowth and morphology were influenced by underlying replica topography. A-D. Diagrammatic representation of experimental approach. Black circles represent DRG explant bodies. Neurites are excluded from cartoon for simplification. Blue lines represent orientation of underlying replica topography for unpatterned (A), random (B), parallel (C), and perpendicular (D) replicas. Red dashed boxes represent 434.93 x 331.37 µm FOVs that were imaged as oriented in the diagrams. Neurite directionality was assessed relative to the compass in (A). Shaded areas on compass (i and ii) represent regions of neurite growth (-90° to -85°, -5° to +5°, 85° to 90°) that were compared to quantify directional preference among neurite angle distributions. E-L. Overlaid phase contrast and fluorescent micrographs of DAPI-positive nuclei (E-H) with corresponding fluorescent micrographs of neurofilament-positive neurites (I-L) from DRG explants on unpatterned (E,I), random (F,J), parallel (G,K), and perpendicular (H,L) replicas after 3 days in culture. Scale bar, 50 µm.

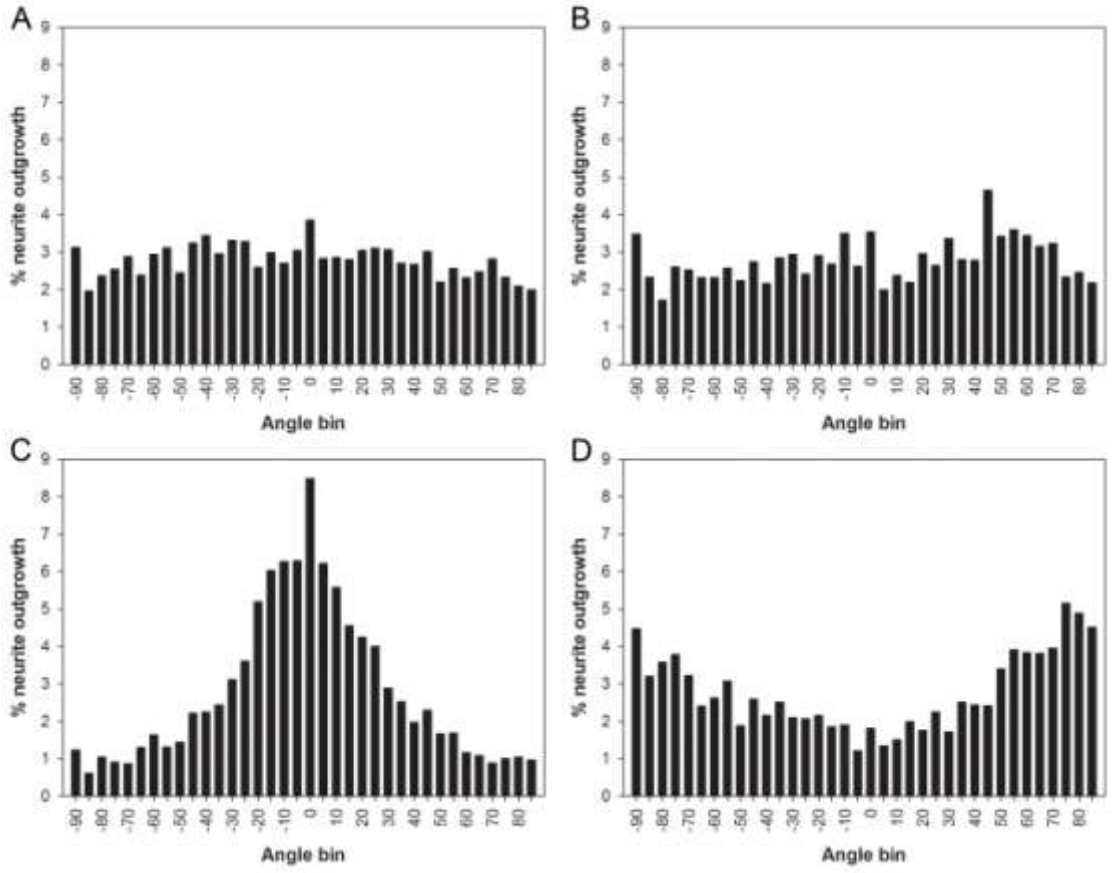

Figure 2.5. Neurite outgrowth angular distributions were directed by underlying topography of two-dimensional replicas. Graphs of unpatterned (A), random (B), parallel (C), and perpendicular (D) neurite distributions. Percentage of neurite length within each 5˚ angle bin is plotted from -90˚ to +90˚. n=6 FOV for each condition.

To quantify the biases in neurite outgrowth directionality depicted by neurite angle distributions in Fig. 2.5, we compared percent neurite outgrowth in the 10° occupied by region i versus region ii for each condition (Figure 2.6; student t-tests assuming equal variance). In the unpatterned control condition, where growth reflects background directionality deriving from initial emergence of neurites from the explants, region i contained a greater percentage of neurite outgrowth than region ii with 3.45±0.24% in region i and 2.56±0.26% in region ii ($P<0.05$). No significant differences in percent neurite outgrowth between regions i and ii were observed for the random condition. In the parallel condition, region i contained a greater percentage of neurite outgrowth than region ii with 7.39±0.73% in region i and 1.10±0.14% in region ii ($P<1.0E-07$). In

the perpendicular condition, region i contained a lower percentage of neurite outgrowth than region ii with 1.51±0.25% in region i and 4.50±0.39% in region ii ($P<1.0E-05$).

Comparing across replicas, a significantly greater percentage of neurite outgrowth was observed within region i in the parallel condition when compared to all other conditions (ANOVA, $P<0.001$). In the perpendicular condition, a significantly lower percentage of neurite outgrowth was observed within region i when compared to the unpatterned and parallel conditions (ANOVA, $P<0.05$). No significant differences were observed between unpatterned and random or between random and perpendicular conditions within region i.

Correspondingly, a significantly lower percentage of neurite outgrowth was observed within region ii in the parallel condition when compared to all other conditions (ANOVA, $P<0.05$). In the perpendicular condition, a significantly greater percentage of neurite outgrowth was observed within region ii when compared to all other conditions (ANOVA, $P<0.01$). No significant differences were observed between unpatterned and random conditions within region ii.

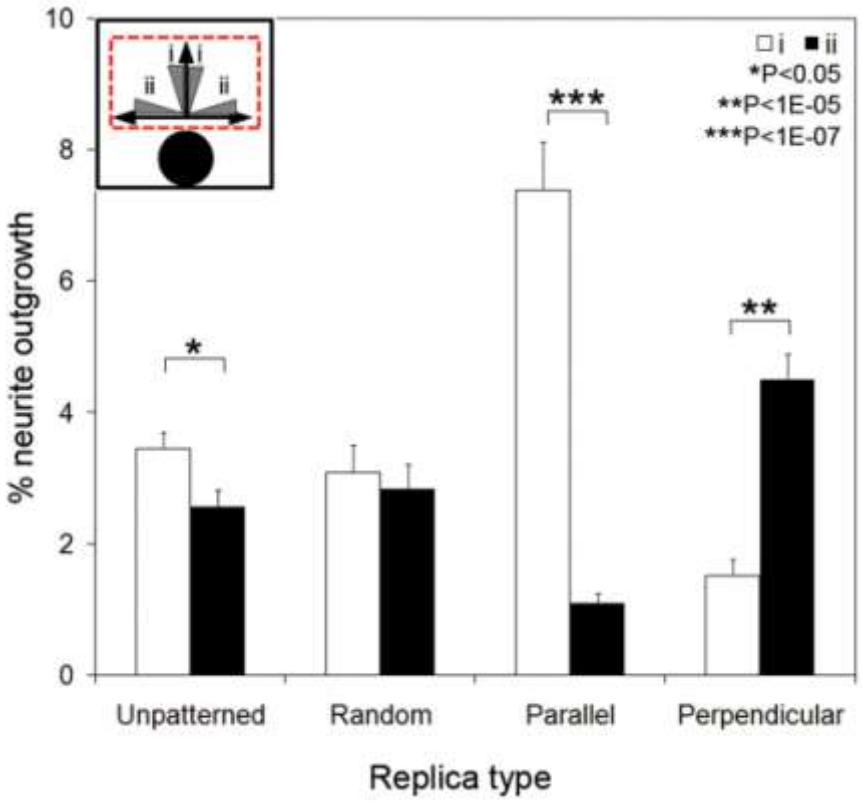

Figure 2.6. The distribution of neurite outgrowth was directed by underlying topographical features. Percentage of neurite length in regions i and ii was compared. n=6 FOV for each condition. (*P<0.05, **P<1E-05, ***P<1E-07 by two-tailed Student's *t*-test assuming equal variances; error bars are standard error of means).

2.4.4. Rate of neurite outgrowth was greatest for parallel conditions.

Neurite outgrowth proceeded fastest into the parallel conduits and in the parallel direction on replicas (969.71±104.89 μm/day, 785.42±50.71 μm/day, respectively). Outgrowth occurred at 613.27±55.03 μm/day and 529.80±49.94 μm/day into unpatterned conduits and on unpatterned replicas, respectively. Outgrowth occurred at 700.99±50.32 μm/day and 590.23±33.98 μm/day into random conduits and on random replicas, respectively. Outgrowth proceeded most slowly into perpendicular conduits and in the perpendicular direction on replicas (373.80±64.96 μm/day, 374.01±31.42 μm/day, respectively).

Neurites in parallel conduits grew 36.75% faster than those in unpatterned conduits, 27.71% faster than those in random conduits, and 61.45% faster than those in perpendicular conduits. Neurites extending in the parallel direction on replicas grew 48.25% faster than those on unpatterned replicas, 33.07% faster than those on random replicas, and 110.00% faster than those extending in the perpendicular direction on replicas.

Rates of neurite outgrowth into conduits and on replicas were greatest in parallel conduits and replicas compared to all other conditions ($P<0.05$). Rates of neurite outgrowth into conduits and on replicas were least in perpendicular conduits and replicas compared to all other conditions ($P<0.05$). No significant differences in neurite outgrowth rate were observed between unpatterned and random conduits and replicas.

2.4.5. Over time, neurite outgrowth and SC migration from DRG explants followed replica topography, and neurite outgrowth exceeded SC migration by Day 2.

We also investigated the interactions between live migrating SC and extending neurites as they encountered the SC topography of the underlying substrates at different orientations (Figure 2.7, Supplemental Figure 2.1). The total area occupied by neurite and SC arbors was determined by fitting an ellipse to the projected area of NF-positive or S100-positive immunostaining and subtracting the projected area of the explant body. The aspect ratios of the neurite and SC arbors were determined from the ratio of lengths of the major and minor axes of the fitted ellipses. SC migration and neurite outgrowth were assessed over a timecourse of three days. For both neurites and SC, total arbor areas increased over time, ranging from 3.72 ± 1.41 mm^2 to 4.76 ± 1.94 mm^2 on day 1; 16.14 ± 5.71 mm^2 to 20.42 ± 7.72 mm^2 on day 2; and 34.97 ± 14.28 mm^2 to 49.93 ± 18.87 mm^2 on day 3 (Figure 2.8A). No significant differences in arbor area were observed between neurites and SC for any condition at any timepoint. At each timepoint, arbor areas were

similar among unpatterned, random, and aligned materials. For neurites and SC growing from DRG explants on unpatterned or random materials, aspect ratios ranged from 1.10 $\pm$ 0.45 to 1.23 $\pm$ 0.47 (Figure 2.8B), and no significant differences in aspect ratio were observed at any timepoint. Neurites from DRG explants on aligned replicas showed significantly greater aspect ratios than corresponding migrating SC, at day 2 (1.86 + 0.76 for neurites vs. 1.31 + 0.50 for SC) and at day 3 (2.00 $\pm$ 0.67 for neurites vs. 1.68 $\pm$ 0.63 for SC; $P<0.05$).

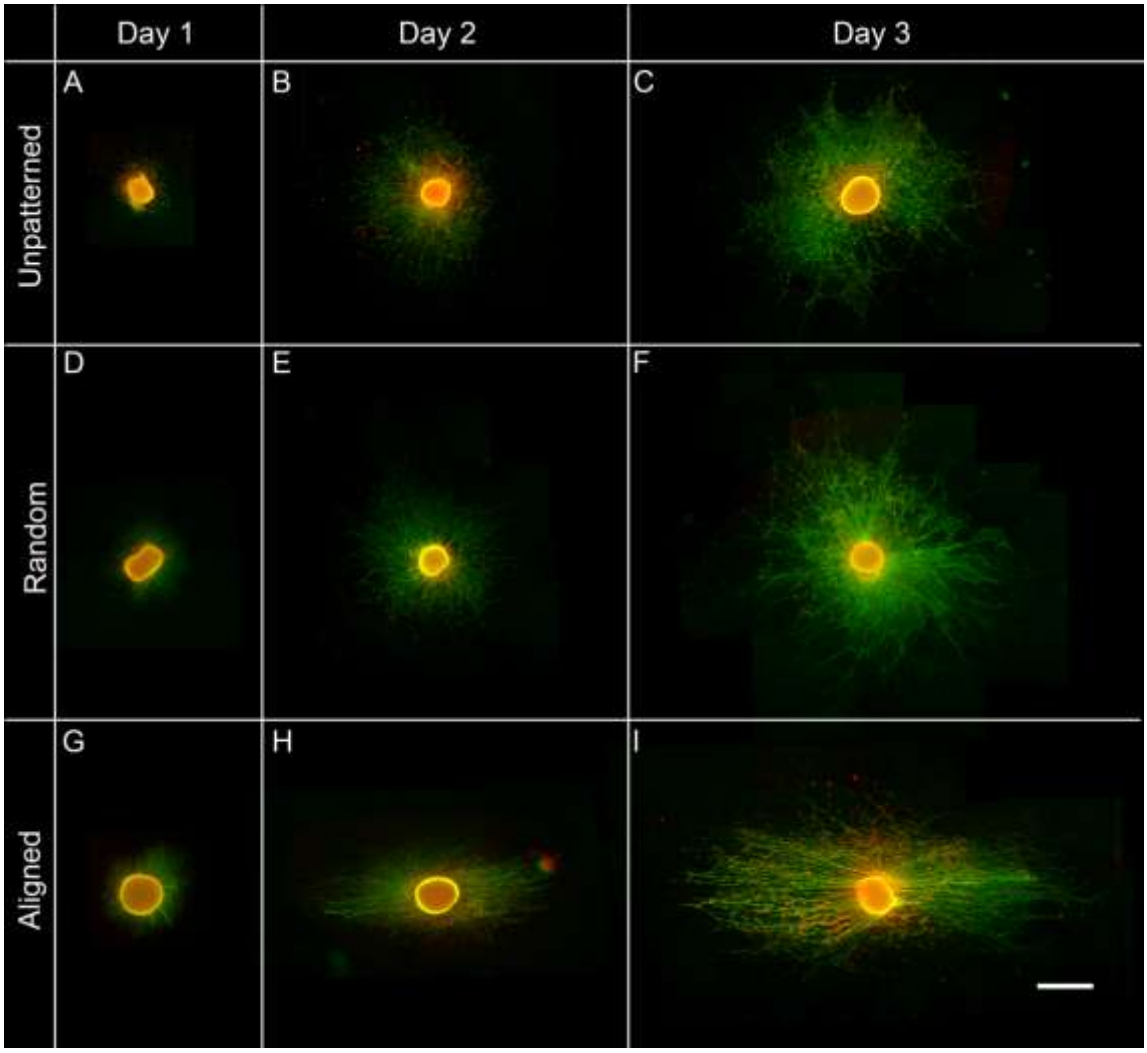

Figure 2.7. Neurite outgrowth and SC migration from DRG explants followed replica topography over time. Epifluorescent micrographs of DRG explants cultured for 1 (A,D,G), 2 (B,E,H), or 3 (C,F,I) days on unpatterned (A-C), random (D-F), and aligned (G-H) replicas and stained for anti-neurofilament (green) and anti-S-100 (red). Scale bar represents 1 mm.

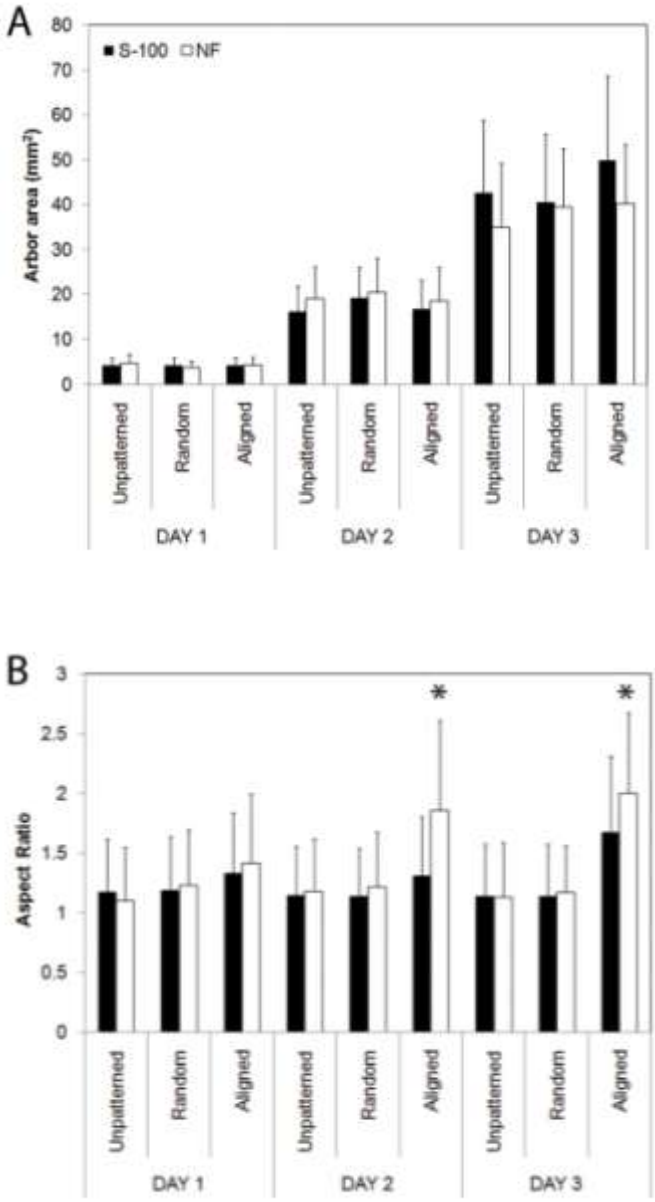

Figure 2.8. Extended neurite and migrated SC arbor areas and aspect ratios were contrasted after 1, 2, and 3 days in culture. A. Neurite and migrated SC arbor areas were similar across all conditions at days 1, 2, and 3. B. Neurite arbor aspect ratio was significantly greater than migrated SC aspect ratio on aligned replicas at day 2 and day 3 (B). (*$P<0.05$ by two-tailed Student's *t*-test assuming equal variances) ($n\geq6$ explants for all conditions; error bars are standard error of means).

2.5. Discussion

A principal objective of this work was to determine how SC topography directed neurite outgrowth from DRG. Due to their ability to promote growth following peripheral nerve injury in vivo, SC have been utilized extensively and the relative contributions of their regeneration-enhancing attributes has been assessed in order to inform strategies for nerve repair [28, 30-32]. Rat spinal neurites have been shown to align to underlying SC monolayers, suggesting that a combination of SC topographical and molecular features is responsible for neurite guidance [28]. To evaluate the individual contributions of SC-based guidance cues, we have developed a replica molding technique to separate SC topography from the secreted factors presented by live SC [24]. By isolating SC topographical components, we can assess neurite guidance in the presence of SC topography in vitro [33].

Toward this end, we analyzed neurite outgrowth and morphological characteristics within PDMS conduits fabricated from replicas containing SC topography in random or aligned orientations. Nerve guidance conduits containing live SC and SC-based molecular components can promote nerve growth through conduits both in vivo and in vitro [19-22, 34-35]. Here, conduits containing SC topography in various orientations were used to investigate neurite outgrowth. We hypothesized that contact between extending neurites and the underlying topographical cues would guide outgrowth, and consequently that the orientation of SC-based topographical features on the conduit lumen would result in distinct neurite outgrowth and morphological responses. As a complement to the guidance channel experiments and to quantify the specific cell-biomaterial interactions, we also used neurite tracing to analyze neurite directionality on corresponding two-dimensional SC topography replicas adjacent to a DRG explant.

2.5.1. Neurite alignment to SC topography

In the simplest condition, the neurite front within unpatterned conduits extended 1839.81±165.09 μm into the conduits. Within unpatterned conduits, neurites showed relatively limited branching and turning. These growth patterns were correlated with the lack of topographical features and obstructions to linear outgrowth within the conduits. Similarly, uniform outgrowth of neurites on the corresponding unpatterned two-dimensional substrates also suggested neurite outgrowth was not preferentially guided along any particular direction in the absence of topography.

When unoriented SC topography was incorporated in the lumen walls of the random replica conduits, the neurite front extended a similar distance (2102.96±150.95 μm) as the front in unpatterned conduits. In contrast to neurites in the unpatterned conduits, neurite morphology within random conduits was complex. The randomly oriented replica topography presented frequent decision points to navigating neurites, and neurites exhibited a high degree of turning and branching. This turning and branching behavior was generally evenly distributed, as it resulted in an overall uniform growth response of neurites to the random SC topography when presented in the analogous two-dimensional substrates. Of note, the exploration in the conduits of the random SC topography did not inhibit the rate of overall neurite front extension.

A distinctly different response was seen in perpendicular replica conduits, where the neurite front extended the shortest distance to 1121.40±194.88 μm. Sharp neurite turning was often evident, as neurites oriented to the direction of the orthogonal SC replica topography. In this case, neurites not only explored the perpendicular SC topography but appeared to align to the features. This alignment was quantified and confirmed in the direction of the underlying SC topography, in the corresponding two-dimensional substrates. We suggest that this perpendicular neurite alignment

in the direction of the conduit's circumference competed with neurite extension along the conduit's longitudinal axis.

In parallel conduits, whose SC topographical features were oriented to the conduit's long axis, the neurite front extended furthest (2909.13±314.68 μm). Neurite turning and branching were more moderate in the parallel condition, whose oriented SC topography mimics Bands of Büngner, which guide sprouting axons following peripheral nerve injury in vivo [2, 36-37]. Neurites aligned to the SC topography, as confirmed on the analogous two-dimensional substrates. These results suggest that the parallel condition presents multidimensional cues in a cooperative manner; neurite interactions with aligned SC topography enhanced extension along the conduit's longitudinal axis.

In previous studies, neurites have been shown to grow preferentially along the long axis of polypropylene filaments with 25 to 550 μm diameters [38-39]. This bias in outgrowth directionality was enhanced when the filament diameter was decreased to approximate dimensions found in vivo, i.e. less than approximately 100 μm. In the studies presented here, neurites encountered macroscale convex curvature (conduit inner diameter of 1.28±.045 mm) combined with microscale complex curvature (cellular topography of 1-2μm heights). Our results suggest that neurites responded to both types and scales of these topographical cues.

Previous studies have also shown that neurites from DRG explants aligned to oriented PLA nanofibers [40] and to microgrooved PDLA with 10 μm grooves with pre-seeded SC [31]. In the present study, the rate of neurite outgrowth on unpatterned and random SC replica conduits and two-dimensional substrates was over two-fold greater than neurite outgrowth rates in the control conditions of the studies above, i.e. random PLA nanofibers and PDLA without pre-seeded SC.

Neurite outgrowth on parallel SC replica conduits and two-dimensional substrates was over threefold greater than the best conditions documented in those studies [31, 40]. Of note, neurite rates within parallel conduits and on two-dimensional replicas were 27.71% and 33.07% higher than those in random conditions. On highly aligned nanofibers, an increase of 20% was observed compared to randomly oriented nanofibers [40]. These comparisons indicate that neurite outgrowth along the direction of aligned SC replicas is as fast as or faster than that observed by others in the field, although some differences exist among substrates and age of cells tested. Coupled with our observations of neurite alignment on these materials, the influence of SC topography on neurite outgrowth and guidance has been demonstrated in this work.

2.5.2. Interactions of neurons, SC, and SC topography

Using DRG explants that contain SC as well as neurons, this approach has afforded us the opportunity to examine the interactions between migrating SC and extending neurites as they encountered SC replica topography. While SC and neurite arbors were similar to each other regardless of substrate type, the main finding here was that after 2 or 3 days on aligned replicas, the neurite arbor was more strongly aligned than the SC arbor to the underlying replica topography. The intimate dynamics that exist between the migrating SC front and navigating axons have been a topic of much investigation in the quest for enhancement of nerve regeneration [41-42].

Previous studies have shown that following PNS nerve transection and autograft transplantation, regeneration into nerve grafts lacking SC has been shown to be poor [37]. The speed of SC extensions in a similar model limited the speed of axon regeneration, and SC were suggested to function as leaders of regenerating nerves [43]. Studies of nerve regeneration through a guidance channel with an access port for manipulation revealed that in this environment, axons sprouted

quickly but needed close association with SC – whose migration preceded axon growth – in order to grow further [44]. In a sequential nerve crush model, peripheral nerve regrowth was shown to be independent of SC support at early phases after injury, but to depend on SC at later phases [45], thus highlighting the complexity of regenerative dynamics.

Overall, the results of the present study confirm and emphasize the critical role that SC have been shown to play in supporting and directing neurite growth. These results extend those of previous studies by demonstrating close associations of neurites both with live SC and also with SC topography. Our findings that neurite outgrowth exceeded the SC migration front after 2 and 3 days on aligned replica substrates suggest that the underlying SC topography enhanced the growth environment, encouraging neurite outgrowth in the absence of association with live SC, i.e. when it would not otherwise occur. These results are consistent with previous work showing that SC can lead neurites [42-43, 46], and that intact SC basal lamina – likely providing some degree of aligned topography [45] – can contribute to support of nerve regeneration.

2.6. Conclusions and future directions

Based on the studies presented here, we hypothesize that the SC topographical replicas provided a substrate which was favorable to neurite outgrowth, even in the absence of associated SC contact, such that neurite elongation surpassed SC migration distance on aligned replica substrates. This result suggests promise in the use of cellular topographical features as guidance cues to encourage neurite elongation in a directed manner over distances that would otherwise not be possible. Glial-neuronal interactions are quite complex [42, 44, 46-47] and to determine the intimate interactions between SC and neurites as they are guided by underlying cellular topography, in-depth dynamic analysis will be required. Additionally, neurites may be interacting with SC in a complex manner

in which neurites and SC are being directed both by SC replicas and by each other in some capacity.

We have shown that neurite extension was enhanced when DRG were presented with longitudinally oriented SC replicas, both in conduit and two-dimensional geometries. That our substrates encouraged significantly increased outgrowth over controls, and decreased outgrowth with orthogonal presentation of such cues implicates cellular topography as a critical feature for expedient directed neurite outgrowth. Continued research utilizing SC topography will not only shed light on the complex glial-neuronal interactions that occur in vivo, but may inform strategies for nerve repair by determining the optimal topographical features required to support and enhance guided nerve growth to target tissues. To augment these strategies, topographical cell replicas may be combined with other factors such as anisotropic molecular cues and electrical gradients to generate coordinated sets of extracellular cues to promote guidance. Finally, in the future this approach can be extended to replicate other cellular topography in order to study its influence on a variety of cellular behaviors including proliferation, migration, polarization, differentiation, and synapse formation—potentially impacting our understanding of neuronal development and ultimately regeneration.

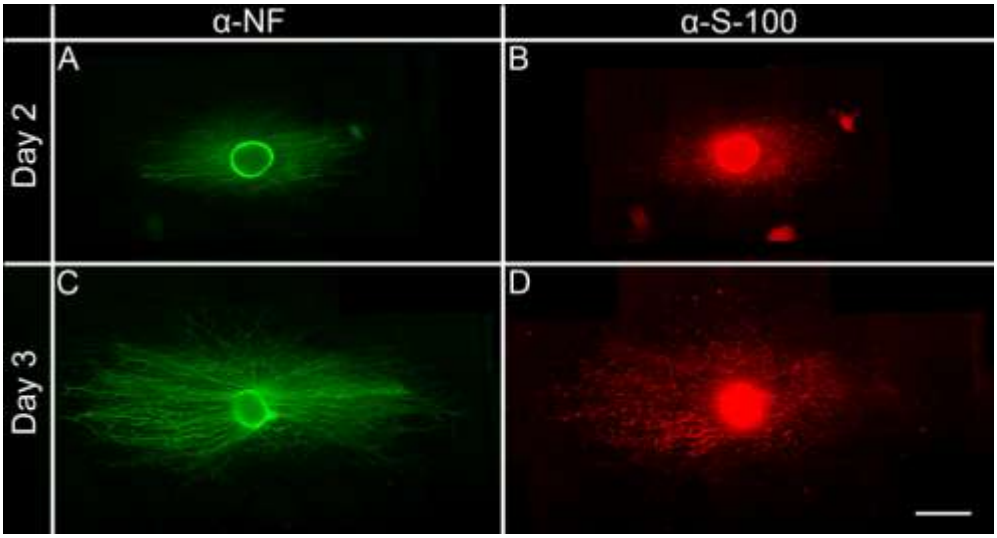

Supplemental Figure 2.1. Neurite outgrowth exceeded SC migration along direction of aligned SC replica at day 2 (A,B) and day 3 (C,D). Corresponding epifluorescent micrographs of DRG explants cultured for 2 (A,B) or 3 (C,D) days on aligned replicas and stained for anti-neurofilament (green; A,C) and anti-S-100 (red; B,D). Scale bar represents 1 mm.

2.7. Acknowledgements

The authors would like to acknowledge Liane Livi, Jennifer Mitchel, and Michael Angelo Santos for their excellent support and helpful discussion about this research. This work was funded by support from the Veterans Administration Center for Regenerative and Restorative Medicine, a VA Rehabilitation Predoctoral Fellowship to JR, and an NSF ADVANCE Career Development Award, Scientific Leadership Award, and R01 EB005722-01 to DHK.

2.8. Literature cited

1. Bunge, R.P., *Tissue-Culture Observations Relevant to the Study of Axon Schwann-Cell Interactions during Peripheral-Nerve Development and Repair.* Journal of Experimental Biology, 1987. **132**: p. 21-34.
2. Bunge, R.P., *The Role of the Schwann-Cell in Trophic Support and Regeneration.* Journal of Neurology, 1994. **242**(1): p. S19-S21.

3. Edgar, J.M. and J. Garbern, *The myelinated axon is dependent on the myelinating cell for support and maintenance: Molecules involved.* Journal of Neuroscience Research, 2004. **76**(5): p. 593-598.

4. Buss, A., et al., *Growth-modulating molecules are associated with invading Schwann cells and not astrocytes in human traumatic spinal cord injury.* Brain, 2007. **130**: p. 940-953.

5. Brook, G.A., et al., *Spontaneous longitudinally orientated axonal regeneration is associated with the Schwann cell framework within the lesion site following spinal cord compression injury of the rat.* Journal of Neuroscience Research, 1998. **53**(1): p. 51-65.

6. Fawcett, J.W. and R.J. Keynes, *Peripheral-Nerve Regeneration.* Annual Review of Neuroscience, 1990. **13**: p. 43-60.

7. Brushart, T.M. and M.M. Mesulam, *Alteration in connections between muscle and anterior horn motoneurons after peripheral nerve repair.* Science, 1980. **208**(4444): p. 603-5.

8. Maeda, T., et al., *Effects of tension at the site of coaptation on recovery of sciatic nerve function after neurorrhaphy: evaluation by walking-track measurement, electrophysiology, histomorphometry, and electron probe X-ray microanalysis.* Microsurgery, 1999. **19**(4): p. 200-7.

9. Miyamoto, Y., *Experimental studies on repair for peripheral nerves. Relationship between circulatory disturbance at nerve stumps caused by tension at suture line and axon regeneration.* Hiroshima Journal of Medical Sciences, 1979. **28**(2): p. 87-93.

10. Nichols, C.M., et al., *Effects of motor versus sensory nerve grafts on peripheral nerve regeneration.* Exp Neurol, 2004. **190**(2): p. 347-55.

11. Mackinnon, S.E. and A.L. Dellon, *A study of nerve regeneration across synthetic (Maxon) and biologic (collagen) nerve conduits for nerve gaps up to 5 cm in the primate.* J Reconstr Microsurg, 1990. **6**(2): p. 117-21.

12. Pfister, L.A., et al., *Nerve conduits and growth factor delivery in peripheral nerve repair.* Journal of the Peripheral Nervous System, 2007. **12**(2): p. 65-82.

13. Evans, G.R., et al., *In vivo evaluation of poly(L-lactic acid) porous conduits for peripheral nerve regeneration.* Biomaterials, 1999. **20**(12): p. 1109-15.

14. Moore, A.M., et al., *Limitations of conduits in peripheral nerve repairs.* Hand (N Y), 2009. **4**(2): p. 180-6.

15. Johnson, E.O. and P.N. Soucacos, *Nerve repair: Experimental and clinical evaluation of biodegradable artificial nerve guides.* Injury-International Journal of the Care of the Injured, 2008. **39**: p. S30-S36.

16. Hazari, A., et al., *A resorbable nerve conduit as an alternative to nerve autograft in nerve gap repair.* Br J Plast Surg, 1999. **52**(8): p. 653-7.

17. Pierucci, A., E.A. de Duek, and A.L. de Oliveira, *Peripheral Nerve Regeneration through Biodegradable Conduits Prepared Using Solvent Evaporation.* Tissue Eng Part A, 2008.

18. Nomura, H., et al., *Extramedullary Chitosan Channels Promote Survival of Transplanted Neural Stem and Progenitor Cells and Create a Tissue Bridge After Complete Spinal Cord Transection.* Tissue Eng Part A, 2008.

19. Evans, G.R.D., et al., *Bioactive poly(L-lactic acid) conduits seeded with Schwann cells for peripheral nerve regeneration.* Biomaterials, 2002. **23**(3): p. 841-848.

20. Rodriguez, F.J., et al., *Nerve guides seeded with autologous Schwann cells improve nerve regeneration.* Experimental Neurology, 2000. **161**(2): p. 571-584.

21. Ansselin, A.D., T. Fink, and D.F. Davey, *Peripheral nerve regeneration through nerve guides seeded with adult Schwann cells.* Neuropathology and Applied Neurobiology, 1997. **23**(5): p. 387-398.

22. Guenard, V., et al., *Syngeneic Schwann-Cells Derived from Adult Nerves Seeded in Semipermeable Guidance Channels Enhance Peripheral-Nerve Regeneration.* Journal of Neuroscience, 1992. **12**(9): p. 3310-3320.

23. Rutkowski, G.E., et al., *Synergistic effects of micropatterned biodegradable conduits and Schwann cells on sciatic nerve regeneration.* J Neural Eng, 2004. **1**(3): p. 151-7.

24. Bruder, J.M., et al., *Fabrication of polymeric replicas of cell surfaces with nanoscale resolution.* Langmuir, 2006. **22**(20): p. 8266-70.

25. Kofron, C.M., V.J. Fong, and D. Hoffman-Kim, *Neurite outgrowth at the interface of 2D and 3D growth environments.* J Neural Eng, 2009. **6**(1): p. 016002.

26. Kofron, C.M. and D. Hoffman-Kim, *Optimization by Response Surface Methodology of Confluent and Aligned Cellular Monolayers for Nerve Guidance.* Cell Mol Bioeng, 2009. **2**(4): p. 554-572.

27. Goldner, J.S., et al., *Neurite bridging across micropatterned grooves.* Biomaterials, 2006. **27**(3): p. 460-72.

28. Thompson, D.M. and H.M. Buettner, *Neurite outgrowth is directed by Schwann cell alignment in the absence of other guidance cues.* Annals of Biomedical Engineering, 2006. **34**(4): p. 669-676.

29. Li, G.N. and D. Hoffman-Kim, *Evaluation of neurite outgrowth anisotropy using a novel application of circular analysis.* J Neurosci Methods, 2008. **174**(2): p. 202-14.

30. Thompson, D.M. and H.M. Buettner, *Oriented Schwann cell monolayers for directed neurite outgrowth.* Annals of Biomedical Engineering, 2004. **32**(8): p. 1120-1130.

31. Miller, C., S. Jeftinija, and S. Mallapragada, *Micropatterned Schwann cell-seeded biodegradable polymer substrates significantly enhance neurite alignment and outgrowth.* Tissue Engineering, 2001. **7**(6): p. 705-715.

32. Schmalenberg, K.E. and K.E. Uhrich, *Micropatterned polymer substrates control alignment of proliferating Schwann cells to direct neuronal regeneration.* Biomaterials, 2005. **26**(12): p. 1423-1430.

33. Bruder, J.M., A.P. Lee, and D. Hoffman-Kim, *Biomimetic materials replicating Schwann cell topography enhance neuronal adhesion and neurite alignment in vitro.* J Biomater Sci Polym Ed, 2007. **18**(8): p. 967-82.

34. Kim, S.M., S.K. Lee, and J.H. Lee, *Peripheral nerve regeneration using a three dimensionally cultured Schwann cell conduit.* Journal of Craniofacial Surgery, 2007. **18**(3): p. 475-488.

35. Hadlock, T., et al., *A polymer foam conduit seeded with Schwann cells promotes guided peripheral nerve regeneration.* Tissue Engineering, 2000. **6**(2): p. 119-127.

36. Bixby, J.L., J. Lilien, and L.F. Reichardt, *Identification of the major proteins that promote neuronal process outgrowth on Schwann cells in vitro.* J Cell Biol, 1988. **107**(1): p. 353-61.

37. Hall, S.M., *Regeneration in cellular and acellular autografts in the peripheral nervous system.* Neuropathol Appl Neurobiol, 1986. **12**(1): p. 27-46.

38. Smeal, R.M. and P.A. Tresco, *The influence of substrate curvature on neurite outgrowth is cell type dependent.* Exp Neurol, 2008. **213**(2): p. 281-92.

39. Smeal, R.M., et al., *Substrate curvature influences the direction of nerve outgrowth.* Ann Biomed Eng, 2005. **33**(3): p. 376-82.

40. Corey, J.M., et al., *Aligned electrospun nanofibers specify the direction of dorsal root ganglia neurite growth.* Journal of Biomedical Materials Research Part A, 2007. **83A**(3): p. 636-645.

41. Bhatheja, K. and J. Field, *Schwann cells: origins and role in axonal maintenance and regeneration.* Int J Biochem Cell Biol, 2006. **38**(12): p. 1995-9.

42. McDonald, D., et al., *Early events of peripheral nerve regeneration.* Neuron Glia Biol, 2006. **2**(2): p. 139-47.

43. Son, Y.J. and W.J. Thompson, *Schwann cell processes guide regeneration of peripheral axons.* Neuron, 1995. **14**(1): p. 125-32.

44. Chen, Y.Y., et al., *Axon and Schwann cell partnership during nerve regrowth.* J Neuropathol Exp Neurol, 2005. **64**(7): p. 613-22.

45. Bajrovic, F., M. Srpcic, and J. Sketelj, *Schwann cell dependence of regenerating rat sensory neurons is inversely related to the quality of axon growth substratum.* J Neuropathol Exp Neurol, 2001. **60**(1): p. 65-74.

46. Corfas, G., et al., *Mechanisms and roles of axon-Schwann cell interactions.* J Neurosci, 2004. **24**(42): p. 9250-60.

47. Popovic, M., M. Bresjanac, and J. Sketelj, *Role of axon-deprived Schwann cells in perineurial regeneration in the rat sciatic nerve.* Neuropathol Appl Neurobiol, 2000. **26**(3): p. 221-31.

CHAPTER 3

COOPERATIVE AND COMPETING COMBINATIONS OF SCHWANN CELL TOPOGRAPHY AND MICROPATTERNED LAMININ INFLUENCE NEURITE GROWTH

J A Richardson*, C Kofron PhD*, C Johnson, J Mitchel, D Chau, J Bruder, D Hoffman-Kim, PhD

***** denotes equal contribution

3.1. Abstract

To inform strategies for nerve repair, neurite response to multiple cues must be determined such that additive and hierarchical neurite response to simultaneous cooperative or conflicting cues may be established. Here, neurite alignment was determined in response to micropatterned laminin (LN) stripes and isolated Schwann cell (SC) topographical cues presented individually,

together in parallel, or orthogonally opposed. Neurite alignment to individual cues was used to pair similar and disparate LN and SC topography cues cooperatively and competitively. Neurites aligned to individually presented LN and SC topography cues. On cooperative cue platforms, neurite alignment was enhanced compared to alignment to individual cues when alignment to individual cues was not maximal. On competitive platforms where neurites were expected to align similarly to each cue, neurite alignment was preferential to one cue. On competitive platforms where neurites were expected to align with greater strength to one cue, the disparity in alignment strength was stronger than expected. These findings demonstrate that neurite alignment to individual guidance cues depends on cue type and dimensions, and that cooperative combinations of directive cues may have an additive effect on alignment response. Additionally, expected similarities and differences in neurite alignment to either cue did not correspond with observed neurite response to competing cues. This suggests that neurite response to individual cues cannot be integrated to infer response to combined cues. Rather, systematic presentation of multiple cues to neurites should be pursued to understand nerve growth decisions and optimally design biomaterials for nerve guidance and repair.

3.2. Introduction

To generate the body's intricate neuronal networks, neurons extend axons along directed paths and connect with appropriate target cells to form synapses. As they navigate, neurons integrate and interpret a variety of cues, including electrical signals from neighboring cells, substrate-bound and diffusible biochemical factors, and physical features of the surrounding cells and extracellular matrix (ECM). Neurons may encounter complex environments at many points – for example, during development; post-injury, during degeneration, glial scar formation, and regeneration; and in the context of transplanted cells or materials. An understanding of how

neurons make growth decisions that incorporate rich combinations of cues can inform strategies to influence neuronal growth in many contexts.

Biochemical cues and topographical cues have been shown individually to influence neurite outgrowth, and are often presented as single lines or parallel stripes[1-4]. Neurites align *in vitro* on tracks of laminin (LN), an adhesive and growth-promoting ECM glycoprotein present in developing and regenerating axon tracts[2, 4-9]. Neurites also orient to microfabricated topographical features, including oriented fibers[10-11], plateaus and grooves[12], and cellular topographies[13-14]. Effective feature sizes range from nanometers to micrometers, similar to the dimensions of features presented by cells and ECM *in vivo*[12, 15-16]. Neurites show directed outgrowth on isolated Schwann cell (SC) topographical features, presenting geometries relevant to the *in vivo* environment[13-14, 17].

Several studies have presented growing neurons simultaneously with multiple cues, including physical, electrical, soluble, and substrate-bound[18-23]. Neurites provided with parallel biochemical and topographical cues have typically shown enhanced growth responses. Neurites provided with orthogonal cues have preferred one cue, but an understanding of the hierarchy of neurite responses to specific cue types has not yet been obtained.

Here we undertook a systematic study of neurite response to multiple cues, employing tailored biomaterial platforms to present defined environments to navigating neurons. First, we determined neurite alignment to aligned SC topographical features and to LN micropatterns with a range of concentrations and dimensions. We then evaluated neurite alignment to combinations of LN micropatterns and SC topography presented in parallel and orthogonal orientations. Once we assessed the relative strength of neurite alignment to defined LN micropatterns and aligned

SC topography, we discuss the correlation between these relative strengths of neurite alignment to individual cues to some of the unexpected neurite alignment responses to multiple cues.

3.3. Materials and Methods

3.3.1. Generation of biomimetic materials presenting SC topography

Biomimetic materials presenting aligned SC topographies were generated as previously described[17]. Briefly, photolithography and soft lithography were used to make poly (dimethylsiloxane) (PDMS) (Dow Corning, Midland, MI, USA) stamps with repeating micron-scaled grooves and plateaus. These patterns were then used to transfer LN protein patterns to glass via micro-contact printing. SCs from adult rat sciatic nerve, a generous gift of Dr. Mary Bunge (University of Miami, Coral Gables, FL, USA), were cultured on the protein patterns and aligned parallel to the protein stripes in Dulbecco's modified eagle's medium (DMEM) (Invitrogen Life Technologies, Carlsbad, CA, USA) with 10% fetal bovine serum (FBS) (Invitrogen), 4 mM L-glutamine (Invitrogen), 100 U/ml penicillin (Invitrogen), and 100 µg/ml streptomycin (Invitrogen) supplemented with 2 µM forskolin (Sigma, St. Louis, MO, USA), 10 µg/ml bovine pituitary extract (Sigma), and 2 µM heregulin (generous gift from Genentech, Vacaville, CA, USA). Cultures were incubated at 37°C with 5% CO_2 in a humidified environment. The cells were fixed at confluence, and PDMS was used to make an impression mold of the cells[24]. A second layer of PDMS was cast from the impression mold to form a relief replica presenting aligned SC topography with micro- and nano-scale resolution of features.

3.3.2. Generation of platforms for neuron guidance

Four different single- or double-cue platforms were generated: (1) a SC replica fully coated with LN (single topographical cue), (2) flat PDMS patterned with LN (single protein cue), (3) a SC replica with LN patterned parallel to the underlying topography (cooperative cues), or (4) a SC

replica with LN patterned orthogonal to the underlying topography (competitive cues) (Figure 3.1). LN concentration, pattern geometry, and pattern dimensions were varied (summarized in Table 3.1). Mouse LN (Invitrogen) was tested at 10 µg/ml (LN_{low}) and 50 µg/ml (LN_{high}). Flat PDMS fully coated with LN was a control. On substrates with a full LN coat, the LN was suspended in Hank's balanced salt solution (HBSS) (Invitrogen), deposited on a plasma-activated PDMS substrate, and allowed to adsorb to the surface for at least 1 h. Before cell plating, the excess LN solution was removed, and the substrate was rinsed with distilled water.

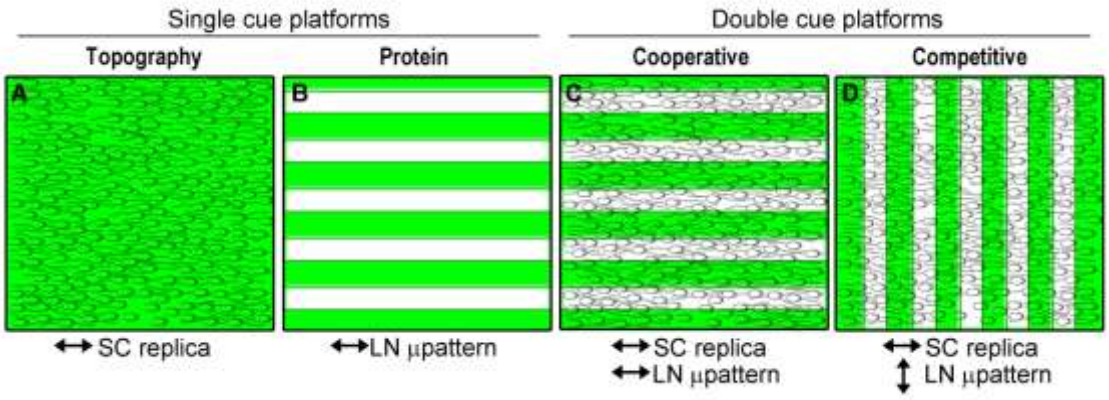

Figure 3.1. Cartoon of single cue and double cue platforms investigated. Single cue platforms presented SC topographical replicas (A) or micropatterned LN stripes (B). Double cue platforms presented micropatterned LN stripes on aligned SC replica topography, with either cooperative (C) or competing (D) orientation. Arrows indicate cue directions. Control substrates were fully coated with LN (not depicted).

		LN concentration *Low = 10μg/ml High = 50μg/ml*	LN micropattern *stripe (μm)-space (μm)*	Topographical cue	n
	Controls	Low	-	flat	68
		High	-	flat	51
Single cue	SC replica topography	Low	-	SC replica	40
		High	-	SC replica	45
	LN micropattern	Low	50-10	flat	39
		Low	500-50	flat	55
		Low	50-50	flat	30
		High	50-50	flat	46
Double cue	Cooperative platforms	Low	50-10	SC replica	40
		Low	500-50	SC replica	36
		Low	50-50	SC replica	30
		High	50-50	SC replica	39
	Competitive platforms	Low	50-10	SC replica	39
		Low	500-50	SC replica	40
		Low	50-50	SC replica	40
		High	50-50	SC replica	43

Table 3.1. Overview of control and experimental platforms investigated. n = number of fields of view analyzed for each condition.

LN was micropatterned in repeating stripes separated by spaces of defined widths. LN micropatterns were transferred to the PDMS substrates via micro-contact printing. PDMS stamps were coated with approximately 200 µl of the appropriate LN solution in HBSS for at least 1 h. Excess protein was removed, and the stamps were rinsed with distilled water and dried with a pressurized air stream. The stamps were then inverted onto plasma-activated flat or SC replica PDMS to transfer the LN pattern for cell culture. Light pressure was applied to the back of the stamps to ensure even contact and LN transfer. Stamps were left in contact for at least 1 h and peeled off directly before cell culture.

3.3.3. Study of dorsal root ganglia alignment

NIH guidelines for the care and use of laboratory animals (NIH Publication #85-23 Rev. 1985) have been observed. Dorsal root ganglia (DRG) explants were dissected from the spinal cords of postnatal rat pups (P0-P4). The explants were cleaned of any blood, axons, or connective tissue, incubated in 0.05% trypsin-EDTA (Invitrogen) in HBSS for 45 minutes, and dissociated by trituration. Dissociated DRG cells were cultured at 37°C and 5% CO_2 in DMEM with 10% FBS, 4 mM L-glutamine, 100 U/ml penicillin and 100 μg/ml streptomycin supplemented with 50 ng/ml nerve growth factor (Invitrogen). Cells were plated at 200,000 cells/well in a standard 12-well tissue culture plate and cultured for 5 days. DRG cells were fixed with 2% parafomaldehyde (Electron Microscopy Sciences, Hatfield, PA, USA) in phosphate buffered saline (PBS) (Invitrogen) for 15-20 min and then rinsed 3 times with PBS. Cell nuclei were stained with 1% 4,6-diamidino-phenylindole (DAPI; Sigma) and 0.1% Triton-X (VWR International, West Chester, PA, USA) in PBS. Neurites were labeled with anti-β(III)tubulin (1:500) primary antibody (Covance Research Products, Inc., Berkeley, CA, USA) and Cy3 conjugated goat anti-mouse secondary antibody (1:200) (Jackson). LN was labeled with rabbit anti-LN (1:200) primary antibody (Biomedical Technologies, Stoughton, MA, USA) and Cy2 conjugated goat anti-rabbit (1:200) secondary antibody (Jackson). Non-specific labeling was blocked by incubating samples with 10% normal goat serum (Jackson) and 0.1% Triton-X in PBS for 60 minutes. Samples were then incubated with the first primary antibody overnight at 4°C and rinsed with PBS. Next, samples were incubated with the second primary antibody overnight at 4°C and rinsed. Finally, samples were incubated with the first secondary antibody for 1 h at room temperature, incubated with the second secondary antibody for 1 h at room temperature, and rinsed 3 times with PBS. During and after this step, the samples were protected from light with aluminum foil. Wells without primary antibodies and wells with cross-matched primary and secondary antibodies were kept as controls.

3.3.4. Microscopy and analysis

Phase contrast and fluorescent images were captured with a Nikon Eclipse TE2000-S microscope at 100X, and outputted to OpenLab v4.0.4 (Improvision, Lexington, MA, USA). At least 10 fields of view (FOV) with the corresponding channels for phase, DAPI, protein, and neurite staining were captured for each sample.

3.3.5. Quantification of neurite orientation

Neurites were traced and analyzed using Neurient, an automated, open-source, custom, Matlab-based software toolset developed by our lab[25]. Briefly, the method uses aspects of exploratory vector tracking, described previously[26-27] combined with global processing of the images, and was designed to be appropriate for analysis of highly confluent, dense neurite images. The algorithm was performed in three phases: (1) generation of a directional lookup table; (2) generation of seed points; (3) exploratory vector tracing of the images. Following this process, traced coordinates were obtained for each image, consisting of the location and angle of short line segements corresponding to neurites from the input image.

Phase I, or generation of the directional lookup table, consisted of two aspects. Resulting from this step was a dataset with dimensions $LxWxN_\theta$, where L and W are the length and width, in pixels, of the original image, and N_θ was a user-determined parameter specifying the number of discrete angles desired by the user. Here, N_θ was set to 36, giving us an angular precision of delta $\theta=10°$. In the first step of Phase I, the images were blurred slightly using a rotation Fourier transform-based method in order to reduce potential bias at the cardinal angles due to losses in the image rotation process. In the second step, each layer of the directional lookup table was generated in the following manner: images were rotated by each possible multiple of $\Delta\theta°$, cross-

correlated with a double edge detection kernel, and rotated back to their original orientation. This processed a LxW dataset where edges at each location were represented by high values, and was performed for each possible value of θ.

Phase II, or generation of seed points, was performed based on previously described methods[28]. In order to identify structures in the images which were neurites that should be traced, a set of initial seed points was generated, defined as points on or near the centerline of neurite segments. The seed point detection method found local maxima along a set of grid lines. We considered M vertical and N horizontal lines, spaced γ pixels apart. The grid lines were low-pass filtered using a one-dimensional Gaussian kernel approximation in order to remove high frequency noise. In order to find the local maxima, a threshold was determined according to the image brightness, defined by the formula $\Gamma = \gamma + \sigma/2$, where γ is the median pixel intensity, σ is the standard deviation around the median. Local maxima along the grid lines were considered if they had intensity values equal to or greater than Γ, with at most one maximum found in each γ-pixel length segement of the grid.

Phase III consisted of the tracing algorithm, which utilized both the directional lookup table and the seed points. The following process was repeated for each seed point: For a given seed point, an initial direction was chosen by indexing into the kernel response lookup table at the point's coordinates and determining the direction corresponding to the maximum kernel response. The trace vector was stepped forward 3 pixels in this direction and the location of the tip of this line segment was set as the new point. The process repeated and the current point was used to index into the kernel response lookup table, this time with the additional criteria that the only available directions are within 90° of the previous direction, ensuring the traces continued forward along a given neurite. Traces were terminated if the following criteria were met: if the trace is no longer

following a neurite, is too close to the edge of the image, or is within a part of the image has already been traced.

Traced images were used to determine alignment relative to topographical and protein cues. For each image, the angles of the line segments corresponding to traced neurites were analyzed for alignment information. These angles had a resolution of $\Delta\ \theta = 10°$ as specified above. For each image, alignment relative to horizontal and vertical cues was determined by calculating the percentage of line segments aligned to with +/- 20° of the horizontal and vertical axes, respectively. At least 30 images were analyzed for each condition.

3.3.6. Statistical analysis

One-way analysis of variance (ANOVA) tests were performed on percent neurite alignment . Post hoc multiple comparison analyses were performed using Tukey's test. A P-value of 0.05 was taken to be significant.

3.4. Results

3.4.1. Single cue and double cue platforms presenting topographical and protein cues were fabricated.

We utilized the versatility of the microcontact printing technique in conjunction with PDMS replicas of aligned SC topography to present single, cooperative, and competitive cues to DRG neurons (Fig.3.1). LN micropatterns can be adsorbed to plasma-activated PDMS surfaces easily and reproducibly. Flat PDMS and PDMS presenting aligned SC topography were coated or microcontact printed with LN at 10 μg/ml (LN_{low}) or 50 μg/ml (LN_{high}). For single cue platforms presenting topographical cues, SC replicas were fully coated with LN (Fig. 3.1A). For single cue platforms presenting protein cues, flat PDMS substrates were microcontact printed with LN

stripes (Fig. 3.1B). For double cue cooperative platforms, LN stripes were microcontact printed parallel to aligned SC replica topography (Fig. 3.1C; Fig. 3.2A,B). For double cue competitive platforms, LN stripes were microcontact printed orthogonal to aligned SC replica topography (Fig. 3.1D; Fig. 3.2C,D). Immunofluorescence confirmed that on double cue platforms, LN stripes appeared continuous and uninterrupted by the topography (Fig. 3.2B,D), and the topographical features were unaffected by the microcontact printing (Fig. 3.2A,C). Fully coated, flat PDMS served as a control. Specifications of each platform are presented in Table 3.1.

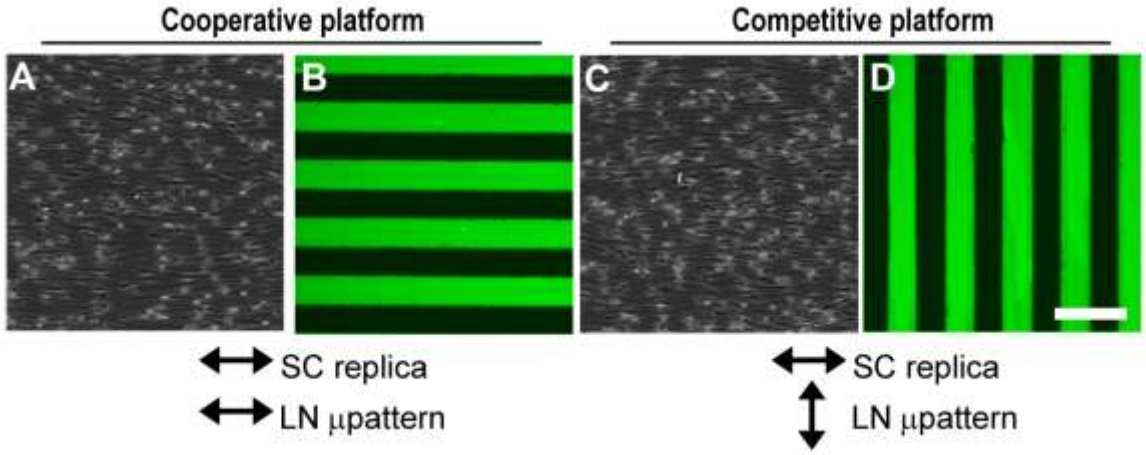

Figure 3.2. Corresponding fields of view of cooperative cue (A-B) and competing cue (C-D) platforms demonstrate independence of orientation of topographical (A,C) and LN cues (B,D). A,C. Phase contrast micrographs. B,D. Fluorescent micrographs showing immunofluorescence for anti-LN. Scale bar, 100μm.

3.4.2. Neurite alignment on single cue platforms depended on underlying cue type and dimensions.

Fluorescent micrographs of neurites positive for anti-β-III tubulin show neurite orientation on all experimental platforms (Fig.3.3). Neurite alignment for all substrate types was quantified and plotted as circular histograms, where the angles of neurite segments were grouped into 10° bins (Fig.3.4). Quantification of neurite alignment to the horizontal and vertical directions for all

substrates is shown in Figure 3.5, where black bars represent neurite alignment to the horizontal direction and gray bars represent neurite alignment to the vertical direction.

CONTROLS
SINGLE CUE PLATFORMS
A
Low
B
High
C
Low/50-10
D
High/SC replica
SINGLE CUE PLATFORMS
E
Low/SC replica
F
Low/500-50
G
Low/50-50
H
High/50-50

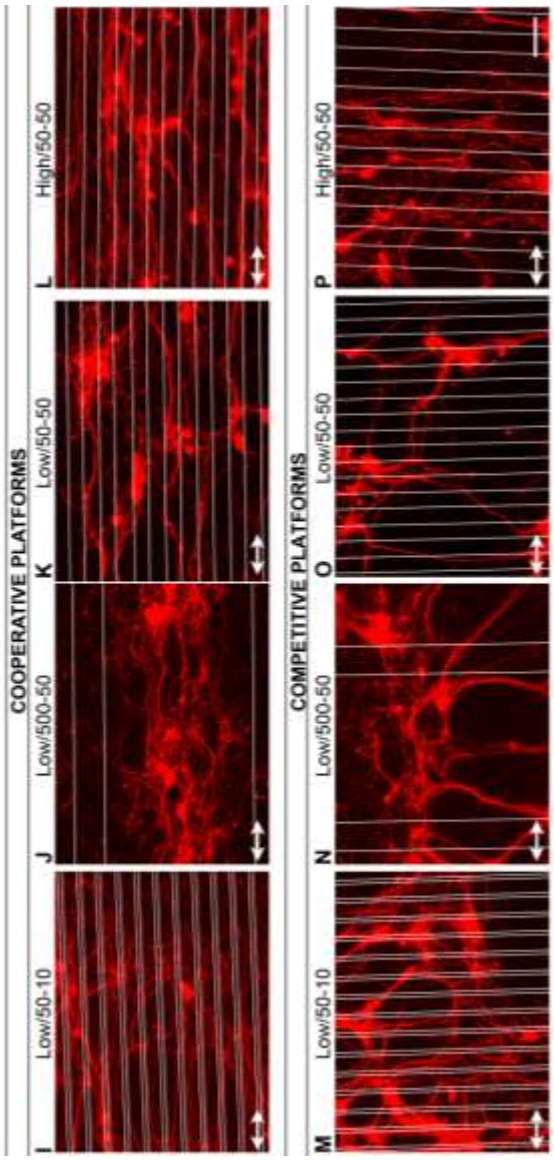

Figure 3.3. DRG neurites responded to underlying directive cues on single, cooperative, and competing cue platforms. Text above images indicates LN concentration (Low=10 μg/ml; High=50 μg/ml) and LN micropattern (stripe width-space width in μm) when applicable. Fluorescent micrographs show neurites positive for anti-β-III tubulin. White lines indicate borders of micropatterned LN stripes. Horizontal white arrows indicate the direction of the underlying SC replica topographical cue. Scale bar, 100μm.

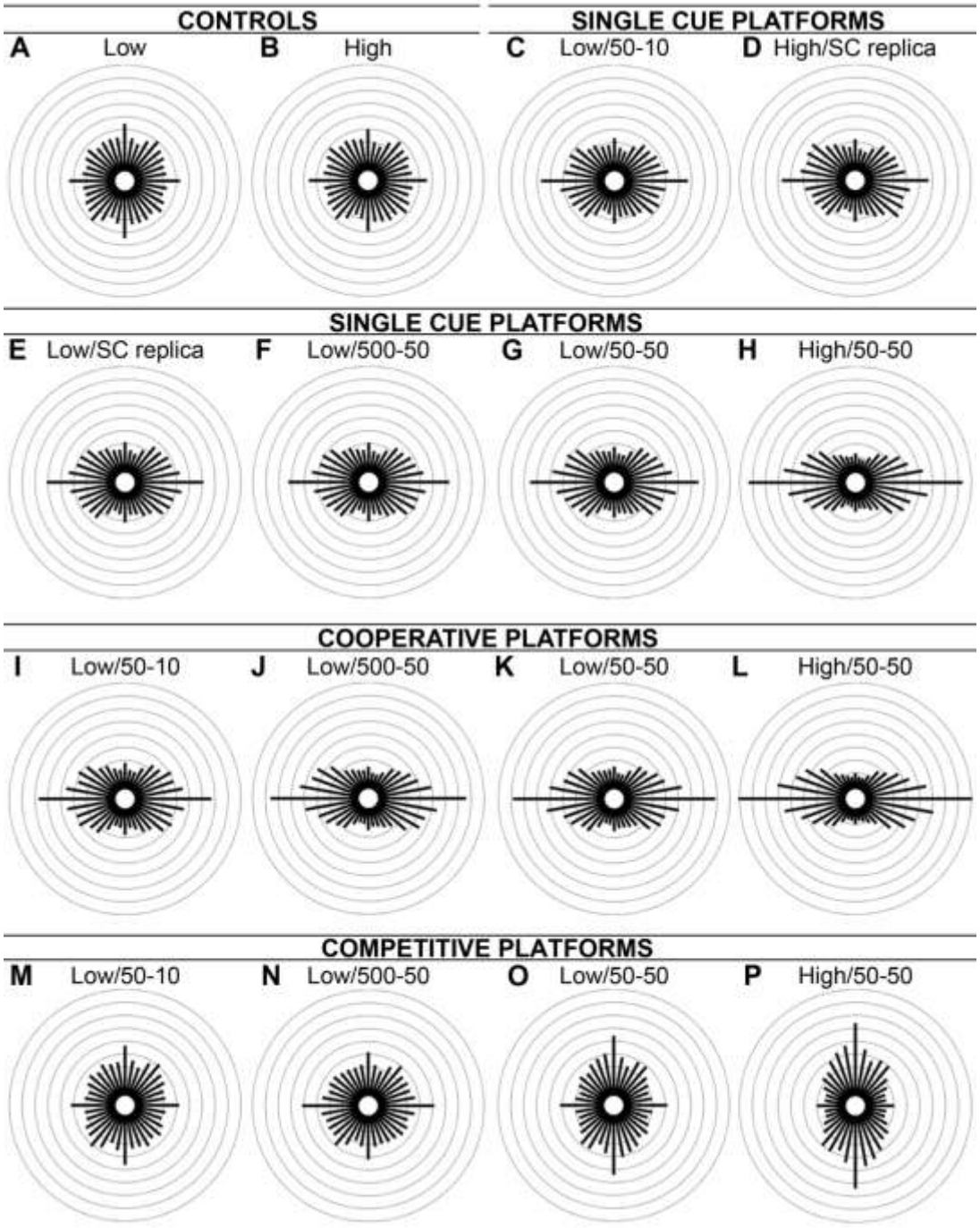

Figure 3.4. DRG neurite response to directive cues depicted in Figure 3.3 is shown quantitatively on circular histograms. The angles of traced neurite segments, modulo 180°, were grouped into 10° bins and plotted on a circular axis. The length of each bar is proportional to the percentage of the total neurite segments at the corresponding angle. Each reference circle represents 1% of the total neurite segments, with the outermost circle at 9%. A,B. Neurite orientation on control substrates is uniformly distributed. C-L. Neurite orientation on single and cooperative cue platforms is aligned horizontally in the direction of the cue(s). M-P. Neurite orientation on competitive cue platforms is complex (see text for details).

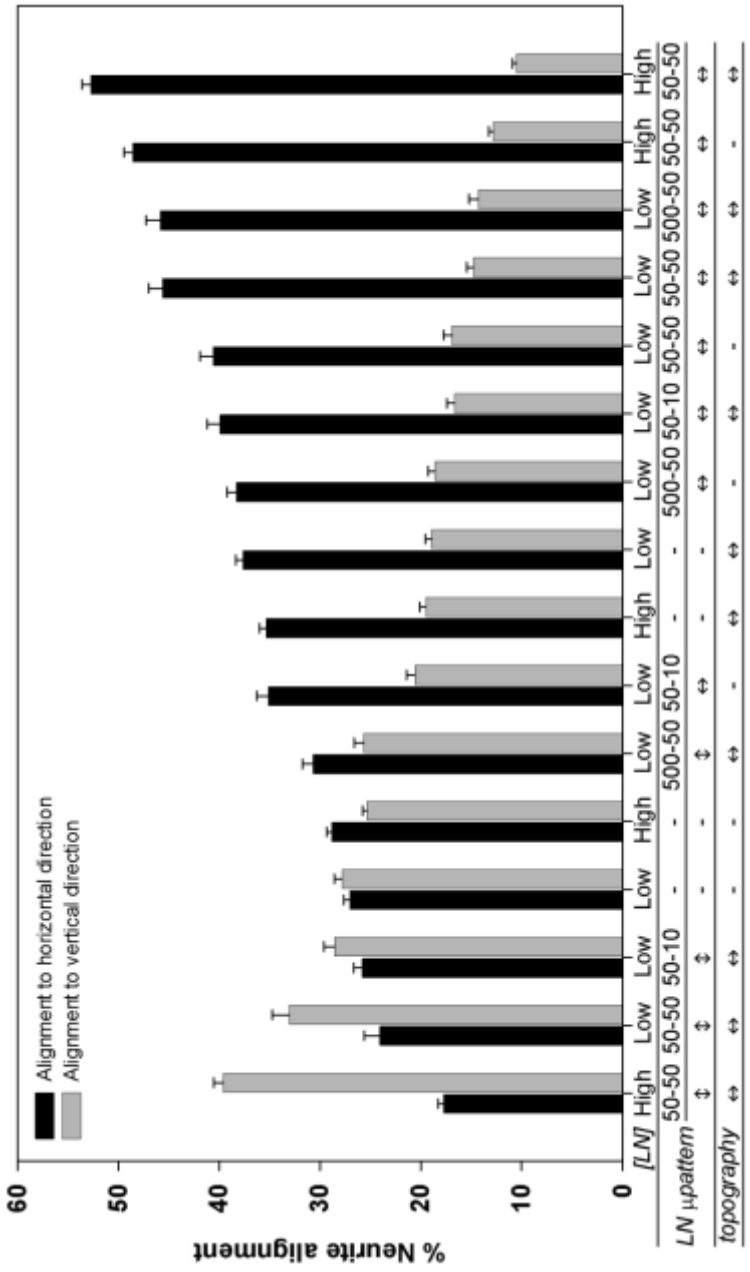

Figure 3.5. Single, cooperative, and competitive cue platforms. Graph of percent neurite alignment to horizontal (black) and vertical (gray) directions for each condition investigated. Platform LN concentration, micropattern dimensions, and topographical cues are noted below graph. Percent neurite alignment was calculated within $\pm$20 degrees of each axis. Statistical differences within and among conditions are depicted in Figures 6-8. Arrows indicate cue directions. Error bars are SEM.

When DRGs were cultured on flat PDMS controls fully coated with LN_{low} or LN_{high}, neurites exhibited random outgrowth (Fig. 3.3A,B; Fig. 3.4A,B). 27.0±0.6% and 28.9±0.5% of neurites were aligned to an arbitrarily defined horizontal direction on fully coated LN_{low} and LN_{high} controls, respectively. These observed values are consistent with the theoretical 27.8% neurite alignment to the horizontal direction when neurites are uniformly distributed.

When DRGs were cultured on single cue platforms presenting either microcontact printed LN stripes or aligned SC topographical replicas, neurites aligned in the direction of the underlying single cue (Fig. 3.3C-H; Fig. 3.4C-H). Neurites appeared most aligned on substrates where 50 μm wide LN stripes were separated by 50 μm wide spaces, presenting either LN_{low} (Fig. 3.3G; Fig. 3.4G) or LN_{high} (Fig. 3.3H; Fig. 3.4H). Quantitative analysis (Fig. 3.5, 3.6) showed that when DRGs were cultured on 50 μm wide stripes of LN_{low} separated by 10 μm spaces, 35.1±1.1% of neurites aligned in the direction of the stripes. When DRGs were cultured on aligned SC topographical replicas uniformly coated with LN_{high}, 35.3±0.7% of neurites aligned in the direction of the topography. When DRGs were cultured on aligned SC topographical replicas uniformly coated with LN_{low}, 37.6±0.8% of neurites aligned in the direction of topography. When DRGs were cultured on 500 μm wide stripes of LN_{low} separated by 50 μm spaces, 38.3±0.9% of neurites aligned in the direction of the stripes. When DRGs were cultured on 50 μm wide stripes of LN_{low} separated by 50 μm spaces, 40.6±1.3% of neurites aligned in the direction of the stripes. Neurite alignment on this single cue platform was significantly greater than alignment to 50 μm wide stripes of LN_{low} separated by 10 μm spaces, and significantly greater than alignment to aligned SC topographical replicas uniformly coated with LN_{high} (Fig. 3.6; $P<0.05$, ANOVA). When DRGs were cultured on 50 μm wide stripes of LN_{high} separated by 50 μm spaces, 48.6±0.9% of neurites aligned in the direction of the stripes. Neurite alignment on this single cue platform was significantly greater than on all other single cue conditions examined. ($P<0.001$,

ANOVA). Neurite alignment on all single cue platforms was significantly greater than average neurite alignment to an arbitrarily defined horizontal direction on control platforms (Fig.3.6 dashed line; P<0.05, ANOVA).

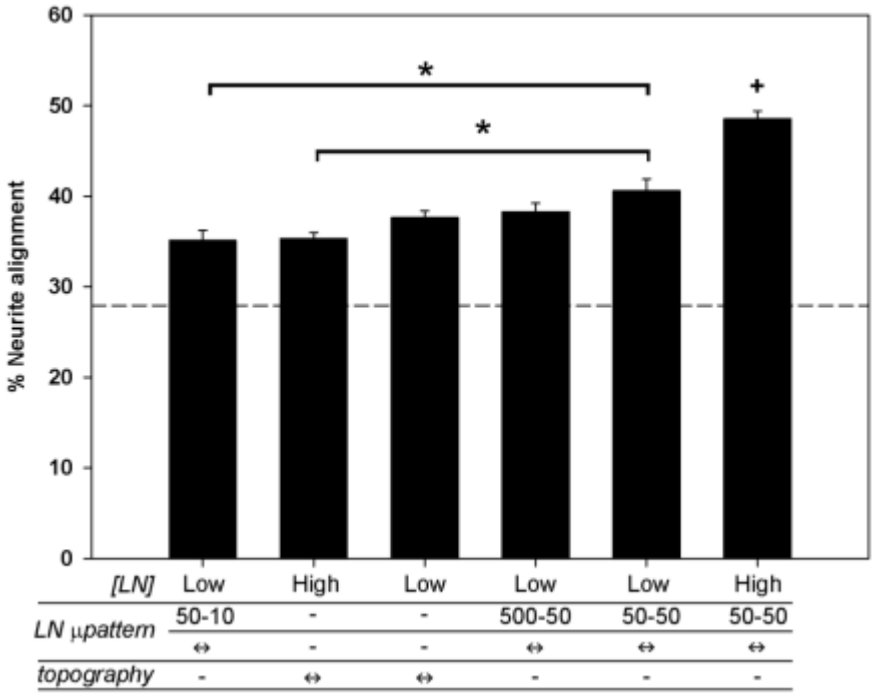

Figure 3.6. Single cue platforms. Neurites aligned to cues on single cue platforms. Graph of percent neurite alignment to cues. There was significantly greater neurite alignment on all conditions compared to control substrates (P<0.05, one way ANOVA). Dashed horizontal line indicates average alignment to an arbitrarily defined horizontal direction on control substrates. Percent neurite alignment was calculated within $\pm$20 degrees of each axis. Arrows indicate cue directions. +P<0.05 significantly greater than all other conditions; *P<0.05 significantly different by one way ANOVA assuming equal variance and Bonferroni's posthoc analysis; error bars are SEM.

3.4.3. Neurite alignment on cooperative cue platforms was enhanced along cue direction and correlated with relative strength of individual LN cues.

When DRGs were cultured on cooperative cue platforms presenting simultaneous microcontact printed LN stripes in parallel with aligned SC topographical replicas, neurites aligned in the

direction of the cooperative cues (Fig.3.3I-L; Fig.3.4I-L). Percent neurite alignment to cooperative anisotropic cues was quantified (Fig.3.5, Fig.3.7). Neurite alignment on platforms with 50 μm wide stripes of LN_{low} separated by 10 μm spaces was 39.9±1.6% when the protein cue was presented cooperatively with the aligned SC topographical replica, and was significantly higher than 35.1±1.1% alignment when the protein cue was presented singly (Fig.3.7; 13.6% increase, $P<0.05$, ANOVA). Neurite alignment on platforms with 500 μm wide stripes of LN_{low} separated by 50 μm spaces was 45.8±1.4% when the protein cue was presented cooperatively with the aligned SC topographical replica, and was significantly higher than 38.3±0.9% alignment when the protein cue was presented singly (19.7% increase, $P<0.001$ ANOVA). Neurite alignment on platforms with 50 μm wide stripes of LN_{low} separated by 50 μm spaces was 45.6±1.3% when the protein cue was presented cooperatively with the aligned SC topographical replica, and was higher than 40.6±1.3% alignment when the protein cue was presented singly (12.5% increase). Neurite alignment on platforms with 50 μm wide stripes of LN_{high} separated by 50 μm spaces was 52.7±0.9% when the protein cue was presented cooperatively with aligned SC topographical replica, and was higher than 48.6±0.9% alignment when the protein cue was presented singly (8.6% increase).

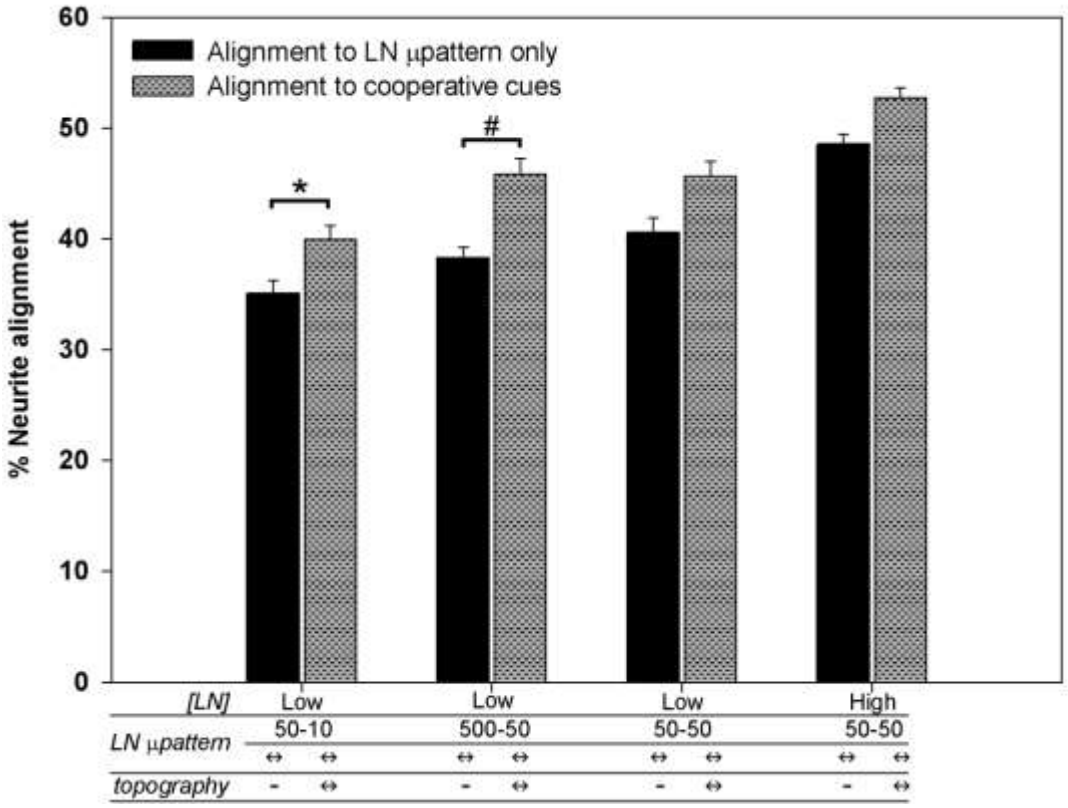

Figure 3.7. Cooperative cue platforms. Neurite alignment to cue direction was enhanced on cooperative cue platforms. Graph of percent neurite alignment on single-cue platforms presenting micropatterned LN (black bars) and percent neurite alignment on cooperative double-cue platforms presenting SC replica topography and micropatterned LN (gray bars). Percent neurite alignment was calculated within $\pm$20 degrees of each axis. Arrows indicate cue directions. *P<0.05; #P<0.001 by Student's t-test; error bars are SEM.

3.4.4. Neurite morphology on competing cue platforms was complex and depended on underlying cue combinations.

When DRGs were cultured on competitive cue platforms presenting simultaneous microcontact printed LN stripes perpendicular to the direction of aligned SC topographical replicas, neurites exhibited complex outgrowth responses (Fig.3.3M-P; Fig.3.4M-P). Neurite alignment to the LN stripes was compared to neurite alignment to the SC perpendicular topographical replica on competing cue platforms (Fig.3.8). On competing cue platforms with 50 μm wide stripes of LN_{low}

separated by 10 μm spaces, neurite alignment to the LN stripes was 28.6±1.1%, and was significantly higher than 25.8±0.9% alignment to the SC replica topography ($P<0.05$, Student's t-test). On competing cue platforms with 500 μm wide stripes of LN_{low} separated by 50 μm spaces, neurite alignment to the LN stripes was 25.6±1.0%, and was significantly lower than 30.7±1.1% alignment to the SC replica topography ($P<0.001$, Student's t-test). On competing cue platforms with 50 μm wide stripes of LN_{low} separated by 50 μm spaces, neurite alignment to the LN stripes was 33.1±1.7%, and was significantly higher than 24.1±1.5% alignment to the SC replica topography ($P<0.001$, Student's t-test). On competing cue platforms with 50 μm wide stripes of LN_{high} separated by 50 μm spaces, neurite alignment to the LN stripes was 39.6±0.9%, and was significantly higher than 17.7±0.6% alignment to the SC replica topography ($P<0.0001$, Student's t-test).

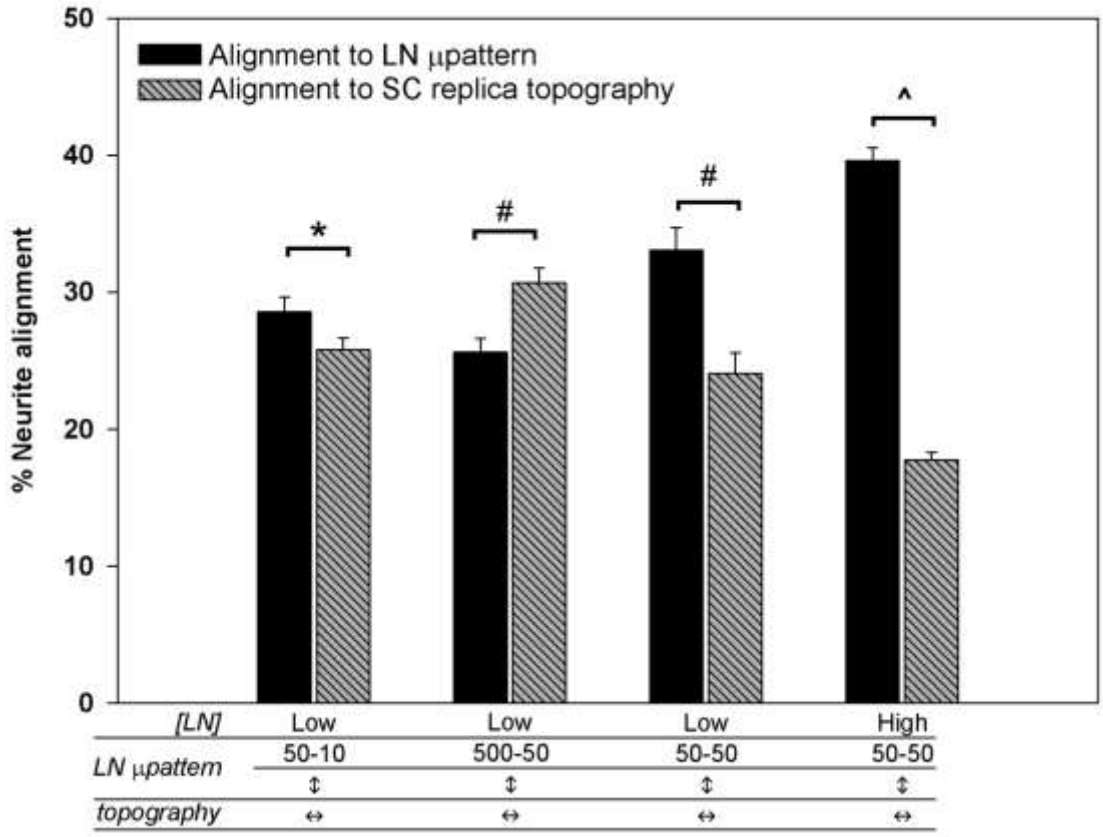

Figure 3.8. Competitive cue platforms. Cue preference was complex on competing double cue platforms presenting micropatterned LN orthogonal to SC replica topography. Graph of percent neurite alignment to simultaneously presented LN micropattern (black bars) and SC replica topography (gray bars) on competing cue platforms. Percent neurite alignment was calculated within ±20 degrees of each axis. Arrows indicate cue directions. *P<0.05, #P<0.001, ^P<0.0001 by Student's t-test; error bars are SEM.

3.4.5. Neurite alignment on competing cue platforms did not always correlate with neurite alignment to constituent single cues

To determine whether neurite alignment to single cues correlated with neurite response on competitive platforms where those cues were presented orthogonally, neurite alignment to SC replica topography and LN stripes on competitive cue platforms was compared with neurite alignment to the individual cues comprising the competitive cue platforms. Table 3.2 compares neurite preference when presented with single topographical (Fig.3.1A) or micropatterned LN

(Fig.3.1B) cues and when presented with simultaneous, orthogonal topographical and micropatterned LN cues on competing cue platforms (Fig.3.1D; Fig.3.2C,D).

Neurite alignment to topographical cues on single cue platforms was compared to neurite alignment to LN stripes on single cue platforms (Table 3.2, white rows). The percent difference in neurite alignment was determined using Equation 3.1 where T is percent neurite alignment in the direction of the SC replica topography and P is percent neurite alignment in the direction of the LN stripes.

$$\%\, difference = 100 \times \frac{|T-P|}{\langle T,P \rangle},$$

Equation 3.1. Percent difference between alignment to SC replica topography (T) and to LN stripes (P).

For single-cue platforms, T and P were measured on separate platforms presenting either SC replica topography or micropatterned LN stripes. For competing cue platforms, T and P were measured on platforms presenting simultaneous orthogonal SC replica topography and LN stripes. The gray rows in Table 3.2 illustrate the differences in neurite alignment to the SC replica topography and to the LN stripes on competing cue platforms. The p-value associated with the difference in alignment to the single cue SC replica and to the single cue LN stripes (Table 3.2, white rows) was used to project the expected alignment preference when neurites were presented with the competing cues. For neurites on competing cue platforms, the percent difference in alignment to the SC replica and to the orthogonal LN stripes was calculated (Table 3.2, gray rows).

	[LN]/Topography	LN cue	% difference between neurite alignment to topography and to LN stripes	Cue preference
Single cue platforms	Low/SC replica	Low/50-10	n.s	Expected: none
Corresponding competing cue platform	Low/50-10 vs. SC replica		10.2*	Observed: LN
Single cue platforms	Low/SC replica	Low/500-50	n.s	Expected: none
Corresponding competing cue platform	Low/500-50 vs. SC replica		17.9#	Observed: SC replica
Single cue platforms	Low/SC replica	Low/50-50	n.s	Expected: none
Corresponding competing cue platform	Low/50-50 vs. SC replica		31.6#	Observed: LN
Single cue platforms	High/SC replica	High/50-50	31.6#	Expected: LN
Corresponding competing cue platform	High/50-50 vs. SC replica		76.2^	Observed: LN

Table 3.2. Comparison of neurite alignment to topographical or micropatterned LN cues presented on single cue platforms (white rows) with neurite alignment to topographical and micropatterned LN cues when cues were presented simultaneously and orthogonally on corresponding competing cue platforms (gray rows). Based on the percent difference in alignment to single cues and associated p-value of comparison, the expected preference for neurite alignment when presented with simultaneous competing cues was determined. Based on the percent difference in alignment to each cue when presented simultaneously on competing cue platforms and associated p-value, the cue to which preferential neurite alignment occurred was determined. (n.s. indicates nonsignificant percent difference. *P<0.05, #P<0.001, ^P<0.0001 by Student's t-test).

While neurite alignment to SC replicas was 6.9% higher than alignment to 50 μm wide stripes of LN_{low} separated by 10 μm spaces, this difference in alignment was not significant, suggesting that when combined on competing cue platforms there would be no preferential alignment to either cue. When these cues were presented on competing cue platforms, neurites aligned more strongly to the LN stripes than to the orthogonal SC replica (10.2% difference, P<0.05). Similarly, while neurite alignment to SC replicas was 1.8% lower than alignment to 500 μm wide stripes of LN_{low} separated by 50 μm spaces, this difference was not significant, suggesting that when combined on competing cue platforms there would be no preferential alignment to either cue. When these cues were presented on competing cue platforms, neurites aligned more strongly to the SC replica than

to the orthogonal LN stripes (17.9% difference, P<0.001). Further, while neurite alignment to SC replicas was 7.6% lower than alignment to 50 μm wide stripes of LN_{low} separated by 50 μm spaces, this difference was not significant, suggesting that when combined on competing cue platforms there would be no preferential alignment to either cue. When these cues were presented on competing cue platforms, neurites aligned more strongly to the LN stripes than to the orthogonal SC replica (31.6% difference, P<0.001). In contrast, there was a significant 31.6% difference (P<0.001) in neurite alignment between neurites on SC replica and neurites on 50 μm wide stripes of LN_{high} separated by 50 μm spaces, suggesting that when these cues were combined on competing cue platforms, there would be preferential alignment to the LN stripes. When these cues were presented on competing cue platforms, neurites aligned more strongly to the LN stripes than to the SC replica (76.2% difference, P<0.0001).

3.5. Discussion

The goal of this study was to investigate the alignment response of navigating DRG neurites to complex multi-cue environments. The study aimed to answer fundamental questions about how navigating neurites make growth decisions, which can be extended to the development of materials for nerve regeneration. Toward this end, we first determined neurite alignment response to micropatterned LN stripes and SC replica topography individually and subsequently quantified neurite alignment response to these cues when combined in cooperative and competitive formats. We systematically combined directive cues whose neurite alignment responses we had measured, enabling the evaluation of neurite alignment response in complex environments where strength of neurite alignment to the individual cues presented was known. We chose serum-containing media and five days culture time as experimental conditions, as we have shown that under these conditions, neurites exhibit a strong response to biomimetic topography [13].

3.5.1. Neurite response to individual LN micropattern and SC replica cues

The working hypothesis in this study was that neurite responses to paired cues would reflect neurite responses to the respective single cues. LN micropatterns are characterized by their concentration, stripe width, and space width. With these parameters, we designed the single-cue platforms to determine alignment responses to a range of cues, to then be combined to present defined multi-cue environments.

On single cue platforms presenting SC replica topography, neurite alignment to SC replica topography coated with LN_{high} was not different from alignment to SC replica topography coated with LN_{low}. This result is somewhat expected, because the LN on these platforms was adsorbed but not oriented. Previous work has shown that rat DRG neurite length was unaffected by LN concentration (of 10 vs. 50 μg/ml) when LN was uniformly presented on glass [29], which is consistent with the present results. In contrast, when these two LN concentrations were presented in stripe form, neurite alignment was significantly higher in response to LN_{high} versus LN_{low}, when stripe and space width were kept constant (50 μm stripes, 50 μm spaces). LN concentration has been shown to affect the location of neurite adhesion on micropatterned stripes, where the percentage of rat hippocampal neurons located along LN stripe edges increased as the concentration of LN increased from 0.8 to 100 μg/ml[30], suggesting a potential mechanism for the enhanced neurite alignment.

On LN micropattern single cue platforms, neurite response was more complex, such that for the conditions investigated neurite alignment strength was affected by LN concentration and space width, but not by stripe width. Neurite alignment was significantly higher in response to space width of 50 μm versus 10 μm when LN concentration and stripe width were the same (LN_{low}, 50 μm stripes). These results suggest that spaces wider than a soma may enhance neurites' abilities

to align to distinct stripes of guidance molecules. In contrast, neurite alignment strength did not differ in response to LN stripe width of 500 μm versus 50 μm when LN concentration and space width were the same (LN_{low}, 50 μm spaces). Numerous studies have investigated neuronal outgrowth and alignment to micropatterned LN of varied dimensions[2, 6, 31-32]. Many cell types, including neurons, respond to stripes of molecules by aligning along the stripe-space border [24, 30], and previous studies have shown that in the case of SC, cells subsequently align to each other to reinforce the overall alignment response. We suggest that a similar mechanism may underlie the present results, particularly with the 500 μm stripes.

Next, we presented navigating DRG neurites with combined LN micropattern and SC replica topography cues whose individual neurite alignment response strengths we had evaluated. With double cue platforms, we aimed to investigate neurite response to simultaneous directive cues. Our goal was to determine whether the relative neurite alignment responses to single cues would be conserved when the cues were presented in pairs in competitive orientations. The specific cues we chose afforded a range of cue types and cue strengths to generate combinations for testing hypotheses regarding complex nerve growth decisions. Several interesting nerve outgrowth events were observed.

3.5.2. Neurite response to cooperative cues

Across all cooperative cue platforms investigated, neurite alignment to the combination of LN stripes and SC replica was stronger than alignment to either cue presented individually. These results agree with previous work, supporting the overarching idea that neurite growth and guidance can be enhanced by simultaneous versus single presentation of cues, including such cues as adhesive tracks and topographic gratings[20], live SC and electric field[33], microgrooves and LN stripes[19], and microchannels and immobilized NGF[34]. Of note, here the difference in

alignment between combination and individual cues was largest when the individual LN cue was the weaker of the pair. Specifically, neurite alignment to the stronger cues (50 μm LN_{high} stripes separated by 50 μm spaces; or 50 μm LN_{low} stripes separated by 50 μm spaces) was not significantly higher when presented cooperatively with the less directive SC replica topography, but in contrast, neurite response to the weaker cues (500 μm LN_{low} stripes separated by 50 μm spaces; or 50 μm LN_{low} stripes separated by 10 μm spaces) was significantly higher when presented cooperatively with the SC replica topography cue.

Miller et al. have shown that postnatal rat DRG neurite alignment was influenced by LN concentration within poly(lactide-co-glycolide) PLGA or poly(D,L-lactic acid) PDLA microgrooves. Although neurite alignment was significantly greater when LN concentration was 200 μg/ml compared to 0 μg/ml, alignment strength was not further enhanced with 1000 μg/ml LN[19]. Britland et al. have shown that rat DRG neurite alignment increased with groove depth when LN stripes were oriented parallel to microgrooves on silica slides. However, for 25 μm and 50 μm LN stripe widths, the effect of increasing groove depth was maximal at groove depths of 0.1 μm or greater[20]. These studies, together with the present study, suggest that when cues are presented to neurons in cooperative combinations, there may be a maximal neurite response for certain types of cues.

3.5.3. Neurite response to competing cues

Across the competing cue platforms, we found several unexpected results: in cases where comparison of neurite responses to single cues suggested no neurite alignment preference, we observed preferential alignment to one cue over the other. This was the case when SC replica topography was presented competitively with 50 μm stripes of LN_{low} separated by 50 μm or 10 μm spaces. When presented individually, the strength of neurite alignment to the LN micropattern

was not different from neurite alignment to the directive SC topography. However, in both cases, on corresponding competitive platforms, neurites preferentially aligned to the LN micropattern over the SC replica topography. We also observed preferential alignment when neurites were presented with SC topography on competitive platforms with 500 μm stripes of LN_{low} separated by 50 μm spaces, but in this case, alignment was to the topographical cue. One possible explanation of these results is that for the 50 μm stripes, the high frequency of LN stripe edges encountered by neurites navigating in the direction of SC replica topography resulted in a corresponding reduction of continuous guidance along the aligned SC topography. In this case, the ability of the neurites to follow the direction of the topography may have been disrupted by the high frequency of discontinuities of the LN in the orthogonal direction. In contrast, the wider regions of LN provided by the 500 μm stripes may have provided more continuous space for the neurite to interact with the underlying topography without encountering a stripe-space border. As integrin expression has been suggested to enhance the ability of cells to respond to topographical features[35-38], disruptions in integrin expression correlating with disruptions in LN along the direction of the topographical cue may play a role here.

Last, a preferential neurite alignment response to the LN cue was expected/indicated when SC topography was competitively combined with 50 μm stripes of LN_{high} separated by 50 μm spaces. This preference was observed on the competitive platforms, and was in fact more than two-fold higher than the expected/indicated alignment based on the alignment to the individual cues.

In a previous study of orthogonal guidance cues, alignment also depended upon multiple cue parameters. Rat DRG neurons were presented with alternating LN and vitronectin stripes of 12-100 μm widths orthogonal to microgrooves of 0.05-6.0μm depths. Neurite alignment was strongest to the adhesive tracks with microgroove depth less than 1 μm, weakest to the adhesive

tracks when microgroove depth was 6 μm, and balanced to both cues when the groove depth was 0.5-1.0 μm[36].

Previous work has suggested that exposure to multiple soluble cues may result in altered neurite sensitivity to one or both of the cues compared to a cue presented individually. The level of cAMP altered growth cone guidance by netrin-1 during Xenopus retinal pathfinding, such that neurites were either attracted to or repelled by netrin-1 based on the local level of cAMP[39]. Navigating Xenopus neurites were also desensitized and resensitized to altered levels of netrin-1 and brain-derived growth factor[40]. The basis for such altered response to cues is thought to better enable long range chemotaxis of neurites in response to various levels of the same guidance molecules, and implicates such responses as having an analogous role in neurite navigation to extracellular cues during nerve regeneration. It is interesting to consider the possibility that neurites may respond in an analogous manner to exposure to multiple substrate and topographical cues..

3.6. Conclusions

We have investigated neurite alignment response to independent and combined presentations of LN micropattern and SC replica topography cues. With a systematic method of cue presentation to navigating neurites, we elucidated several characteristics of neurite response in multi-cue environments. In future work, dynamic studies of neurite alignment in complex environments will reveal mechanisms of neurite alignment in complex environments. Ultimately neurite response to biologically relevant and increasingly complex combinations of microenvironmental cues could be assessed as a microarray assay, in which neurite alignment reaponse to a panel of cue combinations could be quantified and compared to generate a model to predict neurite alignment in response to complex cue combinations and further inform the design of therapeutic biomaterial

strategies for nerve repair. Ultimately, these findings inform the design of therapeutic biomaterials toward nerve regeneration and improve upon the comprehension of basic science issues regarding nerve growth in complex environments.

3.7. Acknowledgements

The authors would like to thank Andrea Lee, Liane Livi and Cristina López-Fagundo for their contributions to data collection and thoughtful discussion. The authors acknowledge the VAMC predoctoral fellowship to JR, VA CRRM, NSF ADVANCE CDA and Career Awards to DHK, AAUW to CK, and Brown UTRA to DC and CJ, PLME and SRA to DC. IMSD and NSF to CLF; GAANN to JM.

3.8. Conflict of interest

The authors state that they are unaware of any conflicts of interest associated with the research presented in this manuscript.

3.9. Literature cited

1. Snow, D.M., J.D. Smith, and J.A. Gurwell, *Binding characteristics of chondroitin sulfate proteoglycans and laminin-1, and correlative neurite outgrowth behaviors in a standard tissue culture choice assay.* J Neurobiol, 2002. **51**(4): p. 285-301.
2. Clark, P., S. Britland, and P. Connolly, *Growth cone guidance and neuron morphology on micropatterned laminin surfaces.* J Cell Sci, 1993. **105 (Pt 1)**: p. 203-12.
3. Esch, T., V. Lemmon, and G. Banker, *Local presentation of substrate molecules directs axon specification by cultured hippocampal neurons.* J Neurosci, 1999. **19**(15): p. 6417-26.

4. Kofron, C.M., V.J. Fong, and D. Hoffman-Kim, *Neurite outgrowth at the interface of 2D and 3D growth environments.* J Neural Eng, 2009. **6**(1): p. 016002.

5. Luckenbill-Edds, L., *Laminin and the mechanism of neuronal outgrowth.* Brain Res Brain Res Rev, 1997. **23**(1-2): p. 1-27.

6. Hammarback, J.A., et al., *Guidance of neurite outgrowth by pathways of substratum-adsorbed laminin.* J Neurosci Res, 1985. **13**(1-2): p. 213-20.

7. Yeung, C.K., et al., *Modulation of the growth and guidance of rat brain stem neurons using patterned extracellular matrix proteins.* Neurosci Lett, 2001. **301**(2): p. 147-50.

8. Song, H.K., et al., *Micropatterns of positive guidance cues anchored to polypyrrole doped with polyglutamic acid: a new platform for characterizing neurite extension in complex environments.* Biomaterials, 2006. **27**(3): p. 473-84.

9. Song, M. and K.E. Uhrich, *Optimal micropattern dimensions enhance neurite outgrowth rates, lengths, and orientations.* Ann Biomed Eng, 2007. **35**(10): p. 1812-20.

10. Dubey, N., P.C. Letourneau, and R.T. Tranquillo, *Guided neurite elongation and schwann cell invasion into magnetically aligned collagen in simulated peripheral nerve regeneration.* Exp Neurol, 1999. **158**(2): p. 338-50.

11. Smeal, R.M., et al., *Substrate curvature influences the direction of nerve outgrowth.* Ann Biomed Eng, 2005. **33**(3): p. 376-82.

12. Rajnicek, A., S. Britland, and C. McCaig, *Contact guidance of CNS neurites on grooved quartz: influence of groove dimensions, neuronal age and cell type.* J Cell Sci, 1997. **110 (Pt 23)**: p. 2905-13.

13. Bruder, J.M., A.P. Lee, and D. Hoffman-Kim, *Biomimetic materials replicating Schwann cell topography enhance neuronal adhesion and neurite alignment in vitro.* J Biomater Sci Polym Ed, 2007. **18**(8): p. 967-82.

14. Richardson, J.A., et al., *Guidance of dorsal root ganglion neurites and Schwann cells by isolated Schwann cell topography on poly(dimethyl siloxane) conduits and films.* J Neural Eng, 2011. **8**(4): p. 046015.

15. Clark, P., et al., *Topographical control of cell behaviour: II. Multiple grooved substrata.* Development, 1990. **108**(4): p. 635-44.

16. Mahoney, M.J., et al., *The influence of microchannels on neurite growth and architecture.* Biomaterials, 2005. **26**(7): p. 771-8.

17. Bruder, J.M., et al., *Fabrication of polymeric replicas of cell surfaces with nanoscale resolution.* Langmuir, 2006. **22**(20): p. 8266-70.

18. Charest, J.L., A.J. Garcia, and W.P. King, *Myoblast alignment and differentiation on cell culture substrates with microscale topography and model chemistries.* Biomaterials, 2007. **28**(13): p. 2202-10.

19. Miller, C., S. Jeftinija, and S. Mallapragada, *Synergistic effects of physical and chemical guidance cues on neurite alignment and outgrowth on biodegradable polymer substrates.* Tissue Eng, 2002. **8**(3): p. 367-78.

20. Britland, S., Perridge, C., Denyer, M., Morgan, H., Curtis, A., Wilkinson, C, *Morphogenetic guidance cues can interact synergistically and hierarchically in steering nerve cell growth.* Experimental Biology Online, 1997. **1**: p. 1-15.

21. Britland, S. and C. McCaig, *Embryonic Xenopus neurites integrate and respond to simultaneous electrical and adhesive guidance cues.* Exp Cell Res, 1996. **226**(1): p. 31-8.

22. Greene, A.C., et al., *Combined chemical and topographical guidance cues for directing cytoarchitectural polarization in primary neurons.* Biomaterials, 2011. **32**(34): p. 8860-9.

23. Foley, J.D., et al., *Cooperative modulation of neuritogenesis by PC12 cells by topography and nerve growth factor.* Biomaterials, 2005. **26**(17): p. 3639-44.

24. Kofron, C.M. and D. Hoffman-Kim, *Optimization by Response Surface Methodology of Confluent and Aligned Cellular Monolayers for Nerve Guidance.* Cell Mol Bioeng, 2009. **2**(4): p. 554-572.

25. Kofron, C.M., et al., *Neurite outgrowth at the biomimetic interface.* Ann Biomed Eng, 2010. **38**(6): p. 2210-25.

26. Meijering, E., *Neuron tracing in perspective.* Cytometry A, 2010. **77**(7): p. 693-704.

27. Zhang, Y., et al., *A novel tracing algorithm for high throughput imaging Screening of neuron-based assays.* J Neurosci Methods, 2007. **160**(1): p. 149-62.

28. Al-Kofahi, K.A., et al., *Rapid automated three-dimensional tracing of neurons from confocal image stacks.* IEEE Trans Inf Technol Biomed, 2002. **6**(2): p. 171-87.

29. Li, G.N., J. Liu, and D. Hoffman-Kim, *Multi-molecular gradients of permissive and inhibitory cues direct neurite outgrowth.* Ann Biomed Eng, 2008. **36**(6): p. 889-904.

30. Xing, S., et al., *Development of neurons on micropatterns reveals that growth cone responds to a sharp change of concentration of laminin.* Electrophoresis, 2010. **31**(18): p. 3144-51.

31. Rogers, S.L., et al., *Neurite extension by peripheral and central nervous system neurons in response to substratum-bound fibronectin and laminin.* Dev Biol, 1983. **98**(1): p. 212-20.

32. Kam, L., et al., *Axonal outgrowth of hippocampal neurons on micro-scale networks of polylysine-conjugated laminin.* Biomaterials, 2001. **22**(10): p. 1049-54.

33. Koppes, A.N., A.M. Seggio, and D.M. Thompson, *Neurite outgrowth is significantly increased by the simultaneous presentation of Schwann cells and moderate exogenous electric fields.* J Neural Eng, 2011. **8**(4): p. 046023.

34. Gomez, N., et al., *Immobilized nerve growth factor and microtopography have distinct effects on polarization versus axon elongation in hippocampal cells in culture.* Biomaterials, 2007. **28**(2): p. 271-84.

35. Poole, K., et al., *Molecular-scale topographic cues induce the orientation and directional movement of fibroblasts on two-dimensional collagen surfaces.* J Mol Biol, 2005. **349**(2): p. 380-6.

36. Lim, J.Y. and H.J. Donahue, *Cell sensing and response to micro- and nanostructured surfaces produced by chemical and topographic patterning.* Tissue Eng, 2007. **13**(8): p. 1879-91.

37. Geiger, B. and A. Bershadsky, *Assembly and mechanosensory function of focal contacts.* Curr Opin Cell Biol, 2001. **13**(5): p. 584-92.

38. Hoffman-Kim, D., J.A. Mitchel, and R.V. Bellamkonda, *Topography, cell response, and nerve regeneration.* Annu Rev Biomed Eng, 2010. **12**: p. 203-31.

39. Shewan, D., et al., *Age-related changes underlie switch in netrin-1 responsiveness as growth cones advance along visual pathway.* Nat Neurosci, 2002. **5**(10): p. 955-62.

40. Ming, G.L., et al., *Adaptation in the chemotactic guidance of nerve growth cones.* Nature, 2002. **417**(6887): p. 411-8.

CHAPTER 4

DYNAMICS OF NEURITE GROWTH AND ALIGNMENT TO TOPOGRAPHICAL AND MOLECULAR CUES

4.1. Abstract

We reported characteristics of neurite outgrowth and orientation in response to micropatterned laminin (LN) and Schwann cell (SC) replica topography when presented individually or combined in cooperative or competing formats (Chapter 3). The data were obtained from studies with a five day culture duration. By nature of endpoint studies, the dynamic progression of neurite growth and alignment to the environmental cues that were presented could not be determined. In particular, neurite alignment response to platforms presenting LN micropatterns and to platforms presenting competitive arrangements of LN micropatterns and SC replica topography gave rise to several hypotheses regarding how nerve growth decisions occur over time in response to these cues. The goal of this study was to quantify the progression of neurite alignment and cell characteristics of cell behavior response to single cue platforms presenting

micropatterned LN stripes and to competitive platforms presenting orthogonally opposed LN stripes and SC replica topography. Sequential endpoint studies were employed to determine the progression of neurite alignment on LN stripes, and dynamic timelapse microscopy was utilized to determine neurite growth events in real-time in response to LN stripes and to LN stripes and SC replica topography presented simultaneously and orthogonally opposed as competing cue platforms. Neurite alignment to micropatterned LN stripes occurred at the LN stripe-space border initially, and on a combination of LN stripes and local cell interactions as time progressed. Neurite alignment to orthogonally opposed LN stripes and SC replica topography responded to the stripe-space border and the relative stripe and space widths in a complex manner, such that response to SC replica topography was enhanced with increased LN stripe width. This work represents an important step toward determining the physical mechanisms that underlie neurite outgrowth in complex multi-cue environments.

4.1. Introduction

Understanding of the basic biology of nerve growth decision-making in response to environmental cues may inform the design of therapeutic biomaterials for nerve repair where nerve guidance is needed. Information regarding nerve growth and behavior over time is critical in determining how neurites respond to the stimuli of their environment. In particular, events of neurite initiation and early elongation and retraction during pathfinding take place rapidly after cells adhere to their underlying substrate, on the timescale of minutes[1-2]. Dynamic imaging is one method by which cell growth events may be visualized, wherein sequential images are captured at frequent time intervals and assembled as videos. Several groups have discovered key outgrowth events with dynamic imaging[2-4]. A study by Laketa et al. revealed the protein expression patterns involved in neurite outgrowth response to NGF using a combination of timelapse microscopy and real time quantitative RT-PCR[3]. Lautermilch et al. investigated the Ca^{2+} dependence of Xenopus

neurite extension via timelapse microscopy[4], and Kofron et al. used timelapse microscopy combined with endpoint studies with SC, astrocytes, and HUVECs to reveal distinctions in cell-type-specific alignment response to micropatterned protein tracks[2]. Additionally, sequential endpoint analysis affords the opportunity to understand cell behavior at progressive time points while affording full opportunity to fluorescently label key proteins and cell markers for in depth quantitative analysis. The sequential endpoint studies described in this chapter incorporate analysis of cell culture experiments at successive intervals of time in order to determine cell behavior and morphology events over time. When combined, dynamic imaging and sequential endpoint studies illuminate cell growth patterns and behaviors that may not be observed with classic endpoint studies. Here, we have employed such experimental techniques to further investigate neurite alignment response to selected experimental conditions described in Chapter 3.

Through the studies presented in Chapter 3, we observed several characteristics of neurite behavior on cell culture platforms presenting individual cues or platforms presenting two cues in cooperative or competing orientations. In particular, interesting neurite outgrowth responses were observed on platforms presenting individual micropatterned LN stripes and on competitive cue platforms presenting orthogonal LN stripes and SC replica topography. Based on these findings, we formed several hypotheses regarding neurite growth and alignment decisions in response to such cues. These observations of neurite alignment were based on five day endpoint studies, such that outgrowth and alignment events leading to those observed at five days were not investigated. To further investigate cellular response to LN micropattern and SC replica cues on competing cue platforms, we performed sequential endpoint studies at one-day intervals beginning at the time of cell seeding and continuing over four days. Based on these studies, we aimed to look more closely at real-time cell behavior during the first day of neurite interaction with the LN and SC replica topography cue platforms via timelapse microscopy. To address our hypotheses, a

combination of dynamic phase contrast microscopy studies and sequential immunolabeled endpoint studies were used to elucidate neurite growth events over time.

4.1.1. Neurite outgrowth on LN micropatterns depended on pattern dimensions

Based on five day endpoint studies described in Chapter 3, among individual LN micropattern cue platforms, neurite outgrowth depended on the parameters of the individual cues on single cue platforms with LN stripes and SC replica topography fully coated with LN. Neurite alignment was affected by LN concentration and LN space width, but not by LN stripe width over the conditions examined. In particular, neurite alignment was higher to stripes of 50 µg/ml LN than to 10 µg/ml LN when the stripes were 50 µm wide and separated by 50 µm spaces. Additionally, neurite alignment was higher to 10 µg/ml LN stripes that were 50 µm wide when the stripes were separated by 50 µm spaces compared to 10 µm spaces. Interestingly, neurite alignment was not different on 500 µm wide stripes of 10 µg/ml LN compared to 50 µm stripes separated by 50 µm spaces, indicating that for the conditions examined, LN stripe width did not play a role in overall neurite alignment at the conclusion of the five day culture period.

Based on these data, we hypothesized that the following physical mechanisms underlie neurite alignment to LN micropatterned stripes. (1.a.) Neurite outgrowth initiates at stripe-space borders, and (1.b.) subsequently propagates inward on the LN stripe. (1.c.) Continued neurite alignment occurs by cell-cell alignment, wherein neurites align to neighboring aligned neurites and proliferative SC, and eventually, (1.d.) the aligned neurites propagate onto the uncoated regions of the micropattern. We hypothesize that these proposed events depend on the dimensions of the LN micropattern, such that wide regions (e.g. 500 µm) of LN presenting lower frequency of stripe-space borders per area promote neurite alignment at a slower pace initially when compared to narrower stripes (e.g. 50 µm) of LN that promote faster initial neurite alignment. Ultimately,

we hypothesize that cell-cell interactions are enhanced throughout the culture time, as neurites extend and live SC proliferate and align, such that the initial neurite alignment response to stripe-space borders may be overcome by cell-cell alignment interactions, wherein local cell-cell alignment may decrease overall neurite alignment to the micropattern over time.

This Chapter discusses the comparison of Chapter 3 data with sequential endpoint studies at day 1, day 2, day 3, and day 4. These experiments were combined with timelapse studies to reveal key aspects of neurite growth and alignment events leading to the alignment observed at the five day endpoint. The combination of endpoint and dynamic data has exposed important characteristics about the physical mechanisms that underlie neurite alignment response to external environmental cues.

4.1.2. Neurite outgrowth on competing cue platforms

Neurite alignment to competing cue platforms presenting LN micropatterned stripes orthogonally opposed to SC replica topography led to hypotheses concerning growth decisions of navigating neurites when presented with conflicting environmental cues. For three competitive cue experimental conditions, we found that neurites exhibited complex and unexpected responses to the underlying cues. When a comparison of neurite alignment to individual LN micropattern and SC replica topography cues indicated no preference in alignment to either cue when presented competitively on double cue platforms, preferential neurite alignment to one cue over the other was indeed observed.

However, the observed preference of neurite alignment was to the LN micropattern direction when the LN micropattern presented 50 μm stripes separated by 50 μm spaces or 10 μm spaces. Contrastingly, when the LN micropattern presented 500 μm stripes separated by 50 μm spaces,

alignment preference was to the SC replica topography direction. For all three conditions, a preferential neurite alignment response was not indicated to occur, but preferential alignment was, in fact, observed. To reveal decision-making events leading to overall neurite alignment preference observed after five days in culture, dynamic and sequential endpoint studies were performed for the conditions described above.

Based on neurite alignment response on competitive platforms presenting orthogonally opposed micropatterned LN stripes and SC replica topography, we hypothesized that the LN stripes provide a surface upon which interaction with the SC replica topography is enhanced such that, for example, wide regions of LN (e.g. 500 μm stripes) provided a relatively large region over which neurites could interact with the orthogonally opposed SC replica topography, and as such, preferential alignment to the topographical alignment was observed. This hypothesis postulates that (2.a.) the preference in neurite alignment depends on stripe and space dimensions, and (2.b.) that exposure to continuous regions of LN enhances the opportunity for neurites to interact with and align to SC replica topography. Further, we propose that (2.c.) discontinuities (i.e. stripe-space borders) occurring along the axis of orientation topographical features will limit neurite interaction and alignment to the topographical features.

4.3. Materials and Methods

4.3.1. Substrate fabrication, cell culture, and analysis

Single and double-cue platforms were fabricated as described in Chapter **3.3**. Postnatal rat DRGs were harvested, dissociated, and seeded at 200,000 cells/well in a standard 12-well culture plate as described in Chapter **3.3.3**. For sequential endpoint studies, DRG were cultured for the prescribed culture period of 24 h (day 1), 48 h (day 2), 72 h (day 3), or 96 h (day 4) and subsequently fixed in 2% paraformaldehyde in PBS, as described in Chapter **3.3.3**. Data for day

1, 2, 3, and 4 was accumulated through identical experimental conditions and setup as described in Chapter 3 and was compared in this chapter to the day 5 data presented in Chapter 3. To visualize the micropatterned LN stripes, neurites, and cell nuclei, cells were fluorescently labeled for anti-LN, anti-β(III) tubulin and DAPI, respectively, as described previously in Chapter **3.3.3**. Sequential endpoint studies were assessed for neurite morphology and alignment relative to the underlying LN stripes as described in Chapter **3.3.4**. Neurite alignment relative to LN stripes was quantified by the custom MATLAB program described in Chapter 3.3.5. Figure 4.1 briefly depicts the process with representative micrographs of fluorescently labeled neurites (Fig4.1A-B) on 50 μm stripes separated by 10 μm spaces as a LN micropattern platform (Fig4.1A) or competing cue platform where LN stripes were oriented along the vertical axis, orthogonally opposed to the SC replica topography (Fig4.1B). The software algorithm generated a 'trace' file from each of the micrographs (Fig.4.1C-D), which depicts the tracing of neurite segments within the micrographs. The percentage of neurite alignment within 20° of the horizontal and vertical directions was output and these values were reported as a bar graph (Fig.4.1E) where percent neurite alignment to the horizontal and vertical directions are reported based on the micrographs of neurites on LN only (Fig.4.1E, black bars) and LN orthogonally opposed to SC replica topography (Fig.4.1E, white bars). Number and alignment of DAPI stained nuclei relative to the LN stripes was assessed by methods described previously[2].

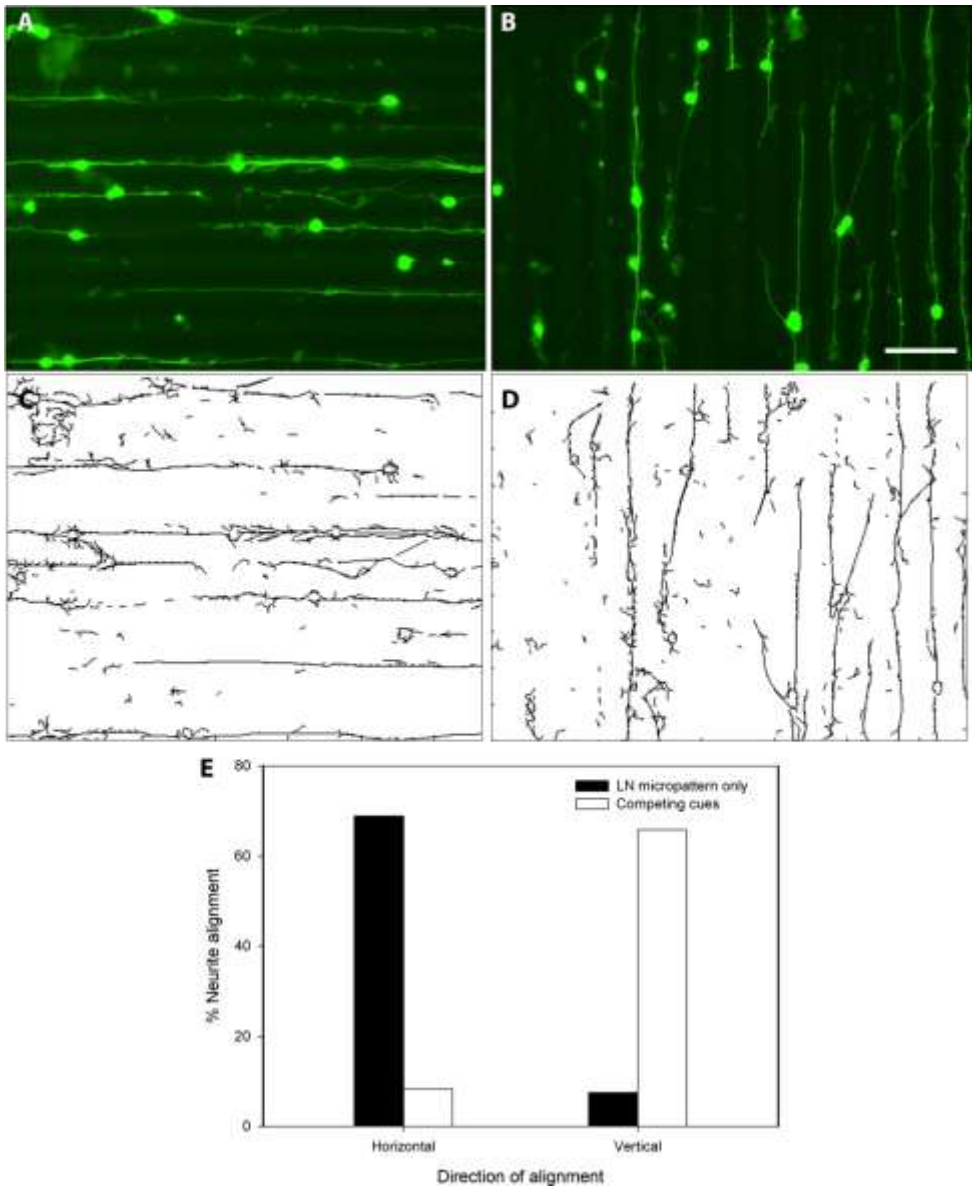

Figure 4.1. Percent neurite alignment data were generated with a custom image tracing algorithm. A,B. Epifluorescent micrographs with neurites labeled for anti-β(III) tubulin on single cue (A) and competing cue (B) platforms presenting 50 μm wide LN stripes separated by 10 μm wide spaces oriented to the horizontal (A) or vertical (B) direction. C-D. Neurite segment traces generated by custom algorithm (described in Chapter 3.3.5). E. Bar graph demonstrates quantification of percent neurite alignment to the horizontal and vertical directions for the fields of view depicted in panels A and B. Black bars represent neurite alignment on A. White bars represent neurite alignment on B. Scalde bar, 100 μm.

Dynamic studies were performed by culturing DRGs within an incubation chamber with 5% CO_2 and 100% humidity, using a motorized xy-stage and automated image capture automation (Warren Automation) developed in Openlab v.4.0.4. (Improvision). For selected fields of view,

10x magnification images were captured every five minutes for 22 or 24 h total duration. For the studies presented here, the first 24 hours of cell culture were imaged for dynamic analysis. Following image capture, image files were assembled into video file formats by exporting Openlab LIFF files as jpegs with Volocity v.6.0.1. Jpeg images were assembled into the .avi video file format with ImageJ v.1.45.

4.3.2. Statistical analysis

One-way analysis of variance (ANOVA) tests were performed on cell count and percent neurite alignment. Post hoc multiple comparison analyses were performed using Tukey's test. A P-value of 0.05 was taken to be significant. Statistical analysis of circular distributions was tested by Rayleigh test. A P-value of 0.05 was taken to be significant.

4.4. Results

4.4.1. Cell proliferation and nuclear alignment to LN micropatterns depended on micropattern dimensions.

To assess overall cell proliferation on substrates presenting LN micropatterns of varied stripe and space widths, the average number of cells per field of view (FOV) was quantified (Fig.4.2). Generally, cell proliferation increased over time, but for each condition examined, cell count was maximal at a time point prior to day 5. The maximal cell count occurred at day 3, with 331 cells/FOV on 50 μm wide LN stripes separated by 10 μm spaces (Fig.4.2 black bars). The maximal cell count occurred at day 4, with 487 cells/FOV on 500 μm wide LN stripes separated by 50 μm wide spaces (Fig.4.2 gray bars). The maximal cell count occurred at day 4, with 361 cells/FOV on 50 μm wide LN stripes separated by 50 μm wide spaces, (Fig.4.2 white bars).

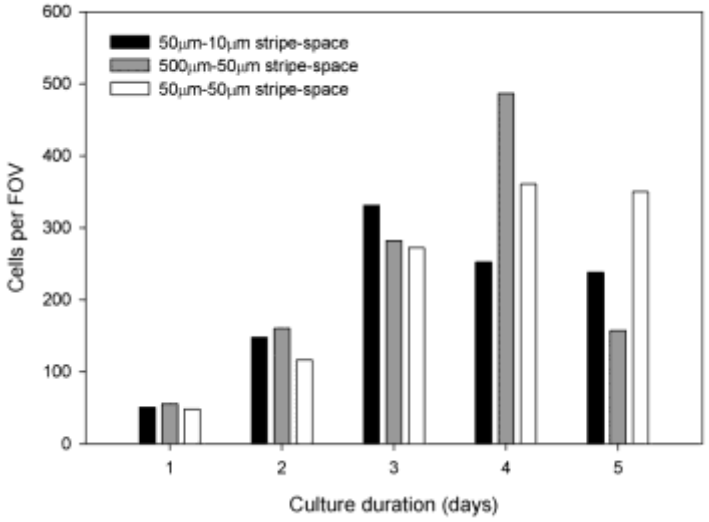

Figure 4.2. The number of cells per field of view with respect to culture duration. Cell number per field of view on 50 μm LN stripes separated by 10 μm (black bars), 500 μm LN stripes separated by 50 μm (gray bars), and 50 μm LN stripes separated by 50 μm (white bars) substrates were evaluated at 1, 2, 3, 4 and 5 days in culture.

DAPI-labeled nuclear alignment was determined on substrates for cell cultures at 1, 2, 3, 4, and 5 days culture duration (Fig.4.3). Circular analysis was used to describe the overall nuclear orientation in response to the LN micropatterns, and circular histograms illustrating nuclear distribution on 50 μm wide LN stripes separated by 10 μm wide spaces, 500 μm wide LN stripes separated by 50 μm wide spaces, and 50 μm wide LN stripes separated by 50 μm wide spaces are depicted in Figures 4.9, 4.12, 4.15, 4.18, 4.21A, B, and C, respectively. The circular distributions of nuclear alignment on LN micropattern platform conditions were significantly different from uniform by Rayleigh test ($P<0.001$).

Mean vector length (MVL) was used as a descriptor of alignment strength, where a MVL approaching 1 indicated strong clustering of nuclear alignment to the micropattern and a MVL approaching 0 indicated no clustering in alignment. Nuclear alignment clustering along the direction of the LN micropattern was maximal at day 2, and subsequently decreased at each

sequential time point on 50 μm wide LN stripes separated by 10 μm wide spaces (**Fig.4.3** black bars) and on 50 μm wide LN stripes separated by 50 μm wide spaces (Fig.4.3 white bars). MVL was lowest at day 1, and subsequently tended to increase with culture duration on 500 μm wide LN stripes separated by 50 μm wide spaces (Fig.4.3 gray bars).

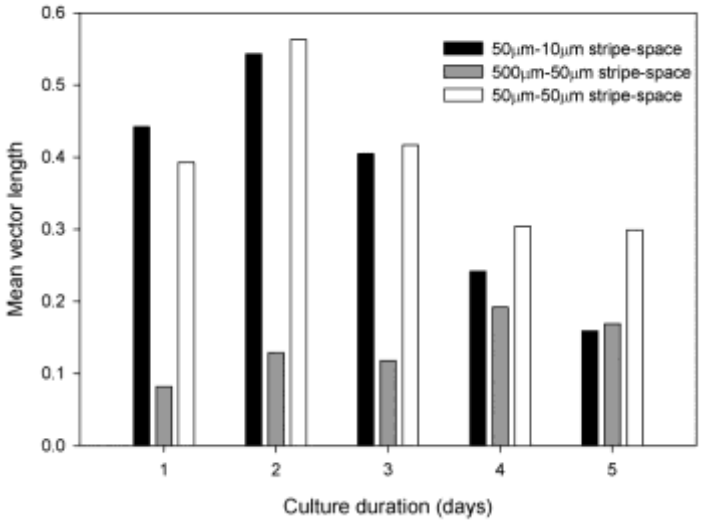

Figure 4.3. Mean vector lengths of circular distributions of nuclear orientation on 50 μm LN stripes separated by 10 μm (black bars), 500 μm LN stripes separated by 50 μm (gray bars), and 50 μm LN stripes separated by 50 μm (white bars) substrates were evaluated at 1, 2, 3, 4 and 5 days in culture.

4.4.2. Over time, neurite alignment depended on LN micropattern dimensions and cell-cell interactions

DRG neurite outgrowth was assessed on platforms presenting micropatterned LN stripes either 50 μm wide separated by 10 μm, 500 μm wide separated by 50 μm, or 50 μm wide separated by 50 μm. Sequential endpoint studies over 5 days revealed characteristics of neurite alignment to LN micropatterns with distinct dimensions.

Cellular morphology, neurite alignment and nuclear alignment to LN micropatterns were observed and quantified following 1, 2, 3, and 4 days of culture duration. Cellular morphology, neurite alignment, and nuclear alignment to LN micropatterns at day 5 were determined as

previously described in Chapter 3, and were compared to outgrowth characteristics at the earlier time points assessed here.

Neurite alignment to 50 μm wide LN stripes separated by 10 μm wide spaces was quantified at sequential endpoints (Fig.4.4). At day 2, neurite alignment to 50 μm LN stripes separated by 10 μm spaces was 61.45±0.8%, which was significantly greater than alignment at day 3 (55.9±0.5%), day 4 (42.48±0.7%) and day 5 (35.1±1.1%) ($P<0.001$; Fig.4.4). Alignment to LN stripes at day 4 and day 5 was significantly different from alignment at all other time points ($P<0.001$), and alignment to LN stripes at day 3 was significantly different from alignment at all other time points ($P<0.05$ significantly different from day 1 (59.2±1.3%); $P<0.001$ significantly different from day 2, day 4, day 5).

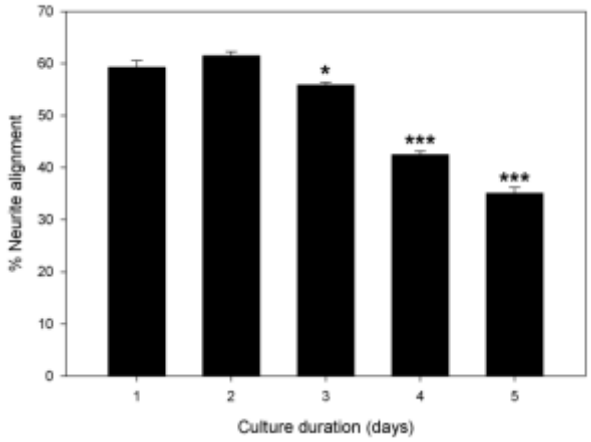

Figure 4.4. Percent of neurites aligned within 20° of 50 μm LN stripes separated by 10 μm at 1, 2, 3, 4, and 5 days culture duration. (*$P<0.05$, ***$P<0.001$ significantly different from all other conditions by one-way ANOVA).

At day 1, neurite alignment to 500 μm LN stripes separated by 50 μm spaces was 35.6±0.6%, which was significantly lower than alignment to the micropattern at day 3 (38.6±0.4%) and day 5 (38.3±0.9%) ($P<0.05$; Fig.4.5.).

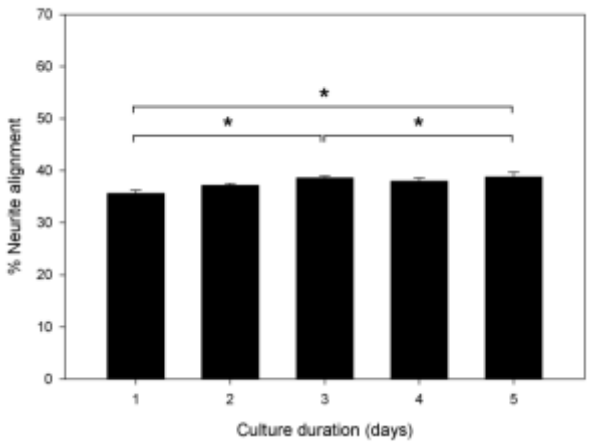

Figure 4.5. Percent of neurites aligned within 20° of 500 μm LN stripes separated by 50 μm at 1, 2, 3, 4, and 5 days culture duration. (*P<0.05 significantly different from each other by one-way ANOVA).

At day 2, neurite alignment to 50 μm LN stripes separated by 50 μm spaces was 64.9±0.5%, which was significantly greater than neurite alignment to the micropattern at all other time points examined (56.4±1.2% at day 1; 57.5±0.4% at day 3; 44.3±0.5% at day 4, 40.6±1.3% at day 5; P<0.001; Fig.4.6). Additionally, at day 5, neurite alignment to 50 μm LN stripes separated by 50 μm spaces was significantly lower than neurite alignment to all other conditions (P<0.01).

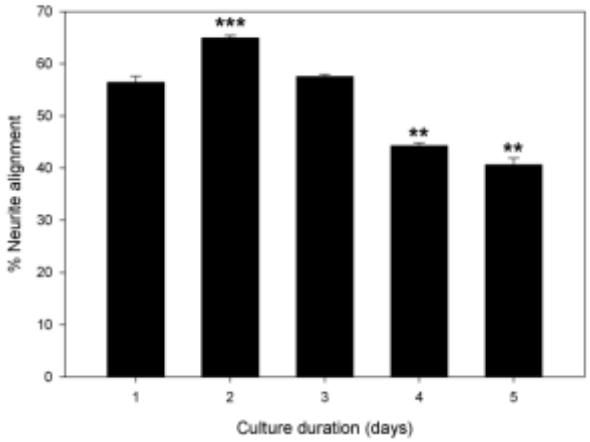

Figure 4.6. Percent of neurites aligned within 20° of 50 μm LN stripes separated by 50 μm at 1, 2, 3, 4, and 5 days culture duration. (**P<0.01, ***P<0.001 significantly different from all other conditions by one-way ANOVA. n>30 FOV for all conditions. Error bars are SEM).

4.4.3. Cell morphology, neurite alignment, and nuclear alignment response depended on micropattern dimensions over time

Neurite morphology, neurite alignment, and nuclear alignment were assessed at day 1, day 2, day 3, and day 4 and compared with corresponding day 5 data presented in Chapter 3. At day 1, neurites on 50 μm stripes of LN separated by 10 μm or 50 μm spaces appeared highly aligned to the direction of the LN stripes (Fig.4.7A,C), while neurites on 500 μm LN stripes separated by 50 μm spaces appeared to be more randomly oriented on the regions of LN (Fig.4.7B). Neurites adhered almost exclusively on the LN stripes for all three conditions (Fig.4.7A-C).

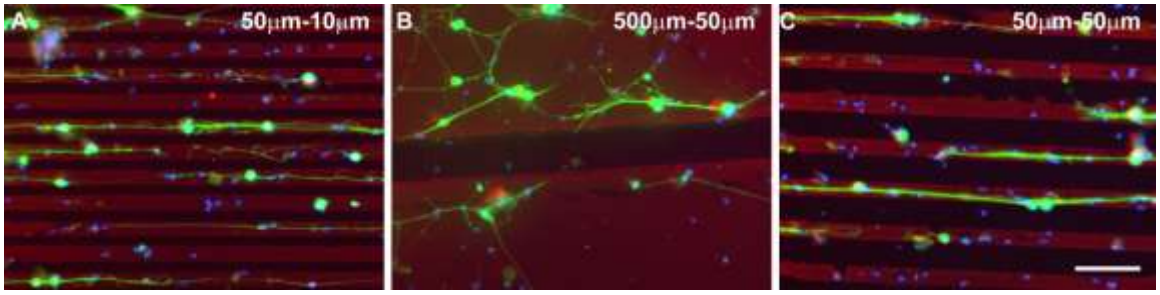

Figure 4.7. DRG neurites responded to environmental cues at day 1. Fluorescent micrographs show neurites positive for anti-β(III) tubulin (green), nuclei labeled with DAPI (blue) and LN stripes positive for anti-LN antibody (red) on 50 μm LN stripes separated by 10 μm (A), 500 μm LN stripes separated by 50 μm (B), and 50 μm LN stripes separated by 50 μm (C). Scale bar = 150 μm.

The percentage of neurites aligned within 20° of the direction of the LN stripes was quantified at day 1 (Fig 4.8). The percentage of neurites aligned to the direction of 500 μm LN stripes separated by 50 μm spaces (35.6±0.6%) was significantly less than the percentage of neurites aligned to 50 μm LN stripes separated by either 10 μm spaces (59.2±1.3%) or 50 μm spaces (56.4±1.2%; P<0.001; Fig.4.8).

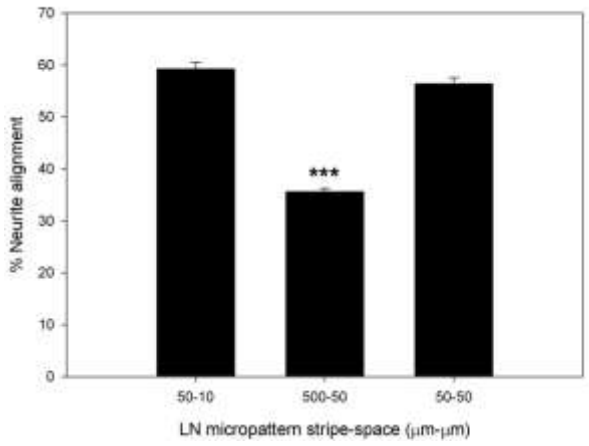

Figure 4.8. Percent neurite alignment at day 1 within 20° of 50 μm LN stripes separated by 10 μm, 500 μm LN stripes separated by 50 μm, and 50 μm LN stripes separated by 50 μm. (***P<0.001 significantly different from all other conditions by one-way ANOVA. n>30 FOV for all conditions. Error bars are SEM).

The distribution of nuclear alignment response on micropatterned substrates was used to determine overall cellular alignment at day 1. Circular histograms depict the distribution of nuclear alignment on micropatterned platforms at day 1 (Fig4.9A-C). The circular distributions correlate with the neurite alignment response on substrates at day 1. The distribution of nuclear orientation at day 1 had a MVL of 0.44 at 1.05° on 50 µm LN stripes separated by 10 µm spaces (Fig.4.9A). Nuclear alignment distribution at day 1 had a MVL of 0.08 at 167.3° on 500 µm LN stripes separated by 50 µm spaces (Fig.4.9B), and a MVL of 0.39 at 2.08° on 50 µm LN stripes separated by 50 µm spaces (Fig.4.9C).

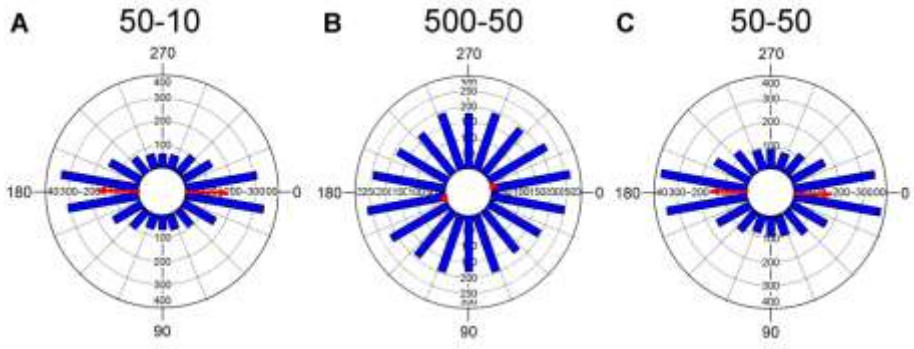

Figure 4.9. Day 1 DRG neurite response to directive cues depicted in Figure 4.7. is shown quantitatively on circular histograms. Circular histograms depict distribution of nuclear alignment on 50 µm LN stripes separated by 10 µm (A), 500 µm LN stripes separated by 50 µm (B), and 50 µm LN stripes separated by 50 µm (C). The length of each bar is proportional to the percentage of the number of DAPI-stained nuclei at the corresponding angle. Mean vector is represented in red. Direction of LN micropattern lies along the 0-180° axis. All distributions were significantly different from uniform ($P<0.001$, Rayleigh test).

At day 2, neurites were predominantly adhered to the regions of LN, but on 50 µm LN stripes separated by 10 µm or 50 µm spaces, neurites were present between the stripes to a limited extent (Fig.4.10A,C). Neurites appeared to be aligned to the direction of the LN micropattern on substrates presenting 50 µm LN stripes separated by either 10 µm or 50 µm spaces (Fig.4.10A,C), but neurite orientation appeared to be more randomly distributed on 500 µm LN stripes separated by 50 µm spaces (Fig.4.10B). Additionally, neurites on 500 µm LN stripes separated by 50 µm

spaces did not tend to extend on the space between LN stripes, but neurites tended to extend to the LN stripe-space border, where neurite alignment to the direction of the border appeared to a limited extent (Fig.4.10B).

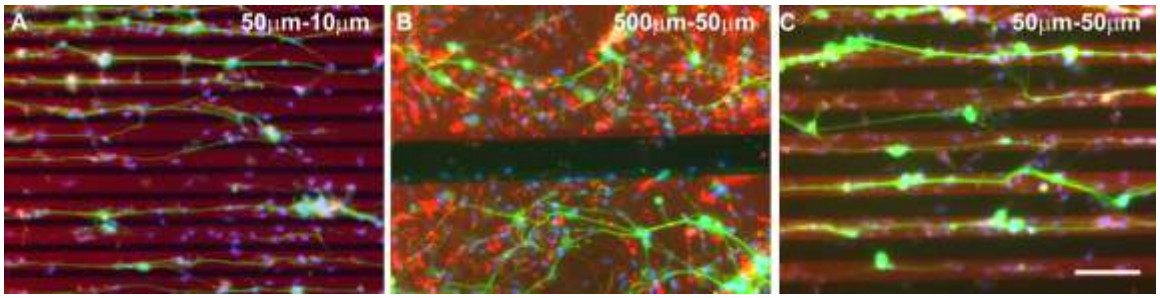

Figure 4.10. DRG neurites responded to environmental cues at day 2. Fluorescent micrographs show neurites positive for anti-β(III) tubulin (green), nuclei labeled with DAPI (blue) and LN stripes positive for anti-LN antibody (red) on 50 μm LN stripes separated by 10 μm (A), 500 μm LN stripes separated by 50 μm (B), and 50 μm LN stripes separated by 50 μm (C). Scale bar, 100 μm.

The percentage of neurites aligned within 20° of the LN stripes was quantified at day 2 (Fig.4.11). Percent neurite alignment to all three conditions was significantly different from all other conditions at day 2 ($P<0.001$; Fig.4.11). Neurites were 61.4±0.8% aligned to 50 μm LN stripes separated by 10 μm spaces. Neurites were 37.2±0.5% aligned to 500 μm LN stripes separated by 50 μm spaces. Neurites were 64.9±0.5% aligned to 50 μm LN stripes separated by 50 μm spaces.

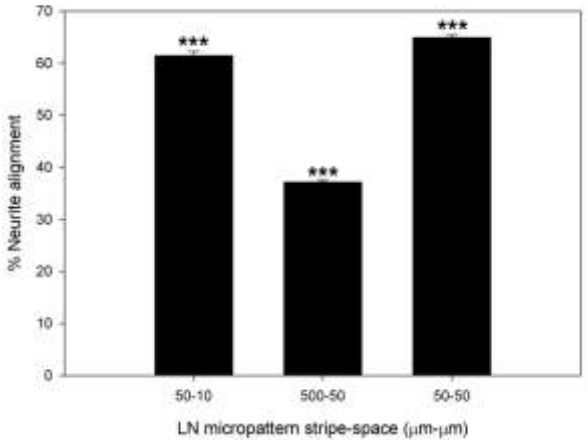

Figure 4.11. Percent neurite alignment at day 2 within 20° of 50 μm LN stripes separated by 10 μm, 500 μm LN stripes separated by 50 μm, and 50 μm LN stripes separated by 50 μm. (***P<0.001 significantly different from all other conditions by one-way ANOVA. n>30 FOV for all conditions. Error bars are SEM).

Circular histograms representing nuclear alignment at day 2 relative to the LN micropatterns was reflective of the cellular morphology and alignment depicted in Figure 4.10 and Figure 4.11. The nuclear angle distribution on 50 μm LN stripes separated by 10 μm spaces had a MVL of 0.54 occurring at 0.15° (Fig.4.12A). The nuclear angle distribution on 500 μm LN stripes separated by 50 μm spaces had a MVL of 0.13 occurring at 179.9° (Fig.4.12B). The nuclear angle distribution on 50 μm LN stripes separated by 50 μm spaces had a MVL of 0.56 occurring at 0.91° (Fig.4.12C).

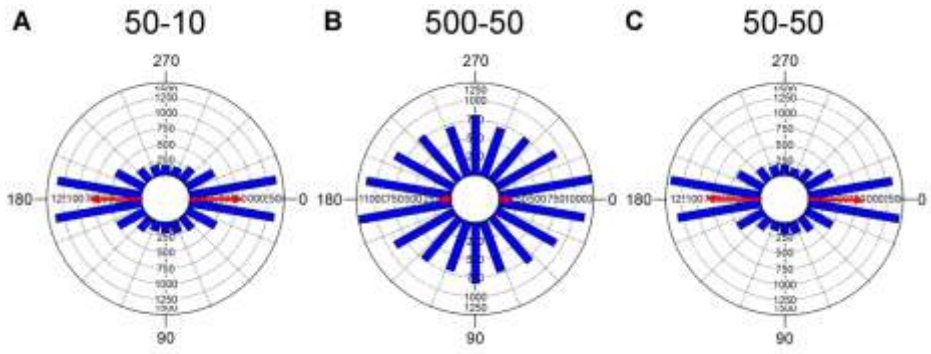

Figure 4.12. Day 2 DRG neurite response to directive cues depicted in Figure 4.10. is shown quantitatively on circular histograms. Circular histograms depict distribution of nuclear alignment on 50 μm LN stripes separated by 10 μm (A), 500 μm LN stripes separated by 50 μm (B), and 50 μm LN stripes separated by 50 μm (C). The length of each bar is proportional to the percentage of the number of DAPI-stained nuclei at the corresponding angle. Mean vector is represented in red. Neurite orientation was not uniformly distributed. Direction of LN micropattern lies along the 0-180° axis. All distributions were significantly different from uniform ($P<0.001$, Rayleigh test).

At day 3, neurites on substrates presenting 50 μm LN stripes separated by either 10 μm or 50 μm spaces appeared to be significantly more numerous than at either day 1 or day 2, and neurites on these conditions demonstrated local alignment to each other and to other neighboring cells (Fig.4.13A,C). Neurites grew between the LN stripes on these conditions, and the overall orientation of neurite outgrowth occured in the direction of the LN micropattern. Neurites on 500 μm LN stripes separated by 50 μm spaces appeared aligned along the direction of the LN stripes, although a proportion of the neurites appeared to be randomly aligned on the LN regions (Fig.4.13B). Neurites appeared to be localized to the regions of LN on 500 μm LN stripes separated by 50 μm spaces.

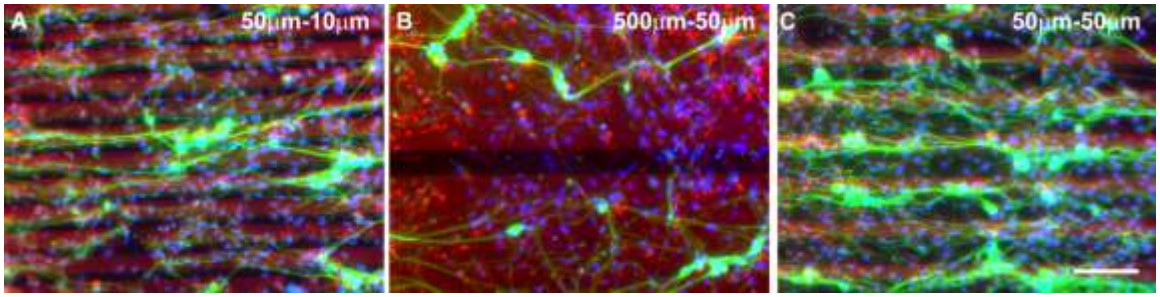

Figure 4.13. DRG neurites responded to environmental cues at day 3. Fluorescent micrographs show neurites positive for anti-β(III) tubulin (green), nuclei labeled with DAPI (blue) and LN stripes positive for anti-LN antibody (red) on 50 μm LN stripes separated by 10 μm (A), 500 μm LN stripes separated by 50 μm (B), and 50 μm LN stripes separated by 50 μm (C). Scale bar, 100 μm.

The percentage of neurites aligned within 20° of the LN stripes was quantified at day 3 (Fig.4.14). Percent neurite alignment to 500 μm LN stripes separated by 50 μm spaces was 38.6±0.4%, which was significantly lower than the percentage of neurite alignment to 50 μm LN stripes separated by either 10 μm spaces (55.9±0.5%; $P<0.001$) or 50 μm spaces (57.5±0.4%; $P<0.001$). Additionally, the percentage of neurites aligned to 50 μm stripes separated by 50 μm spaces was significantly higher than the percentage of neurites aligned to 50 μm stripes separated by 10 μm spaces ($P<0.05$).

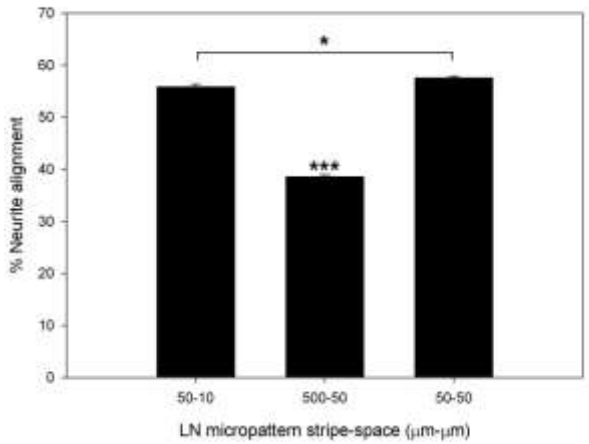

Figure 4.14. Percent neurite alignment at day 3 within 20° of 50 μm LN stripes separated by 10 μm, 500 μm LN stripes separated by 50 μm, and 50 μm LN stripes separated by 50 μm. (*$P<0.05$ significantly different from each other by one-way ANOVA; ***$P<0.001$ significantly different

from all other conditions by one-way ANOVA. n>30 FOV for all conditions. Error bars are SEM).

Circular histograms reflected the differences observed in neurite alignment and described overall nuclear alignment at day 3 (Fig.4.15). The nuclear angle distribution on 50 µm LN stripes separated by 10 µm spaces had a MVL of 0.41 occurring at 0.57° (Fig.4.15A). The nuclear angle distribution on 500 µm LN stripes separated by 50 µm spaces had a MVL of 0.12 occurring at 178.05° (Fig.4.15B). The nuclear angle distribution on 50 µm LN stripes separated by 50 µm spaces had a MVL of 0.42 occurring at 0.38° (Fig.4.15C).

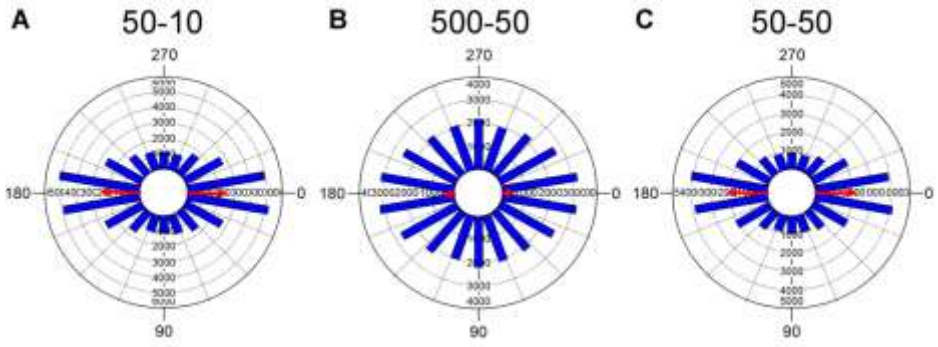

Figure 4.15. Day 3 DRG neurite response to directive cues depicted in Figure 4.13. is shown quantitatively on circular histograms. Circular histograms depict distribution of nuclear alignment on 50 µm LN stripes separated by 10 µm (A), 500 µm LN stripes separated by 50 µm (B), and 50 µm LN stripes separated by 50 µm (C). The length of each bar is proportional to the percentage of the number of DAPI-stained nuclei at the corresponding angle. Mean vector is represented in red. Neurite orientation was not uniformly distributed. Direction of LN micropattern lies along the 0-180° axis. All distributions were significantly different from uniform ($P<0.001$, Rayleigh test).

At day 4, neurites appeared to have higher density on the substrates (Fig.4.16A-C). Neurites on all three conditions appeared to be oriented along the LN micropattern, and neurites appeared to have overgrown onto the spaces between 50 µm LN stripes separated by either 10 µm or 50 µm (Fig4.16A,C).

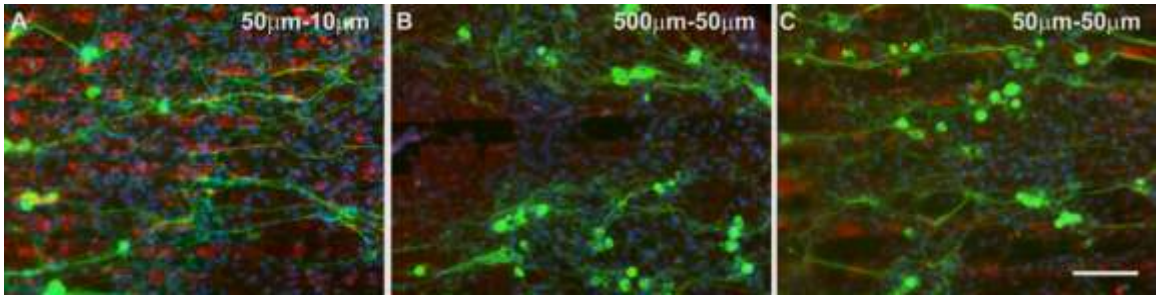

Figure 4.16. DRG neurites responded to environmental cues at day 4. Fluorescent micrographs show neurites positive for anti-β(III) tubulin (green), nuclei labeled with DAPI (blue) and LN stripes positive for anti-LN antibody (red) on 50 μm LN stripes separated by 10 μm (A), 500 μm LN stripes separated by 50 μm (B), and 50 μm LN stripes separated by 50 μm (C). Scale bar, 100 μm.

The percentage of neurites aligned within 20° of the LN stripes was quantified at day 4 (Fig.4.17). Percent neurite alignment to 50 μm LN stripes separated by 50 μm spaces was 44.3±0.5%, which was significantly greater than alignment to 50 μm LN stripes separated by 10 μm spaces (42.5±0.7%; $P<0.01$) and alignment to 500 μm LN stripes separated by 50 μm spaces (38.0±0.6%; $P<0.001$).

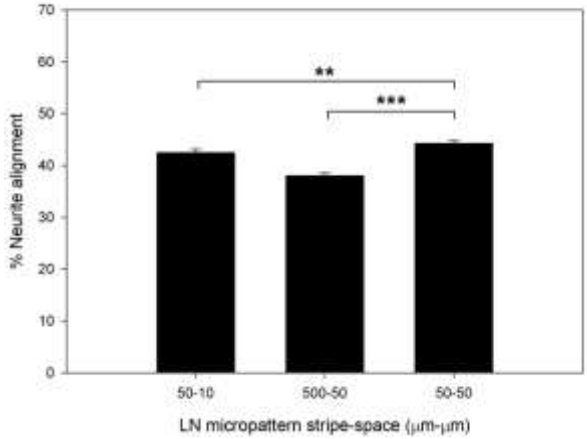

Figure 4.17. Percent neurite alignment at day 4 within 20° of 50 μm LN stripes separated by 10 μm, 500 μm LN stripes separated by 50 μm, and 50 μm LN stripes separated by 50 μm. (**P<0.01, ***P<0.001 significantly different from each other by one-way ANOVA. n>30 FOV for all conditions. Error bars are SEM).

Circular histograms demonstrate that at day 4, nuclear distribution appeared to be less clustered around the 0°-180° axis than at previous time points (Fig.4.18A-C). The nuclear angle distribution on 50 µm LN stripes separated by 10um spaces had a MVL of 0.24 occurring at 179.6° (Fig.4.18A). The nuclear angle distribution on 500 µm LN stripes separated by 50 µm spaces had a MVL of 0.19 occurring at 175.5° (Fig.4.18B). The nuclear angle distribution on 50 µm LN stripes separated by 50 µm spaces had a MVL of 0.30 occurring at 177.3° (Fig.4.18C).

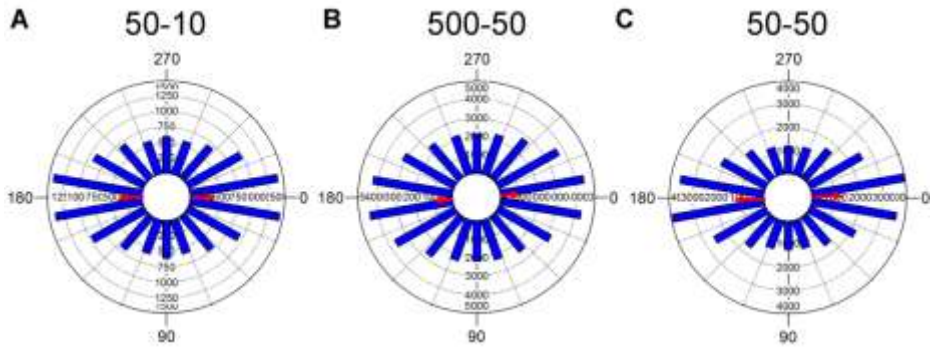

Figure 4.18. Day 4 DRG neurite response to directive cues depicted in Figure 4.16. is shown quantitatively on circular histograms. Circular histograms depict distribution of nuclear alignment on 50 µm LN stripes separated by 10 µm (A), 500 µm LN stripes separated by 50 µm (B), and 50 µm LN stripes separated by 50 µm (C). The length of each bar is proportional to the percentage of the number of DAPI-stained nuclei at the corresponding angle. Mean vector is represented in red. Neurite orientation was not uniformly distributed. Direction of LN micropattern lies along the 0-180° axis. All distributions were significantly different from uniform ($P<0.001$, Rayleigh test).

At day 5, neurites on all micropattern conditions appeared to be associated with neighboring neurites and cells (Fig.4.19A-C; note that immunolabeling colors are reversed from day 1 – day 4 micrograph figures). For all conditions, neurites appeared to have overgrown onto the spaces separating LN stripes, and although overall neurite and cell alignment appeared along the direction of the LN micropatterns, the neurite alignment and morphology appeared to be more highly dominated by cell-cell alignment.

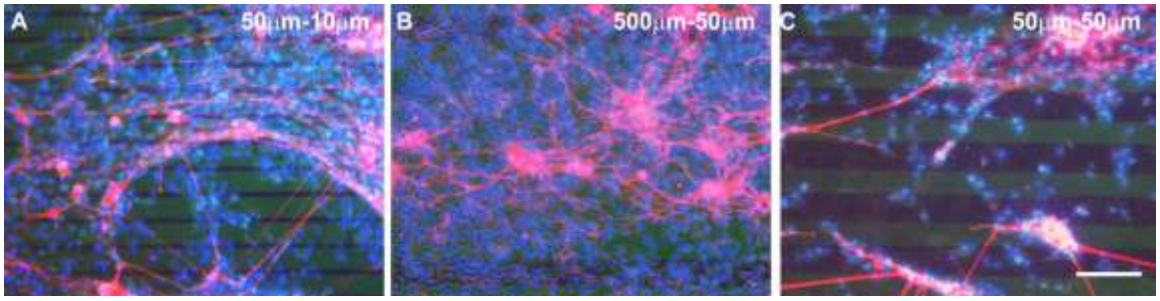

Figure 4.19. DRG neurites responded to environmental cues at day 5. Fluorescent micrographs show neurites positive for anti-β(III) tubulin (red), nuclei labeled with DAPI (blue) and LN stripes positive for anti-LN antibody (green) on 50 μm LN stripes separated by 10 μm (A), 500 μm LN stripes separated by 50 μm (B), and 50 μm LN stripes separated by 50 μm (C). Scale bar, 100 μm.

The percentage of neurites aligned within 20° of the LN stripes was quantified at day 5 and reported in Chapter 3 (Fig.4.20). Percent neurite alignment to 50 μm LN stripes separated by 50 μm spaces (40.6±1.3%) was significantly greater than percent neurite alignment to 50 μm LN stripes separated by 10 μm spaces (35.1±1.1; $P<0.01$). Percent neurite alignment to 500 μm LN stripes separated by 50 μm spaces (38.8±0.9%) was not significantly different from alignment to LN stripes of the other two conditions.

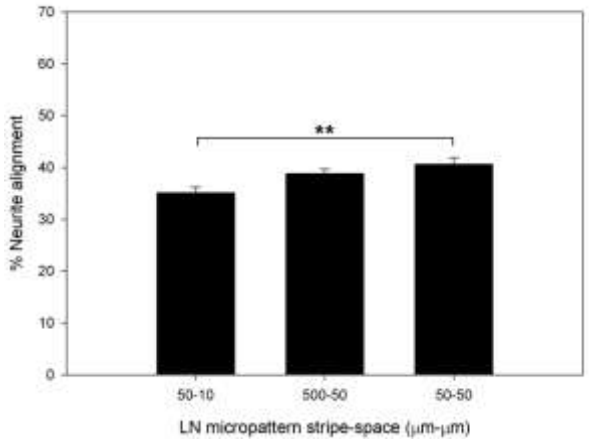

Figure 4.20. Percent neurite alignment at day 5 within 20° of 50 μm LN stripes separated by 10 μm, 500 μm LN stripes separated by 50 μm, and 50 μm LN stripes separated by 50 μm. (**$P<0.01$ significantly different from each other by one-way ANOVA. $n>30$ FOV for all conditions. Error bars are SEM).

Circular histograms depict an overall decreased clustering of nuclear orientation at day 5 compared to previous time points (Fig.4.21A-C). Additionally, the clustering of nuclear alignment at day 5 appeared to be more similar among conditions at day 5 when compared to previous time points. The nuclear angle distribution on 50 µm LN stripes separated by 10 µm spaces had a MVL of 0.16 occurring at 0.64° (Fig.4.21A). The nuclear angle distribution on 500 µm LN stripes separated by 50 µm spaces had a MVL of 0.17 occurring at 176.3° (Fig.4.21B). The nuclear angle distribution on 50 µm LN stripes separated by 50 µm spaces had a MVL of 0.30 occurring at 179.4° (Fig.4.21C).

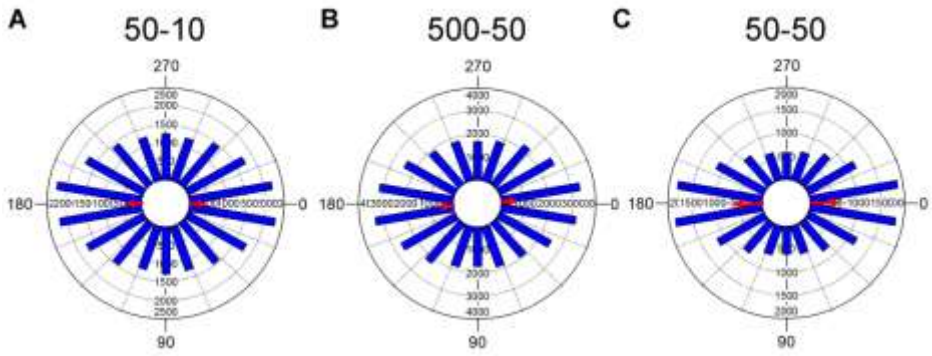

Figure 4.21. Day 2 DRG neurite response to directive cues depicted in Figure 4.19. is shown quantitatively on circular histograms. Circular histograms depict distribution of nuclear alignment on 50 µm LN stripes separated by 10 µm (A), 500 µm LN stripes separated by 50 µm (B), and 50 µm LN stripes separated by 50 µm (C). The length of each bar is proportional to the percentage of the number of DAPI-stained nuclei at the corresponding angle. Mean vector is represented in red. Neurite orientation was not uniformly distributed. Direction of LN micropattern lies along the 0-180° axis. All distributions were significantly different from uniform ($P<0.001$, Rayleigh test).

4.4.4. Dynamic analysis of neurite alignment to LN micropatterns over 24 hours supported hypothesized physical alignment mechanism

Timelapse microscopy was utilized to identify behavioral events leading to alignment response of dissociated DRG to the LN micropattern conditions for which sequential endpoint studies were conducted. Phase contrast images were captured every 5 minutes over the course of 24 hours beginning at the time that cells were seeded onto substrates presenting 50 µm LN stripes

separated by 10 μm spaces (Fig.4.22), 500 μm LN stripes separated by 50 μm spaces (Fig.4.23), or 50 μm LN stripes separated by 50 μm spaces (Fig.4.24). Several interesting morphological events were visible through analysis of these images.

On substrates presenting 50 μm LN stripes separated by 10 μm spaces, cells had adhered to the substrate surface by 6 h after seeding, and at this point, the orientation of cells appeared to be somewhat randomly distributed (Fig.4.22 panel 2). By 12 h, adhered cells had begun to spread, initiation of neurites was evident, and the majority of the cells were oriented along the direction of LN stripes (Fig.4.22 panel 3). At 18 h, cells were clearly aligned to the LN micropattern, and aligned cells appeared to contact neighboring cells along the stripes (Fig.4.22 panel 4). Finally, at 24 h, cell-cell interactions were highly present and a cable-like formation of cellular alignment was observed along the direction of the LN stripes (Fig.4.22 panel 5).

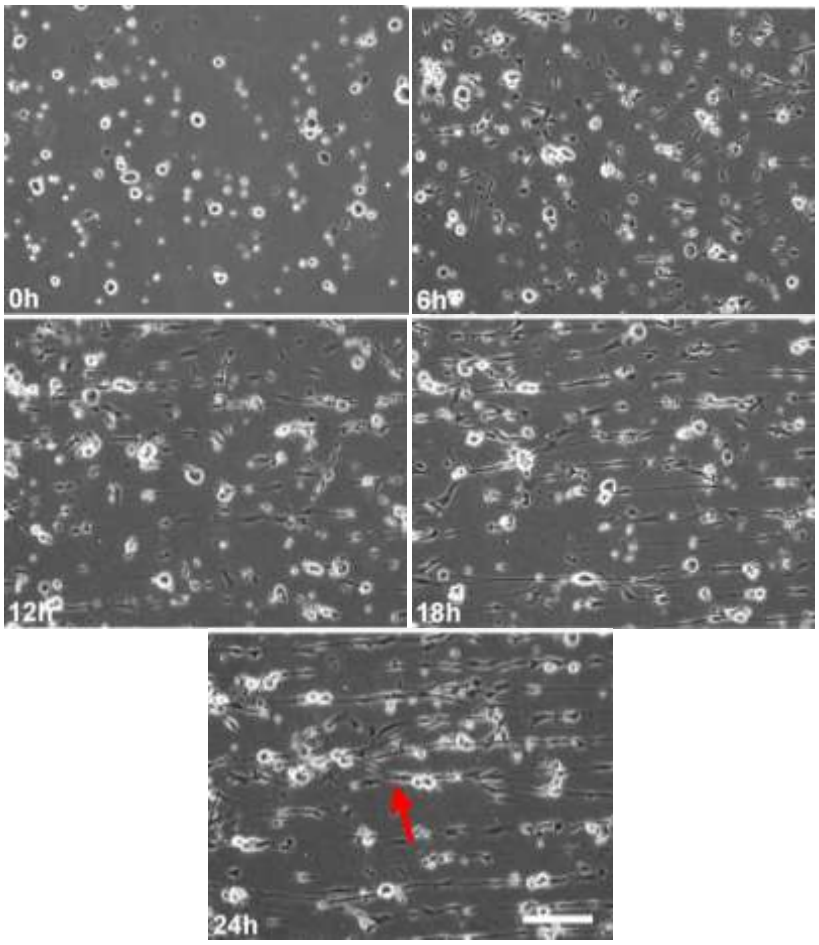

Figure 4.22. Phase contrast images obtained by timelapse microscopy of DRGs after 0 h, 6 h, 12 h, 18 h, and 24 h on 50 μm LN stripes with 10 μm spaces. Arrows indicate events described in text. Scale bar, 100 μm.

On substrates presenting 500 μm LN stripes separated by 50 μm spaces, cells had adhered to the substrate surface by 6 h after seeding, and the orientation of cells was not obviously aligned to any particular direction (Fig.4.23 panel 2). Throughout the remainder of the timelapse culture period, cells continued to spread and extend neurites, but the directedness of neurite extension was not evident except for regions of cell clustering and alignment that presumably occupied the LN stripe-space border (Fig.4.23 panels 4-5).

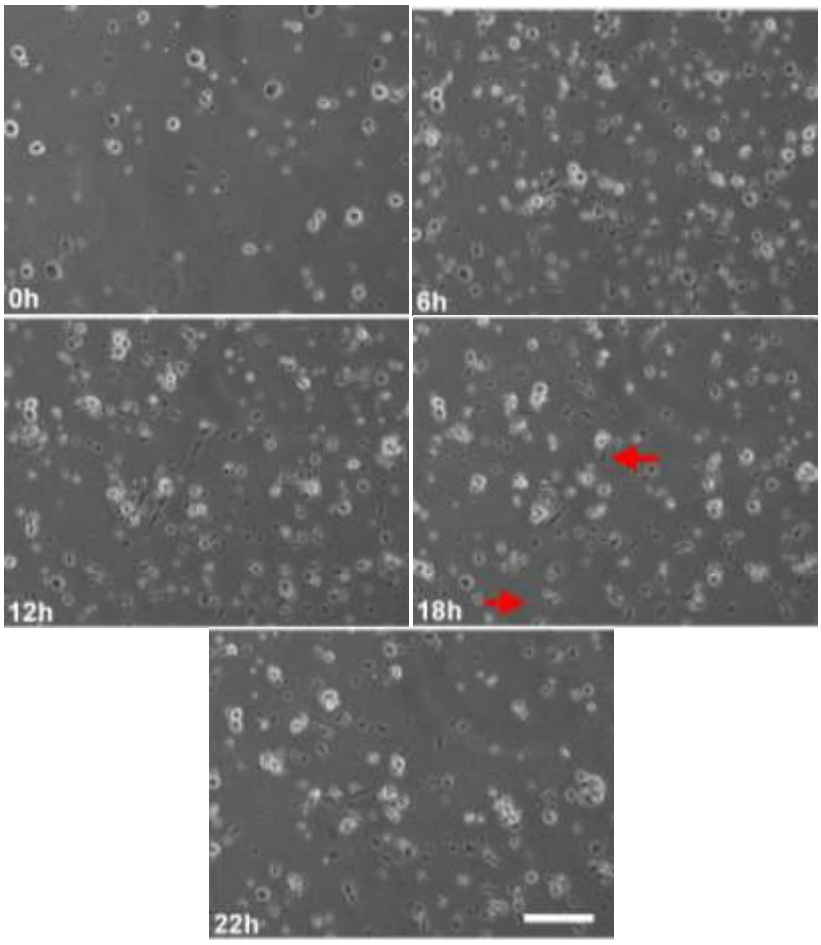

Figure 4.23. Phase contrast images obtained by timelapse microscopy of DRGs after 0 h, 6 h, 12 h, 18 h, and 24 h on 500 μm LN stripes with 50 μm spaces. Arrows indicate events described in text. Scale bar, 100 μm.

On substrates presenting 50 μm LN stripes separated by 50 μm spaces, cells had begun to adhere to the substrate surface by 6 h after seeding, and at this point, the orientation of cells appeared to be randomly distributed (Fig.4.24 panel 1). At 12 h, neurites began to extend along the LN stripes (Fig.4.24 panel 3), and by 18 h and 24 h, alignment to the stripes was evident (Fig.4.24 panels 4-5).

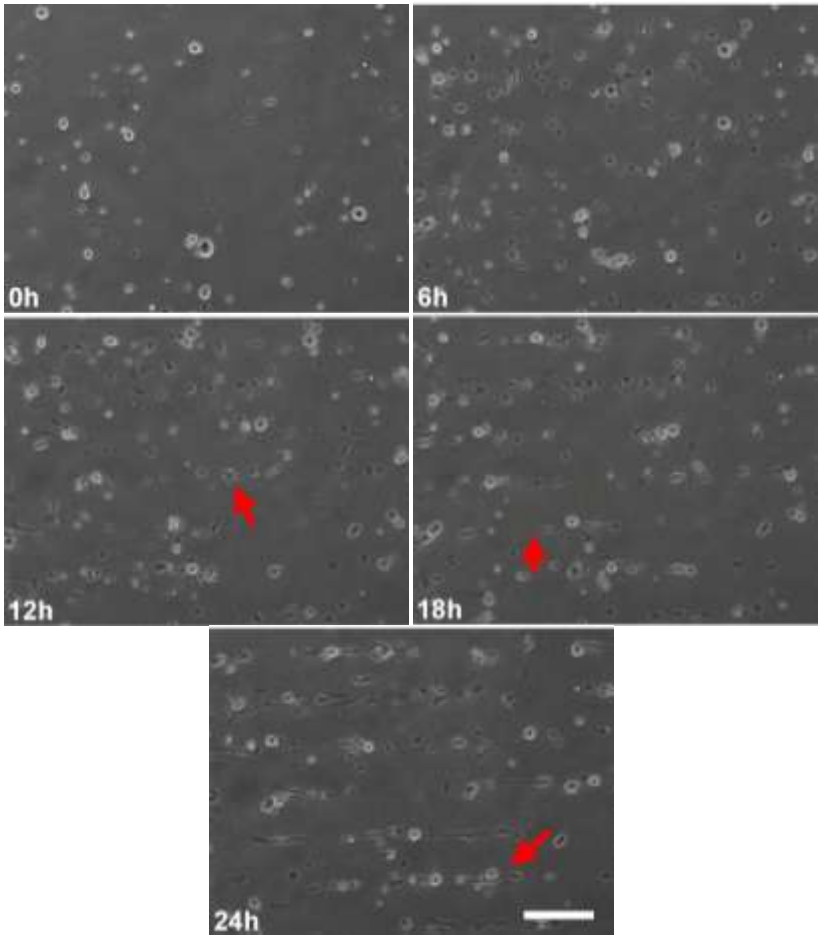

Figure 4.24. Phase contrast images obtained by timelapse microscopy of DRGs after 0 h, 6 h, 12 h, 18 h, and 24 h on 50 μm LN stripes with 50 μm spaces. Arrows indicate events described in text. Scale bar, 100 μm.

4.4.5. DRG response to competing cue platforms at day 1 and day 5

The following sections present results of cell response to competing cue platforms, on which SC replica topography was orthogonally opposed to LN micropatterns, as illustrated in Figure 4.25 below. For all images and circular histograms representing competing cue platforms, the SC replica topography was oriented to the horizontal direction, while the LN micropattern was oriented along the vertical direction. In figures presenting select micrographs of timelapse studies, the SC replica topography can be identified along the horizontal direction, as it remains constant over time.

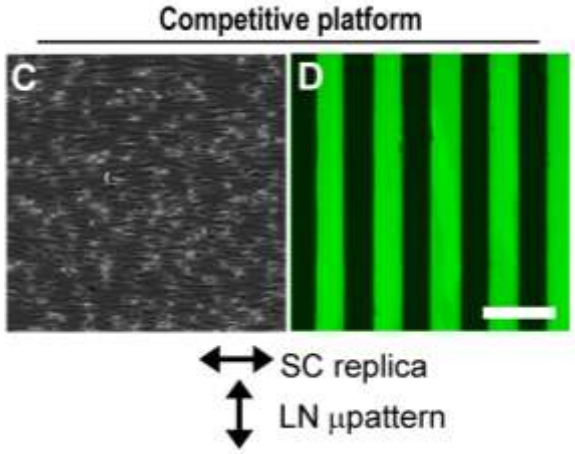

Figure 4.25. Competitive cue platforms. Phase contrast micrograph shows SC replica topography was oriented along the horizontal axis (C), while fluorescent micrograph shows LN micropattern was oriented along the vertical axis (D). Adapted from Chapter 3, Scale bar, 100 μm).

4.4.5.1. Neurite alignment on competitive cue platforms was complex

Based on the observations of neurite outgrowth response to competing cue platforms at 5 days (Chapter 3.4.4), we further investigated neurite response to competing cue platforms at earlier time points, to determine alignment events as neurite alignment is initiated and progresses. Toward this end, neurite alignment was quantified on competing cue platforms presenting 50 μm wide LN stripes separated by 10 μm wide spaces, 500 μm LN stripes separated by 50 μm wide spaces, and 50 μm wide LN stripes separated by 50 μm wide spaces. Further, neurite morphology

and alignment at day 1 were assessed in comparison to morphology and alignment day 5 that were described in Chapter 3. Additionally, timelapse microscopy was used to capture neurite alignment and cell growth events over the course of 24 hours on the competing cue platforms described.

4.4.6. Cell proliferation and nuclear alignment on competing cue platforms depended on micropattern dimensions.

To assess cell adhesion on competing cue substrates presenting SC replica topography orthogonally opposed to LN micropatterns of varied stripe and space widths, the average number of cells per field of view (FOV) was quantified at day 1 and day 5 (Fig.4.26). For all three conditions, cell number increased over time. On competing cue platforms presenting 50 μm LN stripes separated by 10 μm spaces there were 155 cells per FOV at day 1 and 253 cells per FOV at day 5 (Fig.4.26 black bars). On competing cue platforms presenting 500 μm LN stripes separated by 50 μm spaces there were 140 cells per FOV at day 1 and 180 cells per FOV at day 5 (Fig.4.26 gray bars). On competing cue platforms presenting 50 μm LN stripes separated by 50 μm spaces there were 131 cells per FOV at day 1 and 180 cells per FOV at day 5 (Fig.4.26 white bars).

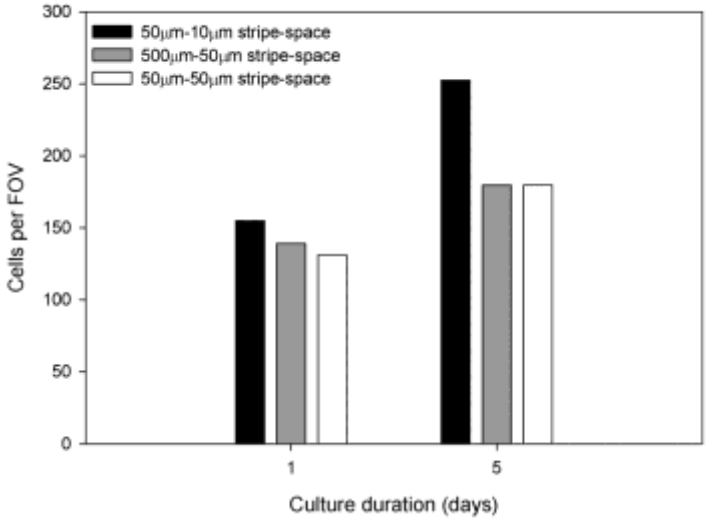

Figure 4.26. On competitive cue platforms, the number of cells per field of view increased with culture duration. Cell number per FOV on SC replica topography orthogonally opposed to 50 μm LN stripes separated by 10 μm (black bars), 500 μm LN stripes separated by 50 μm (gray bars), and 50 μm LN stripes separated by 50 μm (white bars) substrates evaluated at day 1 were compared to that at day 5 (Chapter 3).

Alignment of DAPI-labeled nuclei was determined on competing cue substrates at day 1 and day 5 (Fig.4.27). Circular analysis was used to describe the overall nuclear orientation in response to the LN micropatterns, and circular histograms illustrating nuclear distribution on competing cue platforms presenting SC replica topography orthogonally opposed to 50 μm wide LN stripes separated by 10 μm wide spaces, 500 μm LN stripes separated by 50 μm wide spaces, and 50 μm wide LN stripes separated by 50 μm wide spaces are depicted in Figures **4.30 and 4.33** A, B, and C, respectively. MVL and mean vector direction are discussed in the following section, and Figure 4.27 shows the MVL for all three competing cue platforms at day 1 and day 5.

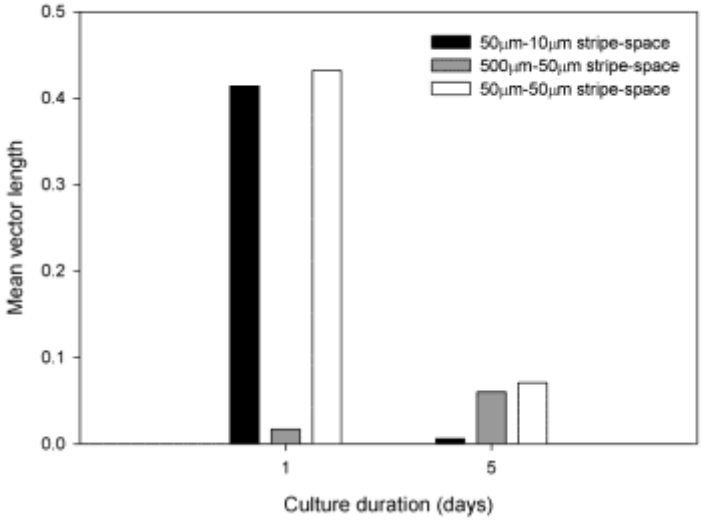

Figure 4.27. Mean vector lengths of circular distributions of nuclear orientation on competing cue platforms presenting SC replica topography orthogonally opposed to 50 μm LN stripes separated by 10 μm (black bars), 500 μm LN stripes separated by 50 μm (gray bars), and 50 μm LN stripes separated by 50 μm (white bars) substrates evaluated at day 1 were compared to that at day 5 (Chapter 3).

4.4.7. At day 1, cell morphology, neurite alignment, and nuclear alignment on competing cue platforms depended on micropattern dimensions

DRG morphology, neurite alignment behavior, and nuclear alignment were assessed on competing cue platforms presenting the three LN micropatterns described above in orthogonal opposition to SC replica topography. Neurite morphology, neurite alignment, and nuclear alignment on competing cue platforms were assessed at day 1 and compared with corresponding day 5 data presented in Chapter 3. Specifically, the percentage of neurite alignment to the direction of the LN micropattern was contrasted with the percentage of neurite alignment to the direction of the SC replica topography. It is of importance to note that the fluorescently labeled micrographs of competing cue platforms depict LN micropattern orientation along the vertical axis and SC replica topography orientation along the horizontal axis.

Neurite alignment response to the direction of micropatterned LN stripes and to the direction of SC replica topography on competing cue platforms described in Chapter 3 was assessed after 1 day culture duration. For all three of the conditions examined, neurite alignment was significantly higher to the direction of the LN stripes than to the direction of the SC replica topography ($P<0.001$; $n\geq18$ FOV; Figure 4.29). In particular, on competing cue platforms presenting 50 μm wide LN stripes separated by 10 μm wide spaces, 54.21±1.41% of neurites aligned to the LN stripes while 13.10±0.80 % of neurites aligned to the SC replica topography. On competing cue platforms presenting 500 μm wide LN stripes separated by 50 μm wide spaces, 30.03±0.76% of neurites aligned to the LN stripes while 24.94±0.65 % of neurites aligned to the SC replica topography. On competing cue platforms presenting 50 μm wide LN stripes separated by 50 μm wide spaces, 57.07±1.34% of neurites aligned to the LN stripes while 11.75±0.54 % of neurites aligned to the SC replica topography.

At day 1, neurite outgrowth on competing cue platforms presenting 50 μm LN stripes separated by either 10 μm spaces or 50 μm spaces appeared to be strongly aligned to the LN micropattern direction, although there appeared to be a limited extent of neurite outgrowth along the direction of the topographical features (Fig.4.28A,C). Neurite outgrowth on competing cue platforms presenting 500 μm LN stripes separated by 50 μm spaces appeared to be randomly distributed on the region of the LN furthest from the stripe-space border, with neurite a portion of outgrowth occurring along the direction of the topographical features within the LN stripe regions (Fig.4.28B).

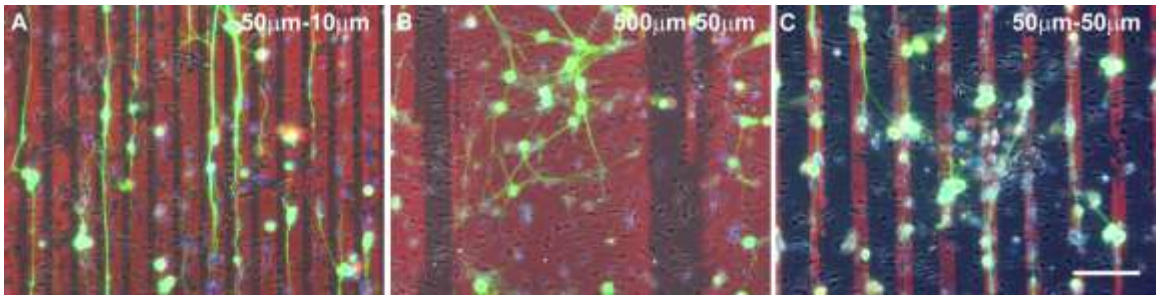

Figure 4.28. DRG neurites responded to environmental cues at day 1. Fluorescent micrographs show neurites positive for anti-β(III) tubulin (red), nuclei labeled with DAPI (blue) and LN stripes positive for anti-LN antibody (green) on SC replica topography (horizontal) orthogonally opposed to 50 μm LN stripes separated by 10 μm (A), 500 μm LN stripes separated by 50 μm (B), and 50 μm LN stripes separated by 50 μm (C). Scale bar, 100 μm.

Neurite alignment to the LN micropattern was compared across competing cue platforms presenting varied LN micropattern dimensions (Fig.4.29). Strength of neurite alignment to the LN stripes was significantly lower on competing cue platforms presenting 500 μm LN stripes separated by 50 μm wide spaces (30.03±0.76%) compared to competitive cue platforms presenting 50 μm wide LN stripes separated by 10 μm wide spaces (54.21-1.41%) or 50 μm wide spaces (57.07±1.34%). Correspondingly, strength of neurite alignment to the SC replica topography was significantly higher on competing cue platforms presenting 500 μm LN stripes separated by 50 μm wide spaces (24.94±0.65%) compared to competitive cue platforms presenting 50 μm wide LN stripes separated by 50 μm wide spaces (11.75±0.54%) or 50 μm wide LN stripes separated by 10 μm wide spaces (13.10±0.80%; Fig.4.29)

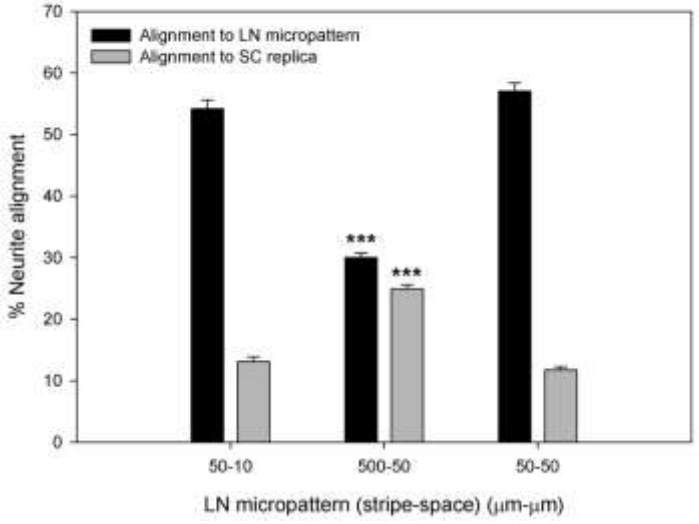

Figure 4.29. Neurite alignment on competing cue platforms at day 1. Percent neurite alignment within 20° of LN micropattern direction (black bars) and to SC replica topography (gray bars) at day 1 on competing cue platforms presenting 50 μm LN stripes separated by 10 μm, 500 μm LN stripes separated by 50 μm, and 50 μm LN stripes separated by 50 μm orthogonally opposed to SC replica topography. (***P<0.001 significantly different from all other conditions by one-way ANOVA. n≥18 FOV for all conditions. Error bars are SEM).

Circular histograms depict the nuclear angle distribution on competing cue platforms at day 1 (Fig.4.30). The orientation of SC replica topography lies along the 0°-180° axis, while the orientation of LN stripes lies along the 90°-270° axis. The nuclear angle distribution on competing cue platforms presenting SC replica topography orthogonally opposed to 50 μm LN stripes separated by 10 μm spaces had a MVL of 0.4 occurring at 89.6°, which was significantly different from uniform (Fig.4.30A; Rayleigh test; P<0.001). The nuclear angle distribution on competing cue platforms presenting SC replica topography orthogonally opposed to 500 μm LN stripes separated by 50um spaces had a MVL of 0.02 occurring at 43.16°, which was not significantly different from uniform (Fig.4.30B; Rayleigh test; P=0.42). The nuclear angle distribution on competing cue platforms presenting SC replica topography orthogonally opposed to 50 μm LN stripes separated by 50 μm spaces had a MVL of 0.43 occurring at 91.7°, which was significantly different from uniform (Fig.4.30C, Rayleigh test; P<0.001).

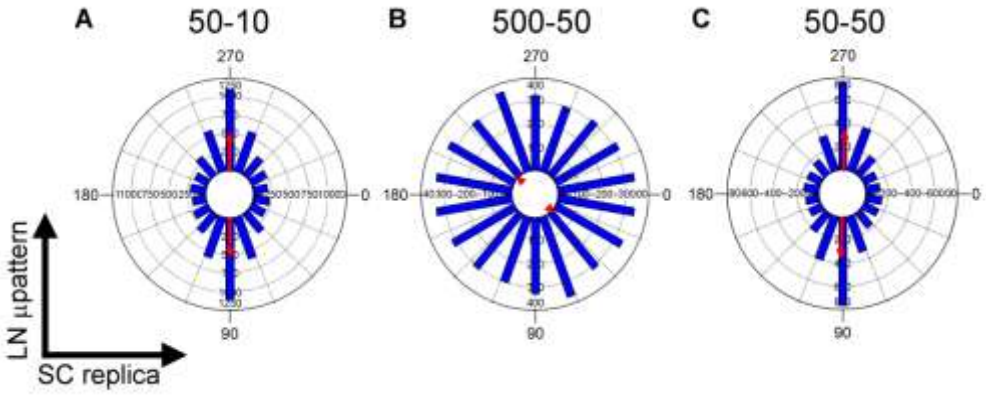

Figure 4.30. Day 1 DRG neurite response to competing cue platforms depicted in **Figure 4.28** is shown quantitatively on circular histograms. Circular histograms depict distribution of nuclear alignment on competing cue platforms presenting SC replica topography (horizontal) orthogonally opposed to 50 µm LN stripes separated by 10 µm (A), 500 µm LN stripes separated by 50 µm (B), and 50 µm LN stripes separated by 50 µm (C). The length of each bar is proportional to the percentage of the number of DAPI-stained nuclei at the corresponding angle. Mean vector is represented in red. Neurite orientation was not uniformly distributed by Rayleigh's test and Rao's test for uniformity. Direction of LN micropattern lies along the 90°-270° axis. Direction of SC replica topography lies along the 0°-180° axis.

4.4.8. At day 5, cell morphology, neurite alignment, and nuclear alignment on competing cue platforms depended on cell-cell interactions and micropattern dimensions

At day 5, neurite outgrowth on competing cue platforms appeared to be aligned with less strength to either of the two substrate cues. In particular, neurite outgrowth occured between the LN stripes for all conditions, and outgrowth along the direction of the SC replica topography was evident across all three conditions, with more apparent alignment to the SC replica on competing cue substrates presenting 500 µm LN stripes separated by 50 µm spaces (Fig.4.31B). Neurite outgrowth appeared to be associated strongly with neighboring neurites and cells for all three conditions (Fig.4.31A-C).

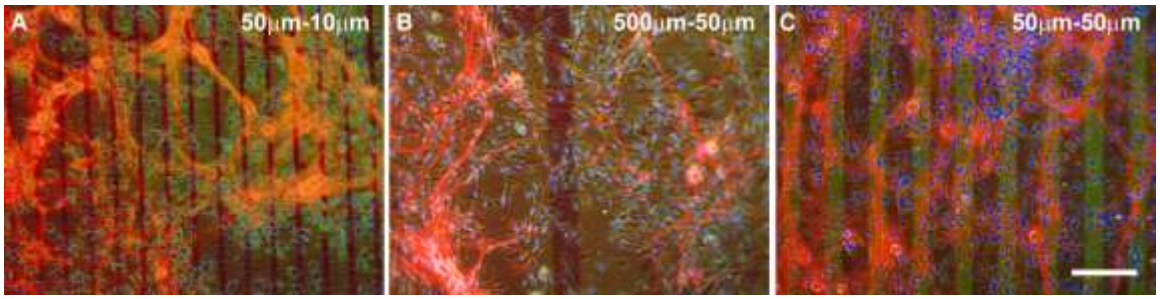

Figure 4.31. DRG neurites responded to environmental cues and neighboring cells at day 5. Fluorescent micrographs show neurites positive for anti-β(III) tubulin (red), nuclei labeled with DAPI (blue) and LN stripes positive for anti-LN antibody (green) on SC replica topography (horizontal) orthogonally opposed to 50 μm LN stripes separated by 10 μm (A), 500 μm LN stripes separated by 50 μm (B), and 50 μm LN stripes separated by 50 μm (C). Scale bar, 100 μm.

Neurite alignment on competing cue platforms at day 5 was assessed in Chapter 3. Briefly, neurite alignment was significantly higher to the direction of LN stripes on competing cue platforms presenting SC replica topography orthogonally opposed to 50 μm LN stripes separated by either 10 μm spaces (28.6±1.1% to LN vs. 25.8±0.9% to SC replica; $P<0.05$) or 50 μm spaces (3.1±1.7% to LN vs. 24.1±1.5% to SC replica; $P<0.001$). In contrast, neurite alignment was significantly higher to the direction of the SC replica topography on competing cue platforms presenting SC replica topography orthogonally opposed to 500 μm LN stripes separated by 50 μm spaces (25.6±1.0% to LN vs. 40.7±1.1% to SC replica topography; $P<0.001$).

Neurite alignment response to the LN micropattern was compared across competing cue platforms presenting distinct LN micropattern dimensions described above (Fig.4.32). The strength of neurite alignment to the LN stripes was significantly higher on competing cue platforms presenting 50 μm LN stripes separated by 50 μm spaces (33.1±1.7%) compared to alignment on competing cue platforms presenting 500 μm LN stripes separated by 50 μm spaces (25.6±1.0%) or competing cue platforms presenting 50 μm LN stripes separated by 10 μm spaces (28.6±1.1%; $P<0.05$; Fig.4.32 black bars).

When compared to other conditions, neurite alignment to the direction of the SC replica topography was significantly higher on competing cue platforms presenting 500 μm LN stripes separated by 50 μm spaces (30.7±1.1%) compared to neurite alignment to the SC replica topography on competing cue platforms presenting 50 μm LN stripes separated by either 10 μm spaces (25.8±0.9%) or 50 μm spaces (24.1±1.5%) ($P<0.05$; Fig.4.32 gray bars).

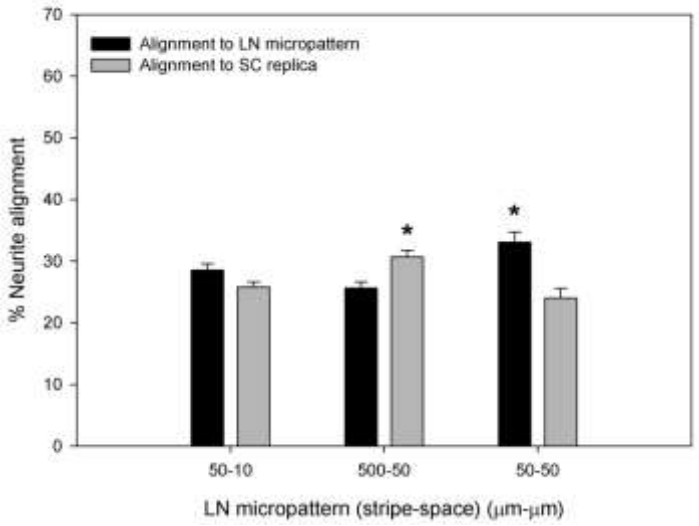

Figure 4.32. Neurite alignment on competing cue platforms at day 5. Percent neurite alignment within 20° of LN micropattern direction (black bars) and to SC replica topography (gray bars) at day 5 on competing cue platforms presenting 50 μm LN stripes separated by 10 μm, 500 μm LN stripes separated by 50 μm, and 50 μm LN stripes separated by 50 μm orthogonally opposed to SC replica topography. (*$P<0.05$ significantly different from alignment to the specified direction of other conditions by one-way ANOVA. $n\geq39$ FOV for all conditions. Error bars are SEM. Data was reproduced from Chapter 3).

Circular histograms depict the nuclear angle distribution on competing cue platforms at day 5 (Fig.4.33). The nuclear angle distribution on competing cue platforms presenting SC replica topography orthogonally opposed to 50 μm LN stripes separated by 10 μm spaces had a MVL of 0.01 occurring at 72.4°, which was not significantly different from uniform (Fig.4.33A; Rayleigh test; $P=0.57$).The nuclear angle distribution on competing cue platforms presenting SC replica topography orthogonally opposed to 500 μm LN stripes separated by 50 μm spaces had a MVL of

0.06 occurring at 169.7°, which was significantly different from uniform (Fig.4.33B; Rayleigh test; P<0.001). The nuclear angle distribution on competing cue platforms presenting SC replica topography orthogonally opposed to 50 μm LN stripes separated by 50 μm spaces had a MVL of 0.07 occurring at 97.4° which was significantly different from uniform (Fig.4.33C; Rayleigh test; P<0.001).

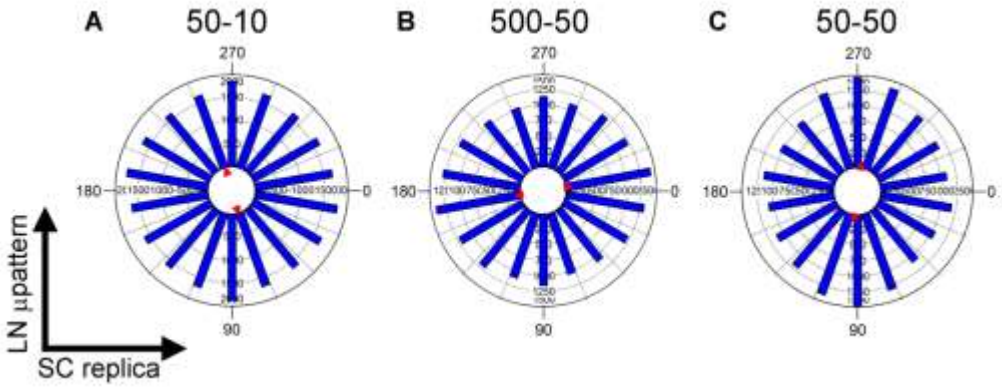

Figure 4.33. Day 5 DRG neurite response to competing cue platforms depicted in **Figure 4.31**. is shown quantitatively on circular histograms. Circular histograms depict distribution of nuclear alignment on competing cue platforms presenting SC replica topography (horizontal) orthogonally opposed to 50 μm LN stripes separated by 10 μm (A), 500 μm LN stripes separated by 50 μm (B), and 50 μm LN stripes separated by 50 μm (C). The length of each bar is proportional to the percentage of the number of DAPI-stained nuclei at the corresponding angle. Mean vector is represented in red. Neurite orientation was not uniformly distributed. Direction of LN micropattern lies along the 90°-270° axis.

4.4.9. Dynamic analysis of neurite alignment to competing cue platforms over 24 hours supported hypothesized physical alignment mechanism

Timelapse microscopy was used to visualize DRG cell behavior events at early time points when cell adhesion and initial neurite extension and decision-making take place. Figures 4.34 - 4.36 depict sequential phase contrast micrographs from timelapse experiments on the three competing cue platforms investigated. In each of the micrographs, the SC replica is oriented along the horizontal axis, while the LN micropattern is oriented along the vertical axis.

On competing cue platforms presenting SC replica topography orthogonally opposed to 50 µm LN stripes separated by 10 µm spaces, cells had adhered by 6 h in culture, and apparent cell alignment to the direction of the LN micropattern was visible by 6 h (Fig.4.34 panels 1-2). Cell spreading and neurite alignment progressively aligned to the direction of the LN micropattern as culture time advanced, and by 18 h and 24 h, obvious preference for the LN micropattern direction versus the SC replica topography direction was observed (Fig.4.34 panels 3-5). Although some alignment of cells to the direction of the SC replica topography could be seen at 18 h, the predominant direction of neurite and cell alignment occurred to the LN micropattern direction.

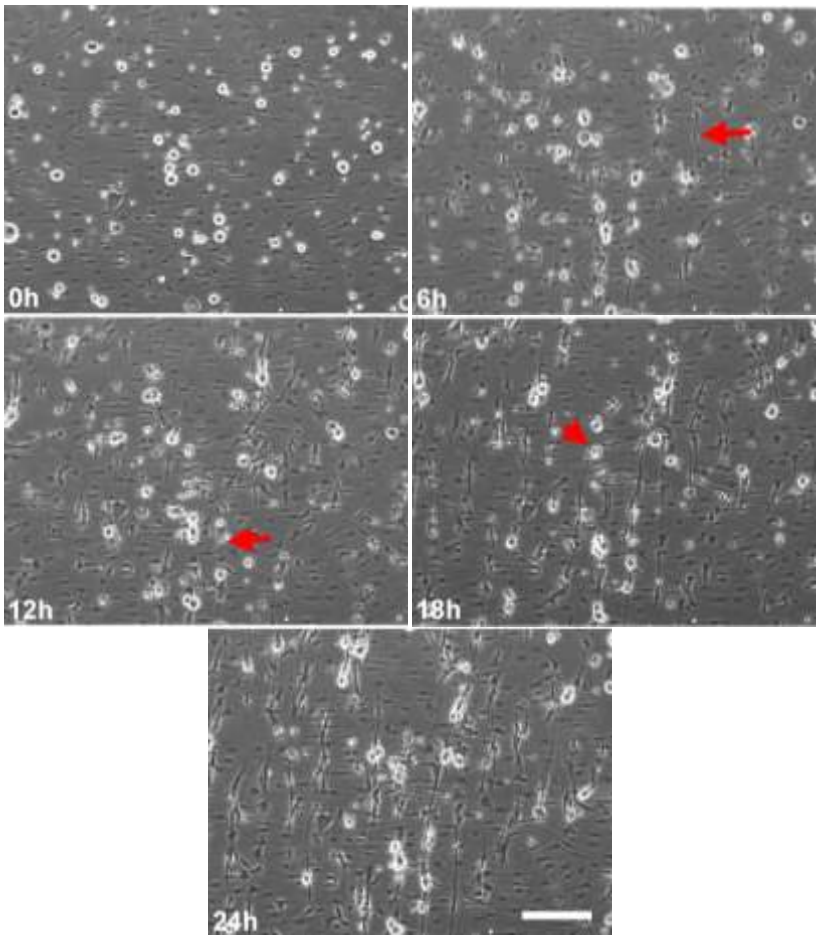

Figure 4.34. Phase contrast images obtained by timelapse microscopy of DRGs after 0 h, 6 h, 12 h, 18 h, and 24 h on 50 μm LN stripes with 10 μm spaces (vertical) orthogonally opposed to SC replica topography (horizontal). Arrows indicate events described in text. Scale bar, 100 μm.

On competing cue platforms presenting SC replica topography orthogonally opposed to 500 μm LN stripes separated by 50 μm spaces, cells had adhered by 6 h in culture, but there did not appear to be a preferential direction of cell alignment until later time points (Fig.4.35 panel 1-2). At 18 h, cell alignment along the apparent LN stripe-space border was observed, although cell movement and alignment to the direction of the SC replica topography dominated within the suggested LN stripe region (Fig.4.35 panel 4). At 24 h, cells were visibly aligned to the LN micropattern along the suggested LN stripe-space borders, but at locations interior to the stripe-space borders, cell and neurite alignment were not obviously preferential toward either cue (Fig.4.35 panel 5).

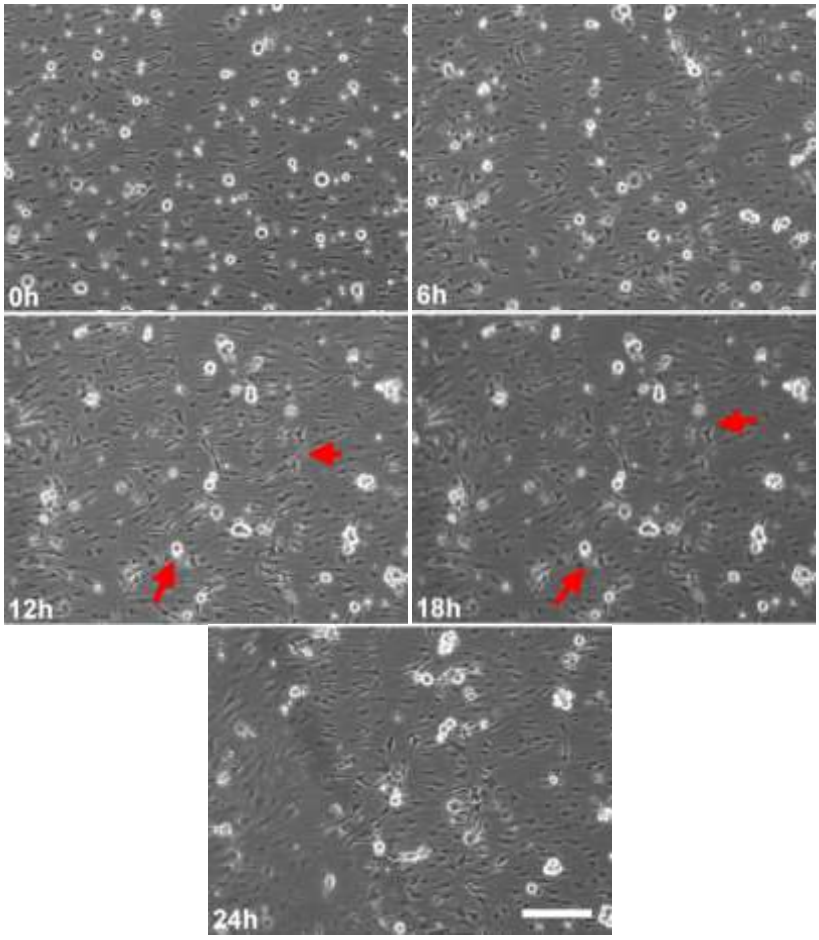

Figure 4.35. Phase contrast images obtained by timelapse microscopy of DRGs after 0 h, 6 h, 12 h, 18 h, and 24 h on 500 μm LN stripes with 50 μm spaces (vertical) orthogonally opposed to SC replica topography (horizontal). Arrows indicate events described in text. Scale bar, 100 μm.

On competing cue platforms presenting SC replica topography orthogonally opposed to 50 μm LN stripes separated by 50 μm spaces, cells had adhered by 6 h in culture, and apparent cell alignment to the direction of the LN micropattern was visible by 6 h (Fig.4.36 panels 1-2). Cell spreading and neurite alignment progressively aligned to the direction of the LN micropattern as culture time advanced, and by 18 h and 24 h, obvious preference for the LN micropattern direction versus the SC replica topography direction was observed (Fig.4.36 panels 3-5). The predominant direction of neurite and cell alignment occurred to the LN micropattern direction.

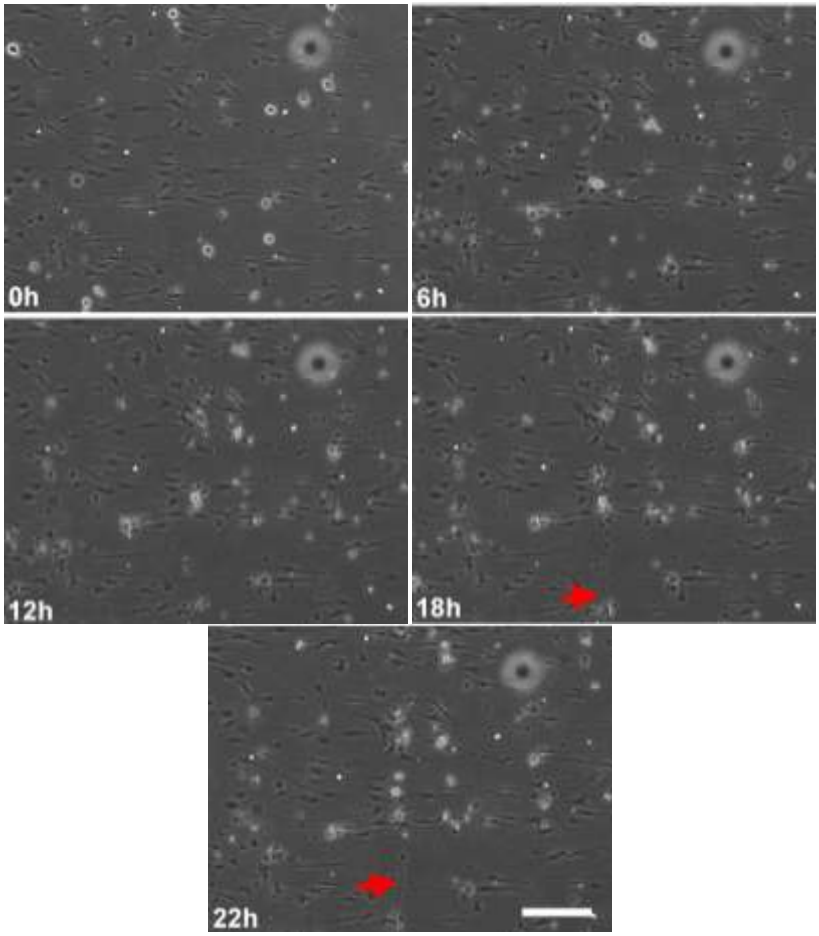

Figure 4.36. Phase contrast images obtained by timelapse microscopy of DRGs after 0 h, 6 h, 12 h, 18 h, and 24 h on 50 μm LN stripes with 50 μm spaces (vertical) orthogonally opposed to SC replica topography (horizontal). Arrows indicate events described in text. Scale bar, 100 μm.

4.5. Discussion

The hypotheses based on the findings of Chapter 3 prompted the further investigation of neurite outgrowth on micropatterned LN stripes and biomimetic topographical features via timelapse microscopic techniques, in order to capture dynamic events as navigating neurites encounter complex environmental cues. Vital aspects of cell behavior and morphological changes have been illuminated by the sequential endpoint and timelapse microscopy studies presented here. These techniques enabled the visualization of incremental and real-time neurite growth and alignment events on platforms presenting micropatterned LN stripes and on competitive cue platforms presenting LN stripes orthogonally opposed to SC replica topography.

4.5.1. Cell number and nuclear alignment changed with time on platforms presenting LN micropatterns

That overall cell count increased with increased duration of culture time was expected, as the SC within the heterotypic culture are proliferative. However, the trend by which cell count increased to either day 3 (50 μm wide stripes separated by 10 μm) or day 4 (500 μm or 50 μm wide stripes separated by 50 μm), may be an indication of different cell response to substrates based on the percentage of the substrate containing LN. In the case of 50 μm wide LN stripes separated by 10 μm spaces, approximately 91% of the surface contained LN, and maximal cell count was observed at day 3. For the condition presenting 500 μm wide stripes of LN separated by 50 μm wide spaces, approximately 83% of the substrate surface contained LN, and maximal cell count was observed at day 4. For the condition presenting 50 μm wide stripes of LN separated by 50 μm wide spaces, 50% of the substrate surface contained LN, and maximal cell count was observed at day 4, although this difference was marginal compared to other time points. It warrants further experimentation to determine the degree to which LN surface coverage affects cell proliferation on micropatterned substrates. Additionally, serum deposition onto the substrate surface may impact cell attachment and proliferation over time, as shown previously[5-6].

An alternate explanation for the observation of a peak in cell count lies in the method by which DAPI nuclei are counted. Through NIH ImageJ (v.1.45) software particle analysis, the total number of DAPI-labeled nuclei was quantified. As cell density increased, neighboring cells approached confluence, resulting in nuclear clustering. This nuclear clustering may have resulted in the artificial underestimation of cell count, as multiple neighboring cells would have been counted as a single cell. Although either or both of these explanations have the potential to have influenced the quantification of cell count, we observed robust cell growth and morphology

throughout all of the experiments documented in this Chapter, wherein SC proliferation and neurite extension were representative of healthy cell culture conditions.

Taken together, the cell number and nuclear alignment data indicate that multiple physical mechanisms of alignment may take place on LN micropatterns presenting different dimensions. Because SC make up nearly 90% of the cells comprising DRG, nuclear orientation is a rough estimate of overall SC orientation. As cells proliferated, nuclear alignment strength decreased on substrates presenting 50 μm LN stripes separated by either 10 μm spaces or 50 μm spaces, whereas nuclear alignment to the micropattern direction remained relatively constant with a slightly increasing trend on substrates presenting 500 μm LN stripes separated by 50 μm spaces. These data are supported by previous work that has shown that the stripe-space border is a critical determinant of neurite alignment behavior[7], but that on wide regions of LN, exploring growth cones interpret the region of LN as a homogenous substrate[6].

4.5.2. Neurite alignment to LN micropatterns presented individually and via competing cue platforms depended on time and micropattern dimensions

Sequential endpoint studies over the first 4 days and timelapse microscopy over the first 24 hours of culture time revealed in depth dynamic analysis of neurite alignment to micropatterned LN stripes. Competing cue platforms were assessed for neurite outgrowth response at day 1 and compared to that at day 5 in addition to timelapse analysis at day 1. Based on the conditions examined here, it is suggested that neurite alignment to micropatterned LN stripes takes place as a sequence of orchestrated events, all of which depend on cell density and micropattern dimensions. Below, the major events are discussed for each of the conditions investigated, along with potential explanations for their occurrence.

On substrates presenting 50 μm LN stripes separated by 10 μm spaces, there was a strong alignment response initially, as neurites extended and contacted LN stripe borders soon after cell adhesion. As time progressed, SC proliferation increased, and the relatively small 10 μm spaces between LN stripes were overgrown such that cell-cell interactions detracted from the overall alignment to the micropattern as cells and neurites grew laterally across the spaces between the stripes.

On substrates presenting 500 μm LN stripes separated by 50 μm spaces, alignment to the LN micropattern was not as strong as it was to the other cues examined, and occurred at a relatively slow pace, such that initial cell adhesion to the wide LN stripe was followed by extension and outgrowth on a wide region of LN before local cell-cell interactions and local cell-cell alignment result in eventual neurite alignment to the direction of the stripe. In this case, there was a delay in the alignment response, as initial neurite growth encountered stripe-space borders with less frequency compared to the other conditions examined. It can be speculated that the large regions of LN were interpreted as homogeneous in nature, and as such, neurites aligned randomly except for at the stripe-space borders. As time progressed, the extending neurites eventually encountered and followed the direction of the stripe-space borders. Based on the level of alignment at later time points, it can be suggested that alignment at the stripe-space border propagated toward the interior of the stripe, resulting in a slight increase in overall alignment as time progressed. However, as time progressed, cell proliferation occurred, so the level to which alignment was able to propagate toward the interior of the 500 μm stripe was likely limited by established cell and neurite orientation at those regions.

On substrates presenting 50 μm LN stripes separated by 50 μm spaces, neurite alignment response was strong initially, and was maintained at the highest level among the conditions

investigated. This may be because 50 μm LN stripes separated by 50 μm spaces approaches the optimal dimensions to promote DRG neurite guidance. It has been shown that dimensions on this order were optimal to promote SC alignment response[2], and as DRG cultures contain SC, it is a reasonable speculation that similar dimensions would elicit a strong alignment response to the culture overall.

On competing cue substrates presenting SC replica topography orthogonally opposed to 50 μm LN stripes separated by 10 μm spaces there was a strong alignment response to the direction of the LN micropattern at day 1. This response may be attributed to the high frequency of stripe-space borders, at which neurites preferentially aligned to the LN micropattern rather than the orthogonally opposed SC replica topography. At the 5 day endpoint, the difference in alignment response to each cue decreased. This may suggest, therefore, that the relatively narrow 10 μm space was small enough that the growth cone filopodia could readily pass over the stripe to reach the next region of LN with lateral movement. Although the alignment strength to the LN stripes was higher than to the SC replica topography at day 5, the level of significance in the difference had greatly decreased from day 1 to day 5, suggesting that the orthogonally opposed topographical cue and the relatively low space between LN stripes, in conjunction with cell proliferation and local alignment, resulted in a decrease in alignment strength to the LN cue over time.

On competing cue substrates presenting SC replica topography orthogonally opposed to 500 μm LN stripes separated by 50 μm spaces, it is likely that the large region of LN was interpreted as a homogenous region with respect to LN but as an anisotropic region of SC replica topography, such that higher relative alignment to the direction of the SC replica took place on the LN stripe region. It can be speculated that although alignment to the LN stripes occurred at the stripe-space

borders, the large regions of homogenous LN encouraged alignment to the SC replica topography. This was evident by day 5, when neurite alignment to the SC replica was significantly greater than alignment to the LN stripes.

On competing cue substrates presenting SC replica topography orthogonally opposed to 50 μm LN stripes separated by 50 μm spaces, neurite alignment response to the LN stripes was strong initially and dominated the alignment response throughout the culture duration. It can be speculated that neurite alignment response to the stripe-space borders was sustained because the 50 μm spaces between stripes was large enough to preclude lateral outgrowth along the direction of the SC replica topography.

4.5.3. Neuronal-glial interactions governed a significant portion of neurite alignment as time progressed

Neuronal interactions with glial cells, such as SC, play a significant role in neurite alignment along the direction of micropatterned LN stripes and the SC replica topography. There are multiple events at play, in which SC and neurite align to themselves, each other, and the underlying micropatterned stripes. These effects may be enhanced or limited over time as SC proliferation increases the proportion of the substrate surface occupied by SC that exhibit local alignment to each other[8-9]. Neurite alignment to neighboring neurites may also impact overall alignment, such that local alignment of neurites to other neurites and neighboring SC may overpower the neurite alignment response to the underlying LN micropatterned stripes[10].

As SC proliferated over time, they became more numerous, occupying an increasing proportion of the substrate surface, and because SC present both topographical and chemical guidance to navigating neurites, this increase in SC presence may have ultimately overpowered the initial

alignment response to the underlying LN micropattern, such that the initial response strength was greater than the sustained neurite alignment response to the micropattern. Neurites and glia responded to the specific micropattern dimensions of each substrate, such that the optimal alignment response depended heavily on micropattern stripe and space dimensions as well as the local heterotypic and homotypic cell interactions.

4.6. Conclusions

Based on the quantification and dynamic observations from this study, several proposed neurite behaviors were observed. These behaviors align with our hypotheses, where it is suggested that neurite alignment is highly dependent on stripe-space border frequency at early time points, and that as SC proliferation takes place over time, local cell-cell interactions progress to eventually dominate overall neurite and cell alignment on micropatterned substrates. We proposed, therefore, that the rate of initial neurite alignment and the rate of cell proliferation coordinate to result in overall neurite alignment over an extended culture period. We proposed that maximal neurite alignment may be achieved with the combination of expedient initial alignment and a lag in local cell alignment, such that neurite alignment to stripe space borders dominates the overall culture directedness, and that subsequent cell proliferation and consequential local cell-cell alignment progress with maintained neurite orientation along the micropattern direction. Based on the observations of this research, it has become evident that the role of glia (SC) in neurite alignment response may both enhance and detract from neurite and overall cell alignment to an intended direction. Neuron-glial interactions may enhance alignment in the case when neurites are already strongly oriented along the micropatterned LN stripes. In contrast, neuron-glial interactions may limit alignment response when local alignment events occur with less strength to the intended direction, either as a result of relatively weak neurite alignment or relatively weak alignment to the micropatterned LN stripes.

When adapted toward an application-based approach, these data may be used to inform improved design of therapeutic biomaterials to improve nerve repair after injury. Along these lines, nerve guidance conduits have been implemented to encourage directed nerve growth toward the distal target nerve stump. The findings here lead to the suggestion that nerve guidance conduits should promote expedient neurite alignment at the onset of implantation, and that the subsequent infiltration of native SC should be encouraged to strongly align to the intended neurite growth direction, as local cell alignment plays a significant role in overall neurite alignment over time.

A topic worth consideration is that the responses observed here are specific to postnatal rat DRG cultures, and are likely to vary with cell type and culture conditions. For example, in a study by Rajnicek et al, an unexpected observation was made, wherein Xenopus spinal neurites aligned along the direction of microgrooves on a quartz substrate, while rat hippocampal neurites aligned perpendicularly to the shallow grooves[11], indicating the cell-type distinctions which arise when investigating outgrowth response to environmental cues.

Further, the observations made here were dependent on culture conditions, wherein all conditions described were based in serum-containing media, which promoted proliferation of the SC and fibroblasts that comprise DRG explants. In vivo, SC are highly active following nerve injury, migrating and proliferating at the site of injury, such that neurite-glia interactions play a pivotal role in overall cell behavior. Thus, these complexities must be kept in mind in the design of therapeutics for repair of nerve injury, and data collected from contributing research should note the physiological response and cell interactions which inevitably occur upon implantation and during regeneration.

4.7. Literature cited

1. Snow, D.M. and P.C. Letourneau, *Neurite outgrowth on a step gradient of chondroitin sulfate proteoglycan (CS-PG).* J Neurobiol, 1992. **23**(3): p. 322-36.
2. Kofron, C.M. and D. Hoffman-Kim, *Optimization by Response Surface Methodology of Confluent and Aligned Cellular Monolayers for Nerve Guidance.* Cell Mol Bioeng, 2009. **2**(4): p. 554-572.
3. Laketa, V., et al., *High-content microscopy identifies new neurite outgrowth regulators.* Mol Biol Cell, 2007. **18**(1): p. 242-52.
4. Lautermilch, N.J. and N.C. Spitzer, *Regulation of calcineurin by growth cone calcium waves controls neurite extension.* J Neurosci, 2000. **20**(1): p. 315-25.
5. Grinnell, F. and T.V. Phan, *Deposition of fibronectin on material surfaces exposed to plasma: quantitative and biological studies.* J Cell Physiol, 1983. **116**(3): p. 289-96.
6. Britland, S., Perridge, C., Denyer, M., Morgan, H., Curtis, A., Wilkinson, C., *Morphogenetic guidance cues can interact synergistically and hierarchically in steering nerve cell growth.* Exp biol online, 1996. **1**(2): p. 1-15.
7. Clark, P., S. Britland, and P. Connolly, *Growth cone guidance and neuron morphology on micropatterned laminin surfaces.* J Cell Sci, 1993. **105 (Pt 1)**: p. 203-12.
8. Koppes, A.N., A.M. Seggio, and D.M. Thompson, *Neurite outgrowth is significantly increased by the simultaneous presentation of Schwann cells and moderate exogenous electric fields.* J Neural Eng, 2011. **8**(4): p. 046023.
9. Thompson, D.M. and H.M. Buettner, *Schwann cell response to micropatterned laminin surfaces.* Tissue Eng, 2001. **7**(3): p. 247-65.
10. Thompson, D.M. and H.M. Buettner, *Oriented Schwann cell monolayers for directed neurite outgrowth.* Ann Biomed Eng, 2004. **32**(8): p. 1120-30.

11. Rajnicek, A., S. Britland, and C. McCaig, *Contact guidance of CNS neurites on grooved quartz: influence of groove dimensions, neuronal age and cell type.* J Cell Sci, 1997. **110 (Pt 23)**: p. 2905-13.

CHAPTER 5

PHARMACOLOGICAL INHIBITION OF MECHANOSENSITIVE TREK-1 CHANNELS: A MECHANISTIC INVESTIGATION OF NEURITE RESPONSE TO TOPOGRAPHICAL FEATURES

5.1. Abstract

Contact guidance is the process by which cells and cellular processes, such as neurites, respond to and track along the topographical features that make up their environmental landscape. In vivo, neurites are guided by several forms of topography, including microscale and nanoscale features of the extracellular matrix (ECM), macroscale tissue architecture, and cellular topographical features. It is of particular interest to determine how such guidance takes place from a mechanistic standpoint, so that the process of neurite alignment and navigation in response to

environmental cues may be more clearly understood to identify targets for therapeutic intervention to nerve injury.

The intracellular mechanisms that govern events of neurite alignment to cell-based topographical cues have yet to be fully understood. The TREK-1 channel is a candidate for investigation of such a mechanism, as it is the most well-understood of the three known mechanosensitive two-pore potassium (K_{2P}) channels present in the neuronal membrane and has been shown to respond to membrane deformation by mechanical stimulus to the cell membrane[1-2]. Additionally, it has been demonstrated that TREK-1 channels respond differentially to convex versus concave membrane deformation[3-4], indicating a potential role of TREK-1 in mechanotransduction response to cellular-based topographical features fabricated by our lab, representing cell-based geometric topographical features in both inverted and protruding formats.

To date, the effect of TREK-1 inhibition on contact guidance of neurons has not been researched, providing a significant opportunity for systematic investigation. The study presented in this Chapter aimed to determine the intracellular events that lead to contact guidance and mechanosensing of cell-based topographical features by TREK-1 channels. Toward this aim, we pharmacologically inhibited TREK-1 channels by fluoxetine hydrochloride (FLX).

5.2. Introduction

5.2.1. The growth cone

The growth cone resides at the neurite tip and senses the local environment, responding to this sensory information with continuation or disruption in outgrowth along a particular direction, based on the nature of the environmental cues[5-6]. In our lab we have observed that neurite alignment strength depends on different topographical features of the in vitro environment[7-10],

supporting the idea that growth cone sensitivity and response are pivotal in neurite guidance by topographical features[11]. Seemingly minor changes in topographical features may result in distinct growth responses, and as such, an understanding of how such topographical cues are relayed into growth decisions is essential for the design of therapeutic biomaterials and to further our knowledge regarding how nerves make growth decisions.

5.2.2. Schwann cell topography directs neurite outgrowth

Schwann cells (SC) proliferate, migrate, and organize into aligned bands, known as Bands of Büngner, to promote peripheral regeneration after injury. SC provide a complex simultaneous milieu of cues to navigating axons, including secreted neurotrophic factors, permissive surface molecules and secreted ECM molecules, as well as topographical guidance in the form of their soma and process architectural organization[12-14].

In Chapter 3 and in previous work, we have found that isolated SC topography presented as polymeric replicas is sufficient to guide DRG neurite outgrowth[9, 15]. We have also shown in Chapter 2 that inverted impression replicas (IR) are sufficient for guided neurite outgrowth. Based on the behavior of SC in vivo and the previous work of our lab and others, we hypothesize that critical guidance information is encoded in the spatial organization and geometry of SC topography[12-13].

5.2.3. Mechanosensing and mechanotransduction

During development of the nervous system and in the injured state, neurites navigate through and around the local environment and are constantly exposed to multiple simultaneous cues. Mechanical cues comprise a subset of environmental information which are sensed by navigating neurites and relayed through intracellular mechanisms which result in cytoskeletal reorganization

and ultimate morphological response by navigating neurites. This process, known as mechanosensing, is complex and depends heavily on the substrate type, stiffness, and topology, and varies among cell types[16-24]. Contact guidance is a form of mechanosensation and mechanotransduction by which the geometrical form of a substrate imparts morphological changes and directional guidance to navigating cells and cell processes[25].

5.2.4. TREK-1 channels are mechanosensitive

Mechanosensitive, or stretch-activated, ion channels are sensitive to the mechanical properties of the local substrate and are sensitive to membrane tension[2, 26] Additionally, some studies have suggested that potassium channels may play a role in neurite elongation by modulation of membrane voltage[27]. The TWIK-related K^+ (TREK-1) channel is the most widely-studied mechanogated two-pore potassium (K_{2P}) channel[1]. TREK-1 channels are present in growth cones of mammalian neurons, including DRG neurons[28-29], and they co-localize with cytoskeletal proteins actin and ezrin[27], suggesting their role in transduction of mechanical signals to the cytoskeletal network. There is evidence to suggest that the presence of TREK-1 at the growth cone may contribute to hyperpolarization of the plasma membrane, subsequently moderating calcium ion entry, leading to changes in axonal guidance and pathfinding[1, 27, 30]. TREK-1 has been shown to be critical to filopodial formation and sensing of substrate geometry[4], indicating a role for TREK-1 during early developmental stages, axonal migration, and formation of synapses. TREK-1 channel opening is induced by membrane stretch[3, 31], and although they are activated by concave membrane curvature, TREK-1 channels are more strongly gated by convex membrane curvature[4].

5.2.5. Fluoxetine inhibits TREK-1 activity

TREK-1 channels are sensitive to several pharmacological agents, including chlorpromazine, venlafaxine, and malprotiline[4] wherein such agents decrease the activity of TREK-1 channels[32].

Fluoxetine hydrochloride reversibly inhibits TREK-1 channel activation, and although the mechanism of action is not yet understood, through patch-clamp recordings, exposure of modified HEK-293 cells to FLX at 100 μM led to an 84% inhibition in TREK-1 activity[33]. In another study, when FLX at 100 μM was presented in a bath solution to HEK-293 cells transfected to express TREK-1, TREK-1 currents were inhibited by 77%, compared to other pharmaceutical inhibitors, which resulted in 60% and 7.5% inhibition of TREK-1[32].

The goal of this study was to gain insight into the mechanism that neurons use for mechanotransduction via pharmacological inhibition of TREK-1 channels by FLX in dissociated DRG cultures.

5.3. Materials and Methods

5.3.1. Substrate fabrication

Flat PDMS served as controls for all experiments conducted. Materials presenting repeating parallel grooves and plateaus were generated as previously described[34]. Briefly, photolithography and soft lithography were used to make poly(dimethyl siloxane) (PDMS) (Dow Corning, Midland, MI, USA) substrates with repeating 40 μm grooves and 40 μm plateaus at a depth of 2 μm. Mouse LN (Invitrogen) was adsorbed to substrate surfaces at 50 μg/ml. LN was suspended in HBSS and applied to oxygen plasma-activated PDMS substrates, allowed to adsorb to the substrates for at least 30 minutes, then excess LN was rinsed away with HBSS, and substrates were kept in HBSS until cells were plated.

5.3.2. Cell culture and TREK-1 inhibition by FLX

DRG were dissected from the spinal cords of postanatal rat pups (P0-P4). The explants were cleaned of blood, axons, and connective tissue and dissociated in 0.05% trypsin-EDTA in HBSS

for 50 minutes, and dissociated by trituration. Dissociated DRG cells were resuspended and cultured at 37°C and 5% CO_2 in neurobasal media (GIBCO) supplemented with 4mM L-glutamine, 100 U/ml penicillin, 100 µg/ml streptomycin, 50 ng/ml NGF (Invitrogen), and B-27 supplement. For all experiments, culture medium without serum was used to limit SC and fibroblast proliferation. Dissociated DRG were seeded at $3x10^4$ cells per well onto PDMS substrates in standard 12-well tissue culture plastic plates. This relatively low cell density was used to allow the identification and visualization of individual neurons with limited influence of cell-cell interaction on cell behavior.

Four hours after cell plating, cultures were imaged to ensure that cells had adhered to the PDMS substrates. The culture medium was removed and replaced with media containing FLX at prescribed molarity diluted in HBSS. Cells remained in the media containing FLX for 24 hours before fixation in 2% paraformaldehyde (Electron Microscopy Sciences, Hatfield, PA, USA) in PBS (Invitrogen) for 15-20 minutes and then rinsed 3 times with PBS. These culture conditions were chosen to permit the observation of neurite outgrowth events in the presence of FLX at early navigational stages. Additionally, because the inhibitory effects of FLX are reversible, FLX remained in the culture medium for 24 h once cells had adhered.

5.3.3. Immunolabeling

5.3.3.1. Nuclear and neurite labeling

Cell nuclei were stained with 1% 4,6-diamidino-phenylindole (DAPI; Sigma) and 0.1% Triton-X (VWR International, West Chester, PA, USA) in PBS. Neurites were labeled with anti-β(III) tubulin (1:500) primary antibody (Covance Research Products, Inc., Berkeley, CA, USA) and Cy2 conjugated goat-anti-mouse (1:200) secondary antibody (Jackson). Non-specific labeling was blocked by incubating samples with 10% normal goat serum (Jackson) and 0.1% Triton-X in

PBS for 60 minutes. Samples were then incubated with the primary antibody overnight at 4°C and rinsed with PBS. Then samples were incubated with the secondary antibody for 1 hour at room temperature and rinsed 3 times with PBS. During the secondary immunolabeling steps, samples were protected from light with aluminum foil.

5.3.3.2. TREK-1 immunolabeling

Optimization of TREK-1 immunolabeling was performed for select samples (Fig.5.1). Several anti-TREK-1 antibodies were investigated to determine ideal concentration and microscopic imaging parameters. Non-specific labeling was blocked as described above, then samples were incubated with polyclonal goat-anti-TREK-1 (N20; 1:50) primary antibody (Santa Cruz Biotech) overnight at 4°C. Samples were then incubated with mouse-anti-β(III) tubulin (1:500) overnight. Then samples were incubated with Cy-2 rabbit-anti-goat secondary antibody (1:200) for 1 hour at room temperature. Finally, samples were incubated with Cy-3 rabbit-anti-mouse (1:200) secondary antibody and rinsed 3 times with PBS. Cell nuclei were labeled with DAPI as described above.

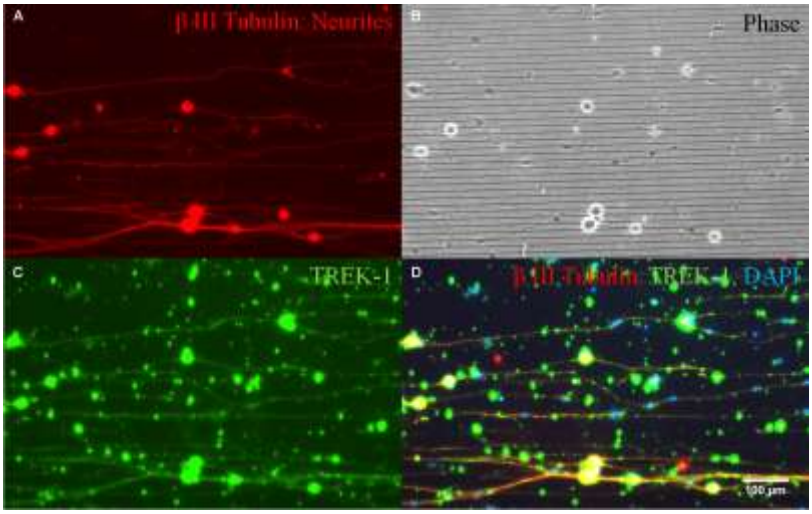

Figure 5.1. Micrographs depict anti-β(III) tubulin positive neurites (A) on PDMS microgrooved substrates (B). TREK-1-positive neurites (C) are overlaid with anti-β(III) tubulin neurites and dapi-positive cell nuclei (D). Figure courtesy of Danielle Chau.

5.3.4. Imaging

Phase contrast and epifluorescent images were captured with a Hamamatsu Orca-ER camera, Orbit shutter controller, and a Ludl stage controller at 4x or 10x magnification on a Nikon Eclipse TE2000-S microscope, outputting to Openlab v4.0.4. (Improvision, Lexington, MA, USA). Samples were oriented such that the microgrooves were consistently directed along the horizontal axis. For neurite and DAPI analysis, at least four fields of view (FOV) were captured per sample, with corresponding phase, DAPI, and neurite images for each sample.

5.3.5. Quantification of cell viability

Images of DAPI-labeled nuclei were used to determine cell counts among substrates tested with incremental FLX concentrations to optimize FLX dosing. Briefly, DAPI-labeled images were converted to 8-bit grayscale with NIH ImageJ v.1.45., inverted, and thresholded. Nuclei number and alignment angle were assessed with the particle analysis function in ImageJ.

5.3.6. Neurite analysis

A custom MATLAB software algorithm generated by our lab was used to quantify percentage of neurite alignment within 20° of the arbitrarily-defined horizontal and vertical directions of anti-β(III) tubulin-labeled images. For microgrooved substrates, the horizontal direction was defined as being parallel to the microgrooves. A description of this software can be found in Chapter 3.3.5.

5.3.7. Statistical analysis

One-way analysis of variance (ANOVA) tests were performed on cell count and percent neurite alignment. Post hoc multiple comparison analyses were performed using Tukey's test. A P-value of 0.05 was taken to be significant. Statistical analysis of circular distributions was tested by Rayleigh's test uniformity. A P-value of 0.05 was taken to be significant.

5.4. Results

We hypothesized that TREK-1 channels play a role in neurite mechanosensing of cell-based topographical features. As a first step toward testing this hypothesis, we quantified cell viability on flat PDMS and subsequently determined neurite alignment response to microgrooves presented by PDMS substrates.

5.4.1. Maximal FLX dose was defined as 150 μM or greater

We tested a panel of FLX concentrations for their effects on cell viability, based on FLX concentrations that have been used previously to inhibit TREK-1 channels[32-33]. Culture medium was treated with 30, 50, 80, 100, 130, 150, 200, and 300 μM FLX. Media without FLX (0 μM) served as controls. Neuronal adhesion and viability were assessed on flat PDMS platforms and on PDMS platforms presenting 40 μm wide microgrooves separated by 40 μm wide plateaus of 2 μm

depth. Cells did not survive when the concentration of FLX ([FLX]) was above 150 μM (Fig.5.2). Representative micrographs demonstrate that intact neuronal cell bodies were not present and that neurite extension was not observed for these conditions.

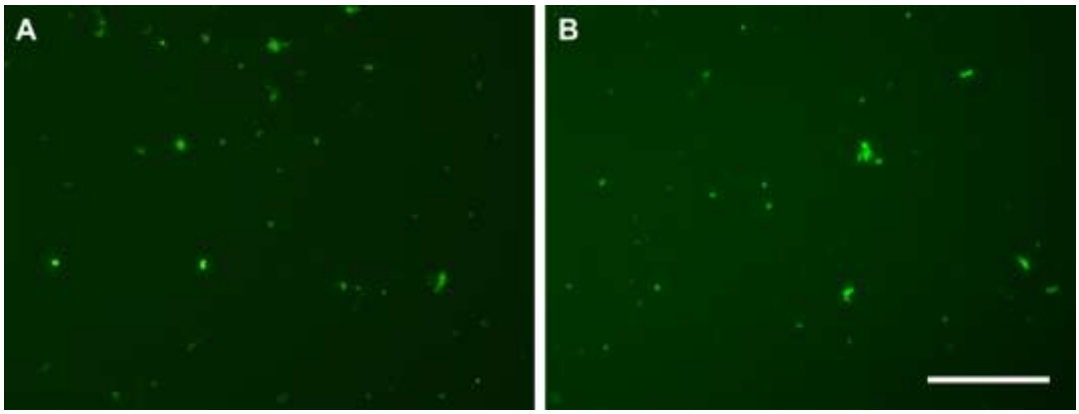

Figure 5.2. Dissociated DRG cells did not survive in culture medium treated with 200 μM (A) and 300 μM (B) FLX concentration. Punctate green labeling depicts nonspecific staining of cellular debris by ant- β(III) tubulin. Scale bar, 200 μm.

DAPI-labeled nuclei and neuronal cell bodies from randomly positioned FOV were counted to determine cell viability with respect to [FLX] on flat PDMS. As DRG cultures are heterotypic in nature, total cell viability consisted of all cell types present, while neuronal cell viability consisted exclusively of neuronal cell bodies. As [FLX] increased from 0 μM to 150 μM, cell and neuron viability decreased (Fig.5.3). In particular, cell number in the absence of FLX (37.8±5.2 cells/FOV) was significantly higher than cell number in the presence of 100, 130, and 150 μM [FLX] (24.0±2.0 cells/FOV, 20.1±3.1 cells/FOV, and 22.9±2.7 cells/FOV, respectively; Fig. 5.3.A). The total cell counts in the presence of 50 and 80 μM FLX were 32.1±5.2 cells/FOV and 28.9 cells/FOV, respectively, and were not statistically different from the total cell count in the presence of 0 μM FLX.

As [FLX] increased from 0 μM to 150 μM, the number of neurons present decreased overall. In particular, there were significantly more neurons present on flat PDMS substrates without FLX (6.1±1.0 neurons/FOV) when compared to 80, 130, and 150 μM FLX conditions, where there were 3.4±0.3, 2.13±0.4, and 2.8±0.5 neurons/FOV, respectively.

Neurite morphology was observed via epifluorescent micrographs with neurites labeled for anti-β(III)tubulin. Continuous, viable neurites were observed for all concentrations of FLX except 200 μM and 300 μM, as shown in representative micrographs (Fig.5.4). Neurites on flat PDMS with 0 μM, 30 μM, 50 μM, 80 μM, 100 μM, 130 μM, and 150 μM appeared to be randomly oriented.

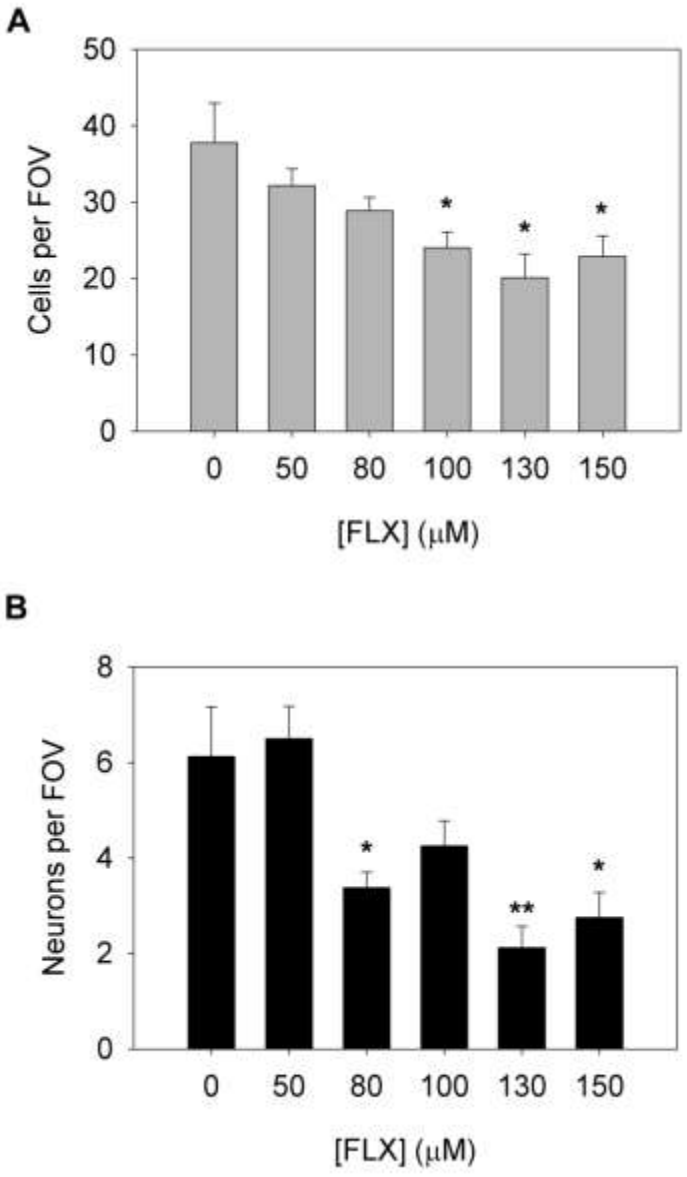

Figure 5.3. Cell viability on flat PDMS. A. Total cell count per FOV. B. Neuron count per FOV. (*P<0.05 significantly different from 0 μM, **P<0.01 significantly different from 0 μM; Error bars are SEM.)

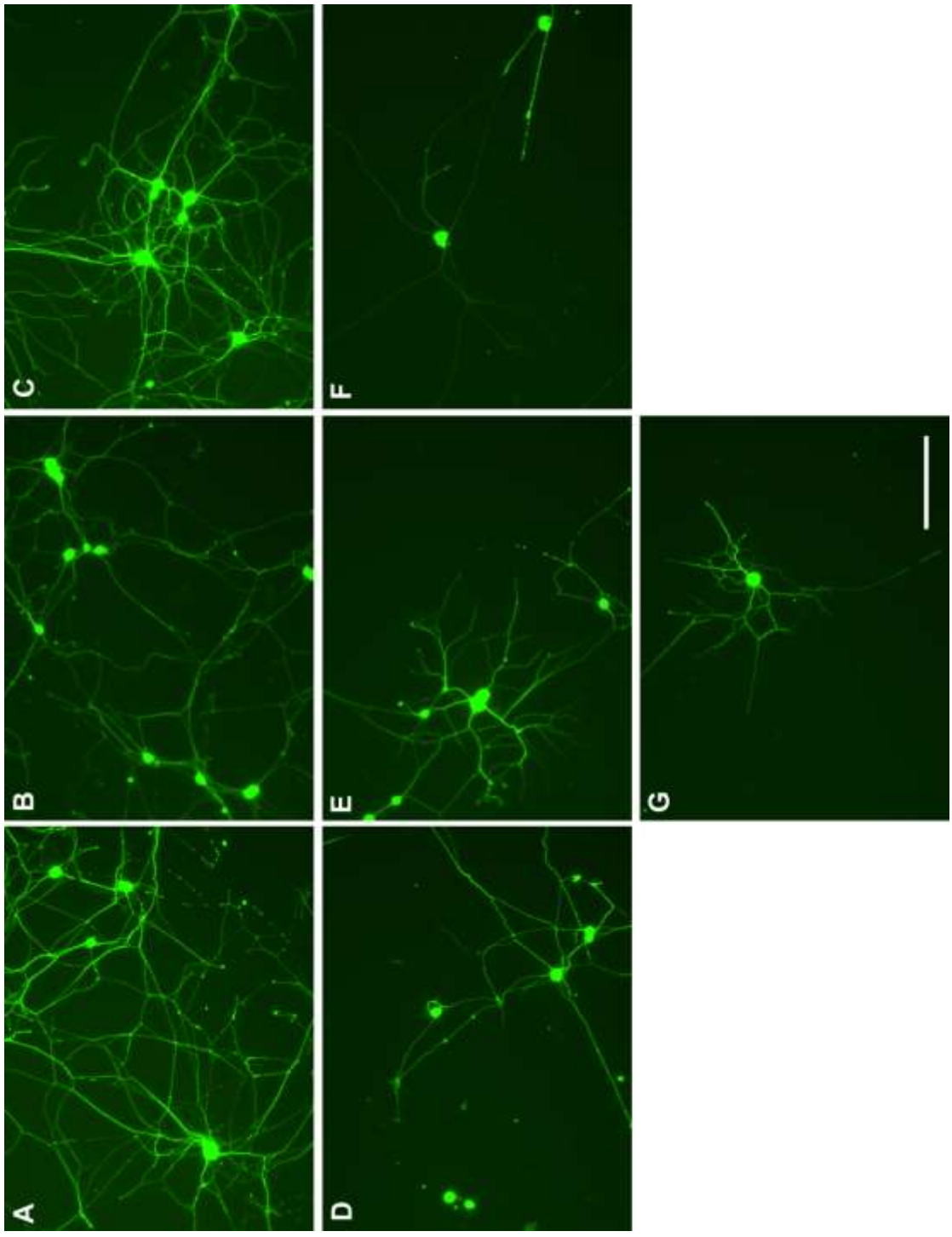

Figure 5.4. Neurite outgrowth on flat PDMS in response to FLX at (A) 0 μM, (B) 30 μM, (C) 50 μM, (D) 80 μM, (E)100 μM, (F) 130 μM, and (G) 150 μM. Scale bar, 200 μm.

5.4.2. Neurite orientation on flat PDMS was not affected by [FLX].

Percent neurite alignment within 20° of the arbitrarily defined horizontal direction on flat PDMS was quantified. There were no significant differences among percent neurite alignment to the horizontal direction with respect to the concentration of FLX (Fig.5.5A) Percent neurite alignment within 20° of the arbitrarily defined vertical direction was also quantified. There were no significant differences among percent neurite alignment to the vertical direction with respect to the concentration of FLX (Fig.5.5B).

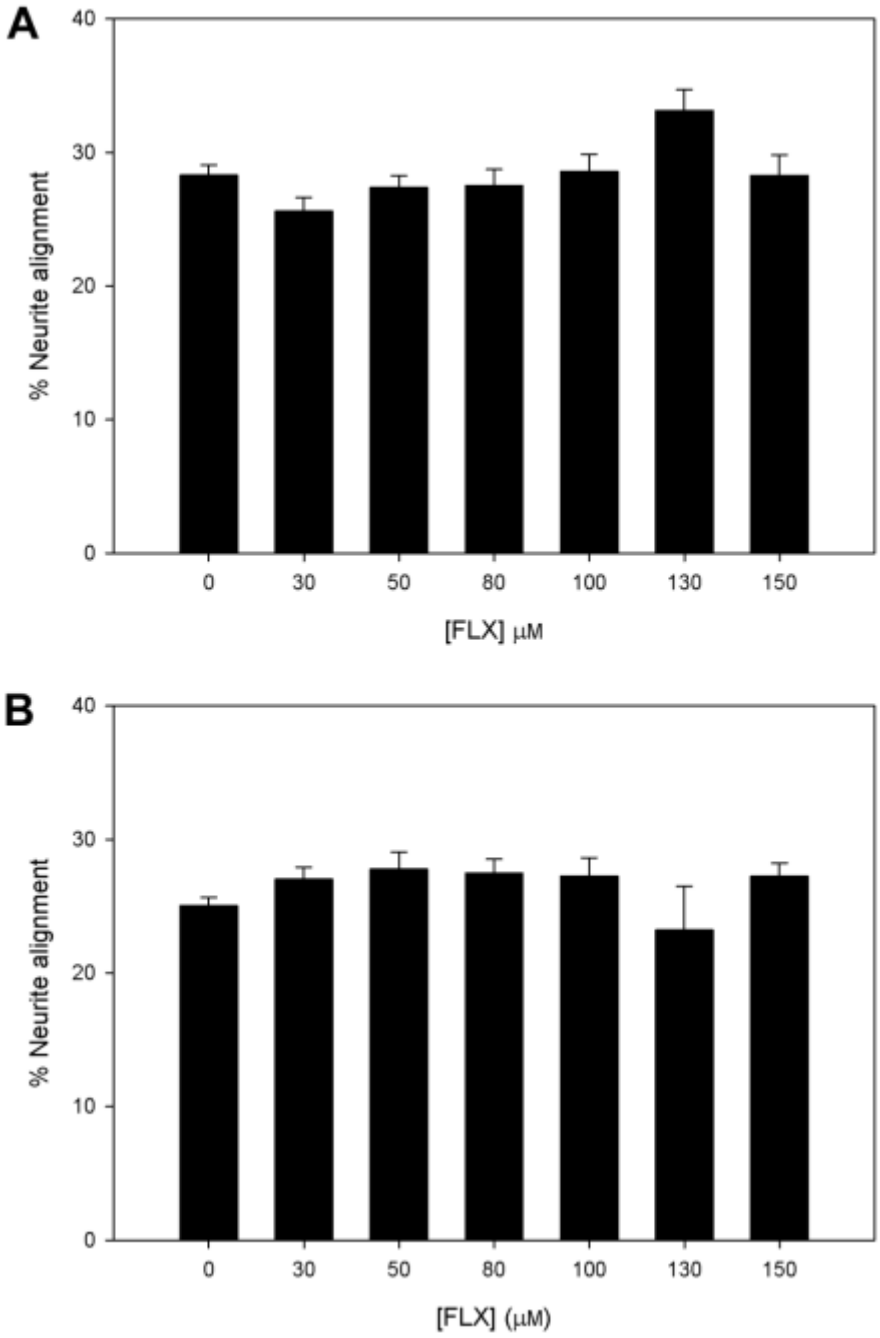

Figure 5.5. Percent neurite alignment within 20° of arbitrarily defined horizontal (A) and vertical (B) axes on flat PDMS. Error bars are SEM.

5.4.3. Nuclear orientation was affected by [FLX] on microgrooved PDMS substrates

DAPI-labeled nuclei and neuronal cell bodies were counted to determine cell viability on microgrooved PDMS with respect to [FLX] (Fig.5.6). Generally, cell count and neuronal count decreased with increasing [FLX] (Fig.5.6A). In particular, there were significantly fewer cells present on 130 μM substrates (11.8±1.1 cells/FOV) and on 150 μM substrates (9.5±1.6 cells/FOV) when compared to 0 μM substrates without FLX (17.7±1.9 cells/FOV; $P<0.05$). In addition, there were significantly fewer cells on 150 μM substrates than on 80 μM substrates, which had 17.25±1.8 cells/FOV ($P<0.05$).

The number of neuronal cell bodies were also quantified on microgrooved substrates (Fig.5.6B). In particular, there were significantly fewer viable neurons on 130 μM (0.9±0.2 neurons/FOV) and 150 μM (1.3±0.5 neurons/FOV) substrates when compared to 0 μM substrates, which had 2.9±0.5 neurons/FOV ($P<0.001$ and $P<0.05$, respectively).

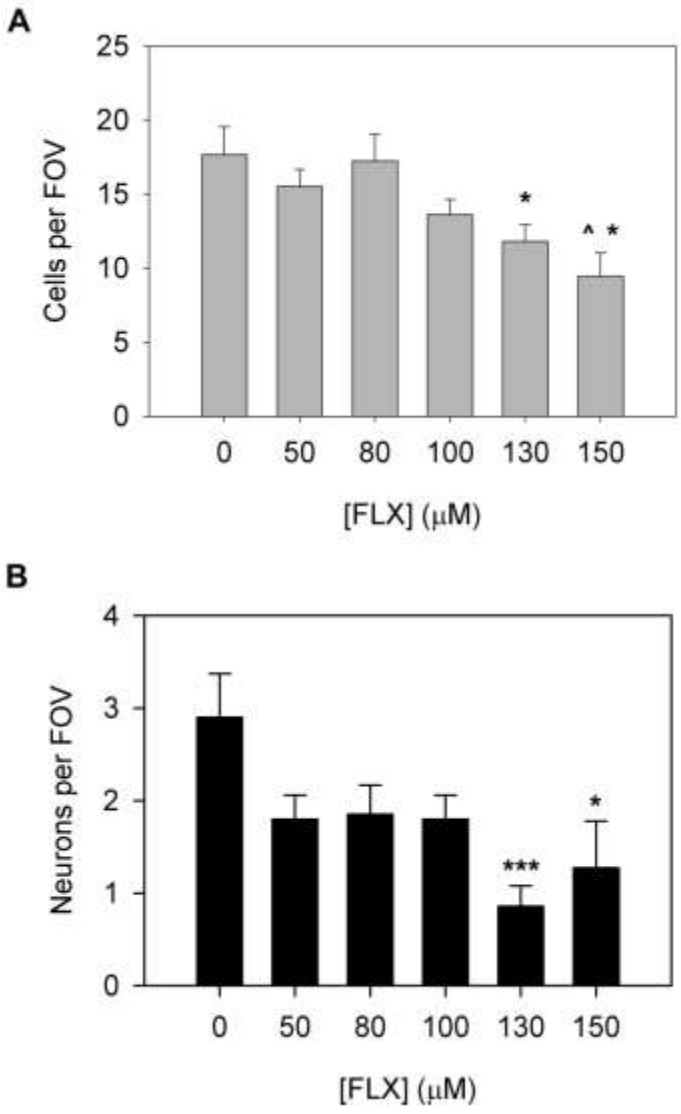

Figure 5.6. Cell counts on platforms presenting microgrooves depended on [FLX]. A. Number of viable cells per FOV. B. Count of viable neurons per FOV. (*P<0.05 significantly different from 0 μM, ***P<0.001 significantly different from 0 μM, ^P<0.05 significantly different from 80 μM; Error bars are SEM.)

Neurite morphology was assessed on microgrooved PDMS in the presence of FLX at prescribed concentrations. Generally, neurites aligned along the direction of the microgrooves (Fig.5.7). Though not quantified, neurites tended to exhibit somewhat less extended, more branched morphology in the presence of higher [FLX], as exemplified in Figure 5.7 (D-E, G).

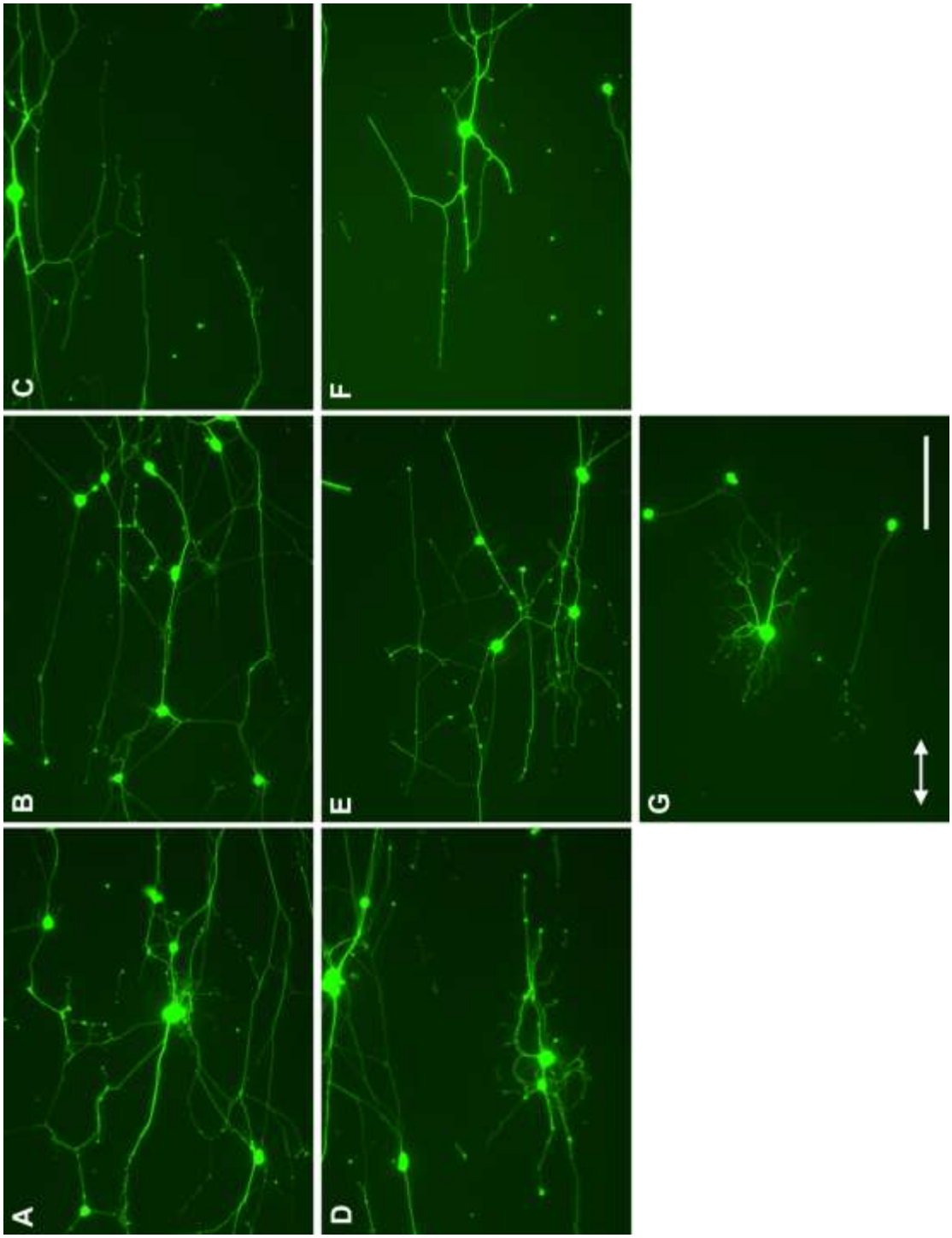

Figure 5.7. Neurite outgrowth on microgrooved PDMS in response to FLX at (A) 0 μM, (B) 30 μM, (C) 50 μM, (D) 80 μM, (E)100 μM, (F) 130 μM, and (G) 150 μM. White arrow indicates orientation of microgrooves. Scale bar, 200 μm.

5.4.4. FLX inhibitor disrupted neurite alignment to microgrooves in a dose-dependent manner

Percent neurite alignment within the 20° region parallel to the direction of the microgrooves and perpendicular to the direction of microgrooves was quantified (Fig.5.8). Generally, neurite alignment to the direction of the microgrooves decreased as [FLX] increased (Fig.5.8A), while neurite alignment perpendicular to the microgrooves increased with increasing [FLX] (Fig.5.8B). P-values for comparisons among neurite alignment with respect to [FLX] are indicated in Figure 5.8 and detailed in Table 5.1 and Table 5.2. Overall, neurite alignment to the microgrooves was lowest (36.1±1.0%) and alignment perpendicular to the microgrooves was highest (21.4±0.7%) in the presence of 130 μM FLX when compared to other conditions.

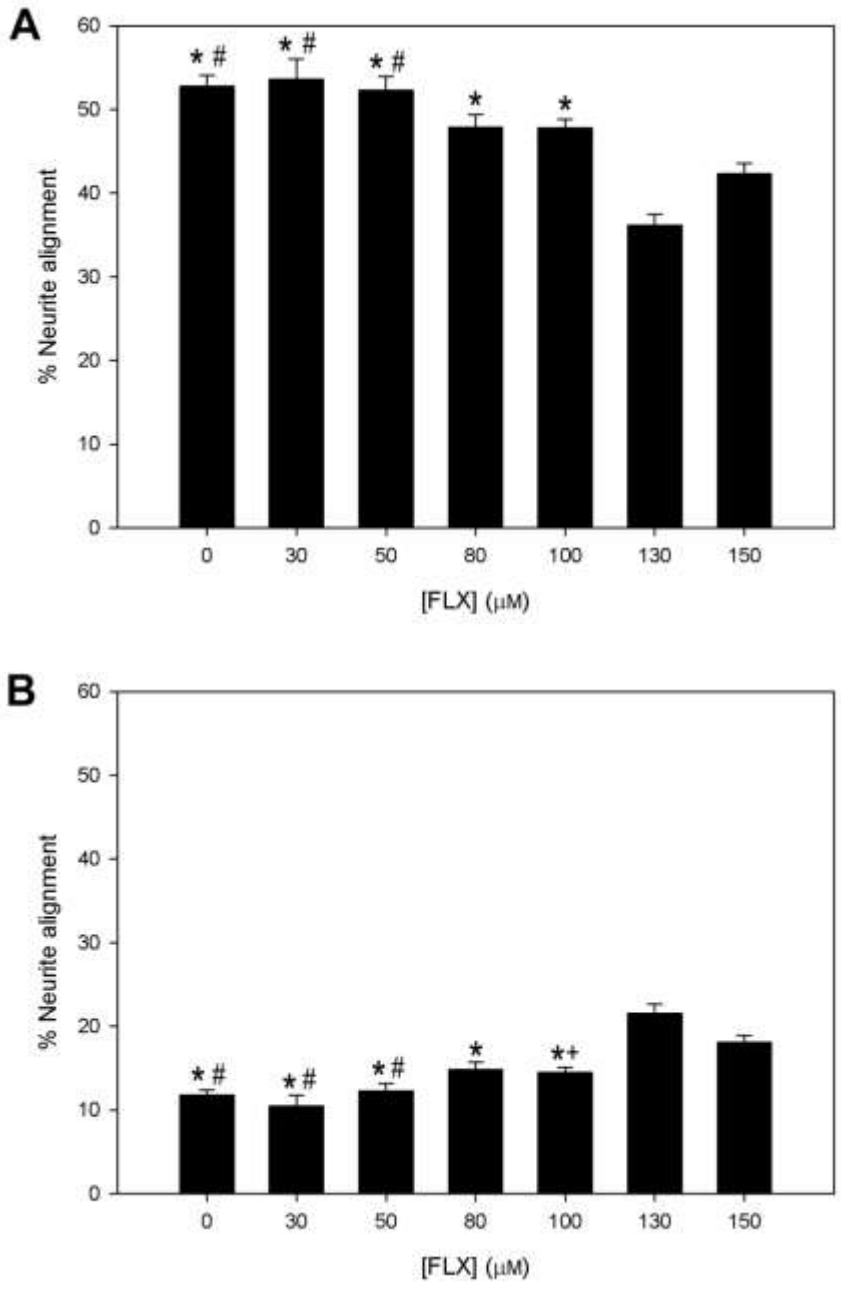

Figure 5.8. Percent neurite alignment within 20° (A) parallel and (B) perpendicular to direction of microgrooves in the presence of FLX. (*P<0.001 significantly different from 130 μM, #P<0.001, +P<0.05 significantly different from 150 μM; Error bars are SEM.)

	0 µM	30 µM	50 µM	80 µM	100 µM	130µM	150 µM
0 µM	-	-	-	-	-	-	-
30 µM	n.s.	-	-	-	-	-	-
50 µM	n.s.	n.s.	-	-	-	-	-
80 µM	n.s.	n.s.	n.s.	-	-	-	-
100 µM	n.s.	n.s.	n.s.	n.s.	-	-	-
130µM	0.000	0.000	0.000	0.000	0.000	-	-
150 µM	0.000	0.001	0.000	n.s.	n.s.	n.s.	-

Table 5.1. Comparison of neurite alignment to microgrooves. P-values by One-way ANOVA and Tukey's post hoc analysis. n.s. = not significant.

	0 µM	30 µM	50 µM	80 µM	100 µM	130µM	150 µM
0 µM	-	-	-	-	-	-	-
30 µM	n.s.	-	-	-	-	-	-
50 µM	n.s.	n.s.	-	-	-	-	-
80 µM	n.s.	n.s.	n.s.	-	-	-	-
100 µM	n.s.	n.s.	n.s.	n.s.	-	-	-
130µM	0.000	0.000	0.000	0.000	0.000	-	-
150 µM	0.000	0.000	0.000	n.s.	0.032	n.s.	-

Table 5.2. Comparison of neurite alignment perpendicular to microgrooves. P-values by One-way ANOVA and Tukey's post hoc analysis. n.s. = not significant.

Circular statistical analysis of DAPI-labeled nuclear alignment on microgrooved substrates was used to examine the distribution of nuclear angles in the presence of FLX. In general, nuclear angle distributions correlated with neurite alignment data, as the clustering of nuclear alignment along the direction of the microgrooves tended to decrease as [FLX] increased (Fig.5.9).

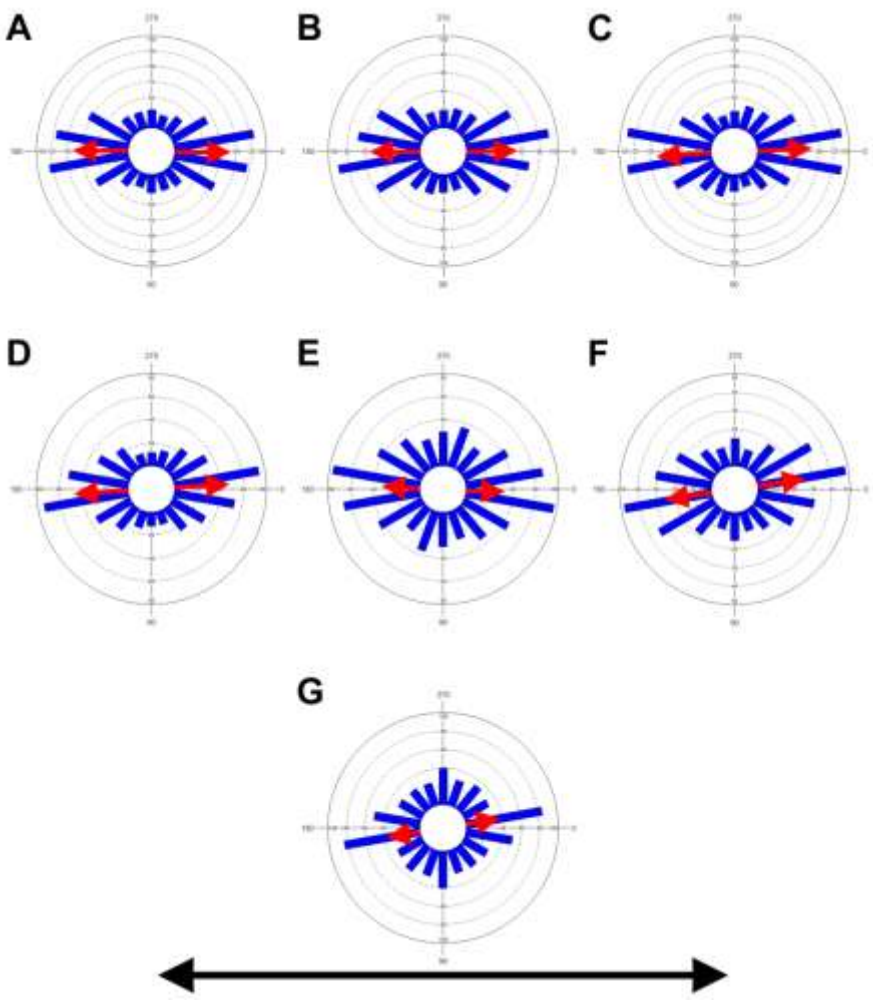

Figure 5.9. Circular histograms represent angular distribution of DAPI-labeled nuclei on microgrooved substrates in response to [FLX] at 0 μM (A), 30 μM (B), 50 μM (C), 80 μM (D), 100 μM (E), 130 μM (F), and 150 μM (G). Red arrows are mean vectors. Black arrow indicates orientation of microgrooves.

Combined, the mean vector direction and mean vector length (MVL) are mathematical descriptors of the angular clustering of a set of data points. MVL ranges from 0-1 and indicates the strength of clustering of alignment around a particular angle. Higher MVL indicates increased clustering of alignment around a particular angle. The circular histograms depicted in Figure 5.9 are graphical representations of the neurite angular distribution, where the red arrows are the mean vectors for each [FLX] condition.

For the studies presented here, the angles of 0° and 180° represent the orientation of microgrooves, such that the mean vector angle along this axis indicated overall nuclear alignment clustering along the direction of the microgrooves, and increased MVL indicated increased strength of clustering along the direction of the microgrooves. All nuclear angle distributions examined were statistically different form a uniform distribution by Rayleigh's test and Rao's spacing test ($P<0.05$). The distribution of nuclear alignment in response to 0 μM FLX had a mean vector length of 0.42 at 178.3° (Fig.5.9A). The distribution of nuclear alignment in response to 30 μM FLX had a mean vector length of 0.38 at 179.4° (Fig.5.9B). The distribution of nuclear alignment in response to 50 μM FLX had a mean vector length of 0.40 at 177.5° (Fig.5.9C). The distribution of nuclear alignment in response to 80 μM FLX had a mean vector length of 0.37 at 178.0° (Fig.5.9D). The distribution of nuclear alignment in response to 100 μM FLX had a mean vector length of 0.27 at 0.30° (Fig.5.9E). The distribution of nuclear alignment in response to 150 μM FLX had a mean vector length of 0.35 at 171.6° (Fig.5.9F). The distribution of nuclear alignment in response to 150 μM FLX had a mean vector length of 0.25 at 172.2° (Fig.5.9G).

Figure 5.10 depicts MVL for nuclear alignment to microgrooves with respect to [FLX]. MVL tended to decrease with increasing [FLX], indicating a decrease in strength of alignment as [FLX] increased.

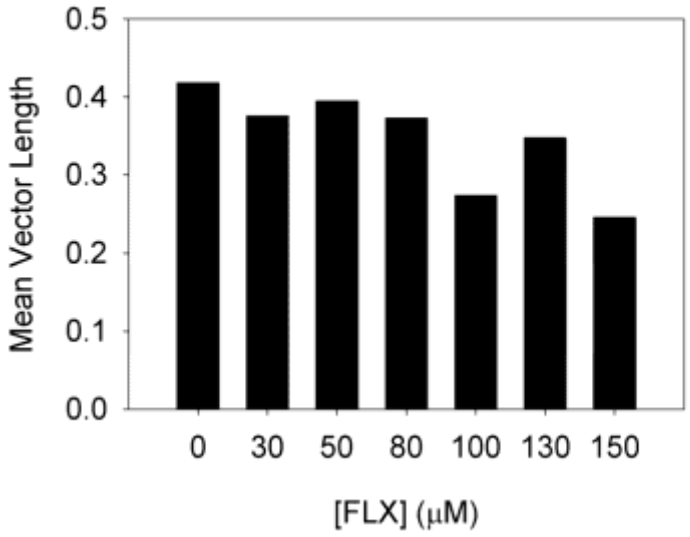

Figure 5.10. Mean vector length (MVL) with respect to [FLX] on microgrooved substrates. (n>45 nuclei for each condition.)

5.5. Discussion

Through the studies presented in this chapter, we investigated DRG response to topographical features from a mechanistic standpoint. In particular, pharmacological inhibition of mechanosensitive TREK-1 channels by FLX was utilized to determine the relevance of TREK-1 channel activation in the mechanotransduction of topographical cues by navigating neurites. Thus far, we have investigated DRG cell viability with respect to a panel of FLX concentrations. Further, we assessed neurite and overall cell alignment to microgrooved substrates in response to FLX concentration.

5.5.1. Assessment of cell viability in the presence of FLX

The experiments outlined here utilized serum-free cell culture medium supplemented with B27 and NGF to limit proliferation of SC, enabling closer evaluation of neuronal behavior and morphology while limiting secondary influences due to highly heterotypic culture conditions.

Additionally, a relatively low cell culture density of $3x10^4$ cells per standard 12-well culture plate was used to improve the visualization of individual cell and neurite behavior and morphology.

Viable cells were counted within random fields of view to determine the heterotypic cell count and neuronal cell count on each substrate type. DAPI-labeled cell nuclei were counted to determine the number of all cells in each field of view, while DAPI co-localized with anti-β(III) tubulin was used to determine the number of neurons in each field of view. Overall, the number of all cells and the number of neurons decreased with increasing [FLX]. Further, the cell counts on microgrooved substrates were lower than their flat PDMS correlate conditions. This observation may be due to an interruption in cell adhesion by the relatively shallow (2 μm) grooves, rather than confinement of cells demonstrated by deeper grooves[35].

Pharmacological inhibitor studies must determine acceptable criteria within which a reasonable proportion of cell health is expected. Here, we showed that increased [FLX] correlated with a decrease in overall cell count, but that cell adhesion to PDMS in the presence of 100 μM [FLX] persisted at greater than 50% of that of 0 μM [FLX]. It can therefore be speculated that 100 μm [FLX] is the most promising dosage as it results in a balance of maintaining cell viability and disrupting alignment response, while corresponding with the concentration that has been reported previously to effectively inactivate TREK-1 channels via electrophysiological studies of TREK-1 inactivation.

5.5.2. On microgrooved substrates, neurite orientation and nuclear angle distributions decreased in alignment strength in response to increasing [FLX]

Neurite orientation to the horizontal and vertical directions on flat PDMS controls was statistically similar among all conditions tested. This agrees with the expectation that neurite

outgrowth was randomly distributed on flat PDMS regardless of [FLX]. Overall, neurites appeared to be shorter in length as [FLX] increased, although further analysis is warranted to justify this observation, as it is not yet clear whether the decrease in cell number contributed to a decrease in neurite length.

It has been established that DRG neurites grow along microgrooves of specific dimensions by contact guidance[25, 36-37]. We assessed neurite alignment response to microgrooved PDMS substrates to determine the effects of TREK-1 inhibition by FLX on neurite alignment. We hypothesized that FLX inhibition of TREK-1 channels would impair channel activation in response to mechanosensation of environmental topography, such that inhibition of TREK-1 would dampen neurite alignment to microgrooved topography. Morphological assessment of neurite outgrowth demonstrated overall neurite alignment to the direction of the microgrooves. As [FLX] increased, however, neurite association with the microgroove orientation tended to decrease (Fig.5.7; Fig.5.8), suggesting a role for TREK-1 channel activity in neurite alignment response to topographical features.

As expected, percent neurite alignment along the direction of the microgrooves decreased with increasing [FLX]. This finding suggests that the presence of FLX disrupts downstream cytoskeletal events which lead to contact guidance response of neurites to local topographical features, and is supported by a study which has demonstrated TREK-1 association with actin and ezrin cytoskeletal proteins[27]. Further, as [FLX] increased, neurite alignment perpendicular to the microgroove orientation increased, suggesting that neurite orientation approached a more random distribution with increased [FLX].

The orientations of DAPI-labeled nuclei were used to generate circular histograms to represent overall nuclear alignment on microgrooved substrates in the presence of FLX. The nuclear

distributions corresponded with the trend of decreasing alignment to the direction of the microgrooves with increasing [FLX], as demonstrated by the mean vector direction and length (Fig.5.9 red arrows; Fig.5.10).

5.6. Conclusions and future directions

These initial experiments have demonstrated potential for the use of FLX to study TREK-1 channel activation in mechanosensing of extracellular topographical features by navigating neurites. The topic of mechanosensation and mechanotransduction by neurites, which leads to morphological and guidance decision-making, is of importance in the understanding of nerve guidance in response to extracellular cues, and may inform strategies for promoting guidance following injury[16, 18, 38]

Further analysis must be done to determine the relevance of TREK-1 activation in response to cellular-based topographical features, including cellular replicas, biomimetic inspired materials, and geometric cell-based materials. In particular, the level of structural detail of such features that is able to be mechanotransduced to the cytoskeleton via TREK-1 signaling is an area that merits further investigation. In particular, how FLX inhibition of TREK-1 affects neurite alignment to microgrooves, microposts, bioinspired cell features including soma and processes, and cell replicas is of interest, as described in Chapter 2.

It has been shown that TREK-1 is more strongly activated by convex membrane curvature than by concave membrane curvature[4]. We hypothesize that the activation of TREK-1 channels depends on the geometry of the topographical features, wherein TREK-1 mechanotransduction and subsequent neurite guidance is dependent on feature type and dimensions. It is therefore relevant to determine how TREK-1 inhibition disrupts neurite alignment in response to concave

and convex variations of the topographical features described above. An improved understanding of this subject will illuminate the role of TREK-1 in neurite guidance during peripheral nerve regeneration, where navigating neurites encounter and respond to the convex curvature of SC that comprise the Bands of Büngner[39-41], or to the concave curvature of the endoneurium as they reconnect with their targets[42]. An additional likely curvature-dependent event occurs when regenerating nerves follow along the fibrin cable that forms between distal and proximal nerve fibers within nerve guidance conduits that bridge large nerve gaps[43]. Elucidating the role that TREK-1 has in guiding nerve growth decisions in such environments may lead to the identification of a target for pharmaceutical therapeutics or inform improved design of biomaterials to enhance nerve guidance.

5.7. Literature cited

1. Dedman, A., et al., *The mechano-gated K(2P) channel TREK-1*. Eur Biophys J, 2009. **38**(3): p. 293-303.
2. Honore, E., *The neuronal background K2P channels: focus on TREK1*. Nat Rev Neurosci, 2007. **8**(4): p. 251-61.
3. Maingret, F., et al., *Mechano- or acid stimulation, two interactive modes of activation of the TREK-1 potassium channel.* J Biol Chem, 1999. **274**(38): p. 26691-6.
4. Patel, A.J., et al., *A mammalian two pore domain mechano-gated S-like K+ channel.* Embo Journal, 1998. **17**(15): p. 4283-90.
5. Kalil, K., G. Szebenyi, and E.W. Dent, *Common mechanisms underlying growth cone guidance and axon branching.* J Neurobiol, 2000. **44**(2): p. 145-58.
6. Mueller, B.K., *Growth cone guidance: first steps towards a deeper understanding.* Annu Rev Neurosci, 1999. **22**: p. 351-88.
7. Kofron, C.M., et al., *Neurite outgrowth at the biomimetic interface.* Ann Biomed Eng, 2010. **38**(6): p. 2210-25.

8. Kofron, C.M. and D. Hoffman-Kim, *Optimization by Response Surface Methodology of Confluent and Aligned Cellular Monolayers for Nerve Guidance.* Cell Mol Bioeng, 2009. **2**(4): p. 554-572.

9. Richardson, J.A., et al., *Guidance of dorsal root ganglion neurites and Schwann cells by isolated Schwann cell topography on poly(dimethyl siloxane) conduits and films.* J Neural Eng, 2011. **8**(4): p. 046015.

10. Li, N. and A. Folch, *Integration of topographical and biochemical cues by axons during growth on microfabricated 3-D substrates.* Exp Cell Res, 2005. **311**(2): p. 307-16.

11. Lopez-Fagundo, C.Y., Ramchal, T., Liu, Y-T, Hoffman-Kim, D, *Navigating neurites utilize cellular topography of Schwann cell somas and processes for optimal guidance*, Brown University.

12. Thompson, D.M. and H.M. Buettner, *Neurite outgrowth is directed by schwann cell alignment in the absence of other guidance cues.* Ann Biomed Eng, 2006. **34**(1): p. 161-8.

13. Thompson, D.M. and H.M. Buettner, *Oriented Schwann cell monolayers for directed neurite outgrowth.* Ann Biomed Eng, 2004. **32**(8): p. 1120-30.

14. Thompson, D.M. and H.M. Buettner, *Schwann cell response to micropatterned laminin surfaces.* Tissue Eng, 2001. **7**(3): p. 247-65.

15. Bruder, J.M., A.P. Lee, and D. Hoffman-Kim, *Biomimetic materials replicating Schwann cell topography enhance neuronal adhesion and neurite alignment in vitro.* J Biomater Sci Polym Ed, 2007. **18**(8): p. 967-82.

16. Vogel, V. and M. Sheetz, *Local force and geometry sensing regulate cell functions.* Nat Rev Mol Cell Biol, 2006. **7**(4): p. 265-75.

17. Kung, C., *A possible unifying principle for mechanosensation.* Nature, 2005. **436**(7051): p. 647-54.

18. Pellegrino, M. and M. Pellegrini, *Mechanosensitive channels in neurite outgrowth.* Mechanosensitive Ion Channels, Pt B, 2007. **59**: p. 111-125.

19. Sigurdson, W.J. and C.E. Morris, *Stretch-Activated Ion Channels in Growth Cones of Snail Neurons.* Journal of Neuroscience, 1989. **9**(8): p. 2801-2808.

20. Sachs, F., *Mechanically Sensitive Ion Channels.* Journal of General Physiology, 1991. **98**(6): p. A7-A8.

21. Sachs, F., *Mechanical Transduction by Membrane Ion Channels - a Mini Review.* Molecular and Cellular Biochemistry, 1991. **104**(1-2): p. 57-60.

22. McCarter, G.C., D.B. Reichling, and J.D. Levine, *Mechanical transduction by rat dorsal root ganglion neurons in vitro.* Neuroscience Letters, 1999. **273**(3): p. 179-182.

23. Shim, S. and G.L. Ming, *Roles of channels and receptors in the growth cone during PNS axonal regeneration.* Experimental Neurology, 2010. **223**(1): p. 38-44.

24. Hamill, O.P., *Twenty odd years of stretch-sensitive channels.* Pflugers Archiv-European Journal of Physiology, 2006. **453**(3): p. 333-351.

25. Rajnicek, A., S. Britland, and C. McCaig, *Contact guidance of CNS neurites on grooved quartz: influence of groove dimensions, neuronal age and cell type.* J Cell Sci, 1997. **110 (Pt 23)**: p. 2905-13.

26. Morris, C.E., *Mechanosensitive Ion Channels.* Journal of Membrane Biology, 1990. **113**(2): p. 93-107.

27. Lauritzen, I., et al., *Cross-talk between the mechano-gated K-2P channel TREK-1 and the actin cytoskeleton.* Embo Reports, 2005. **6**(7): p. 642-648.

28. Heurteaux, C., et al., *Deletion of the background potassium channel TREK-1 results in a depression-resistant phenotype.* Nature Neuroscience, 2006. **9**(9): p. 1134-1141.

29. Medhurst, A.D., et al., *Distribution analysis of human two pore domain potassium channels in tissues of the central nervous system and periphery.* Molecular Brain Research, 2001. **86**(1-2): p. 101-114.

30. Chemin, J., et al., *A phospholipid sensor controls mechanogating of the K+ channel TREK-1.* Embo Journal, 2005. **24**(1): p. 44-53.

31. Maingret, F., et al., *TRAAK is a mammalian neuronal mechano-gated K+ channel.* J Biol Chem, 1999. **274**(3): p. 1381-7.

32. Eckert, M., et al., *TREK-1 isoforms generated by alternative translation initiation display different susceptibility to the antidepressant fluoxetine.* Neuropharmacology, 2011. **61**(5-6): p. 918-23.

33. Kennard, L.E., et al., *Inhibition of the human two-pore domain potassium channel, TREK-1, by fluoxetine and its metabolite norfluoxetine.* Br J Pharmacol, 2005. **144**(6): p. 821-9.

34. Goldner, J.S., et al., *Neurite bridging across micropatterned grooves.* Biomaterials, 2006. **27**(3): p. 460-72.

35. Singhvi, R., G. Stephanopoulos, and D.I. Wang, *Effects of substratum morphology on cell physiology.* Biotechnol Bioeng, 1994. **43**(8): p. 764-71.

36. Lin, Y.L., et al., *Sciatic nerve repair by microgrooved nerve conduits made of chitosan-gold nanocomposites.* Surg Neurol, 2008. **70 Suppl 1**: p. S1:9-18.

37. Charest, J.L., et al., *Combined microscale mechanical topography and chemical patterns on polymer cell culture substrates.* Biomaterials, 2006. **27**(11): p. 2487-94.

38. Raoux, M., et al., *Mechanosensor channels in mammalian somatosensory neurons.* Sensors, 2007. **7**(9): p. 1667-1682.

39. Donoff, R.B., *Nerve regeneration: basic and applied aspects.* Crit Rev Oral Biol Med, 1995. **6**(1): p. 18-24.

40. Hu, M.E., et al., *Ultrastructural observations on the progress of nerve degeneration and regeneration at the suture site following vagal-hypoglossal nerve coaptation in cats.* Cells Tissues Organs, 2009. **190**(4): p. 230-45.

41. Madison, R.D., et al., *Factors contributing to preferential motor reinnervation in the primate peripheral nervous system.* J Neurosci, 1999. **19**(24): p. 11007-16.

42. Burnett, M.G. and E.L. Zager, *Pathophysiology of peripheral nerve injury: a brief review.* Neurosurg Focus, 2004. **16**(5): p. E1.

43. Aebischer, P., A.N. Salessiotis, and S.R. Winn, *Basic fibroblast growth factor released from synthetic guidance channels facilitates peripheral nerve regeneration across long nerve gaps.* J Neurosci Res, 1989. **23**(3): p. 282-9.

CHAPTER 6

CONCLUSIONS AND FUTURE DIRECTIONS

The nervous system possesses the remarkable capacity for regeneration, but the potential for repair is often precluded by environmental factors at the injury site. The capacity for nerve regeneration relies heavily on the cellular interactions that follow nerve injury. It is our duty as investigators of nerve guidance by environmental cues to harness the potential that lies in these cellular interactions, such that those which promote growth are emphasized and those that prohibit regeneration are prevented. When we have understood how neuronal response is governed by environmental features, we can employ this knowledge toward the informed design of therapeutic biomaterial-based approaches for improved nerve repair.

The research presented in this thesis investigated cellular and neurite DRG response to engineered platforms presenting individual and simultaneous extracellular matrix protein and

topographical guidance features. The primary goal of this work was to characterize neuronal response to these cues to answer basic biological questions on how nerves and glia make growth decisions and to use the knowledge obtained to inform biomaterial-based strategies for nerve repair.

In Chapter 2, we characterized neurite alignment within nerve guidance conduits with SC topographical features on the lumen surfaces, informing an application-based approach to enhancing nerve growth with parallel presentation of guidance cues to navigating neurites. Additionally, we found that neurite growth on directive SC replica topography progressed further than live SC migration from the DRG, supporting the potential role for biomimetic SC topographical features to promote neurite growth. This research has prompted the continuing evaluation of the combination of biomimetic topographical features and NGC, and as such, attempts toward in vivo evaluation of bioresorbable conduits is under pursuit.

In Chapter 3, we quantified neurite response to permissive extracellular matrix micropatterns and directive SC replica topography presented individually or as strategically designed cooperative or competing combinations. From this research, we improved upon the understanding of the biology of nerve guidance in response to these environmental cues. Nerve growth was enhanced in response to parallel combinations of cues, while outgrowth response was complicated in the presence of conflicting cues. The addition of adhesion-promoting molecules between alignment-promoting micropatterned stripes may enhance alignment response by allowing for increased initial cell adhesion between and on the stripes, resulting in expedient neurite alignment to the stripes, due to the enhancement of local cell to cell alignment response along the direction of interest. Additionally, use of competing cue platforms may lead to the development of a decision-making to inform key aspects of neurite decision making to be addressed. As the orthogonal

opposition of micropatterned protein and cell-based topography disrupted neurite alignment to the direction of either cue, an effort toward maintained directed neurite outgrowth may introduce topography along the intended direction of outgrowth. This work illuminated a portion of the complexities involved in governing neurite outgrowth in the presence of complex combinations of cues, demonstrating the imperative nature of studying neuronal growth in complex environments, as observed neurite growth in the presence of complex multi-cue environments did not always occur as it was anticipated.

The research of Chapter 4 followed the key findings of Chapter 3 with an in-depth analysis of neurite and glial growth and behavior to micropatterned LN stripes and competing cue platforms presenting SC replica topography orthogonally opposed to LN micropatterns. Through sequential endpoint and timelapse microscopy analysis, the progression of neurite outgrowth and neuronal and glial alignment response to the cues was investigated at early time points, when early decision-making events and neurite outgrowth interaction with environmental cues take place. Continuing research will address the neuronal-glial interactions that govern cellular response in complex environments to harness the complexities of these interactions to inform the design of biomaterials for regeneration, especially as they pertain to directing nerve growth to overcome the obstacles of a conflicting cue environment.

To inform engineering strategies to promote nerve growth and guidance, information regarding the dynamic physical mechanisms underlying nerve growth decisions and behaviors must be understood. Through the studies in Chapter 5, we took initial steps toward defining intracellular mechanistic response to extracellular biomimetic topographical features. We observed a disruption in neurite alignment to microgrooves when TREK-1 was pharmacologically inhibited. The potential involvement of the mechanosensitive TREK-1 channel in neurite response to cell-

based topographical features may illuminate TREK-1 as a target for therapeutic intervention after nerve injury. The future of this work should address the sensitivity of TREK-1 in neurite response to cell-based topographies of incremental complexity, and should aim to evaluate the role of TREK-1 in neurite response to concave versus convex deformation of the plasma membrane.

The future of biomaterial-based techniques for nerve repair lies in intelligent combinatorial approach, wherein optimal pairs or sets of guidance cues are employed to promote nerve growth within NGC, enabling the formation proper reconnections and the process of nerve regeneration to take place. The engineered presentation of molecular and topographical guidance cues to direct nerve growth is a promising approach with a wide array of highly tailorable parameters. In order to promote nerve regeneration, however, the approach must be informed such that these cues are optimally combined to promote nerve regeneration and enable recovery to take place.

APPENDIX A

CONFERENCE PROCEEDINGS

Neurite outgrowth in response to electrical and molecular cues

JA Richardson, KM Kim, CM. Kofron, SY Kim, GTR Palmore, D Hoffman-Kim

Biomedical Engineering Society Annual Meeting

October 2008, Podium Presentation

Following nerve injury, damaged neurons encounter permissive and inhibitory molecular cues. Electrical stimulation has demonstrated positive effects on neurite outgrowth and directionality. We have developed a platform on which multiple cues were delivered to neurons. This platform features parallel cell culture chambers, enabling simultaneous control and experimental dissociated rat dorsal root ganglia cell cultures. Neurite outgrowth was assessed after 25h culture on laminin that included 25mV/mm constant electric field for ten minutes. Electrical stimulation onset time was varied to correspond to relative early, intermediate, and late neurite initiation and growth.

Neurons stimulated at 4h had shorter neurites than unstimulated controls (longest neurite 30.9±14.6μm vs. 36.2±16.7μm). Neurons stimulated at 11h had longer average neurite lengths than unstimulated controls (30.2±14.0μm vs. 26.5±10.9μm). Neurons stimulated at 24h had fewer neurites per neuron than unstimulated controls (1.30±0.46 vs. 1.43±0.19). Neurite outgrowth directionality was clustered parallel to the direction of applied voltage when stimulated at 4h and 11h. These results suggest that short-duration electrical stimulation presented with LN cues can affect neurite growth, and in particular,

can influence neurite direction when neurons are permitted to grow for more than 10h after stimulation. Future studies will assess the potential for multiple cues to direct nerve growth in complex environments.

Funding: 1R21 EB004506; 1R01 EB005722; Kaplan fellowship

Novel Platform to Assess Neurite Outgrowth in Response to Multiple Cues

JA Richardson*, KM Kim*, C Kofron*, SY Kim, D Hoffman-Kim, GT Palmore (*co-first authors)

Northeast Bioengineering Conference

April 2008, Podium Presentation

Abstract—After central nervous system (CNS) injury, damaged neurons are exposed to numerous permissive and inhibitory cues in a predominantly inhibitory environment that prevents regrowth. We have developed a novel platform on which multiple cues may be assessed for their effects on neurite outgrowth. Outgrowth was assessed in the presence of electrical stimulation and substrate bound laminin (LN). Short duration of electrical stimulation produced directed neurite outgrowth along the axis of current flow when neurons were allowed to grow more than ten hours after stimulation. The extent of neurite outgrowth was affected by variation in the onset time of stimulation. These preliminary results indicate the importance of electrical and molecular cues to directing and enhancing neurite outgrowth and the usefulness of our platform for assessing combinations of cues required for accurate and effective nerve regeneration.

I. INTRODUCTION

Following traumatic injury to the CNS, nerves fail to regenerate spontaneously. At the site of injury, nerve cells are presented with an overall inhibitory environment, including

the astryocytic glial scar. CNS neurons have the capacity to regenerate, but the post-injury environment contains too many inhibitory cues and too few stimulatory cues. Our working hypothesis is that multiple growth-promoting cues will enable axon growth to overcome this local post-injury inhibitory environment. To test this hypothesis we have developed a novel platform on which combinations of cues may be administered simultaneously in a quantifiable manner. For the preliminary studies presented here, substrate-bound LN in combination with electrical stimulation were studied for their effects on neurite outgrowth and orientation.

II. METHODS

We designed a platform that consists of two parallel chambers in which neurons were examined with and without electrical stimulation (Fig. 1). The platform is comprised of an upper molded poly(dimethyl siloxane) (PDMS) and lower glass substrate for cell adhesion. PDMS was poured onto the acrylonitrile butadiene styrene master and was baked for 50 min at 70ºC. Plasma activation was used to adhere the glass cover slip (25 x 75 mm) to the molded PDMS, forming two identical parallel chambers for cell culture, as well as distal wells for delivering current through salt bridges to the cell chambers. Platinum wires (99.99%, diameter 0.25 mm) were placed through the distal wells on the side of the chamber for stimulation. Wired platforms were cleaned and sterilized. The total surface area of each chamber is 102 mm^2, with width and height measuring 3 and 4 mm, respectively. LN (50 µg/ml) was adsorbed to the glass cover slip via plasma activation.

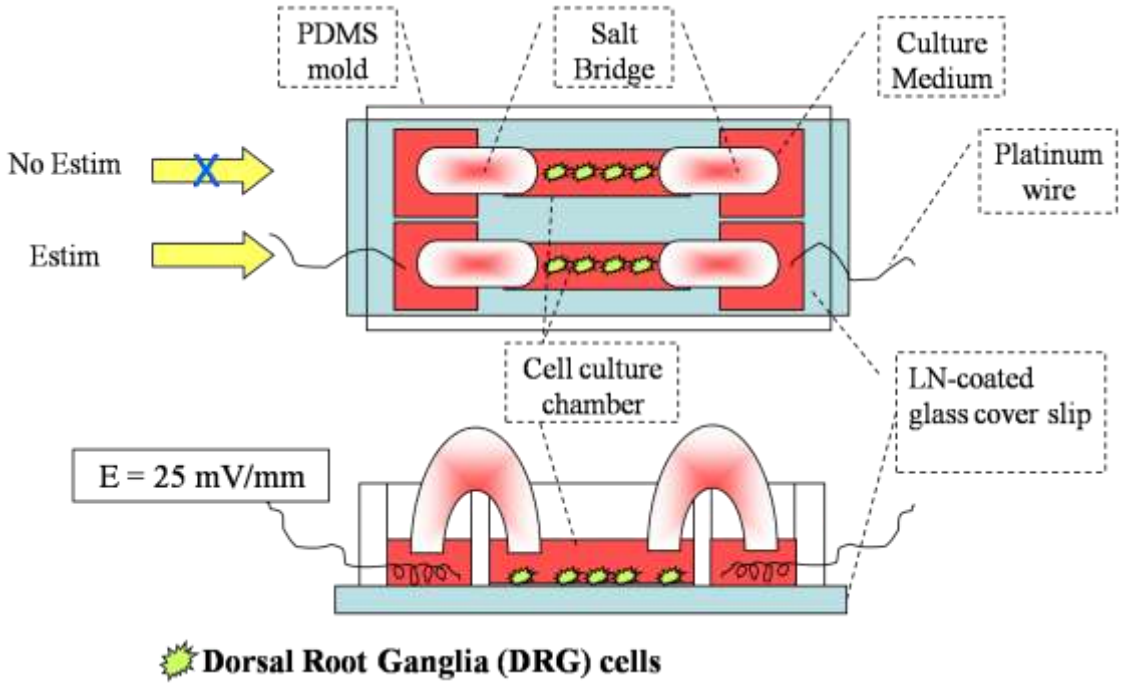

Figure. A.1. Top view (top) and side view (bottom) schematics of cell culture platform, with control and experimental chambers (not to scale)

Dorsal root ganglia (DRG) explants were obtained from postnatal (P1-P4) rat pups, dissociated enzymatically with trypsin and plated at 160cells/mm^2. Cells were allowed to adhere at least 4 h to the LN-coated glass. A constant electric field of 25 mV/mm was applied to the experimental well of each platform for 10 min at 4, 11, or 24 h after plating. To ensure the application of a constant electric field, a potentiostat was used to vary potentials between 5.5V-5.9V. Salt bridges were used as electric connectors during electrical stimulation to protect cells from oxidized substances in the media. During stimulation, the parallel control chamber remained unstimulated. A transparent, gas-permeable culture-foil made of fluoro-ethylene-propylene covered platforms during culture to prevent contamination and evaporation. Upon the initiation of electrical

stimulation, time-elapsed images of 2-3 fields of view of both the control and experimental chambers were obtained to observe dynamic effects of stimulation on neurites. One image was obtained per field of view per minute for 1h.

At 25 h after initial cell seeding all samples were fixed. Images were obtained under phase contrast optics. Neurites extending from cells without contact with neighboring cells were traced from soma to neurite tip using OpenLab software. Measurements of each neurite length and angle of neurite extension from the cell soma were recorded. Extensions smaller than the diameter of the soma (<15 μm) were not included in our analysis. At least 85 neurons were analyzed per chamber. To evaluate the significance of electrical stimulation on outgrowth parameters, student t-tests were used with significance levels taken as $p<0.05$. Directional data were analyzed both unidirectionally and bidirectionally with Oriana 2.02.

III. Results

A. Platform for Simultaneous Presentation of Cues

We fabricated a platform to study neuronal growth, which allows delivery of combinations of cues in a controllable and quantifiable manner. We successfully delivered both molecular (LN) and electrical stimulation to adhered neurons extending neurites. Voltage application can be controlled in magnitude and duration. Our platform allows for a variety of substrates to be utilized including conductive polymers and patterned proteins. Our system permits simultaneous observation of both electrically

stimulated and unstimulated populations under the same culture conditions (e.g. temperature, humidity, CO_2 concentration, etc.).

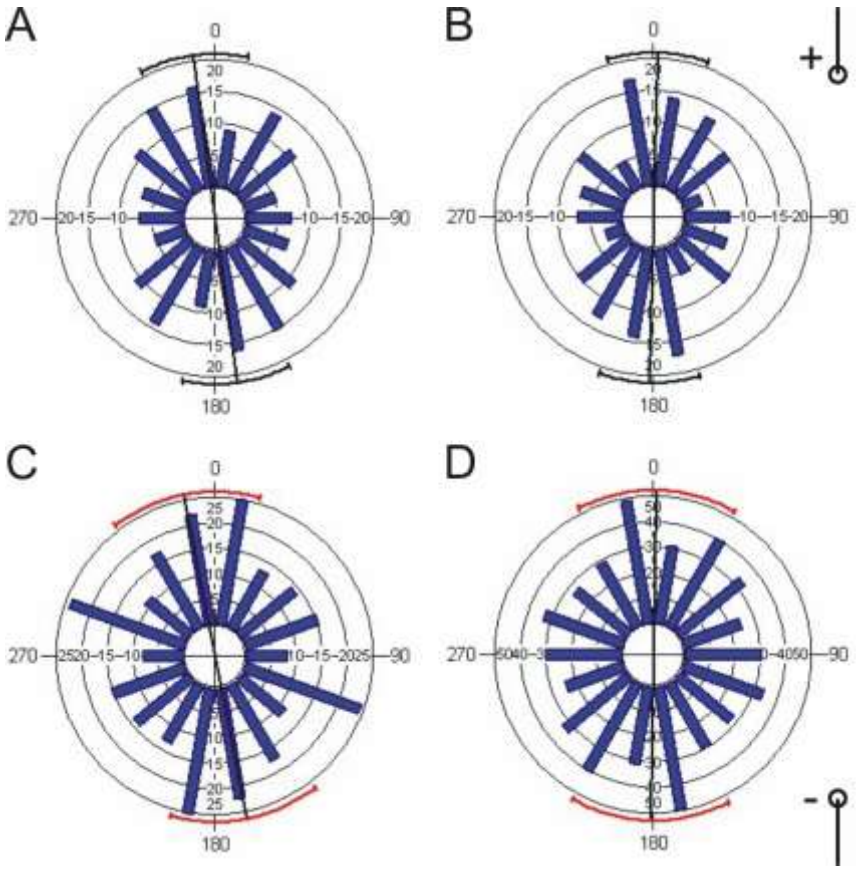

Fig A.2. Neurite Direction Following Short-Duration Electrical Stimulation

Bidirectional circular histograms of the orientation of the longest neurites of neurons cultured for 25 h with stimulation at 4h (A), 11h (B), or 24h (C) or no electrical stimulation (D). Alignment parallel to the direction of field was significant for neurites with stimulation at 4 and 11 hr. Anode and cathode represented on the right.

B. Electrical Stimulation Affects Outgrowth and Direction

Neurons adhered and extended neurites on LN coated glass substrates in all platforms tested. Time-elapsed microscopy did not reveal any significant changes in outgrowth during and up to 1 h after stimulation. With and without stimulation, neurites with active growth cones were observed to initiate, extend, and retract. Neurons that were electrically stimulated at 4h had shorter neurites than unstimulated controls at 25h (length of longest neurite = 30.9±14.6μm vs. 36.2±16.7μm). Neurons that were electrically stimulated at 11h had longer average neurite lengths than unstimulated controls at 25h (30.2±14.0μm vs. 26.5±10.9μm). Neurons that were electrically stimulated at 24h had fewer neurites per neuron than unstimulated controls at 25 h (1.30±0.46 and 1.43±0.19). Stimulation at 4h and 11h also affected directionality of neurite outgrowth (Fig. 2). With bidirectional analysis (0°=180°=360°), neurite outgrowth was clustered parallel to the direction of the applied voltage at 2 h. The mean vector lengths parallel to the voltage were 0.21 and 0.24 for stimulation at 4h and 11h respectively. Unidirectional analysis (0°=360°) showed no significant directional clustering.

IV. Discussion

We successfully developed a platform on which combinations of cues can be presented to neurons. The versatility of our platform provides us with a means by which to test a stimulatory environment against an inhibitory environment, thereby quantifying how guidance cues promote axon growth in an inhibitory environment. The relative effects of these combinations may be evaluated as they affect neurite outgrowth and directionality. In order to demonstrate the capacity of our platform to investigate these parameters, we presented molecular and electrical cues to neurons simultaneously. LN was chosen as a

molecule of interest because it is an extracellular matrix molecule found in the post-injury environment and has been shown to promote and guide neurite outgrowth [1]. Electrical stimulation was also chosen as a cue because previous work has illustrated its potential as a permissive and directive cue [2-4]. Short duration electrical stimulation was chosen because of its effectiveness in promoting neurite outgrowth and alignment towards the cathode *in vivo* [3,4]. *In vitro* assessment of short duration field application has demonstrated that short pulse stimulation can increase neurite outgrowth from whole DRG explants, but results pertaining to alignment of neurites to the axis of applied current were inconclusive [2]. We observed alignment parallel to the axis of current when cells were permitted to grow for more than 10 h post-stimulation. This alignment did not show preference towards the anode or cathode. Neurons exposed to electric field and fixed immediately post-stimulation (Fig. 2C) showed no directionality, indicating that neurite orientation induced by electrical stimulation may occur during post-stimulatory growth. This work suggests the potential of electrical stimulation and molecular cues to be used in combination to promote neurite outgrowth. The platform developed here provides a vehicle to further assess the potential for accurate and effective nerve regeneration in more complex, inhibitory environments.

Acknowledgement

This work was funded by NIH 1R01EB005722 to DHK and GTRP.

References

[1] L. Luckenbill-Edds. "Laminin and the mechanism of neuronal outgrowth," *Brain Res*

Brain Res Rev 23:1-27, 1997.

[2] M. Wood and R. Willits, "Short-duration, DC electrical stimulation increases chick embryo DRG neurite outgrowth," *Bioelectromagnetics*, 27:328-331, 2006.

[3] L. Jaffe and M. Poo, "Neurites grow faster towards the cathode than the anode in a steady field," *J Experimen Zool*, 209(1):115-128, 1979.

[4] N. Patel and M Poo, "Orientation of neurite growth by extracellular electric fields," *J Neurosci*, 2(4):483-496, 1982.

APPENDIX B

THE IMPORTANCE OF DEFINING 'DATA' IN DATA MANAGEMENT POLICIES

JA Richardson and D Hoffman-Kim

Science and Engineering Ethics, 2010. 16(4), 749-751.

Abstract

What comprises 'data' varies from one institution to another based on the information which is deemed important by individual institutions. To effectively and efficiently produce, collect, and retain data, an organization develops specific defining characteristics of data to meet its informational needs. Procedures to maintain and retain knowledge among laboratory members and principal investigators will allow for improved efficiency of data collection. Optimization of communication, maintenance of inventories, record keeping, and updating relevant training programs are all critical to supporting the quality and integrity of a particular organization's data. Concurrent revisions to such procedures will ensure that the definition of data as well as the means by which it is collected and maintained remain appropriate to the needs of the individual organization.

Key Words: data collection, data management, laboratory, defining data.

In the article, "Issues in Data Management," Margi Joshi and Sharon Krag discuss multiple definitions of data and how they vary within specific institutions and between different kinds of institutions (Joshi and Krag 2010). The items placed under the umbrella of 'data' reveal what is deemed valuable information. It is interesting to consider why certain definitions of data develop, and what purpose each definition serves. As a graduate student and faculty member in the interdisciplinary field of biomedical engineering, we encounter these definitions most often in the context of three settings: academic institutions, federal funding agencies, and the regulatory bodies that oversee the first two.

For each definition of data, Joshi and Krag list not only the components that are considered to be data, but also specific exclusions to the definitions of data. These are worthy of further note

because they signal how information is differently valued. For example, the definition of research data, according to Circular A-110 from the federal Office of Management and Budget (OMB), "excludes lab samples, preliminary analyses, drafts of scientific papers, plans for future research, peer reviews, or communications with colleagues" (Office of Management and Budget 2010). Scientific researchers in the academy value highly these components of the research process because of the important role they play in publishing and patenting. Reputations and credibility as academic scientists rely strongly on both written experimental procedures and the ability to determine ownership of specific discoveries. That OMB's interest lies not in the race to publish, but rather in the use of published results, explains why OMB's definition is narrow. For OMB's purposes, data is: "recorded factual material commonly accepted in the scientific community as necessary to validate research findings" (Office of Management and Budget 2010). What constitutes research data for OMB need not include the majority of components of the research process that researchers find to be critical to the pursuit of academic science.

A particular definition of data typically reflects quite broadly the components of research that are most important to that specific organization/group/entity. Often in the academic setting or within a specific field, a single definition of data encompasses broad institutional needs. In practice, however, detailed descriptions of data may vary among subsections of institutions such as particular laboratories or research groups. Further, in order to comply with official institutional definitions and guidelines, research groups often develop additional, more specific definitions and guidelines for the acquisition and management of specific research components. These definitions are often less formal and less clearly articulated, but are critical to the integrity of the research endeavor.

Especially in the academic setting, in which the tenure of researchers may be as little as one semester to an academic year, it is important for the principal investigator and researchers within a group to ensure that data and associated knowledge are retained and preserved despite the flux of researchers. Specific procedural systems regarding the procurement and handling of laboratory data can aid in acquiring and retaining data most efficiently in the laboratory setting. Ideally, data such handling procedures are determined, implemented, monitored for effectiveness, and seamlessly transmitted from senior to incoming group members. Such data handling procedures should be tailored to individual laboratory requirements, and may be based on paper records, or more currently in electronic formats (Elliot 2010). Ongoing clear communication among principal investigator and laboratory researchers is critical for initial training and to relay updates, changes, and new data management topics, ensuring that policies and procedures are adequately implemented and monitored. Time spent on the specifics of data-associated procedures is worthwhile, as the result may streamline data collection and thereby laboratory productivity (Bonetta 2006).

Annual inventories and refreshers of laboratory procedures can aid in monitoring data collection and management. Inventories can include evaluation of the implementation of the procedures as well as of their efficiency. Revisions and modifications may be determined during the monitoring of laboratory data management procedures, and can increase the rate and efficiency of data acquisition. On a more frequent basis, laboratory members may take advantage of regular scientific project status discussions to inform one another of, and make decisions regarding, protocol additions and alterations, and alterations in methods of data acquisition and analysis. Documented discussions will serve to improve the consistency of laboratory methods and enhance the reproducibility of experiments. It is particularly important that all changes in protocols, materials, and methods be communicated to all laboratory personnel, since minor

changes may have major effects on experimental outcomes. Additionally, recording specific steps taken to troubleshoot methods will facilitate swift problem solving in the future.

Finally, a laboratory research group's reputation and credibility are based on the reproducibility and quality of data output. Data (according to both official and laboratory-specific definitions), as well as data management practices, must be maintained from generation to generation within a group. Only in this way will the research group be optimally positioned to uphold research quality and integrity and maintain the momentum required to meet its research goals.

References

1. Joshi, Margi and Krag, Sharon S. (2010). Issues in Data Management. *Science and Engineering Ethics* (this issue).
2. Office of Management and Budget. (1999). Uniform Administrative Requirements for Grants and Agreements With Institutions of Higher Education, Hospitals, and Other Non-Profit Organizations. http://www.whitehouse.gov/omb/rewrite/circulars/a110/a110.html#2. Accessed 13 May 2010.
3. Elliot, M.H. (2010). Considerations for Management of Laboratory Data. Resource Document. Scientific Computing. http://www.scientificcomputing.com/considerations-for-management.aspx?terms=lims. Accessed 4 August 2010.
4. Bonetta, L. (2006). *Making the Right Moves: A Practical Guide to Scientific Management for Postdocs and New Faculty.* Research Triangle Park, NC, USA; Chevy Chase, MD, USA. Howard Hughes Medical Institute and Burroughs Wellcome Fund.

APPENDIX C

POLY(DIMETHYL SILOXANE) NERVE GUIDANCE CONDUIT FABRICATION

The construction of nerve guidance channels featuring biomimetic topographical or other luminal surface features is described in the text and photos that follow.

C.1. Step 1. Mix PDMS monomer and catalyst

For PDMS NGCs, combine Sylgard 184 (Corning) at a ratio of 10:1 wt/wt base:catalyst. Typically, you may make approximately 20 ml to work with for one session of NGC rolling, so 20 g base and 2 g of catalyst should be combined in a 50 ml Falcon tube. Vigorously mix with a glass stirring rod until the entire mixture is thick with small bubbles. Remove air bubbles by centrifugation at 2000 rpm for 1 minute.

C.2. Step 2. Pour and cure PDMS on cell template

Pour approximately 1-2 ml of PDMS onto a clean cell template. Tilt the template to allow the PDMS to flow over the entire surface evenly, and before placing it on the hot plate, tilt the template toward one side to achieve a slight tapering in the PDMS layer on the cell template. This taper will help with rolling the NGC later. Bake the PDMS at 95°C for 20 minutes or until it is firm to the touch. Such a thin layer of PDMS does not need the full curing time as thicker substrates.

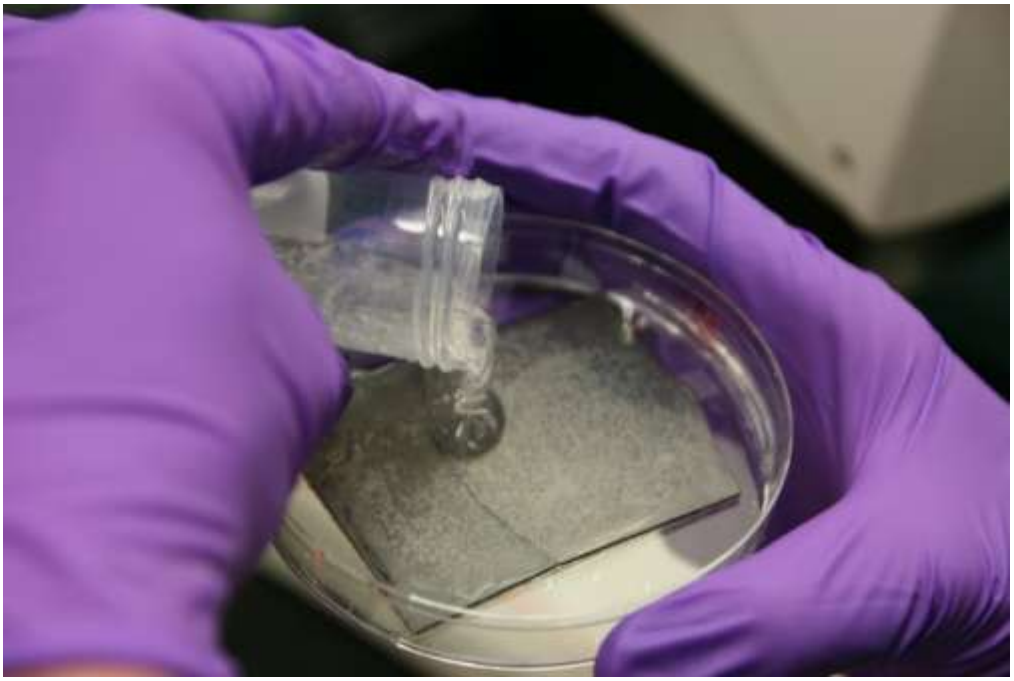

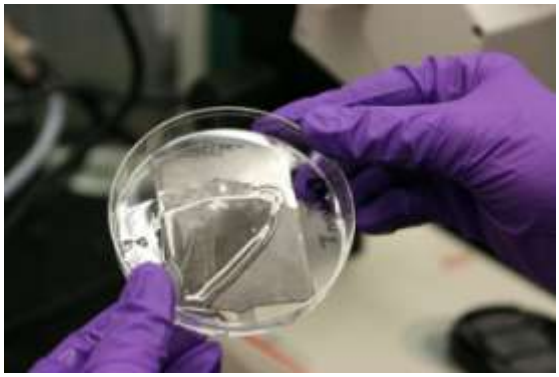

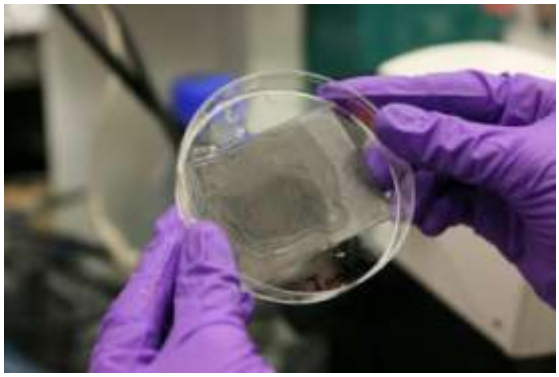

C.3. Step 3. Mise en place

Prepare your workspace. Prepare 1 mm glass mandrels by snapping off the ends of Pasteur pipettes, leaving approximately 7 cm mandrel length.

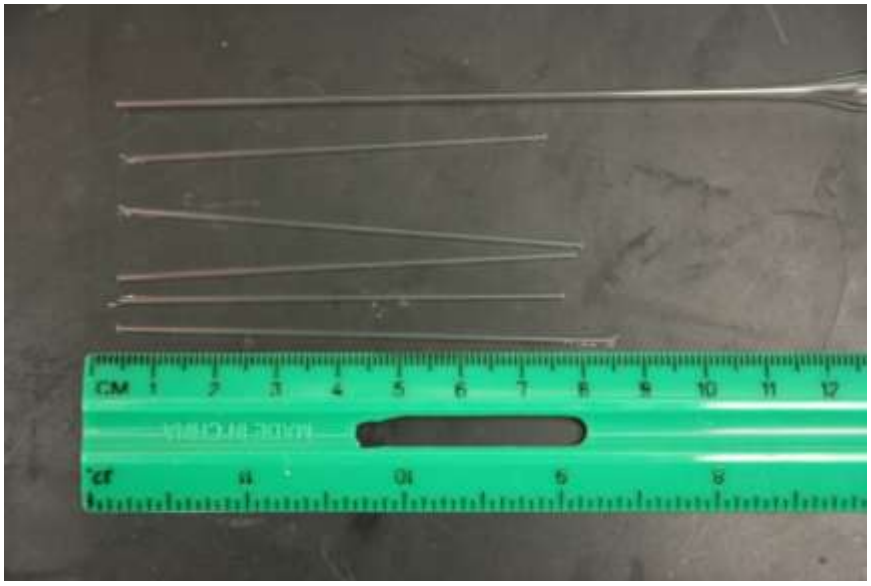

Pour approximately 400 ul of the PDMS into the lid of a 15 ml Falcon tube. Set out several SIZE glass slides, set the hot plate to 175°C.

Use the smallest gloves that your hands will fit into. This trick will help during the rolling step to 'grip' the PDMS to the mandrel as you roll.

C.4. Step 4. Remove PDMS film from template

Under a light microscope, cut out the thin PDMS using a razor blade so that it contains the lumen area of interest (e.g. aligned topographical features). Typically, I have used 1 cm x 2 cm regions, where the 1 cm edge becomes the width of the conduit and is wrapped parallel to the mandrel. Under the microscope, trim the edges of the PDMS so that it is the appropriate shape, invert it, and put on glass slide.

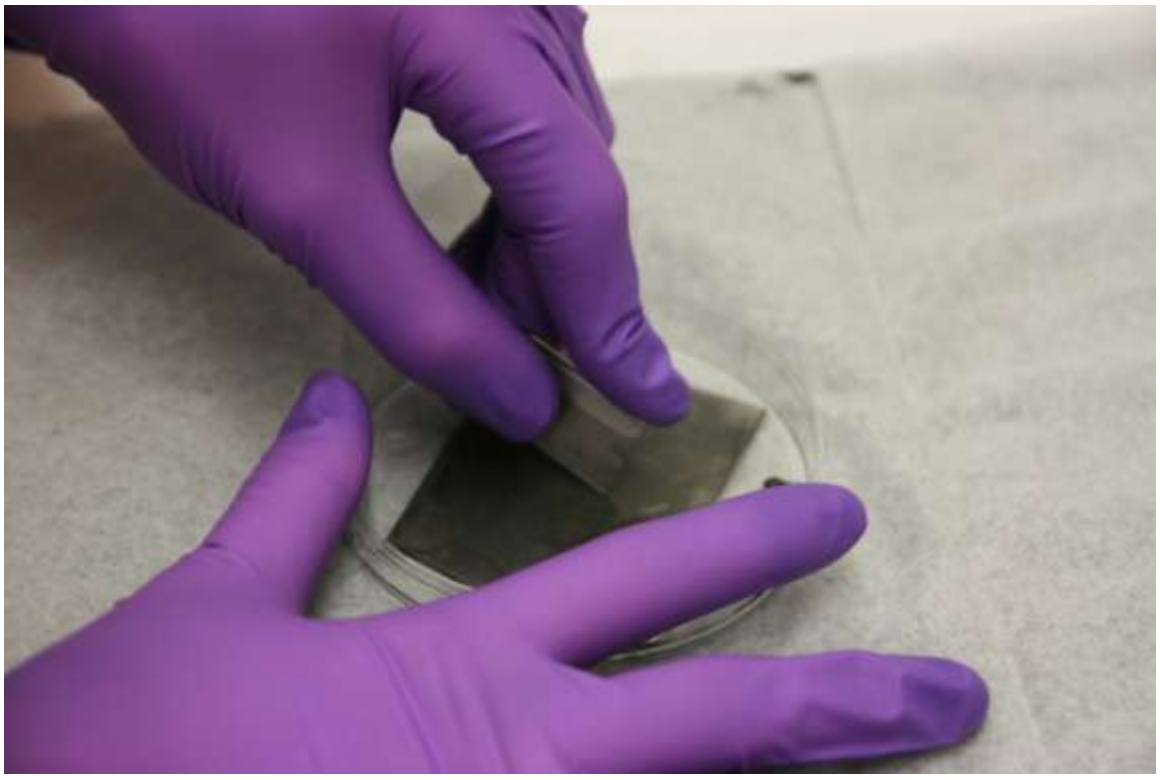

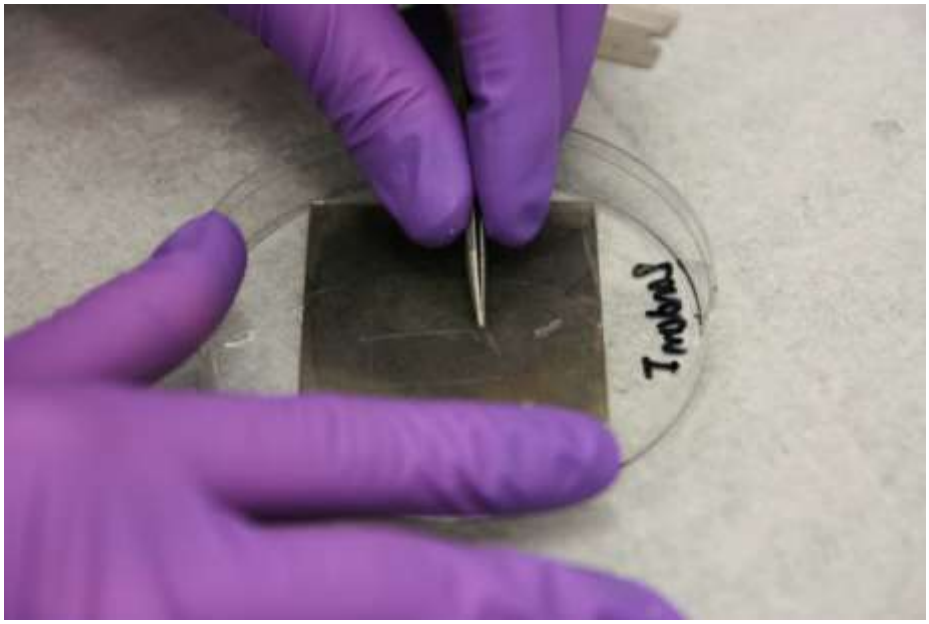

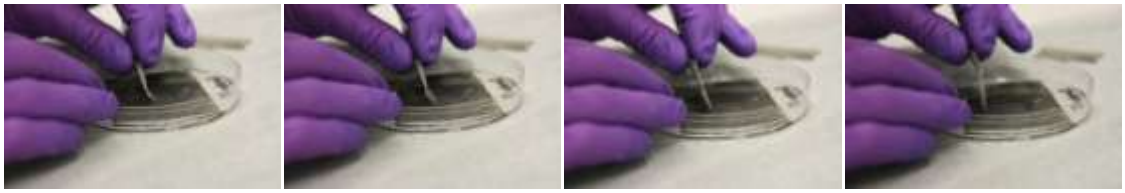

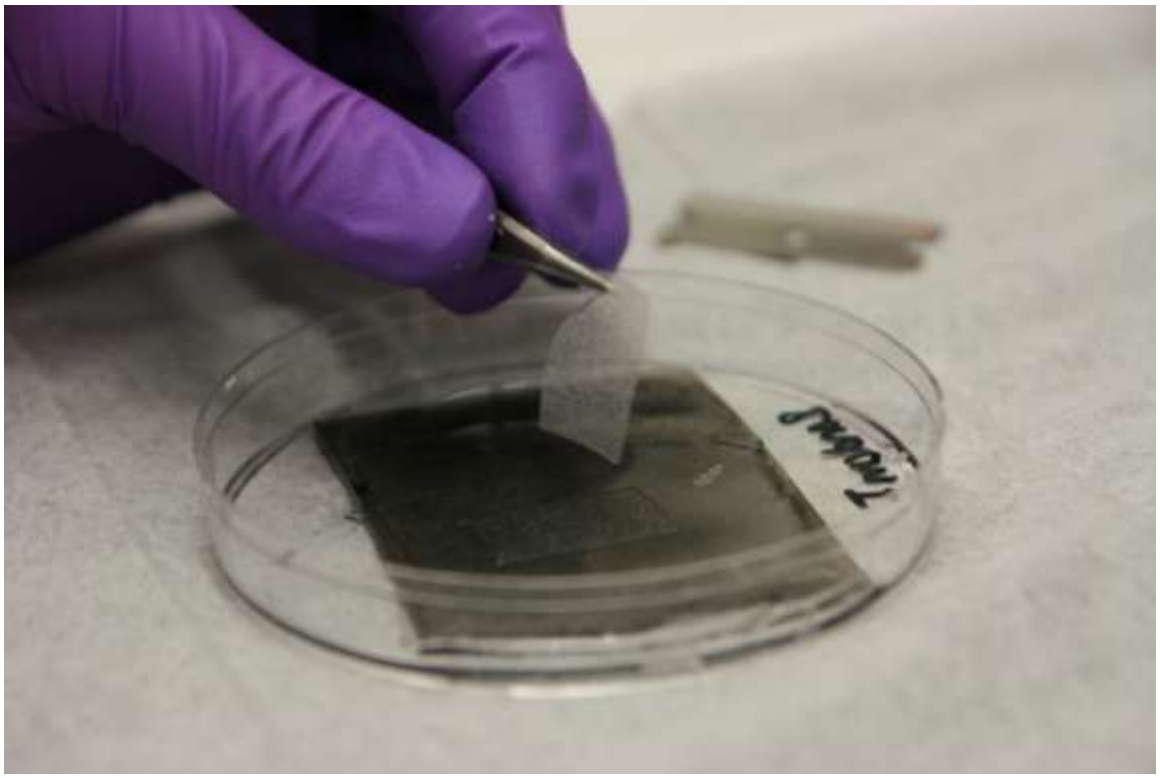

C.5. Step 5. Roll the NGC

Line up a glass mandrel to the edge of the PDMS film that is most tapered and contains your lumen surface of interest. Use one hand to grip the mandrel and your other hand to use forceps to grip the edge of the PDMS and begin to wrap it around the mandrel. Carefully swap the forceps for the index finger of your right hand and use this finger to firmly secure the PDMS to the mandrel. Apply pressure with your finger while rolling the mandrel away from yourself and pushing the PDMS along the contour of the mandrel. Flexing the last segment of your index finger as you hold the PDMS to the mandrel will help to make sure that the PDMS does not fold onto itself during the rolling process. Typically, firmly pressing the PDMS to the mandrel while rapidly rolling achieves the best results, as slower rolling and less pressure leads to 'loose' channels and more opportunity for the PDMS to fold onto itself, disrupting the lumen topography. For this step, the thinnest possible PDMS should be used. Here is where tapering the PDMS can help, in that the tapered end of the PDMS film may be wrapped more easily to the glass mandrel and the tapering leads to smoother lumen topography (less of a PDMS 'step').

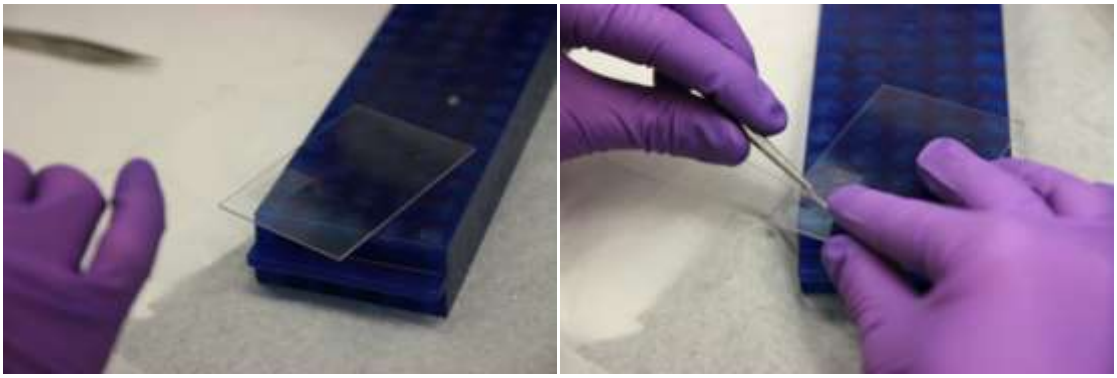

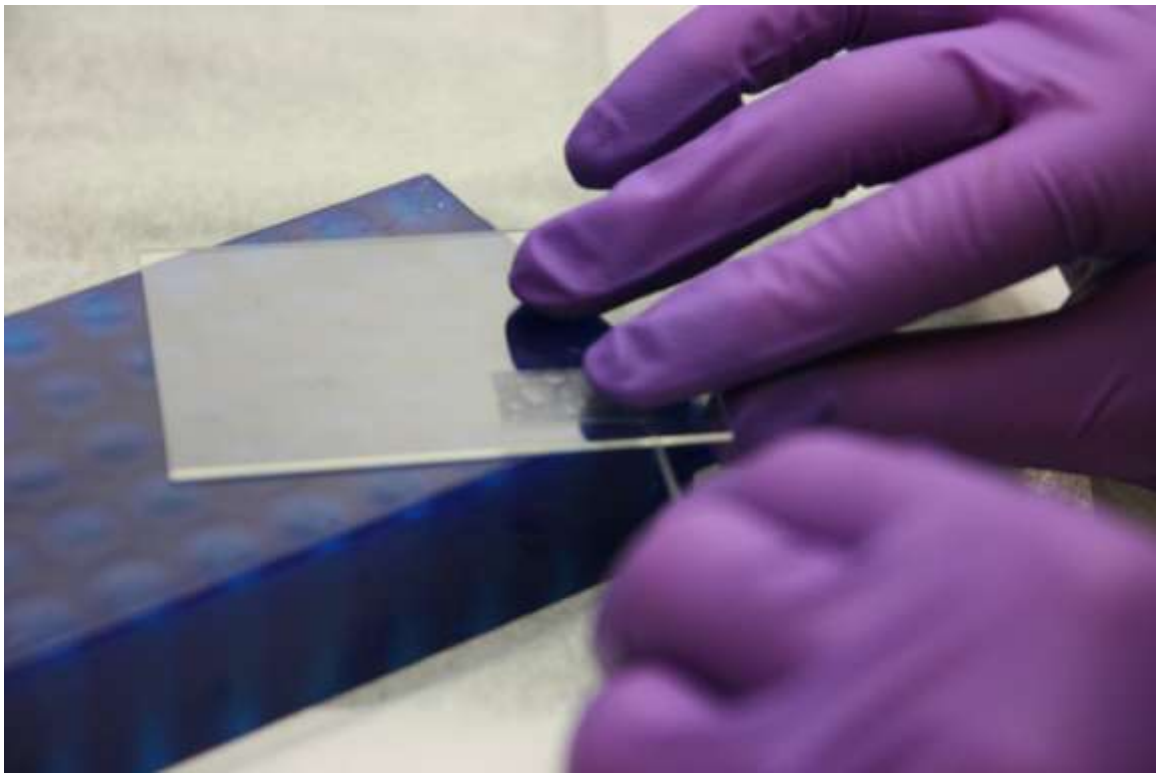

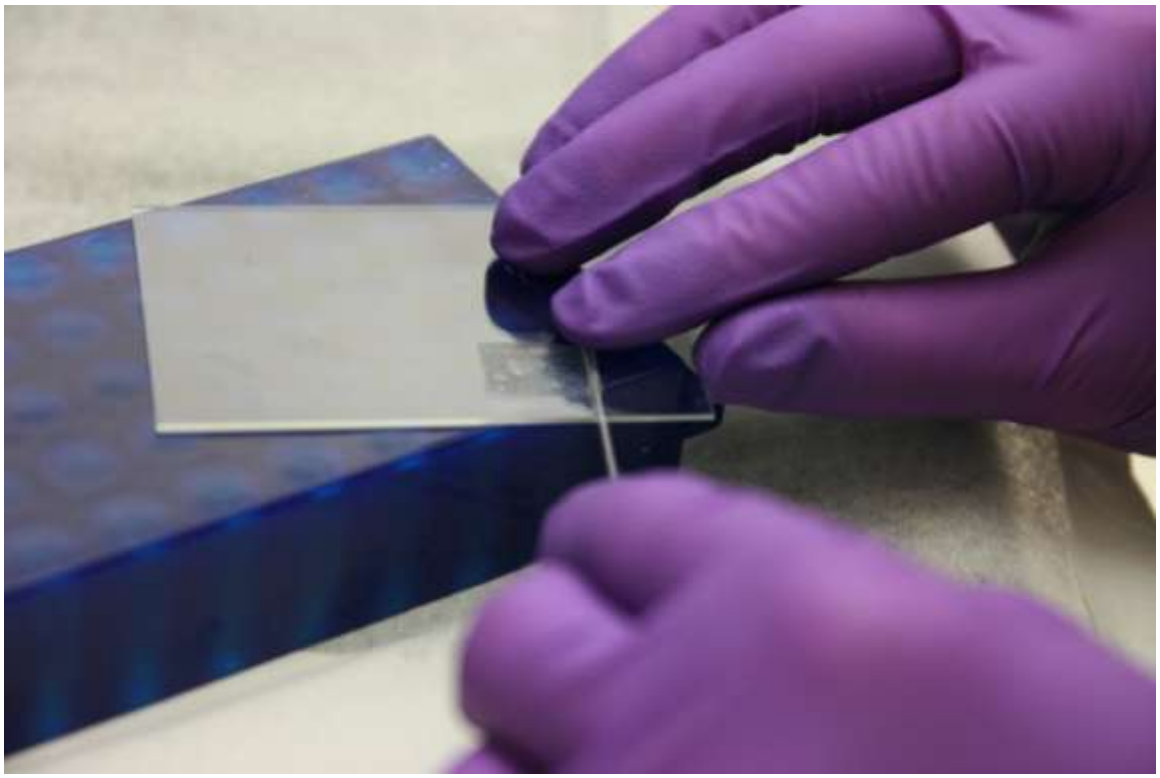

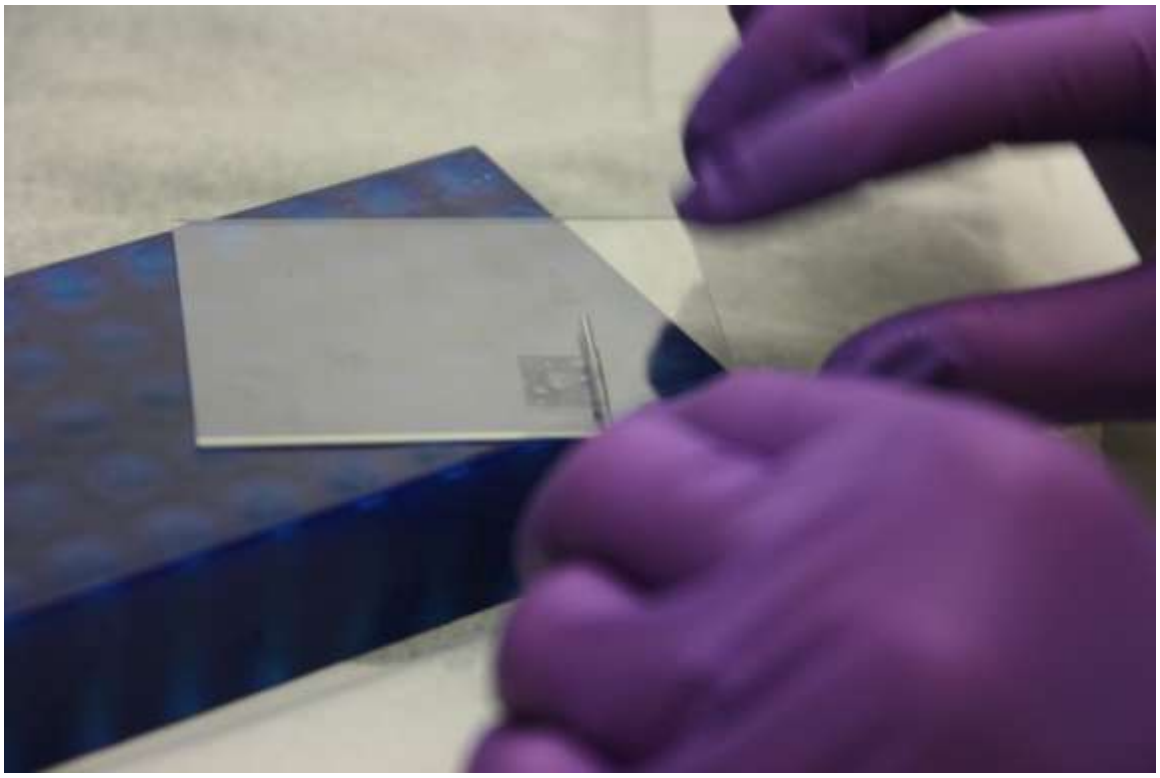

C.6. Step 6. Seal the NGC

Once you have rolled the PDMS so that it is wrapped slightly more than one full revolution around the mandrel, keep the mandrel steady while applying radial pressure away from yourself and use the other hand to dab liquid PDMS onto crease with the mandrel you have set up into the Falcon tube lid with PDMS. The liquid PDMS will be quickly cured and used to seal the conduit.

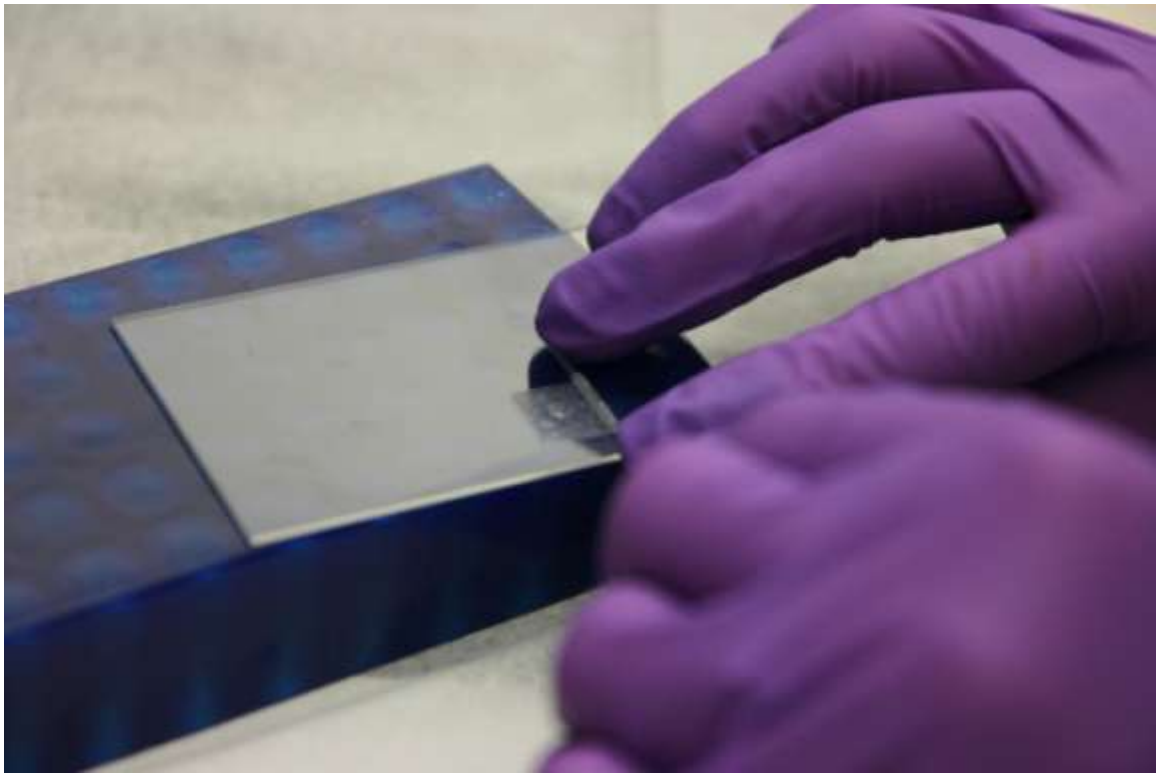

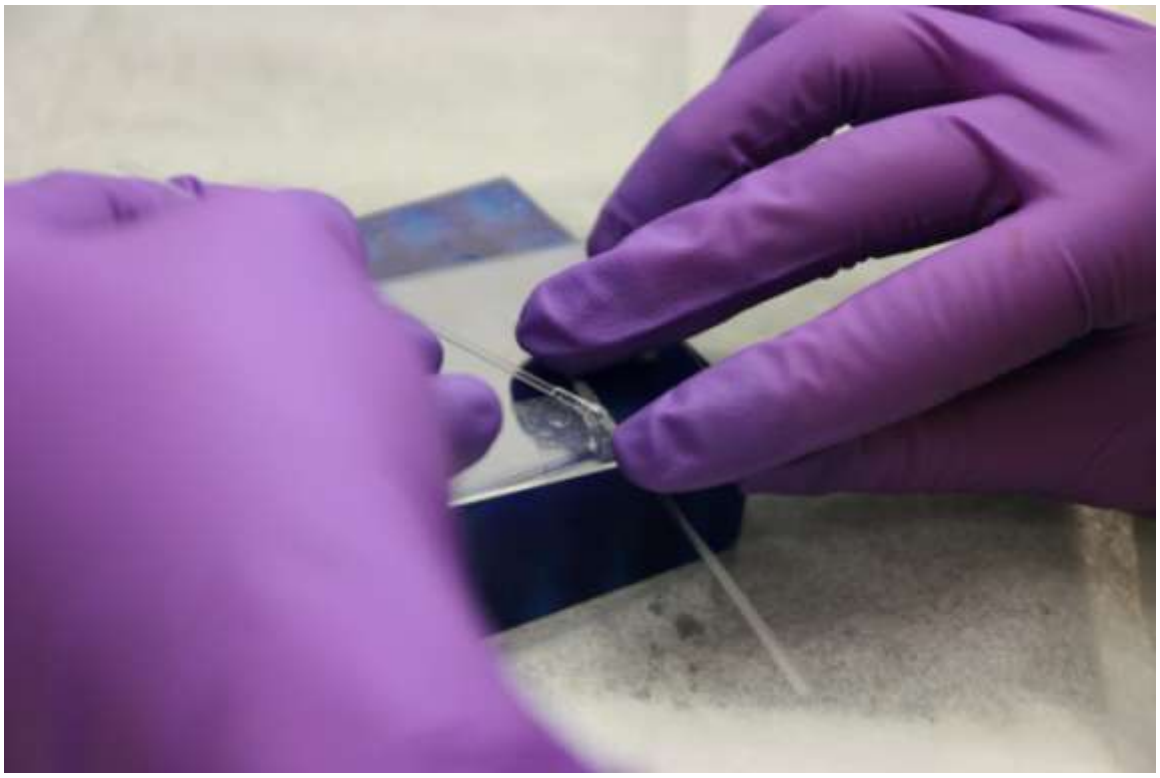

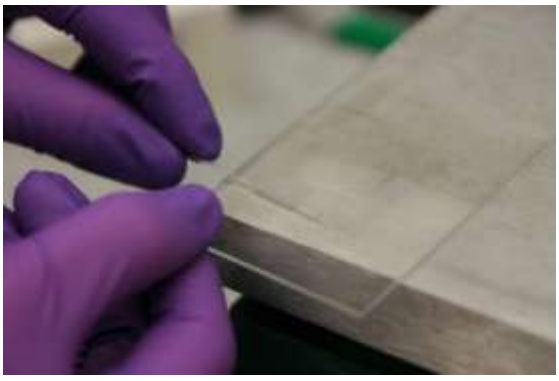

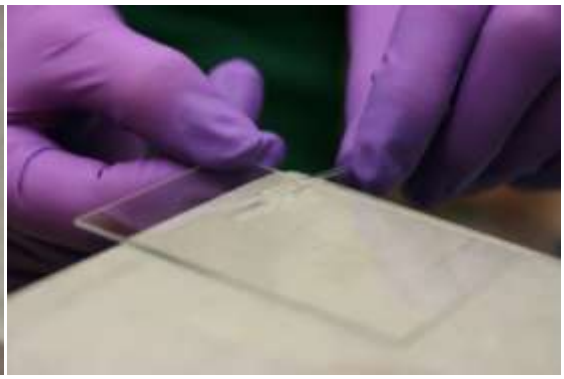

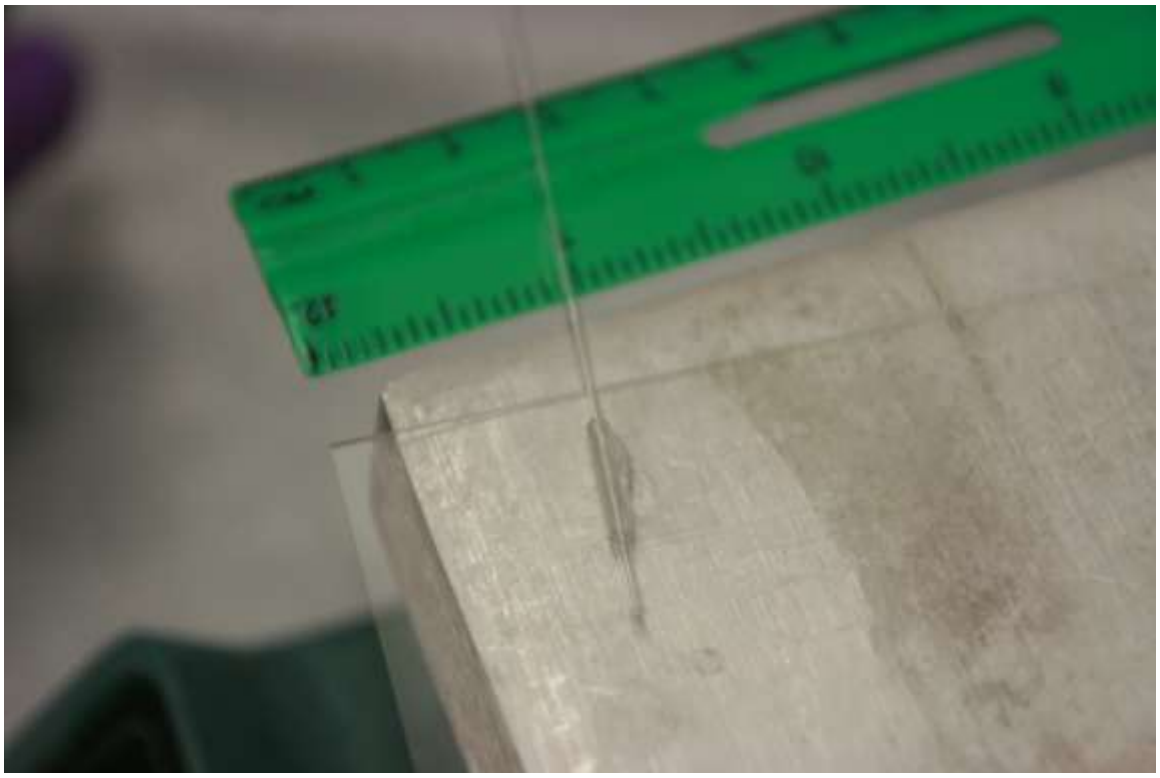

Carefully and steadily transfer the glass, mandrel, and NGC composite to the 175°C hot plate and hold it steady to allow the liquid PDMS to cure and seal channel together (about 30-45 s). After this initial curing period, you may let go and allow the PDMS seal to cure for an additional 10 minutes.

C.7. Step 7. Process the NGC

Once the PDMS seal has fully cured, remove the glass slide/NGC/mandrel complex from hot plate. Using a razor blade, trim the excess thin PDMS closely to the glass mandrel, so that the NGC does not have an excess flap of PDMS extending from it.

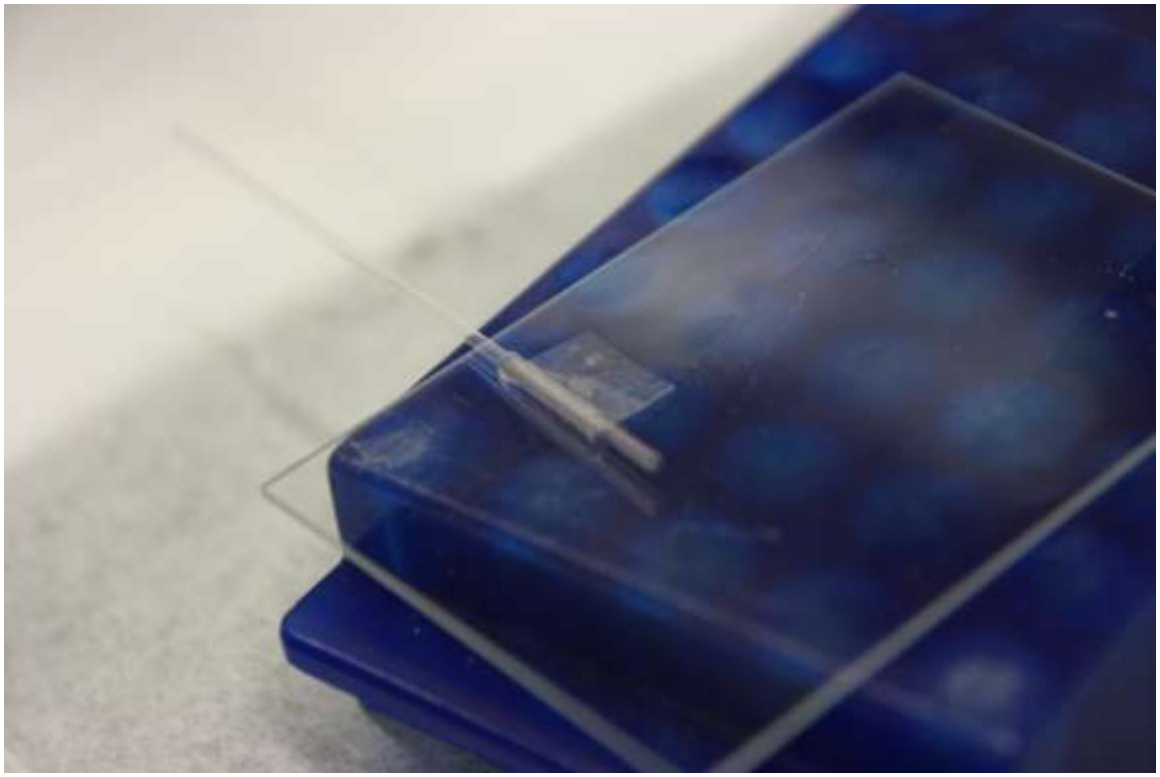

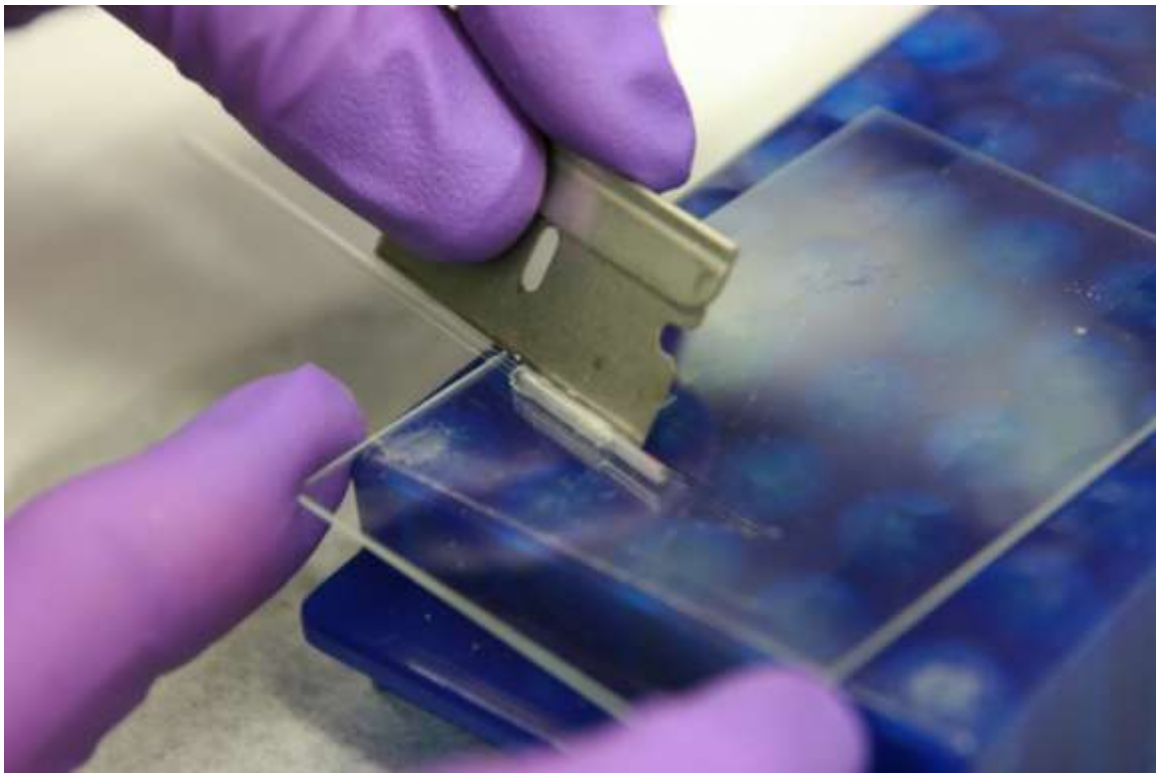

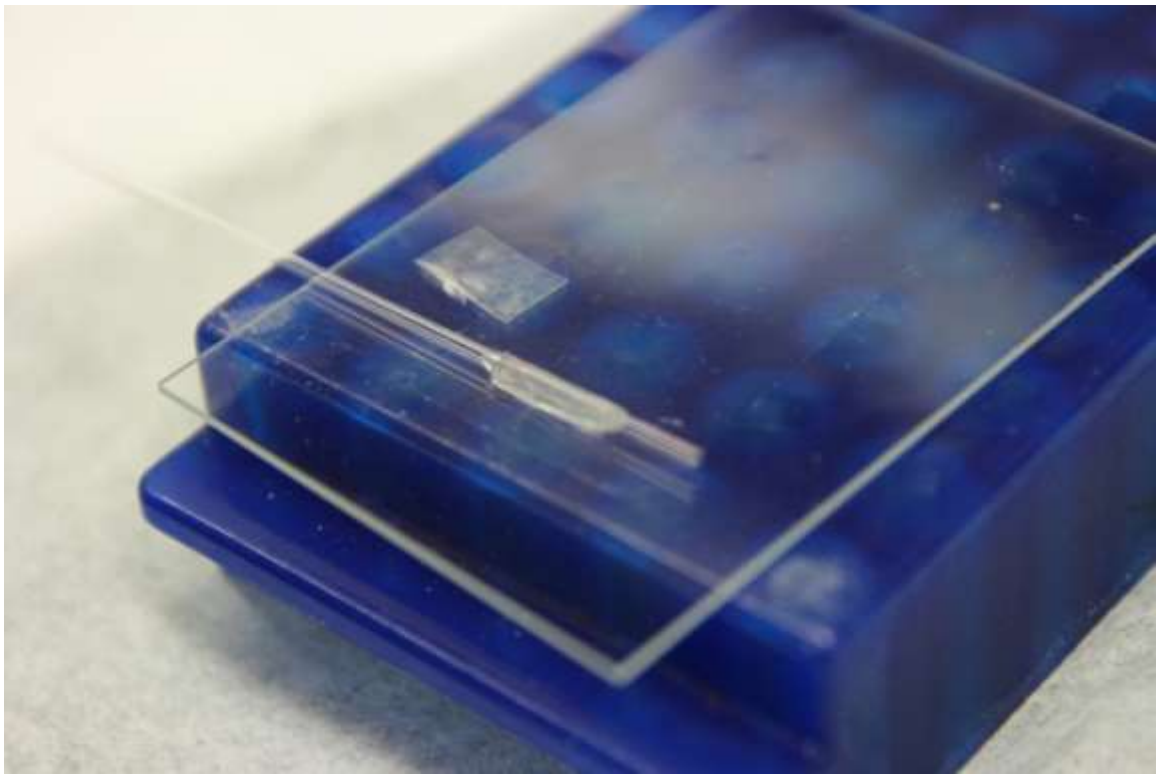

While gripping the mandrel with one hand, gently twist and pull the NGC to remove it from the glass mandrel.

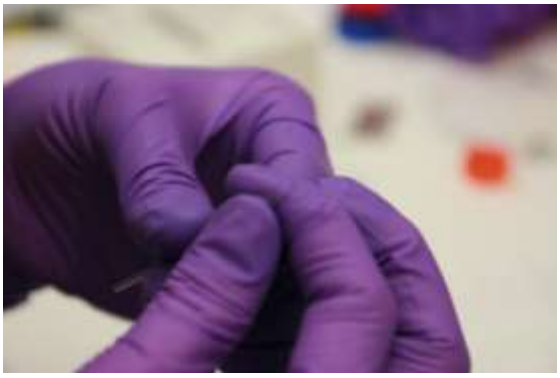

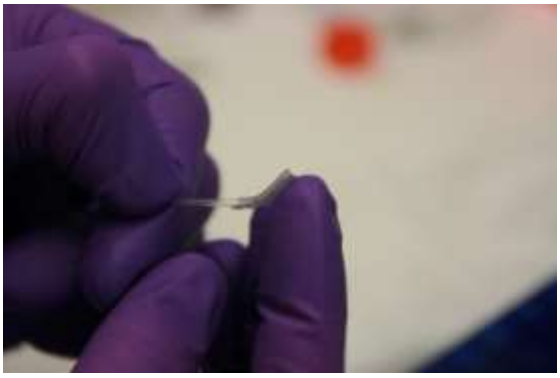

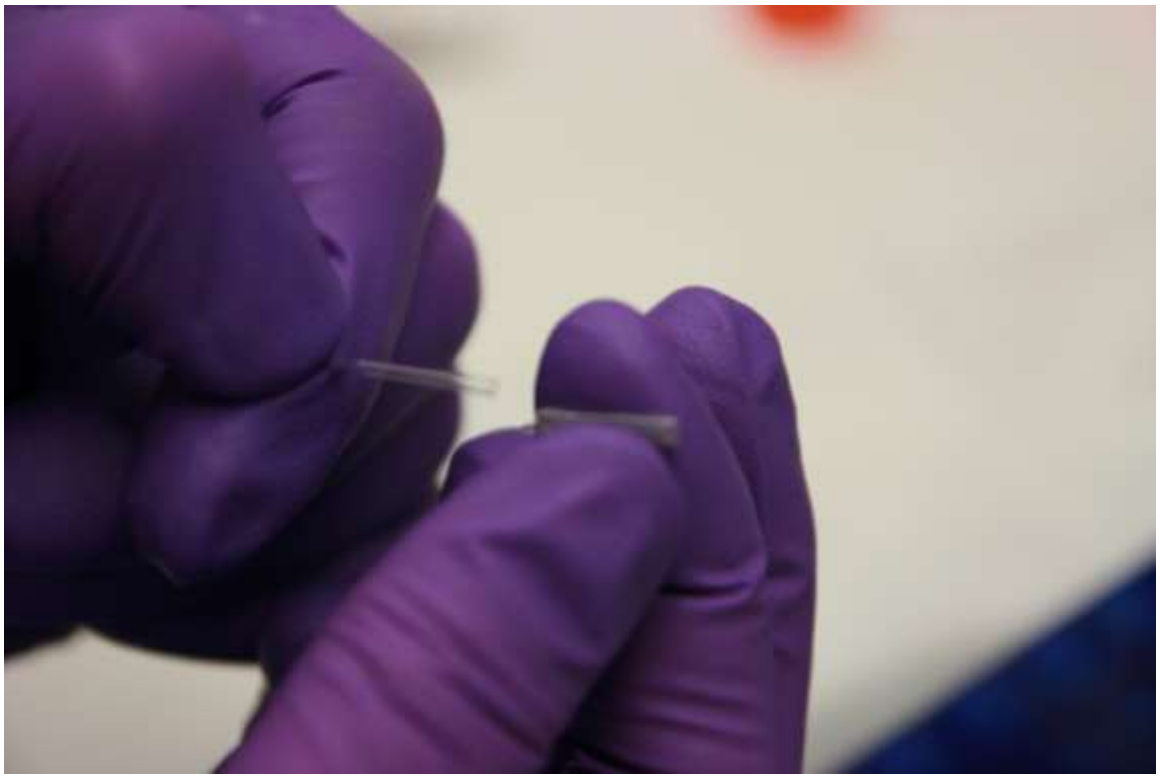

Using a razor blade. trim the NGC to the desired length.

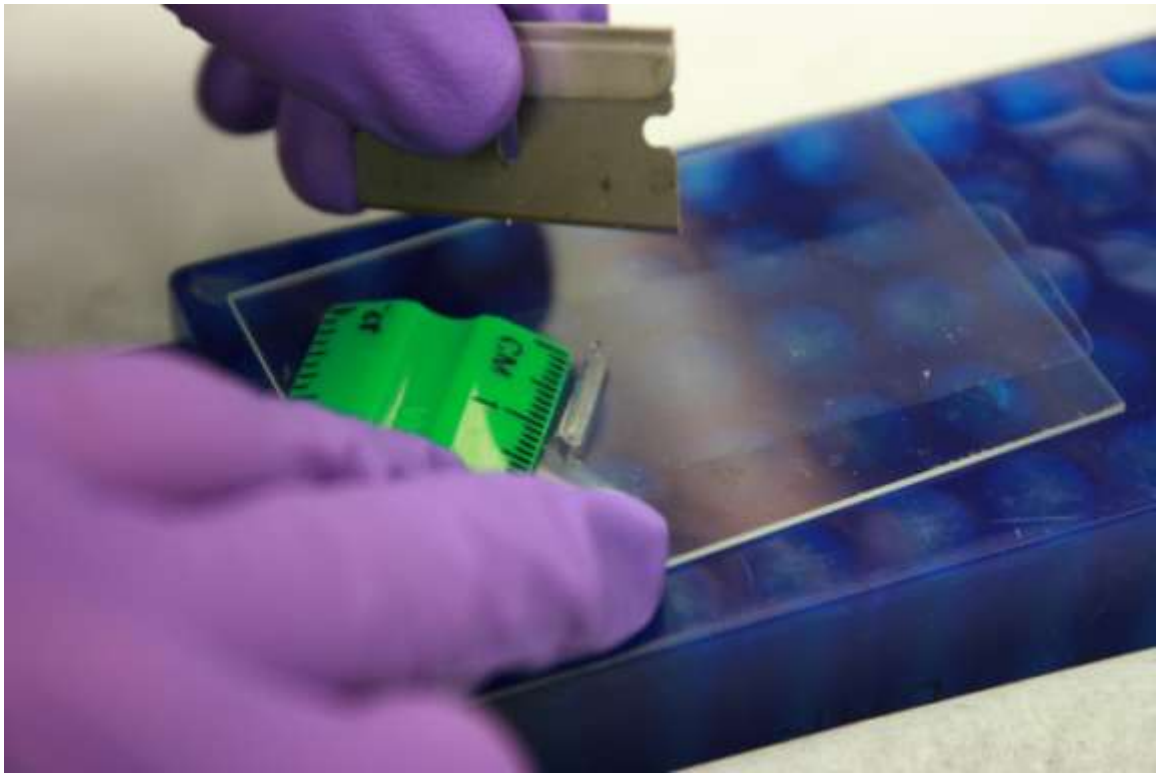

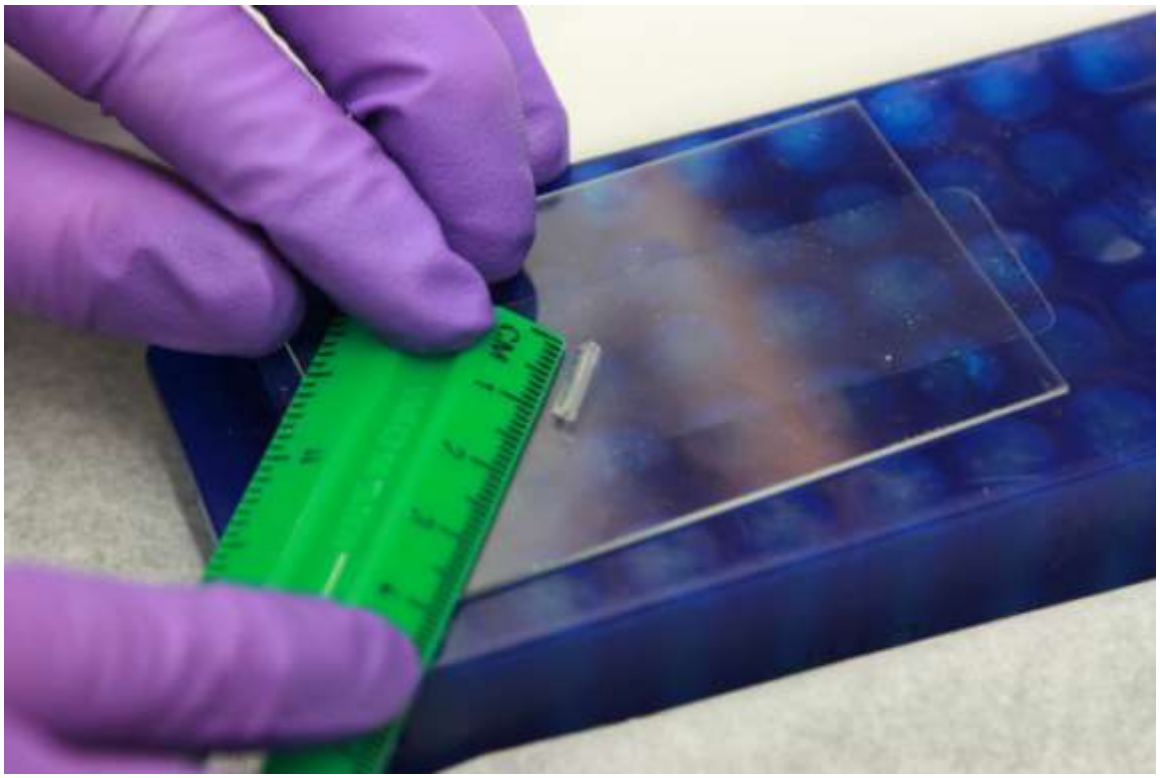

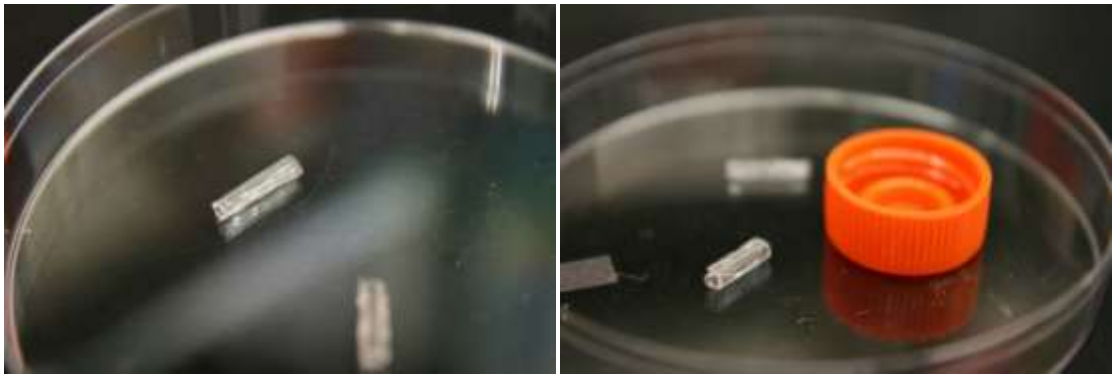

C.8. Step 8. Apply protein coat to lumen of NGC

To apply a protein, such as laminin to the lumen of the NGC, first clean the NGC by flooding it with ethanol then water, then thoroughly dry the lumen surface by gripping the NGC with forceps and flowing pressurized air through the conduit. Plasma etch the conduit for 60 seconds, and then, using a small pipette tip, apply drop of LN to the end of the conduit, allowing capillary action to bring it through to the other end. Allow the protein to adsorb for at least 30 minutes, then flush the NGC with dH_2O and used pressurized air to dry the lumen while holding the NGC steady with forceps.

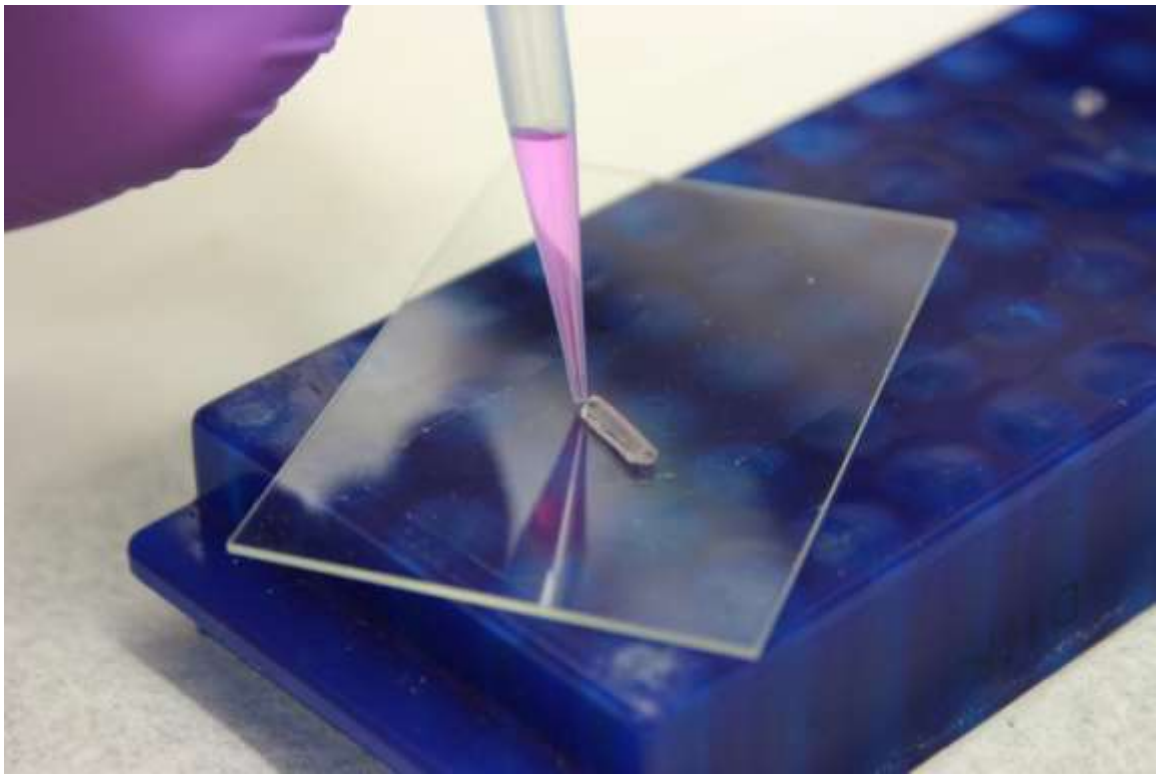

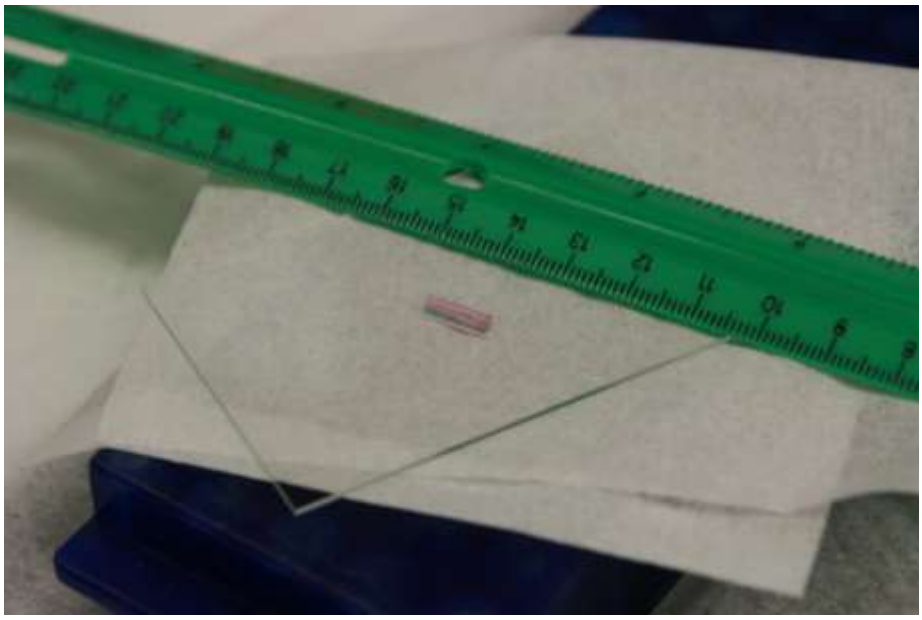

C.9. Step 9. Using NGC for whole DRG culture

To use the NGC in a cell culture experiment, first adhere the NGC to a well plate or to a small glass cover slip within a well using a small dab of silicone grease. Seeding DRGs to conduits works best when the conduit is dry. Use forceps to blot excess moisture from the DRG onto the lid of a 35 mm petri dish. Then, using the same forceps, under the light microscope, place the DRG explants on the lumen of the conduit, within 1 mm from the conduit opening, away from the inner seam of PDMS. Within 30 s, use a needle and syringe to apply a few drops of media to the opposite end of the conduit, allowing capillary action to draw the media through the conduit. Be cautious if you try to apply media to both ends of the conduit, as you may end up with a bubble in the center of the conduit. Once the conduit is flooded with media and the DRG is secure, you may apply media to the well so that the conduit is covered by media. Add the media slowly to avoid dislodging the DRG explant.

C.10. Acknowledgements

Thank you Talisha Ramchal and Danielle Chau for your help with taking these photos.